UNIVERSITY OF GAZİANTEP
GRADUATE SCHOOL OF
NATURAL & APPLIED SCIENCES

ULTIMATE LOAD CARRYING CAPACITY OF THIN-WALLED STIFFENED STRUCTURES

Ph. D. THESIS
IN
CIVIL ENGINEERING

BY
TALHA EKMEKYAPAR
JUNE 2013

Ultimate Load Carrying Capacity of Thin-Walled Stiffened Structures

Ph.D. Thesis
in
Civil Engineering
University of Gaziantep

Supervisor
Prof. Dr. Mustafa ÖZAKÇA
Co–Supervisor
Assist. Prof. Dr. Nildem TAYŞİ

by
Talha EKMEKYAPAR
June 2013

T.C.

UNIVERSITY OF GAZİANTEP
GRADUATE SCHOOL OF
NATURAL & APPLIED SCIENCES
CIVIL ENGINEERING DEPARTMENT

Name of the thesis: Ultimate Load Carrying Capacity of Thin-Walled Stiffened Structures
Name of the student: Talha EKMEKYAPAR
Exam date: 07.06.2013

Approval of the Graduate School of Natural and Applied Sciences

Assoc. Prof. Dr. Metin BEDİR
Director

I certify that this thesis satisfies all the requirements as a thesis for the degree of Doctor of Philosophy.

Prof. Dr. Mustafa GÜNAL
Head of Department

This is to certify that we have read this thesis and that in our opinion it is fully adequate, in scope and quality, as a thesis for the degree of ~~Master of Science~~/Doctor of Philosophy.

Assist. Prof. Dr. Nildem TAYŞİ
Co–Supervisor

Prof. Dr Mustafa ÖZAKÇA
Supervisor

Examining Committee Members	Signature
Prof. Dr. A. Kamil TANRIKULU	
Prof. Dr. İbrahim H. GÜZELBEY	
Prof. Dr. Mustafa ÖZAKÇA	
Assoc. Prof. Dr. Abdülkadir ÇEVİK	
Assoc. Prof. Dr. Mustafa ŞAHMARAN	

I hereby declare that all information in this document has been obtained and presented in accordance with academic rules and ethical conduct. I also declare that, as required by these rules and conduct, I have fully cited and referenced all material and results that are not original to this work.

Talha EKMEKYAPAR

ABSTRACT

Ultimate Load Carrying Capacity of Thin-Walled Stiffened Structures

EKMEKYAPAR, Talha
PhD. in Civil Engineering
Supervisor: Prof. Dr. Mustafa ÖZAKÇA
Co–supervisor: Assist. Prof. Dr. Nildem TAYŞİ
June 2013, 189 pages

To generate more robust designs to serve significant magnitude of compressive forces, plate assemblies are stiffened by specially designed stringers. The benefit of stiffening of a plate structure lies in achieving divided more efficient segments which use compression and bending performances of stringers. The characteristics of structure, expected loading type, used materials, expected performance and employed manufacturing technique are examples of parameters which governs the design and shape of stringers. Generally stiffened panels are constructed as built-up structures, where individual stringers are riveted or welded on thin skins. This way of assembling process has many advantages in conventional stiffened panel manufacturing such as reduction of material cost and production of individual elements with lower imperfection tolerances. In this thesis with the intent of delivering significant key findings, buckling-and post-buckling behaviour of stiffened panels are investigated. Towards this aim, various headings in the field of stiffened panel performance under compressive loadings are studied. Main focus is directed to aircraft stiffened panels. Metallic fuselage and wing panels which comprise the significant components of aircrafts are the main research elements in this thesis. Studied panel configurations selected in such a way that would represent subcomponents of commercial aircrafts. This thesis links experimental and theoretical practices on metallic aircraft panels by laboratory tests and non-linear simulation techniques. Comparisons of the used techniques allowed undertaking some sensitivity and parametric studies on panels' static strength behaviour to deliver the key details. Outcomes of the present study have the potential to guide to build efficient advanced simulation models for compression loaded aircraft panels.

Key Words: Buckling, Post-buckling behaviour, Collapse, Thin-Walled stiffened panels, Stiffened panel tests, Finite element method

ÖZET

İnce Cidarlı Takviyeli Yapıların Nihai Yük Taşıma Kapasitesi

EKMEKYAPAR, Talha
Doktora Tezi, İnş Müh. Bölümü
Tez Yöneticisi: Prof. Dr Mustafa ÖZAKÇA
Yardımcı Tez Yöneticisi: Yrd. Doç. Dr. Nildem TAYŞİ
June 2013, 189 sayfa

Yüksek basınç yükleri altında hizmet görecek tasarımlar oluşturmak için, plak elemanları özel tasarlanmış takviyeler ile güçlendirilirler. Bir plak yapısının takviyelendirilmesindeki fayda belirli parçalar bölünmüş ve takviyelerin basınç ve eğilme performanslarını kullanan daha etkili parçalar oluşturmaktır. Yapı karakteristikleri, beklenen yükleme tipi, kullanılan malzeme, beklenen performans ve üretim teknikleri takviye elemanlarının tasarımında ve şeklinde etkili olan örnek parametrelerdir. Genellikle takviyeli paneller ayrı takviye elemanlarının ince plakların üzerine vidalanması veya kaynaklaması ile oluşturulur. Bu şekildeki birleştirme işlemlerinin geleneksel takviyeli panel üretiminde malzeme tüketimini azaltmak ve daha düşük toleranslarda bağımsız elemanlar üretme gibi bir çok avantajı vardır. Bu tez çalışmasında önemli bulguları sunmak amacıyla takviyeli panellerin burkulma ve burkulma sonrası davranışları incelenmiştir. Bu amaçla basınç yüklerine maruz kalan takviyeli panellerin performansı alanında bir çok başlık çalışılmıştır. Temel olarak uçak panelleri üzerinde odaklanılmıştır. Böylece uçakların önemli parçalarını oluşturan göve ve kanat panelleri çalışmanın temel elemanlarını oluşturmaktadır. Çalışılan panel konfigürasyonları uçakların bileşenlerini temsil edecek şekilde seçilmiştir. Laboratuvar testleri ve lineer olmayan simülasyonlar yardımı ile bu tez çalışması deneysel ve teorik pratikleri birleştirmektedir. Tekniklerin karşılaştırılması bazı parametrik ve hassasiyet çalışmalarının yapılabilmesine olanak sağlamıştır. Bu çalışmanın sonuçları basınç yüklemelerine maruz kalan uçak panelleri için etkili ileri düzey simulasyon modelleri kurulmasında öncülük edecek niteliğe sahiptir.

Anahtar Kelimeler: Burkulma, Burkulma sonrası davranış, Çökme, İnce cidarlı takviyeli paneller, Takviyeli panel testleri, Sonlu elemanlar metodu

ACKNOWLEDGMENTS

I would like to express my sincere thanks to my supervisor, Prof. Dr. Mustafa ÖZAKÇA, for giving his time, support, guidance, advice and generous supervision. His active interest in my work and the discussions with him created and inspired a great working environment. My thanks also go to my co–supervisor, Assist. Prof. Dr. Nildem TAYŞİ and Assist. Prof. Dr. M. Tolga GÖĞÜŞ for their helpful discussions.

Herein also I would like to acknowledge the financial assistance of the Scientific and Technical Council of Turkey (TÜBİTAK) which allowed me to pay a scientific visit to Queen's University Belfast Department of Mechanical and Aerospace Engineering. Advanced laboratory facilities at Queen's University Belfast and testing programs on aircraft panels helped this thesis to combine experimental and theoretical techniques. Moreover, Dr. Adrian MURPHY at Queen's University who supervised me during the six month research period and provided extensive opportunities has great contributions to undertaken investigations in this thesis.

I would like to express my appreciation to Prof. Dr. A. Kamil TANRIKULU for his great interest during the preparation of this work.

My wife and son also deserve many thanks for their patience and encouragements.

TABLE OF CONTENTS

LIST OF FIGURES

page

LIST OF TABLES

page

LIST OF SYMBOLS

Scalars

a	Plate length
A	Cross-sectional area
b	Width of plate
b_e	Effective width of plate
c	Distance from centroid to extreme fiber
C_w	Cross section warping constant
e	Loading eccentricity
E	Elastic modulus of material
E_r	Reduced modulus
E_s	Secant modulus
E_t	Tangent modulus
g	Parameter in Gerard's crippling strength formula
G	Shear modulus
I	Moment of inertia of section about buckling axis
J	St. Venant torsion constant
k_c	Plate buckling coefficient
K	Effective length factor
L	Length of member
P	Axial load
P_{cr}	Critical buckling load
P_E	Eluler buckling load
P_{Ex}	Critical buckling load about x axis
P_{Ey}	Critical buckling load about y axis
P_r	Reduced modulus load
P_t	Tangent modulus load, Torsional buckling load
r	Radius of gyration

r_0	Polar radius of gyration
t	Thickness of plate
x_0	x coordinate of shear centre
y_0	y coordinate of shear centre

Vectors

f^{ext}	External load vector
f^{int}	Internal load vector
r	Residual load vector
u	Displacement vector
Δu	Incremental displacement vector
δu	Iterative displacement vector

Matrices

K_T	Tangent stiffness matrix
K	Elastic stiffness matrix
K_σ	Geometric stiffness matrix

Greek Symbols:

ε_{tol}	Convergence tolerance
ν_e	Poisson's ratio in elastic range
ν_p	Poisson's ratio in fully plastic range
σ_E	Euler buckling stress
σ_c	Compression strength
σ_{cr}	Critical buckling stress
σ_{c-s}	Crippling strength
σ_e	Plate edge stress
σ_y	Yield strength
Δl	Arc-length
η	Plasticity reduction factor
λ	Eigenvalue, Section slenderness
ν	Poisson's ratio in transition range
σ	Normal stress

φ	Eigenvector
ψ	Scaling parameter in Arc-length method

CHAPTER 1

INTRODUCTION

1.1 General Introduction

Thin-walled structures are employed as structural components in many engineering disciplines including civil, aeronautical, mechanical and naval engineering. These types of structures are assembled utilizing thin plates. High strength-weight ratio, significant stiffness and availability of various materials make these types of plated structures favourable in engineering applications. The need and the growth in use of lightweight strong structures also support the progress. Aircrafts, rockets, tanks, submarines, vessels are a few examples of thin-walled structures which are made by joining thin plate elements. High strength, stiffness and straining properties of metals and metallic alloys lead those types of materials to govern the construction of thin-walled structures. But today, new materials such as composites are candidates to be employed in construction process of plated structures. Although composites have different advantages in structural applications, the complexity in nature of mechanical properties and the diversity of manufacturing techniques do not allow these types of materials to be fully adapted in common engineering designs. So, the metallic materials with various types and properties are still good choices and convenient in designs of thin-walled structures.

The high strength-weight ratio of plated assemblies originates from the in-plane load carrying capacity of such members. But buckling phenomena limits the structural response of those thin plated structures when compressive related forces or stresses arise. Since buckling of thin-walled elements generally takes place prior to

achievement of material strength, analysis and design process of compressive loaded thin plated elements entirely focus on buckling behaviour. Compressive forces first initiates local buckling in thin plate elements but the plates do not fail to sustain further magnitudes of compressive action thanks to significant post-buckling reserves'. This reserve of plate elements are exploited during design processes. Generally the collapse of plate occurs far beyond the local buckling when a combined material and geometric failure develops. Due to nonlinear characteristics arise beyond the local buckling; linearized approaches fall short to capture the response in this region. In order to predict the behaviour of plates in post-buckling regions it is compulsory to consult some advanced analytical, empirical, numerical or experimental techniques.

1.2 Objectives of the Thesis

Buckling and ultimate strength of aircraft components have been widely investigated over the decades by using different approaches in the field. Many researchers developed closed form solutions using plate and shell theories to formulate the non-linear behaviour of stiffened panels subjected to compressive forces. Besides the complexity of geometrical configurations, the adoption of non-conventional materials in construction of stiffened panels led to more challenging engineering practices in terms of analytical derivations. Also adversity to represent imperfections developed in manufacturing, storage and transport processes makes it very difficult to deploy the analytical methods to evaluate performance of stiffened panels. In order to generate knowledge for the complicated post-buckling mechanics of stiffened panels experimental testing programs accompanied research projects as a main tool for many years to focus on post-buckling behaviour of stiffened panels. Contribution of material properties, geometric imperfections, different cross sectional shapes and production defects to panel performance can be assessed precisely by means of experimental works. Although experimental programs have many advantages in terms of detailing with structural behaviours, they give rise to significant concerns for research. First, comprehensive experimental programs bring about significant investigation costs including calibrated testing machines and manufacturing of test specimens. Also fully engineered monitoring devices are needed to accurately capture the developed mechanics of test specimens. A further concern in experimental programs is time, since the extensive amount of specimen testing requires a strict agenda. Another complication with the experimental programs is the obligation to test representative components of investigated big structures. Laboratory conditions and huge amount of costs generally do not allow the works to be directed to full scale tests.

Aforementioned challenges compelled researchers in the field to generate some basic approaches for specific applications. Some charts and empirical formulations were developed to deal with focused designs. Unfortunately these charts and formulations have some limited characteristics such as applicability for specific materials or geometrical configurations. The advent of digital computers in 1960s and advances in numerical techniques offered different solutions to buckling problems. Following decades with the progress in computational mechanics and associated development in numerical plate and shell equations made it possible to deal with complicated nature of stiffened panels. Furthermore, as the computers gained power during the time, non-linear problems which entail tremendous amounts of equations to solve became reasonable to deal with. Today advanced virtual testing methods offer high fidelity engineering solutions for behaviour of stiffened panels. The methods have not only the ability to account for non-linear geometric and material characteristics; they allow the designers to investigate the various loading and boundary conditions with very low research costs as well. Using these computational techniques, works in the literature shed some light on modelling buckling, post-buckling and collapse behaviours of stiffened panels. Nevertheless, the demand for more efficient structural components that reduce life cycle costs and provide better performance leads researches to look for further advancements in analysis and design techniques. Complicated failure mechanisms of stiffened panels and interaction of different stability modes in buckling and post-buckling regimes entail very challenging investigations to be undertaken.

In this thesis with the intent of delivering significant key findings, buckling-and post-buckling behaviour of stiffened panels are investigated. Towards this aim, various headings in the field of stiffened panel performance under compressive loadings are studied. Main focus is directed to aircraft stiffened panels. Metallic fuselage and wing panels which comprise the significant components of aircrafts are the main research elements in this thesis. Panel configurations selected in such a way that would represent subcomponents of commercial aircrafts. Both single and multi-stiffened panels are considered through the study. The research is extended to account for the behaviours of both built up and integrally stiffened panels. To provide with the comprehensive knowledge and open the way of innovative designs, one aim of this thesis is to generate virtual testing models with high level of confidence for compression loaded aircraft stiffened panels. To this end, advanced finite element (FE) methods are employed to undertake key challenges of stiffened panel physical behaviours. Developing a robust virtual representation model introduces significant difficulties in terms of achieving accurate responses. Discrepancy between the computationally evaluated load and collapse load of a real field component can be large. Also failure mechanism of an actual structure which triggers the developing mechanics in segments is of importance and has to be predicted accurately. Therefore, verification of virtual testing models is significant for subsequent designs. To circumvent this phenomenon and certify further simulations, in each heading computational models accompanied with experimental test results. All panel experimental test results are provided using the laboratory facilities of Queen's University Belfast, Department of Mechanical and Aerospace Engineering. Some of them are from the published test results of the research group at Belfast directed to different research goals. But the majority of the test results are belong to the outcomes of collaborative research between the author and the research group at Queen's University Belfast.

1.3 Layout of Thesis

Apart from intending to generate robust computational simulation models for buckling and post-buckling behaviours of aircraft panels, this thesis aims several further attributes which are introduced in following paragraphs. The thesis organized as follows;

Chapter 2 expands the literature about stiffened panels. A detailed summary of works done by numerous researchers on buckling and collapse behaviours of stiffened panels are summarized in this chapter. Important references which created the bases of the present thesis are underlined. Extensive amount of works which deliver case studies, experimental tests and numerical simulation models are presented.

Buckling theory is treated in Chapter 2 in conjunction with detailed literature. After a general buckling theory and classifications, several column and plate buckling theories are presented. The derivation of column buckling and plate buckling equations are detailed. Also the theoretical approaches developed for the prediction of stiffened panel buckling are shown in this chapter. Moreover, the empirical approaches which are proposed by different researchers for the prediction of collapse load of stiffened panels are referred. Besides, numerical solution methods, used in non-linear static buckling and collapse simulations of stiffened panels are introduced in this chapter. The advantages and shortcomings of methods with respect to simulation purposes are explained.

Aiming at tracing the best representative virtual test model, in Chapter 3 three built-up lap jointed fuselage panels are modelled with different FE techniques. These panels differ from each other in geometrical configurations. Scales of configurations covers a wide range of stiffened panels which can be testable using laboratory facilities. One panel with single stringer, other single bay with three stringers and a large panel with five stringers and three longitudinal bays are considered for this purpose. Since the panels are manufactured using FSW, measured residual effects of welding are introduced into each simulation to create representative virtual test models as possible. Local buckling, post-buckling, collapse behaviours and failure mechanisms of developed different FE models are compared with test responses of specimens. Conclusions of the chapter deliver crucial knowledge on modelling of lap jointed fuselage stiffened panels.

In Chapter 4 main attention is focused on weld joint integrity of stiffened fuselage panels. Results of the five tests on single stringer panels were used to assess the joint failure during compression loading. A criterion is proposed for the assessment process based on Equivalent Plastic Strains (EPS).

In Chapter 5 to specify contributions of welding residual effects on panel static-strength behaviour FE modelling combined with statistical approaches. Width of effective weld joint, location of the effective weld joint centre, effective strength of heat affected zone (HAZ) material, width of the HAZ and magnitude of tensile residual stress are the investigated key parameters. The large multi-bay panel with five stringers studied in Chapter 3 is considered for this purpose. Effects of parameters on local buckling and collapse behaviour of panel are presented utilizing some statistical methods.

Chapter 6 concludes the thesis with summary of key findings revealed from investigations. Experienced modelling techniques to perform high fidelity virtual tests are summarised in this chapter. The characteristics of fuselage and wing panel static strength behaviours and failure mechanisms are introduced to generate expanded knowledge on modelling and testing techniques. The conclusions presented in this chapter have the potential to be deployed to field and will lead to an improved understanding of the mechanics involved in aircraft stiffened panels.

CHAPTER 2

LITERATURE SURVEY AND THEORY

2.1 Column Buckling

2.1.1 Flexural Buckling

The basic buckling equation dates back to works of Leonhard Euler (1707-1783) who investigated mathematical derivations of columns under compression lading [1]. The studies of Euler comprise isolated columns which are centrally loaded, prismatic, initially straight and simply supported. Equation 2.1 indicates the Euler's critical column buckling load corresponding to a single half wave mode.

$$P_E = \frac{\pi^2 EI}{L^2} \tag{2.1}$$

where E is the elastic modulus of material, I is the moment of the inertia of the cross section perpendicular to buckling and L is length of the simple supported column. The further mathematical equations for the end conditions other than pins were also developed. Hence, the equation accounting for possible boundary conditions takes the general form with effective length factor, K;

$$P_E = \frac{\pi^2 EI}{(KL)^2} \tag{2.2}$$

Effects of out of straightness, loading eccentricity are first realized and presented by Young [2]. It further took several decades to include geometrically non-linear large deflection effects on the column stability behaviour. Doing so, Kirchhoff [3] presented the mathematical derivations for the elastica problem. von Kármán [4] was the first to approach eccentrically loaded column behaviour as a buckling problem and his study underlined the strength reductions of columns due to eccentric loadings. In following years, Westergaard and Osgood [5] presented the analytical solutions for the eccentrically loaded columns. Also in that study the derivations were performed for columns which have initial out of straightness as well. Although there exist many investigations on eccentrically loaded columns, literature cites Young's calculations [2] as the basis for today's governing approach. His study inspired the derivation of equation called secant formula by Sheffler [6] in following decades. Equation 2.3 provides the secant formula for the evaluation of eccentrically loaded columns.

$$\sigma = \frac{P}{A}\left(1 + \frac{ec}{r^2}\sec\frac{L}{2r}\sqrt{\frac{P}{EA}}\right) \tag{2.3}$$

where e is the loading eccentricity, r is the radius of gyration of the section, c denotes the distance from centrodial axis to extreme fibers, P refers the applied loading and A is the cross sectional area. Development of the material yield is the failure criteria of the secant formulation. Thus, column capacity F_c is evaluated as the level of loading that produce the yield stress $\sigma = \sigma_y$.

Consideration of inelastic material effects on buckling behaviour of columns requires a different account to be cited. By the progresses in testing facilities it was realized that for some slenderness ratios test results violates the Euler's buckling load. The reason for such a violation was the development of non-linear material behaviour during the compression loading before column configurations achieve Euler's buckling load. Considère [7] was the first to explain this phenomenon by performing 32 experimental tests in 1889. And he suggested that if the buckling attained above the proportional limit of the material the elastic modulus should be replaced in the Euler formula by an effective modulus. According to his theory the effective modulus should has a value between elastic modulus and tangent modulus. With an independent work in 1889, Engesser [8] proposed replacement of elastic modulus with tangent modulus for the columns in which Euler buckling stress exceeds material yield strength. But in 1895, Engesser [9] proposed another approach which reverses his previous tangent modulus theory. A weighted average approach was his new suggestion which is called reduced modulus or double modulus theory.

Conducted experiments by von Kármán [10] on mild steel rectangular columns supported the proposal of reduced modulus theory. Investigation of support conditions and loading eccentricities were also other concerns of his experiments. Shanley's work [11] which created an improved understanding of inelastic buckling, verified and refined the Engesser' tangent modulus theory. Performing some experimental tests on aluminium alloy columns, he showed that inelastic buckling behaviour of columns can be closely approached by tangent modulus theory provided the out of straightness of columns are extremely small. Also he presented that evaluated loads by using reduced modulus theory are different from those evaluated by using tangent modulus theory. He attributed these discrepancies to the different stress strain curve characteristics of steel and aluminium. Today Shanley's theory provides the basis for several specifications used in inelastic column buckling design. Although tangent modulus approach accounts for nonlinear behaviour of columns, assumption of initially perfect column, which is not the case in real life columns, is a shortcoming of the theory. A work presented by Hoff [12] provides significant review on the development and modification period of column buckling equations between Euler and Shanley. Detailed derivations for reduced modulus and tangent modulus theories are presented by Bleich [13]. Equations 2.4 and 2.5 present the tangent modulus and reduced modulus approaches respectively.

$$P_t = \frac{\pi^2 E_t I}{(KL)^2} \tag{2.4}$$

$$P_r = \frac{\pi^2 E_r I}{(KL)^2} \tag{2.5}$$

2.1.2 Torsional and Flexural-Torsional Buckling

The building block researches of column buckling which have been presented so far are related to doubly symmetric hot rolled or built-up heavy cross sections in which Euler flexural buckling mode is dominant. However, centrally loaded columns have the potential to exhibit torsional buckling modes, in case of singly symmetric or asymmetric cross sections [14]. The columns which have closed sections generally do not exhibit torsional related buckling modes. The reason for such a behaviour is that the large torsional rigidity of closed sections [15]. However, the deployment of thin-walled open sections into field as load carrying columns led to researches to account for torsional buckling problems. Furthermore, use of singly symmetric sections in structural applications is an additional trigger of torsional buckling behaviour. Because in single symmetric forms shear centres are eccentric from cross sectional centroids and for such a column axially loaded along its centroidal axis, the eccentricity of the load from the shear centre may cause buckling in the torsional or flexural-torsional modes [16]. The torsional buckling and flexural torsional buckling of columns was first realised in 1920s, when metal airplanes were assembled across the world. Use of open section columns in forms of channels, zees or angles then spread out in aircraft construction due to ease of connections and convenient inspections [17]. In 1929, Wagner was the first to deliver a theory for torsional buckling behaviour. Pugsley's work [18] was another step which contributed to the progress of torsional buckling theory for columns. Timoshenko [19] derived the torsional buckling equations for an arbitrary thin-walled open section. Further developed cold-formed steel industry during 1940s, in which thin-walled open sections are employed, adopted and significantly improved the torsional buckling experience of aircraft industry. Since Cornell University has a leading position on the evolution process of cold-formed steel, extensive key researches on the torsional buckling behaviour of thin-walled open sections were conducted in Cornell. The works presented by Goodier [20], Fang [21], Chajes and Winter [22], Chajes et al. [23] and Peköz and Winter [24] are the earlier studies which guide today's torsional and flexural-torsional buckling design. Figure 2.1 depicts flexural-torsional buckling mode of an arbitrary open section column with angle of rotation, ϕ. x and y coordinates of shear centre are represented by x_0 and y_0 respectively.

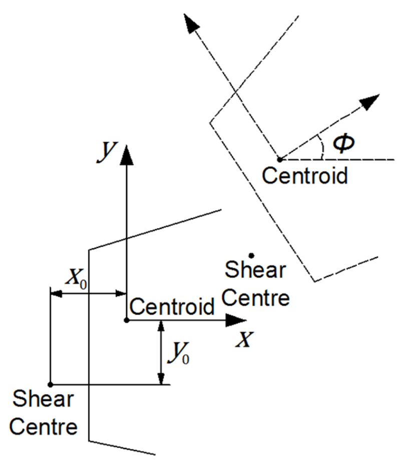

Figure 2.1 Flexural-torsional buckling of an arbitrary open section

Governing equation of the concept can be summarized as follows;

$$r_0^2(P_{cr}-P_{Ex})(P_{cr}-P_{Ey})(P_{cr}-P_t) \\ -(P_{cr})^2(y_0)^2(P_{cr}-P_{Ex})-(P_{cr})^2(x_0)^2(P_{cr}-P_{Ey})=0 \qquad (2.6)$$

in which r_0 is cross section polar radius of gyration, P_{Ex} and P_{Ey} represent Euler buckling loads about x and y axes respectively and P_t is the torsional buckling load of the column;

$$P_t=\left[\frac{\pi^2 E C_w}{(K_t L_t)^2}+GJ\right]\left(\frac{1}{r_0^2}\right) \qquad (2.7)$$

where C_w is cross section warping constant, G refers shear modulus and J represents St. Venant torsion constant. The governing buckling mode of column is determined by evaluating the smallest value of three roots of P_{cr} in Equation 26.

2.1.3 Effects of Manufacturing Residuals on Columns

The preceding works generated theoretical knowledge and background for the evaluation processes of column buckling behaviour. But there were significant further parameters that need to be investigated to fully characterise columns' buckling nature, such as effects of manufacturing residuals, assembling process and stress strain characteristics of different materials. In last century significant amount of researches whether experimental or theoretical, were devoted for this purpose.

Non-uniform cooling after rolling of structural metallic shapes gives rise to residual stresses. Moreover, employment of welding to assemble built-up sections introduces significant amount of residual stresses on metallic shapes along welding direction. Since the column carrying capacity is a key parameter to produce safe designs, effects of these residual stresses have to be addressed. Beedle and Tall [25] characterized the key effects on magnitude and distribution of residual stresses as type of cross section, rolling temperature, cooling conditions, straightening procedures and the material properties. Investigating the effects of residual stresses on columns, a valuable contribution was made by Batterman and Johnston. [26]. Different steel grades, maximum compressive residual stresses, out of straightness and slenderness ratios were the investigated parameters. Drawbacks of the work generated crucial knowledge for the impact of residual stresses on columns' buckling behaviour. The study conducted by Alpsten and Tall [27] detailed the distribution of residual stresses through the thickness of heavy welded shapes. Performing extensive amount of experimental tests on built-up steel sections, they investigated a wide range of column sections. Residual stress distributions on built-up steel cross sections were mapped as stress contours to refer discrepancy of stress distribution through thickness and across the width of members. Brozzetti et al. [28] concluded that the sequence of welding and the number of welding passes are the critical factors that significantly influence the distribution of residual stresses. Also in built-up column manufacturing, the method itself to produce individual plate elements leads to unique residual stress patterns. Bjorhovde [29] investigated built-up column behaviours which are assembled from universal milled and flame cut (oxygen cut) plates. Presented curves for columns, produced employing these methods, illustrate performance of each method against stress free correspondents.

2.1.4 Design Specifications

Variety of applications in field compelled engineers to develop practical guides to undertake complicated designs. Moreover, the evaluation process of structural elements must be standardized to develop certified engineering products. The adaptation of standardized metallic materials and cross sections around the world also required to provide systematic examination techniques. Thus, over the decades, a great many specifications have been generated by the help of research communities. The theoretical knowledge in literature, developed by aforementioned investigations and many others which are not presented in this work was the first consulted resource. Subsequent investigations of laboratory measurements in conjunction with computational simulations were performed to expand the statistical databases and create robust prediction methods. There are several specifications which are accepted by engineering communities as deployable methods to predict axial load capacity of centrally loaded metallic columns. The theoretical and application background of specifications differs mainly due to different experiences. Beedle's work [30] provides the answer of "why specifications are different?" question in detail. The basic theories of each specification never change. However, assumptions in idealizations of structural details are constantly being developed by novel proposals.

Structural Stability Research Council (SSRC), formerly Column Research Council (CRC), has significant contribution to provide improved column curves to be used for design purposes. The council was founded in 1944. The outcomes of the study conducted by Bjorhovde [29] constitute main frame of SSRC column curves. Covering the full practical range of shapes, steel grades and manufacturing methods he developed an extensive database of column strength [14]. Using the database he depicted 112 column curves which need to be narrowed down to be deployable for practical applications in field. The curves account for effects of residual stresses induced by manufacturing methods and initial out of straightness (initial geometrical imperfections). Examining the curves, Bjorhovde observed that the wide spreading band of column curves can be represented by subdividing the band into groups of curves with an average curve for each group. Considering material properties, cross sectional shapes and manufacturing methods he divided the wide range into three groups and represented the regions by corresponding three curves. Today these curves are known as SSRC column strength curves 1, 2 and 3. These column curves accounts for L/1000 initial geometrical imperfection as a form of sinusoidal shape. In same work Bjorhovde [29] also carried out a field study which includes systematic measurements of geometrical imperfections of manufactured columns. As a result of statistical methods, he found that the mean value of geometrical imperfections was equal to L/1470. Accordingly, he presented another three curves which consider L/1470 maximum geometrical imperfections. These curves are named as SSCR 1P, 2P and 3P curves. American Institute of Steel Construction (AISC) specification [31], adopts the SSRC 2P curve for buckling design of steel columns. The curve is known as American single buckling curve. Figure 2.2 delineates SSRC column curves in a comparison form and adapted from the Bjorhovde [29]. λ denotes column slenderness and in vertical axis column capacity is shown in a non-dimensional form.

European Convention of Constructional Steelworks (ECCS) was founded in 1952 and proposes different column strength curves compared to SSCR approach. The discrepancy between European and SSRC curves originates from the used material types and shape sizes commonly used in two regions. High strength steels and heavy

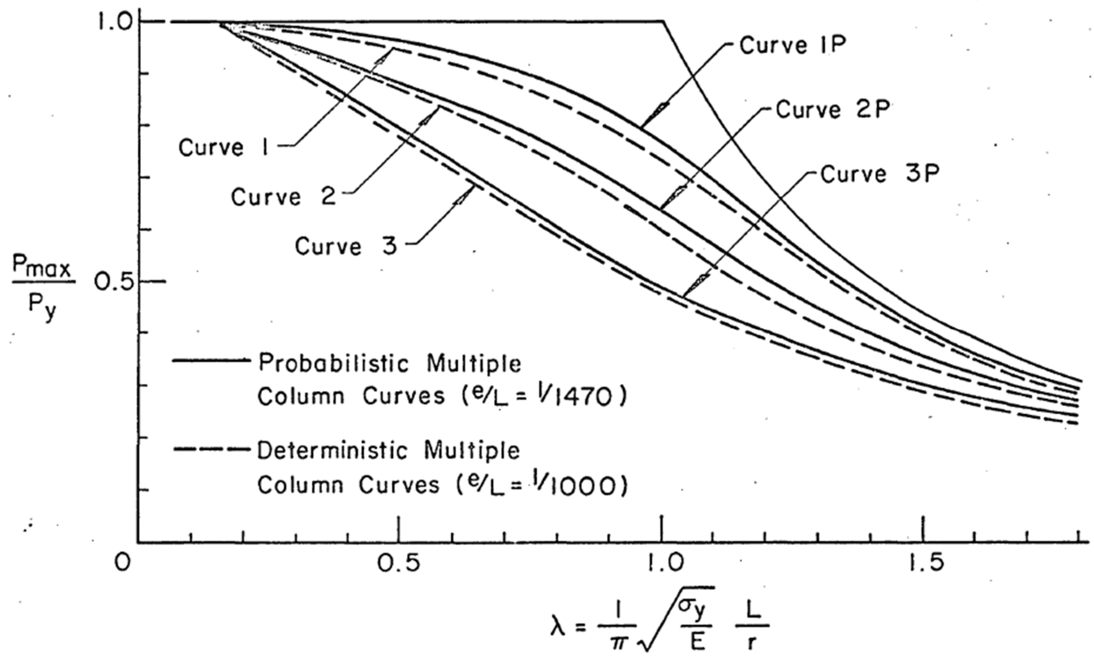

Figure 2.2 SSRC Column curves (from [29])

shapes which are available in construction practices of USA generally do not employed in European construction works [32]. The study conducted by Beer and Schultz [33] has great contribution to development of ECCS column curves. The number of curves originally proposed was three (curves, a, b, c). The curves a^0 and d were further developed for possible future use. Bjorhovde and Tall [32] depicted that a good correlation between SSRC and ECCS is present in case all five European curves are taken into account. Now ECCS suggests the use of total five curves for the prediction of ultimate load carrying capacity of steel columns. The Eurocode 3 [34] which governs the design of steel structures in European countries adopts the ECCS five column curves. The background of ECCS column curves relies on 1000 column tests [35]. To collect representative columns, specimens were taken from various steelwork fabricators which were serving in several European countries [36]. Besides the experimental database, there is a theoretical knowledge behind the buckling equations adopted in Eurocode-3 which is called as Perry-Robertson formula. Perry-Robertson approach of column strength assumes a failure occurs when the stress induced by compression and second order bending achieves yield strength at extreme fibers of cross section. The manual of ECCS describes the development history of five buckling curves in detail [37]. Figure 2.3 presents ECCS column curves. In order to provide compatibility with the curves of SSRC Figure 2.3 adapts Bjorhovde's [29] presentation.

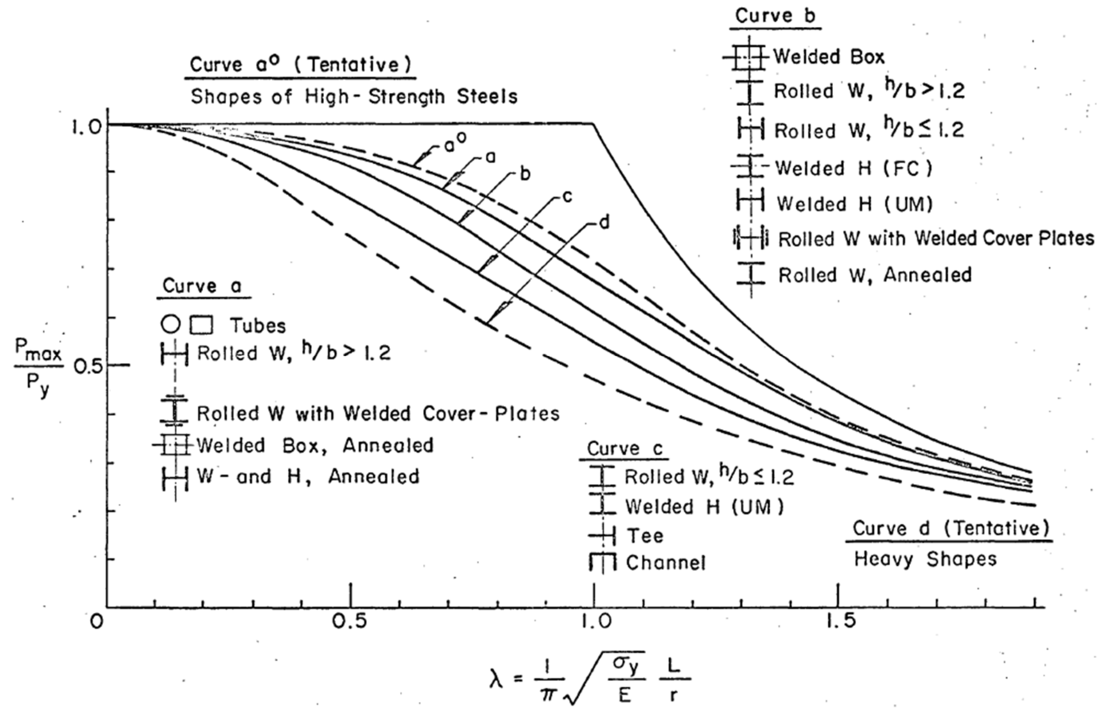

Figure 2.3 ECCS Column curves (from [29])

Due to some physical and economical characteristics of aluminium and its alloys the utilization of aluminium in construction works is not as much as carbon steel. Therefore the literature on aluminium columns is not wide compared to literature on columns made from other structural materials. However, the advantages of aluminium alloy materials in some particular applications and the capabilities of alloys in undertaking extreme environmental conditions extended the research. In design practices of aluminium alloy columns the column capacity prediction approaches have been generally based on the tangent modulus theory, since there exist good agreement with test results [14]. As a consequence of possessing different stress-strain curve characteristics, the proposed analysis and design methods for columns made from aluminium remarkably differ from those for steel columns. Carbon steels exhibit a linear elastic characteristic up to a definite yield point, and then a flat yield plateau follows the material failure. Experiencing some straining within this flat region a strain hardening portion completes material behaviour up to ultimate strength. This kind of material behaviour of carbon steels are represented closely by bilinear material curves in design processes. Unlike the carbon steels, aluminium based materials have nonlinear, or rounded, stress-strain curves which do not disclose sharply defined yield points [13, 14, 38-41]. A general approach in literature in representing this kind of nonlinear stress-strain curves is to use an expression originally proposed by Ramberg and Osgood [42]. Today various approaches are available to predict aluminium column flexural buckling behaviour. Besides codified approaches, soft computing techniques today are used for such initial design procedures. A study conducted by Çevik et al. [43] who used available test data in literature proposed a well correlated formulation for flexural buckling prediction of aluminium alloy columns.

The realization of such a nonlinear material response and lack of test data served as starting point of research into aluminium columns. Investigations conducted during 1960s and 1970s are the leading researches on buckling behaviour of aluminium columns. Employing the tangent modulus theory Johnston [44] investigated the buckling behaviour of initially straight aluminium columns. In a following study, again basing the research on tangent modulus theory and detailing the inelastic buckling gradient, Johnston [45] investigated the buckling behaviour of an aluminium tee section. In the study conducted by Batterman and Johnston [26] the parameters that affect the buckling behaviour of steel and aluminium columns were systematically determined by means of mathematical models. And it was shown that for idealized straight columns of either aluminium alloy or steel, the maximum inelastic post-buckling strength was only a few per cent above the tangent modulus load. The study has also a valuable contribution to improved understanding of effects of initial imperfections on steel and aluminium columns. Plots of load deflection curves for columns with different magnitudes of imperfections provide a significant reference to be cited. Also another work presented by Johnston [46] introduces the mathematical modelling details of Shanley's tangent modulus theory on aluminium alloy columns. Undertaking some experiments and mathematical modelling on tee shaped aluminium columns, Hariri [47] concluded that effect of eccentric loading is more detrimental than the effect of same magnitude geometrical imperfections. Welding causes material degradations within the weld region and introduces residual stresses, thus reduces buckling capacity of metal sections. Transverse welds are generally employed in connection designs, whereas longitudinal welds are utilized in built-up member manufacturing [48]. In a research paper Brungraber and Clark [49] presented the strength results of longitudinal and transverse welded aluminium columns. Lai and Nethercot [50] stated that capacity reduction of welded aluminium columns depend up on the direction, location and number of welds.

As is the basis for column buckling curves, the design specification of U.S., AA 2005 [51], uses Euler column strength in elastic design portion. The inelastic portion of the column curve is based on tangent modulus theory with an associated approximate straight line. There exists single column capacity formulation in AA 2005 specification. Artificially aging process characterise the coefficients in the column formulation. The AA 2005 specification provides equations for determining the buckling coefficients. Also the corresponding magnitudes of coefficients for widely used aluminium alloys in design practices are presented in a tabulated form in specification. The buckling formulation in AA 2005 specification implies the use of simpler equations compared to equations used in steel specification. The basic column strength equation of AA which is based on tangent modulus theory can be summarized as follows;

$$\sigma_c = B_c - D_c\lambda \ \ in\ case\ \lambda < C_c \tag{2.8}$$

where $\lambda = KL/r$ and the coefficients for artificially aged tempers;

$$B_c = \sigma_y\left[1 + \sqrt{(\sigma_y/2250)}\right] \tag{2.9}$$

$$D_c = (B_c/10)\sqrt{(B_c/E)} \tag{2.10}$$

$$C_c = \frac{0.41B_c}{D_c} \tag{2.11}$$

Coefficients take the following form for other tempers;

$$B_c = \sigma_y\left[1 + \sqrt{(\sigma_y/1000)}\right] \tag{2.12}$$

$$D_c = (B_c/20)\sqrt{(6B_c/E)} \tag{2.13}$$

$$C_c = \frac{0.67B_c}{D_c} \tag{2.14}$$

1960s and 1970s are also important in terms of standardization of aluminium column evaluation techniques in Europe. The lack of test data and different strength characteristics of aluminium compared to steel compelled ECCS to support some researches on I shaped and circular hollow section columns. The studies conducted by Arnault [52], Bernard et al. [53], Djalay and Sfintesco [54] and Kloppel and Barsch [55] are the earlier works on aluminium columns under the support of ECCS. Works presented by Mazzolani and co-workers introduced extensive experiences into development of ECCS aluminium column buckling curves. Studies cover the investigations on extruded members, built-up members, residual stresses, initial imperfections and further parameters that lead serious difficulties in column design evaluations. In the reference Mazzolani [56] cites his foregoing works and explains the development process of ECCS aluminium column curves in detail. In the earlier versions of ECCS aluminium structures approach there were three column curves referred to as a, b and c curves. The natures of heat-treated and non-heat-treated alloys, closed or open and symmetric and asymmetric cross sections in buckling behaviour led to development of aforementioned three column curves. As with the ECCS steel specification, ECCS aluminium specification adopts the Perry-Robertson approach in the theoretical column capacity predictions [14]. Serious difficulties encountered in the evaluation processes caused by complicated classification of materials and cross sections gave rise to adaptation of two curves (a and b) instead of three (a, b and c). Therefore, in the final version of ECCS specifications a and b curves are utilized for design purposes and heat-treated or non-heat-treated

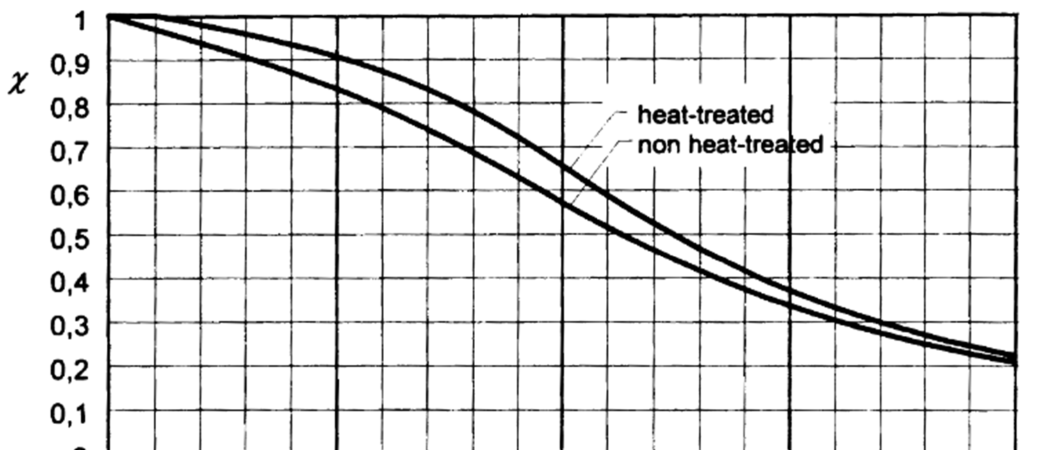

Figure 2.4 Eurocode-9 Aluminium column curves

characteristics of materials are the only parameters on deciding which curve to use. The asymmetry of the cross section is handled by introducing some factors into column capacity formulations. Eurocode-9 [57] which serves as design specification of aluminium structures in European countries is the recommended standard by ECCS. Figure 2.4 provides the aluminium column curves of Eurocode-9. χ represents the reduction factor for flexural buckling evaluations.

Foregoing literature introduces a comprehensive knowledge on the development process of the approaches on flexural buckling phenomenon of metallic columns. On the other hand there exist numerous investigations on column buckling behaviour which were not presented here. In this sense, the bibliography presented by Driver et al. [58] lists hundreds of researches on columns and provides a significant guide for those readers concerned about column buckling. Flexural and torsional buckling modes do not dominate all column stability failures. There exists another mode of stability for columns in case of very slender cross sections. Slender sections are manufactured using thin plate elements with relatively large width/thickness ratios. Consequently, compression action on these columns causes local buckling waves to take place. Since local buckling is plate related behaviour, capacity evaluations of such columns are performed using plate buckling approaches rather than using traditional column buckling equations. Towards this aim, it is necessary to investigate performance of constituent plate elements by considering width/thickness ratios. The inventory presented by Driver et al. [58] also lists local buckling studies on axially loaded columns. But the literature on plate buckling related behaviour is treated in the following section of this chapter.

Stringers used to build stiffened panels serve as columns in case they are used in upper wing or lower fuselage portions of aircrafts. Although the buckling phenomenon of columns never changes, the stringers attached on skins leads to relatively complicated instability behaviours compared to an independent column buckling response. Nevertheless, as is well known the performance of independent stringers directly and strongly influences the load carrying capability of entire panel assembly. The diversity of materials used in industry, complicated configuration of structural elements, the complexity nature of loadings and the sensitivity of the aircraft structure itself lead aerospace industry research to follow different approaches than civil engineering practices. As a result, experiences, laboratory tests and high fidelity engineering simulations generally replace conventional buckling equations. On the other hand to provide basic knowledge and permit initial sizing of stringers some guides are available in literature. The data sheets provided by Engineering Sciences Data Units (ESDU) are very important references in this manner. Citing fundamental works, these data sheets present some parametric analysis and design charts and formulations in conjunction with applied examples for particular applications. Data sheet no 01.01.01 [59] deals with strength of struts considering flexural buckling caused by concentric and eccentric loadings. Flexural and torsional-flexural buckling of thin-walled open section struts are presented in data sheet no 89007 [60]. Torsional buckling of angles which are point symmetric sections is detailed in a particular data sheet 01.01.10 [61]. Buckling of lipped and unlipped Z and channel sections are focused on data sheets 77030 [62] and 76023 [63]. Data sheet 01.01.08 [64] treats local instability of thin-walled sections with flat sides. Local buckling and associated crippling strength of I, Z and channel sections are introduced in data sheet 78020 [65].

2.2 Plate Buckling

2.2.1 Elastic Buckling of Plates

In 1891 Bryan [66] derived buckling equation of simply supported rectangular thin plate subjected to uniform compressive force. He used a sinusoidal type of deflection shape to derive the critical stress equation. Bryan's work was also the first to apply the energy criterion of stability to the solution of a buckling problem. Critical stress for an elastic plate is evaluated using plate width to thickness ratio, b/t;

$$\sigma_{cr} = k_c \frac{\pi^2 E}{12(1-{\nu_e}^2)}\left(\frac{t}{b}\right)^2 \tag{2.15}$$

where ν is Poisson's ratio and k_c is plate buckling coefficient which depends on plate boundary conditions and aspect ratio.

Energy method further employed in treatment of stability problems and solved serious difficulties encountered in the conventional mathematical derivations [13]. Equilibrium and energy approaches for plate buckling problems can be found in the reference by Ventsel and Krauthammer [67]. Employing energy approaches and solving plate differential equations Timoshenko [68] introduced the critical stress equations for rectangular plates with different loading and boundary conditions. Analytical solutions of the plate buckling coefficients for various types of boundary conditions are presented in this study. Hill [69] presented the chart of the buckling coefficients for practical applications. The chart depicted by Hill covers uniformly compressive loaded plates with simply supported or clamped loaded edges and different combinations of unloaded edge boundary conditions. This chart permits a detailed observation of boundary condition effects on buckling of rectangular plates. Figure 2.5 presents the buckling coefficient curves for elastic rectangular plates under various boundary conditions.

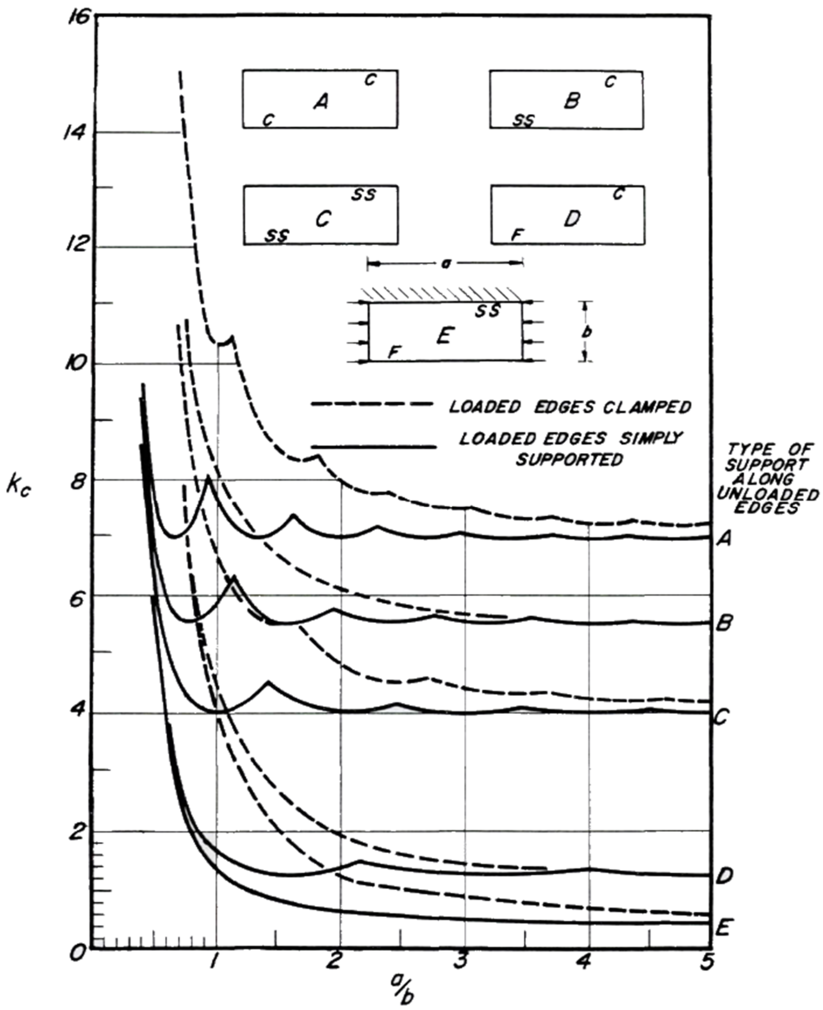

Figure 2.5 Plate buckling coefficients (from [70])

Studies conducted by Lundquist and Stowell improved understanding of the buckling behaviour of plates and plated elements. With a series of investigations they shed light on local buckling of slender sections composed of thin plate elements. Focusing on rectangular tube sections and deriving tabular data and guide charts Lundquist [71] investigated local instability of constituent plate elements. In a following work, considering channel and Z sections Lundquist [72] detailed local buckling evaluations for centrally loaded columns. In another study Stowell and Lundquist [73] presented detailed evaluations for local buckling of I, Z, channel and rectangular tube sections. In a subsequent investigation, examining junctions of conventional cross sections that composed of thin plate elements, Lundquist and Stowell [74] introduced mathematical equations and charts of local buckling coefficients. The study provides comprehensive knowledge on elastically restrained unloaded edge boundary conditions against rotation. The critical stress equations of outstanding flanges of thin-walled columns which are elastically restrained against rotation along one unloaded edge and free at the other unloaded edge were derived by Lundquist and Stowell [75]. It is worth noting that aforementioned works presented by Lundquist and Stowell were devoted to aeronautical technology.

2.2.2 Plastic Buckling of Plates

Before achieving elastic buckling stress material yielding may commence in plates under the compressive loading. Yielding of material may occur locally and/or may cover entire cross section according to geometrical configuration and boundary conditions. In this case it is necessary to account for plastic actions and refer inelastic buckling. Historically, there have been significant amount of attempts to rationally characterize inelastic buckling of plates. Studies on inelastic buckling behaviour of plates up to 1936 were summarized by Timoshenko [68]. Experimentally evaluated column response and behaviour of constituent plate elements of columns were employed to develop plasticity coefficients for plate buckling. However, it required further extensive theoretical and experimental research to develop representative plasticity coefficients for plate buckling problems. Through a series of investigations Bijlaard proposed plastic buckling theories for plates which are accepted as the first satisfactory works [70]. Among the incremental and deformation type theories he suggested deformation type approach, since it founds lower buckling loads compared to incremental approach. In a deformation type plasticity total strain components are evaluated considering current stress state and so presumed to be independent of loading history. Considering inelastic buckling of thin steel plates Bijlaard [76] published his theory first in 1938. By further studies [77] he extended the theory for different loading and boundary conditions and indicated the agreement of the theory with test results. In subsequent studies in conjunction with plate problems Bijlaard also applied his theory to shell buckling problems and obtained reliable results [78, 79]. In following studies [80, 81] examining bending, eccentric loading and associated non-homogenous stress distributions he provided important steps for different cases in inelastic plate buckling phenomenon.

Citing Bijlaard's theory, Ilyushin [82, 83] derived differential equation of flat plates to propose a novel approach based on strain reversal model. In order to satisfy equilibrium condition in plastic zone he adopted Hencky-Mises plasticity theory. The basic idea behind the Hencky-Mises theory is the fact that it presumes isotropy of the material in the plastic zone. But assumption of strain reversal model and associated unloading on the convex side, as the basic idea behind the reduced modulus theory, led to unsatisfactory results when compared with experimental behaviours [13]. The experiences and approaches presented by Bijlaard and Ilyushin created significant references for Stowell's investigations on inelastic buckling of flat plates. Instead of adopting a strain reversal model, improving Ilyushin's theory Stowell [84] used a non-strain reversal model like employed in Shanley's inelastic column approach. In a non-strain reversal model it is assumed that unloading during the early stages of buckling does not take place and buckling and increase in load progress simultaneously. Stowell's study particularly concerned with developing factors of η for different boundary conditions which must be multiplied by elastic critical buckling equation of the corresponding case to give the critical stress for the plastic case.

$$\sigma_{cr} = \eta k_c \frac{\pi^2 E}{12(1-{\nu_e}^2)}\left(\frac{t}{b}\right)^2 \tag{2.16}$$

He obtained values of η by dividing the critical stress of the plated structure in the plastic state by the critical stress evaluated on the assumption of perfect elastic behaviour. As is well known the material characteristics change when the structural elements are stressed beyond the proportional limit. Thus, promising basis of plasticity reduction factor η is the fact that a single factor accounts for the changes in elastic modulus E, Poisson's ratio v and plate buckling coefficient k in plastic state. The plasticity reduction factors for various boundary conditions can be found in data sheet no 83044 [85] provided by ESDU. In 1957 Gerard published a series of guides to address the issue of structural stability for airframes which is named as "Structural Stability Handbook". Part I [70] of the guide deals with buckling of flat plates and is very important reference for researchers who study in the field of plate buckling. The work presents a comprehensive review of plate buckling theories up to published year and provides detailed analysis tools to evaluate failure of plates. Effects of plasticity were incorporated by employing Ramberg-Osgood [42] stress-strain relations. Basic mathematical principles, boundary conditions, derivation of elastic buckling coefficients, a comprehensive treatment of plasticity reduction factors, effect of cladding were delineated in the guide, permitting a detailed understanding of elastic and plastic plate buckling. A compact form of plate buckling is also treated in ESDU data sheet 72019 [86] with practical formulations and basic charts covering all combinations of boundary conditions. Table 2.1 provides plasticity reduction factors for compression loaded rectangular plates in ESDU 8304 [85] format.

Table 2.1 Plasticity reduction factors

Plate configuration	Equation
Long flange, one long edge simply supported, other free	$\eta_1 = \dfrac{E_s(1-\nu_e^2)}{E(1-\nu^2)}$
Long flange, one long edge clamped, other free	$\eta_2 = \eta_1\left[0.33 + 0.335\left(1+3\dfrac{E_t}{E_s}\right)^{1/2}\right]$
Long plate, both long edges simply supported	$\eta_3 = \eta_1\left[0.5 + 0.25\left(1+3\dfrac{E_t}{E_s}\right)^{1/2}\right]$
Long plate, both long edges clamped	$\eta_4 = \eta_1\left[0.352 + 0.324\left(1+3\dfrac{E_t}{E_s}\right)^{1/2}\right]$
Short plate loaded as a column (length/width <<1)	$\eta_5 = \eta_1\left[0.25\left(1+3\dfrac{E_t}{E_s}\right)\right]$
Square plate loaded as a column	$\eta_6 = \eta_1\left[0.114 + 0.886\dfrac{E_t}{E_s}\right]$
Long column (length/width >>1)	$\eta_7 = \eta_1\dfrac{E_t}{E_s}$

E_s is secant modulus, ν_e refers elastic Poisson's ratio and ν represents Poisson's ratio of material in transition range between an elastic and a fully plastic behaviours. Following equation is used to describe the Poisson's ratio in this transition range;

$$\nu = \nu_p - (E_s/E)(\nu_p - \nu_e) \tag{2.17}$$

in which $\nu_p$is the Poisson's ratio in fully plastic range and equal to $1/2$ for isotropic materials [70].

2.2.3 Post-buckling Behaviour of Plates

The foregoing works focused on evaluation of local instabilities in elastic or plastic states and may serve as starting point in detailing stability theory of plates. Because plate structures have more complicated behaviours under the action of compressive loading. It has long been recognized that plates have the potential to sustain further magnitudes of loads up to collapse beyond the local buckling [13, 14, 17], Figure 2.6. The load carrying capability of plates beyond local buckling is referred as post-buckling reserve.

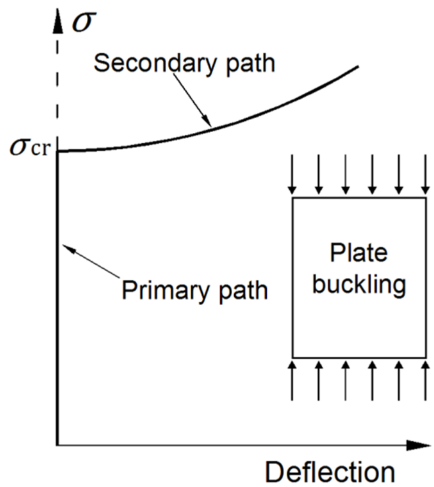

Figure 2.6 Plate post-buckling behaviour

Depending upon material properties, loading and boundary conditions and as well as geometrical configurations collapse load of a plate may widely differ from its local buckling load. This post-buckling reserve of plate structures offers structural efficiency and design versatility in satisfying extreme loading conditions and hence is fully facilitated in weight sensitive structures such as aircrafts. In this manner the credit is given to Koiter who realized and detailed the importance of post-buckling reserve of structures. Investigations of Koiter [87] revealed that stability in the post-buckling region may permit the design loads to be set higher than the critical buckling load of structure. He developed a systematic stability approach to delineate initial post-buckling behaviour of elastic systems. In order to find alternative equilibrium paths beyond the critical point he employed energy methods which alleviate inherent difficulty of pure analytical approaches as mentioned before. In an investigation on behaviour of plates beyond local buckling, Davidson [88] concluded that Koiter's equation is capable of describing the post-buckling range of plates. However, Koiter's approach was limited to initial post-buckling of elastic systems which exhibit bifurcation type of buckling and unfortunately was not the answer of a fully nonlinear behaviour beyond the critical buckling. His work also is important in terms of detailing effects of small imperfections on stability behaviour of structures.

In following decades Sewell [89], Thompson [90] and Supple [91] employed static perturbation methods to develop novel approaches in tracing the post-buckling paths. In order to capture post-buckling behaviour they used derivatives of energy functions and the developed approximate analytical methods, forming the basis of numerical evaluations [92]. For elastic-plastic behaviour Hill [93, 94] developed bifurcation theories which are still referred in post-buckling investigations. Improving Hill's theory, Hutchinson [95, 96] proposed asymptotic approach for post-buckling behaviour which provides detailed understanding of inelastic bifurcation. Referring the cited works above, post-buckling behaviour of structures has been subject of extensive theoretical and experimental researches for decades. However, herein no attempt is made to detail extensive literature on post-buckling theories. Although above investigations are not directly focused on plate behaviour, they are the building blocks of today's post-buckling assessments.

2.2.4 Ultimate Capacity of Plates

As has been detailed before, local buckling does not represent ultimate limit state, since plates have a stable post-buckling behaviour. In design practices the stable behaviour of plates beyond local buckling is fully exploited to develop more efficient thin-walled structures in civil, marine and aeronautical disciplines. For instance aircraft panels are designed in such a way that local buckling would be a small fraction of collapse load. In this manner evaluation of ultimate limit state of plates is very crucial to specify the level of functional loss. Exact solutions of ultimate load carrying capacity of plates address introduction of compatibility and equilibrium differential equations which may not be possible due to high level of complexity and nonlinearity.

In order to proceed in the field of plate ultimate capacity, the earlier investigations consulted experimental techniques which have the potential to explain plate collapse behaviour clearly. In this context undertaken study by Schulman and Back [97] is the earliest experimental work on ultimate strength of plates. Testing plates made from duralumin, stainless iron, Monel metal and nickel under compressive loading they indicated that ultimate strength of a plate can achieve as much as thirty times the critical buckling load evaluated using Bryan's equation. The study was devoted to explain capacities of thin sheets employed in aircraft construction and the materials adopted in tests were very attractive for aeronautical applications in thirties. Further needs and interest of aeronautical engineers on capacity of plates and plated sheets led extensive experimental and theoretical researches to be undertaken in following decades. Sweeney [98] performed compression tests on rectangular steel plates to evaluate ultimate strengths'. Examining ultimate strength of steel plates with free unloaded edges Montgomerie [99] carried out some tests. Lahde and Wagner [100] tested long plates to determine ultimate limit states. Frankland's [101] study which was devoted to ship plating also includes tests of steel plates. Focusing on transversely framed vessels Muckle [102] performed a series of experimental tests on plates with loaded edges clamped and unloaded edges free.

The most important development in that time was the proposal of a semi empirical method by von Kármán [103] to evaluate ultimate load carrying capacity of plates supported along unloaded longitudinal edges. The approach is called as effective width method which implies that only a certain width of plate resists further magnitudes of loading beyond the local buckling. The underlying explanation of the proposal is as follows: The stress distribution in a uniformly loaded plate which is supported along unloaded edges is uniform up to local buckling. As the load tends to larger values the central portion of the plate starts to deflect laterally and would not support any further magnitudes of load. However the portions close to longitudinal supports continue to take stresses beyond local buckling, Figure 2.7. This phenomenon suggests that a redistribution of normal stress takes place after local buckling [17]. In this context, concerning the two strips adjacent to edges of plate and yield stress of material von Kármán [103] stated that it is possible to evaluate ultimate load carrying capacity of plates loaded in compression.

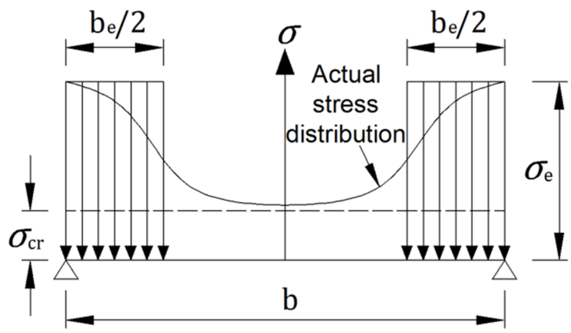

Figure 2.7 Effective plate width

von Kármán's effective width concept can be equated using plate buckling equation and assuming that the effective width, b_e ,would fail at a level of edge stress, σ_e, equal to yield stress of material, σ_y;

$$k_c \frac{\pi^2 E}{12(1-\nu_e{}^2)}\left(\frac{t}{b_e}\right)^2 = \sigma_y \tag{2.18}$$

In order to relate the equation with actual width of plate, b, Equation 2.15 is used. Assuming a simple supported condition with $k = 4.0$ von Kármán's effective width equation takes the form;

$$b_e = b\sqrt{\frac{\sigma_{cr}}{\sigma_y}} \tag{2.19}$$

A few years later from von Kármán's proposal, considering a constant membrane strain in the loaded plate and neglecting the effects of shearing stresses Cox [104] performed an approximate energy analysis of ultimate strength to improve the effective width approach. He performed the theoretical analysis in conjunction with testing duralumin plates clamped at all edges. The proposal was based on geometrical analysis and tended to lead conservative strength and stiffness results.

Accordingly, proposal was later named “lower bound method” and has been used by many investigators. In same year, a study by Sechler [105] provided significant development for application of effective width approach to sheet stringer aircraft panels. Depicting empirical curve he found that constant given in von Kármán’s formulation has to be depend on plate geometrical and material characteristics. In an attempt to improve effective width approach, a valuable contribution to theory was made by Marguerre [106] who employed principle of minimum potential energy and compatibility equation to solve post-buckling problem of simply supported flat plate in compression Later many investigations were conducted combining von Kármán and Marguerre’s approaches. Marguerre’s theory and extensions are presented in detail by Bleich [13]. Testing two sheet stringer panels Ramberg et al. [107] investigated post-buckling strength of constituent plate elements. The importance of their study lies in the fact that they assessed various effective width approaches proposed up to 1939 against their test results. So, the promising basis of various proposals and their drawbacks were detailed.

As a result of promising predictions, effective width method became a tool of particular interest in engineering practice. Adoption of thin-walled structures also promoted civil engineers to employ and improve effective width approach by performing extensive experimental and theoretical researches. In this manner studies conducted by Winter and co-workers are very important in the development history of specification for cold-formed steels, AISI [108]. By treating cold-formed steel members as thin plated sections and performing many experimental studies in conjunction with theoretical work, Winter [109] and Winter et al. [110] proposed an updated type effective width equation. Proposed effective width equation was incorporated the AISI specification of 1946 through 1962 editions. In further studies the effective width approach was extended to cover unstiffened flanges of cold-formed steel sections which are supported along one longitudinal edge. The study conducted by Kalyanaraman et al. [111] who performed tests on short columns and beams and the work by Winter [112] served for this purpose. 1986 edition of AISI specification adopted the proposed equation for unstiffened elements. Equation 2.20 represents Winter type effective width;

$$b_e = b\sqrt{\frac{\sigma_{cr}}{\sigma_e}}\left(1.0 - 0.22\sqrt{\frac{\sigma_{cr}}{\sigma_e}}\right) \quad (2.20)$$

Equation 2.21 presents Winter's type effective width equation in a general format which can be applied for plates with various boundary conditions.

$$b_e = 0.95t\sqrt{\frac{k_c E}{\sigma_e}}\left(1.0 - 0.209\sqrt{\frac{k_c E}{\sigma_e}}\frac{t}{b}\right) \quad (2.21)$$

Since effective width approach has been a major tool for the evaluation of post-buckling strength of thin-walled structures, many disciplines such as civil, aeronautical and marine engineering are contributed to development process and suggested different key points according to considered structure type. Comparisons of various effective width equations developed by foregoing authors and many others that are not presented here were provided and reviewed in detail by Jombock and Clark [113], Faulkner [114], Lind et al.[115], Roorda and Venkataramaiah [116], Rhodes [117], Cui and Mansour [118] and Paik [119]. The works have the potential to deploy significant assessments of various effective width formulations into thin-walled structures field. Today effective width is still in use as a robust prediction method for the post-buckling strength of thin-walled structures and adopted by many other specifications across the world.

2.2.5 Effects of Manufacturing Residuals on Plates

Geometrically perfect structure in field of engineering practice does not exist basically due to manufacturing and assembly processes [38, 120]. Rolling, forming and machining steps introduce different type of geometrical imperfections which need to be included in assessment of structural performance. Also riveting or welding used to assemble structural components lead another type of geometrical imperfections. Moreover, type and magnitude of geometrical imperfections have the potential to promote structural collapse mode shape. In order to develop robust predictive methods and designs with high level of confidence, the geometrical imperfections have to be accounted for in all structural shapes, especially in thin-walled structures. Fortunately, as is well known initial geometrical imperfections do not considerably affect the buckling load and ultimate load of axially compressed plates thanks to their stable post-buckling behaviour. But they cause the buckling to take place gradually unlike a sharp buckle of perfect element, masking the buckling load of structure [17], Figure 2.8.

A theoretical investigation undertaken by Hu et al. in 1946 [121] provides comprehensive assessments of effects of geometrical imperfections on buckling behaviour of simply supported square plates. Performing analysis in elastic limit they indicated that the initial geometrical imperfections have an impact on the vicinity of local buckling of plates as detailed above. And also they presented that in regions

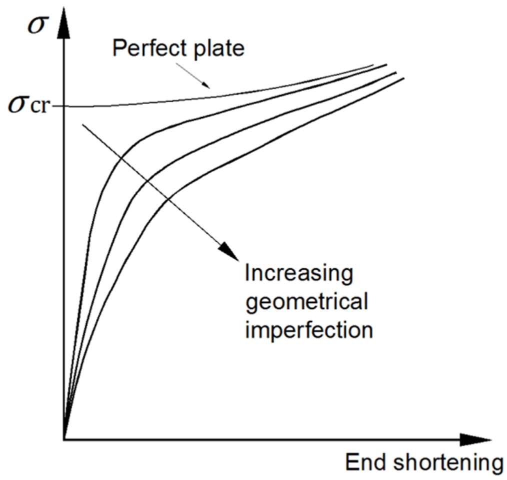

Figure 2.8 Initial geometrical imperfection effects on plate buckling

well below or above the critical stress imperfect plates have behaviour very close to geometrically perfect ones.Effects of imperfections on elastic post-buckling behaviour of square plates were also theoretically studied by Yamaki [122] for different types of boundary conditions. Also in a further work Yamaki [123] studied the case experimentally. Pope [124] also delineated the low imperfection sensitivity of elastic plates by conducting a theoretical study. A further approach by Kmiecik [125] is the first to consider superimposed Fourier components as initial geometrical imperfections for axially loaded plates. In a later study Kmiecik et al. [126] analysed a very significant database of plates for imperfections. The measurements of manufacturing distortions of 1998 ship plates obtained from a 15 years study from a wide range of ship structures statistically analysed by him. A series of studies presented by Rhodes et al. [127, 128] are significant in referring the post-buckling strength of elastic plates with different magnitudes of sinusoidal imperfections. In a combined theoretical and experimental work Rhodes et al. [127] plotted load deflection curves of imperfect plates which support findings of Hu et al [121]. Another work by Rhodes and Harvey [128] considered the imperfect rectangular plates simply supported along loaded edges and various types of supports along unloaded edges..

Many studies also were undertaken to assess effects geometrical imperfections on buckling and collapse behaviour of plates including plastic material characteristics. Considering plastic material behaviour Dwight and Racteliffe [129] coupled theoretical knowledge and experimental testing to analyse imperfection sensitivity. Theoretical work presented by Hutchinson and Budiansky [130] also was devoted to same purpose. A study conducted by Bradfield [131] explains the effects of imperfections experimentally. Conclusion of low imperfection sensitivity of plates in plastic range as with the elastic case is the common key drawback of the works presented above.

As with the columns, manufacturing processes and assembly methods certainly introduce residual stresses into plates. Magnitude and direction of these stresses actually depend on the methods themselves in production and used material characteristics. Since the stresses create configurations different than a stress free condition, they have to be an effect on buckling performance of plates. The primary source of residual stresses in plates or plated elements is usually welding. Thermal cycle of weld introduces heat locally into vicinity of weld. As the weld metal and base metal cool, weld region experiences tensile stresses and compressive stresses far away weld region arise to satisfy the equilibrium, Figure 2.9. The created compressive stresses can reduce buckling strength of plates subjected to compressive loading [132]. Moreover, tensile residual stresses adversely influences mechanical characteristics such as fatigue, creep strength, stress corrosion cracking, and brittle fracture [133]. Also welding leads to material degradation and geometrical imperfections which need to be considered in engineering practices. The work presented by Rao et al. [134] discussed the distribution and magnitude of residual stresses in welded plates.

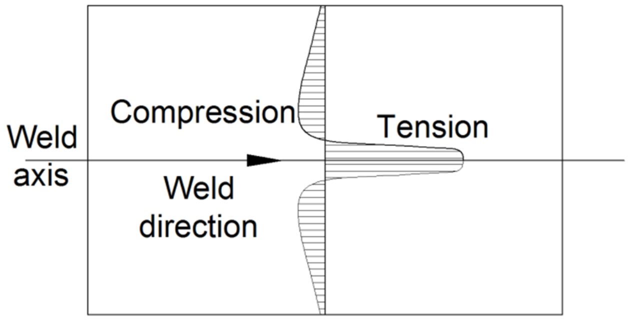

Figure 2.9 Weld induced longitudinal residual stresses

Focusing on ship hull girders Becker et al. [135] tested various square thin-walled tubes which were formed by welding. They concluded that effect of residual stresses on buckling performance depends on plate width/thickness ratio. The study conducted by Frieze [136] is also important which presents effects of residual stresses on plate compression behaviour. Proposing equations to predict profiles and magnitudes of residual stresses White [137, 138] presented the details of welding experiments. Bradfield [139] tested welded plates to assess buckling performances and compared the results with simplified empirical approaches. The study conducted by Bradfield was later summarized in a research paper [131] which presents the test results of welded and unwelded plates. In a comprehensive work which combines theoretical and experimental studies Bambach and Rasmussen [140] concluded that presence of welding residual stresses increases the experimental elastic buckling stress. This behaviour was attributed to the presence of tension fields at both longitudinal edges by authors. However another work [141] conducted by same authors established only marginally less ultimate strengths for plates with residual stresses compared to unwelded ones. Cui and Mansour [118] conducted a theoretical study which gives comprehensive account for previously proposed ultimate strength formulations for plates by various authors. Employing elastic large deflection theory and rigid plastic analysis they proposed a novel formulation set to evaluate ultimate strength of plates including effects of residual stresses and initial geometric imperfections. They observed slight reductions of ultimate strength due to residual stresses that supports the findings of Bambach and Rasmussen [141]. But also they noted that weld induced imperfections have considerable effect on ultimate strength of plates. The importance of paper also lies in the fact that it presents eleven different ultimate strength equations, including von Kármán's, and the equation proposed by authors. Therefore, the work can be addressed as an important reference when dealing with plate buckling problems.

2.3 Buckling of Stiffened Panels

In many engineering disciplines the promising capabilities of plate stable buckling behaviour is facilitated to build efficient structures. Nevertheless, further actions have to be undertaken for plates in order to compensate extreme loading conditions. Increasing thickness of plate is an alternative to improve the buckling performance of structural components. However such a way would lead to expensive designs in terms of engineering practices with waste of material. To arrive at a reliable solution and overcome this challenge with efficiency based approach, stiffening of plate elements have been a robust engineering based technique in field. In this context, stringers are attached on flat plates to constitute stiffened panels which will serve as more powerful building blocks for structures. The bending and compression capacities of stringers combined with post-buckling reserve of thin flat plate (skin) constitute the key force behind the high performance of stiffened panels. Although stringers on flat plates create efficient structural segments, they reduce the predictability of structural behaviour by provoking complicated geometrical configurations. There exist several instability modes for this kind of thin-walled structures such as global and local buckling related to stringer or skin behaviour. A more complicated case is the interaction buckling of skin and stringers which plays a major role in practice and calls for careful prediction techniques.

Since the stiffened panels have been common challenges for many engineering sciences such as civil, aeronautical and marine engineering, literature contains many works devoted to characterize their behaviour under compressive forces. Many experiments, theoretical works and numerical studies were undertaken from around 1930s to present time. In this manner, Timoshenko [142] was the first to deliver the theory into stability of stiffened panels. Considering rectangular plates stiffened by longitudinal or transverse ribs, he investigated required minimum rigidity of the ribs to restrict buckling. Towards this aim, he employed energy methods in deriving approximate solutions of buckling under different loading conditions. The book presented by Timoshenko [68] in 1936 also devotes a chapter to the stability of stiffened panels. Chapter treats evaluation of proper thickness of panel skin and spacing of stringers in detail. Timoshenko's works implied that neglecting torsional rigidity any increase in flexural rigidity of stringers beyond a minimum required value lead no further increase in the critical buckling stress of panel when the buckling of skin between stringers is under consideration. Citing this drawback and considering one longitudinal stringer in the middle of the plate Schleicher [143] evaluated required minimum rigidities of stringers. In an attempt to present elastic buckling of stiffened panels with equally spaced stringers Lokshin [144] derived the exact solutions for longitudinally or transversely stiffened cases. Since the derivations in the study did not introduce general solution of differential equations, his work only achieves the buckling cases of symmetrical modes. Reviewing the works presented by Timoshenko, Barbré [145] investigated the elastic buckling of panels stiffened by one or two equally spaced longitudinal stringers. To this end, he focused on evaluation of proper dimensions for longitudinal stringers which would develop maximum buckling strength for panel with simply supported and fully clamped unloaded edges.

Windenburg [146] introduced the noticeable influence of torsional rigidity of stringers with reinforcing bulbs (Tee stringers) to critical stress of panels. He assumed a simple support condition at skin-stringer junction. In a similar manner, Chwalla [147] investigated the case under the assumption of clamped support at skin-stringer junction. In both studies torsional rigidities of stringers were shown to contribute much to panel critical stress. A further research by Steele and Wang [148] improved understanding of effects of stringer torsional rigidity on stiffened panel buckling. They utilized von Kármán's large deflection theory to investigate the effects on single stringer panels. Effect of imperfections on critical stress of panel stiffened by a central longitudinal stringer was investigated by Schleicher and Barbré [149]. They concluded that a sinusoidal type initial imperfection with magnitude of 10 % web thickness has no considerable effect on panel critical stress and behaviour. Fröhlich [150] studied buckling of simply supported rectangular plate with one longitudinal and one lateral stiffeners crossing at the middle of the plate. He evaluated minimum stringer requirements under pure compression. Main focus of foregoing works was addressing the critical stress of stiffened panels with various configurations and did not made an attempt to evaluate ultimate strength. Herein it should be noted that evaluations of critical stress and ultimate strength of stiffened panels loaded in compression requires different approaches to follow. Although analytical approaches were derived to evaluate ultimate load carrying capacity of unstiffened plates and empirical equations were proposed, in case of stiffened panels mathematical equations become too complex to deploy into ultimate strength assessments.

2.3.1 Stiffened Panels in Aeronautical Engineering

The production of thin-walled metal aircrafts in 1930s provoked aeronautical engineers to improve the research on stiffened panels. Today stiffened panels constitute fuselage and wing portions of all aircrafts, Figure 2.10. Since then the stability performance of stiffened panels under various conditions has been a major subject of numerous theoretical and experimental investigations in aeronautical science. Local buckling or critical buckling of panels constitutes just the first step in aircraft panel designs. Because as documented before, aircraft panels are designed in such a manner that local buckling of the sheet occurs at loads considerably below critical buckling of entire system [13]. Thus, majority of researches in this field mainly focused on ultimate strength rather than critical buckling.

Figure 2.10 A typical fuselage section (from [151])

To the knowledge of author, the history of stiffened panel research for aircraft applications begins with the experimental studies of Newel [152, 153] in 1930 and 1932. Using channel section stringers he performed a series of compression tests on small scale aluminium alloy stiffened panels. He reported that strength of a stiffened slightly curved sheet is lower than that of same configuration with flat sheet. A study presented by Lundquist [154] was particularly concerned with prediction of compressive strength of stiffened panels. His valuable contribution provides employment of the effective width method for ultimate strength prediction of stiffened panel configurations. By comparing three proposed effective width methods, including von Kármán's, he assessed the prediction methods against test results provided by Newel [152, 153] and Schuman and Back [97]. He concluded that a method which presumes a together act of stiffener and effective width of skin as a column leads the best correlation between test results. In following years some authors named this method as "strut approach". For decades experimental works were the most powerful tools for aircraft panel assessments. Figure 2.11 shows a fuselage panel tested to failure by Murphy et al. [155].

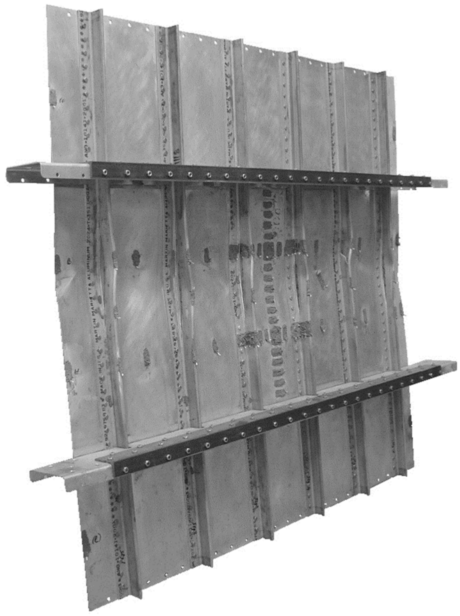

Figure 2.11 Collapse shape of an axially loaded fuselage test panel (from [155])

Sechler [156] conducted a combined analytical and experimental study to investigate buckling behaviour of compression loaded stiffened panels. Conclusions of the study confirmed the Lundquist's findings which underlines column behaviour of stringer with an effective width of sheeting. Also he proposed an equation to characterize effective plate width under the stringers which allows evaluating strength of panel with any number of stringers. Dickinson and Fischel [157] detailed the evaluation techniques of effective width of plating in stiffened panels for experimental and theoretical studies. Reviewing the previous proposals on effective width, Reff [158] extended the application of the approach for various sheet stringer combinations. Considering one or two longitudinal or transverse stringers with various positions on rectangular plate Barbré [159] derived differential equations to investigate buckling behaviour stiffened panels. The study performed by Ramberg et al. [107] includes experimental testing of two stiffened panels under compression. Test results were compared with the theoretical results obtained using different effective width formulas. Test program undertaken by Dunn [160] provided significant amount of data for the strength assessments of panels. He tested 183 aluminium alloy panel stiffened by bulb-angle stringers under compression. It was shown that an increase in the torsional rigidity of stringer increases the effective width of sheeting.

Assessment of attachment methods and investigation of effects on panel strength begins with Hutchins's thesis [161] published in 1934. For various attachment methods he underlined a probable buckling of sheet between rivets, spot welds or bolts. In a further study Howland [162] delineated inter-rivet buckling behaviour experimentally and theoretically. Holt [163] tested stiffened panels which represent the configuration of an actual airplane wing. Potential reduction in panel strength due to the inappropriate spacing of rivets which were used to attach stringer on sheet was reported by him. Also he examined effective width equations proposed by von Kármán [103] and Ramberg et al [107]. In order to address the difficulties encountered in connection of theoretical solutions with experimental results Cox et al. [164] conducted a combined theoretical and experimental study. Inter-rivet buckling was one of the failure modes observed in the test program. Semonian and Peterson [165] proceeded to address inter-rivet buckling for stiffened panels under compression loading. Analysing experimental data they showed inter-rivet buckling has great influence on panel strength and proposed an equation to be employed in inter-rivet buckling checks.

Extending the theory of arbitrary shape of open section stringers Levy and Kroll [166] gave particular attention to investigate the stabilizing effect of the sheets on the buckling load of stiffened panels. Test results presented by Rossman et al. [167] provided valuable numerical database on the critical buckling and ultimate strength of panels stiffened by Z shaped stringers. Testing panels with formed hat section longitudinal stringers Schuette et al. [168] developed some design charts and compared the efficiencies of hat section stringers with that of Z shaped stringers. Dow et al. [169] investigated effects of material characteristics such as elastic modulus and yield strength on critical buckling and ultimate strength of stiffened panels by testing panels made from stainless steel, mild steel, titanium, copper, aluminium alloy and magnesium alloy. The study is very important in terms of indicating the efficiencies of different materials in aircraft construction.

Crippling stress play an important role into buckling design of stiffened panels in aircraft construction. The term crippling refers local compressive failure of stringer or skin-stringer combinations with maximum effective slenderness (L/r) of 20. Considering the aluminium alloy material properties Crockett [170] developed an empirical formula to be used for crippling strength prediction. Investigations conducted by Gatewood and Williams [171] and Bijlaard [172] also aimed to address crippling strength of stiffened panels. Handbook of structural stability presented by Gerard gives comprehensive account for the theoretical buckling evaluation of aircraft components. Particularly, Parts IV and V [173, 174] of these series was devoted to stiffened panel buckling behaviour. Reviewing significant amount of proposals on strength of stiffened panels, Gerard [173, 174] proposed a novel approach to evaluate buckling strength of compression loaded sections and stiffened panels. Considering extruded or formed stringers, his main focus was on determination of crippling strength of short panels. Main idea behind the proposal was to idealize the skin-stringer configuration as flange elements with different boundary conditions at longitudinal edges. For the panels in transition range (between short panels with a maximum slenderness of 20 and long columns) he extended the approach by combining his crippling strength theory with Johnson parabola. The Euler column equation was employed for long columns which buckle at stress levels lower than local buckling stress and material yield strength. In further decades Gerard's theory was employed in many other investigations. In a following work Gerard [175] summarized his theory and extended it to cover various environment conditions such as crippling at elevated temperatures and creep crippling. Herein, it is worth noting that the Johnson's equation combined with Euler's curve serve as an important initial sizing tool for aircraft panels. It is an empirical equation to describe the flexural stability strength of columns with cross sections having elements that are subject to local buckling or crippling [176]. Equation 2.22 presents Euler-Johnson column strength.

$$\sigma_c = \sigma_E \ , \sigma_E \leq 0.5\sigma_{c-s} \qquad (2.22-a)$$

$$\sigma_c = \sigma_{c-s}\left[1 - \frac{\sigma_{c-s}\left(\frac{KL}{r}\right)^2}{4\pi^2 E}\right] , \sigma_E > 0.5\sigma_{c-s} \qquad (2.22-b)$$

where σ_c refers column strength, σ_E is the Euler column strength and σ_{c-s} represents whole cross section crippling strength which can be evaluated as weighted average of crippling strength of constituent strips as follows;

$$\sigma_{c-s} = \frac{\sum b_i t_i (\sigma_{cr})_i}{\sum b_i t_i} \qquad (2.23)$$

Crippling strength of each strip is determined by directly using Equation 2.15 or by employing effective width method for the section. Gerard's [173, 174] approach shows itself here to determine the crippling strength of cross section. For angles, tubes, plates and multi-corner sections such as stiffened panels he proposed following crippling strength equation;

$$\frac{\sigma_{c-s}}{\sigma_y} = 0.56\left[(gt^2/A)\left(E/\sigma_y\right)^{1/2}\right]^{0.85} \qquad (2.24)$$

For T shaped, cruciform and I shaped sections;

$$\frac{\sigma_{c-s}}{\sigma_y} = 0.67\left[(gt^2/A)\left(E/\sigma_y\right)^{1/2}\right]^{0.4} \qquad (2.25)$$

For two corner sections such as Z shaped and channel sections;

$$\frac{\sigma_{c-s}}{\sigma_y} = 3.2\left[(t^2/A)\left(E/\sigma_y\right)^{1/3}\right]^{0.75} \qquad (2.26)$$

In equations 2.24 to 2.26, g is the number of cuts required to divide the cross section into a series of flanges plus resulting number of flanges, Figures 2.12 and 2.13.

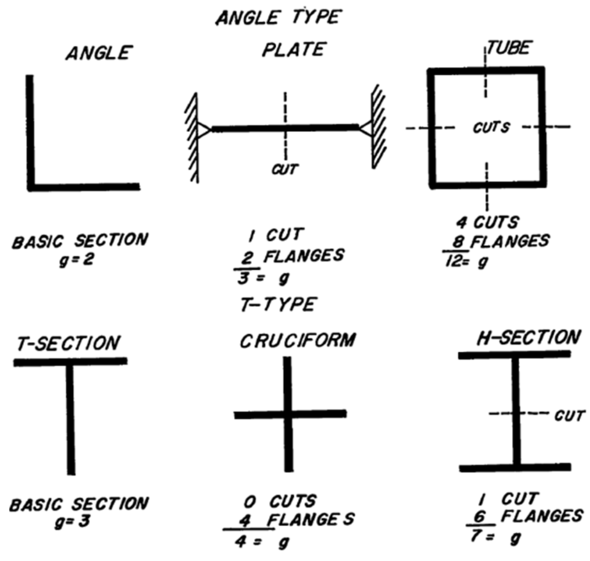

Figure 2.12 Gerard's method of cutting sections to determine g

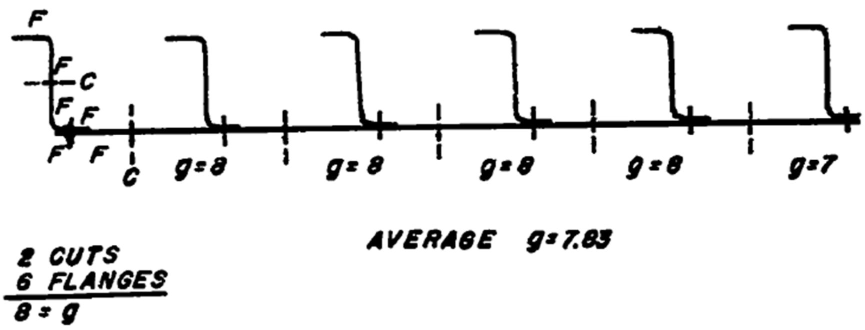

Figure 2.13 Gerard's method of cutting stiffened panels to determine g

With a particular attention to the wing panels, Yusuff [177] reviewed probable instability modes of stiffened panels. He showed that three modes generally commence in stiffened panels under compression loading. An Euler mode associated with a long wavelength, local mode in which the wavelengths are of the order of stiffener spacing and a combined Euler and local mode were in scope of the investigation. In a later study Yusuff [178] investigated local instability of compression loaded stiffened panels using energy equations and verified his approach by comparing the results with test data. Another paper by Yusuff [179] combined his energy approach with previous panel strength equations to develop robust formulations. Study delivered equations for panels covering complete range of slenderness including short panels, long panels and the panels in transition range. Considering strain energy of plastic buckling Sujata [180] investigated panels having one, two and infinite number of stringers. He proposed an approximate approach to evaluate plastic buckling coefficient for stiffened panels with any aspect ratio. In a subsequent study Sujata [181] investigated effective width of sheeting under the stringers accounting for the anisotropy of the material in inelastic range. He indicated that effective plate width in elastic range differs significantly in plastic range.

Aiming at comparing structural efficiencies of conventional stiffened panels and integrally formed panels under compression loading McClaren et al. [182] investigated crippling, panel buckling and overall buckling behaviour of various skin-stringer configurations. Another study [183] presented by same authors detailed the comparisons in terms of structural performance, manufacturing cost and applicability. Investigating failure characteristics of various configurations they concluded that low manufacturing cost, high strength capability and low weight goals can be satisfied by employing integrally formed panels. Mode interaction with stiffened panels was investigated by van der Neut [184]. Considering top-hat stringers he focused on the effects of mode interaction in post-buckling region of axially loaded panels. Also he stated that investigation of multi-bay panels requires incorporation of clamped end boundary conditions instead of simply supported ones to represent similar behaviour of such systems. Focusing on post-buckling behaviour of stiffened panels, Rothwell [185] investigated efficiency of Z shaped stringers. Test set-up generated by him to simulate collapse behaviour of stiffened panels aimed at providing simply supported unloaded edge boundary conditions. Moreover, the study includes geometrical imperfection measurements of stiffened panels. Ekvall and Chellman [186] investigated the compression performances of Aluminium-Lithium alloys to be used in aircraft panels. As a result of experimental tests they reported that weight savings are possible in compression critic parts of aircrafts by means of use of such alloy. Compression performance of aluminium alloys at elevated temperatures in conjunction with assessments against other aircraft materials were presented by Chellman et al. [187]. In order to assess the potential of FSW technology as replacement of conventional riveting methods Hoffman et al. [188] tested aluminium alloy panels stiffened by closed shape stringers. Performances of welded and riveted panel specimens compared using measured characteristics for initial skin buckling and collapse.

As a result of nature of aircrafts, aeronautical engineers are not forced to comply with design specifications. The aerospace structures community has no such codified design rules since their structures and components are far less conventional and repetitive. In addition, their designs are not governed by any usual structures design authority except for governmental aircraft certifiers [38]. The variety of material types used in aircrafts and very complicated geometrical configurations also keep them away from codified approaches. Thus each novel configuration requires a comprehensive research to be deployed carefully beginning from smallest cell of aircraft to complete assembled body. On the other hand analysis and design of such complicated structural forms call for some guidance to be consulted. In this sense the data sheets presented by ESDU fulfil the requirements of aircraft engineers in respect of preliminary analysis and design of aircraft stiffened panels. The data sheets combine research of aircraft structural engineers with theoretical knowledge on mechanics to serve as practical guides. Data sheets 70003 [189], 71014 [190], 02.01.34 [191], 02.01.35 [192], 02.01.36 [193] deal with local buckling of compression panels with different stringer shapes. Inter rivet buckling is treated in data sheets 02.01.08 [194] and 02.01.09 [195]. Strength of stringers in stiffened panels is formulated in data sheets 02.01.16 [196] and 02.01.17 [197]. Data sheet 98016 [198] gives comprehensive account for elastic buckling of stiffened panels and elasto-plastic buckling of panels is introduced in data sheet 01001 [199]. Moreover, the books by Bruhn [200] and Niu [176, 201] provide analyses and design methods accepted by aeronautical communities for buckling of aircraft components. Those books are fundamental resources for aircraft structural engineers.

2.3.2 Stiffened Panels in Civil and Engineering

As underlined previously, stiffened panels constitute main building blocks of most of the thin–walled structures in engineering practices. Promising results from earlier research in aeronautical field was the main reason of employment of such panels in different engineering disciplines such as in civil engineering, Figure 2.14. Nevertheless, required attributes and priorities of each field differs sometimes due to geometrical configurations, used material properties and expected performance. In this context it is convenient to detail each investigation according to its field of application. In this section the research on stiffened panel buckling performance for civil engineering applications are introduced.

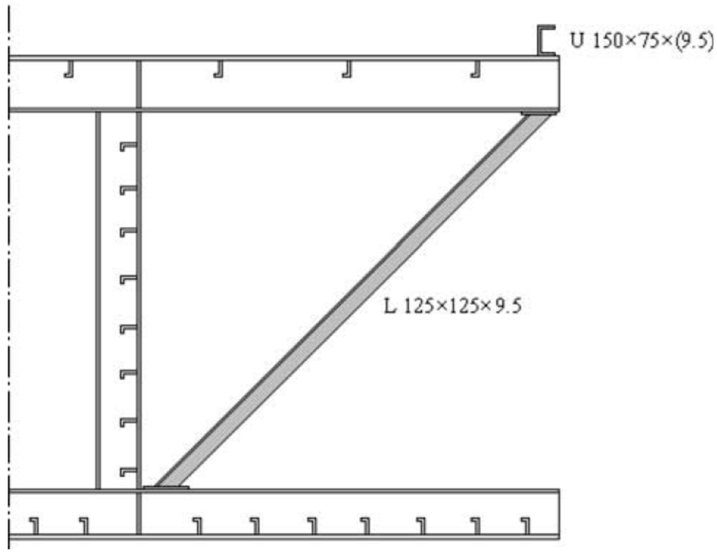

Figure 2.14 Cross section of a stiffened box girder bridge (from [202])

Collapse of box-girder bridges in 1960s and 1970s provoked the interest in plate buckling and performance of stiffened panels in civil engineering. Collapses of bridges during the period of late 1960s and early 1970s were discussed in detail by Åkesson [202]. Also plate buckling theory for bridge components was well documented in that reference. As a consequence of extensive research in field of aeronautical structures civil engineers were aware of the advances in plate buckling theory. Nevertheless, the differences in geometrical configurations and used material properties in civil structures compelled civil engineers to undertake further investigations. Investigations performed by Murray contributed very much to understanding buckling behaviour of stiffened panels in civil engineering. Performing some experimental works on stiffened panels Murray [203] concluded that stringer induced failure is more critical than a failure resulting from plate buckling because a sudden collapse follows a stringer failure. In another [204] work he presented a plastic mechanism analysis method based on elastic-plastic idealization of stiffened panel. The approach was developed throughout a strut idealization of the stringer and associated effective width of plating. Following years he presented [205] extended version of the plastic mechanism approach for thin-walled channel columns. In a later study [206] the details of the plastic mechanism approach for thin-walled structures treated by him in a more definite format.

A series of works presented by Horne and Narayanan [207-210] proposed a method to predict compression performance of continuous stiffened panels. Their formulations were based on Perry-Robertson column equations and idealize the stiffened panels as isolated columns. Stringer and corresponding effective width of plating comprise the isolated column geometry. An elastic behaviour of plate until attainment of local buckling was assumed in the proposal. Development of yield strength in plate portion or in stringer and instability of stringer are the failure criterions of the proposed formulations. Reduced sectional properties also proposed by them to compensate effects of initial geometrical imperfections and residual stresses. Experimental programs also accompanied their theoretical works to understand buckling behaviour of stiffened panels. The isolated column approach (strut approach) was also adopted by Dwight and Little [211], Dowling and Chatterjee [212] and Chatterjee [213].

A simplifying method for prediction of ultimate strength of stiffened panels in literature is orthotropic plate theory. The basic idea behind the theory refers converting of stiffened panel geometry into an equivalent plate that has a constant thickness. This constant thickness is equal to original thickness of plating plus thickness resulting from smearing the stringers over plating, Figure 2.15. However the method has some limitations and disadvantages. Closely spaced stringers are required to obtain satisfying results with this theory. Moreover, the method cannot be used in case of unequally spaced stringers and non-uniform panel geometry. The orthotropic plate theory is well documented in reference book by Troitsky [214]. Many researches were conducted for stiffened panel compression behaviour using this theory. Sherbourne et al. [215] used orthotropic plate theory to investigate buckling and post-buckling behaviour of simply supported aluminium stiffened panels. Using orthotropic plate theory Massonet and Maquoi [216] derived analytical formulations to predict performance of stiffened compression elements of box girder bridges. The study conducted by Murray and Katzer [217] assessed orthotropic plate theory and isolated column approach against test results. The elastic instability of bridge panels was investigated by Williams [218] using orthotropic plate theory. Lind [219] presented a refined version of Timoshenko’s energy method to predict strength of stiffened panels. The orthotropic plate theory was the method behind the Lind’s derivations while discrete stringer approach was used by Timoshenko. Effects of type of stringer on panel buckling mode and ultimate capacity were also discussed in this investigation.

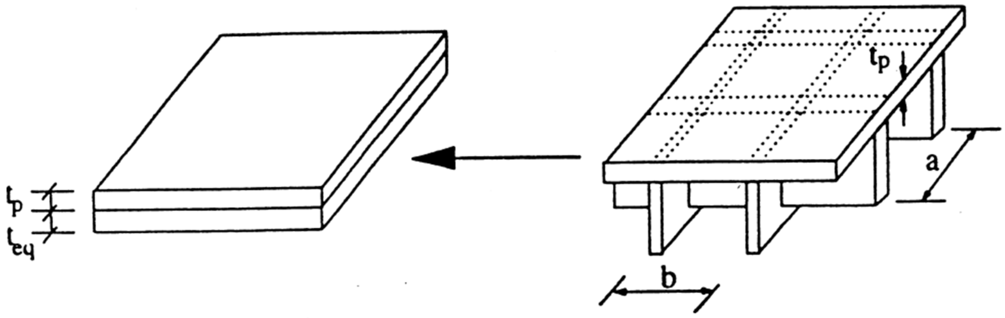

Figure 2.15 Orthotropic plate theory (from [220])

Comprehensive test programs on laboratory specimens were also undertaken to specify buckling and collapse behaviour of stiffened panels in civil structures, Figure 2.16. Experimental study conducted by Barbré et al. [221] focused on 45 stiffened panel specimens. To be able to observe various instability modes involved in stiffened panels like stringer and plate induced failures test specimens were designed with care. Subdividing the test specimens into several groups they aimed to investigate impacts of geometrical imperfections and residual stresses. The test results of stiffened panels having intentionally introduced geometrical imperfections with different shapes and magnitudes and residual stresses were assessed against the test results of nearly perfect specimens. A following study carried out in same institute served as accompanying work of Barbré et al. [221]. In that study Scheer and Vayas [222] tested 20 steel stiffened panels. Unlike free unloaded boundary conditions adopted by Barbré et al., Scheer and Vayas performed the tests under simply supported unloaded boundary conditions.

The investigation conducted by Roik [223] indicated that closed section stringers have numerous advantages over open section stringers. He particularly underlined high torsional stiffness of closed section stringers which lead to greater compressive strength in stiffened panels. Experimental study presented by Dubas [224] confirmed the advantages of closed section stringers. The study concluded that it is possible to design panels with larger stringer spacing using closed section stringers. Referring Marguerre's plate theory and using energy approach Steen [225] derived mathematical equations for elastic post-buckling analysis of stiffened panels.

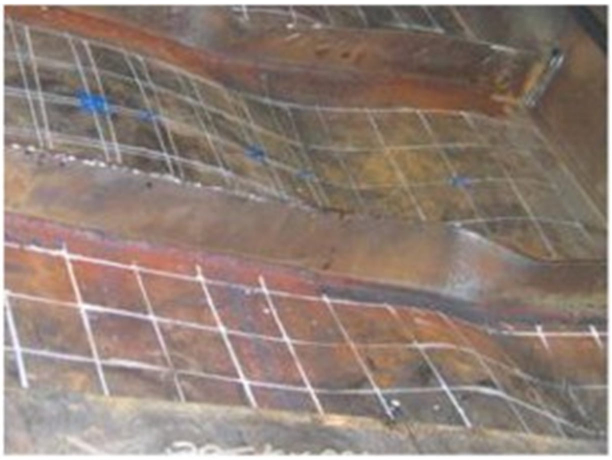

Figure 2.16 Collapse shape of an axially loaded bridge test panel (from [226])

Neglecting local instability modes his research focused on capturing global buckling modes. The case also investigated by Siridharan and Mao-Hua [227] analytically, accounting for local instabilities developed in stiffened panels. Bedair [228] derived analytical energy formulations for elastic behaviour of uniformly compressed stiffened panels. He idealized the multi-stiffened panels as assembled plate and beam elements. The developed formulations were then applied to investigate buckling mode changes due to dimensional shifts. Galéa and Martin [229] assessed the evaluation process of Eurocode-3 for global buckling of stiffened panels and proposed a simple computerized approach for fast calculations.

The specifications and codified methods for box-girder bridges and design approaches for compression loaded stiffened panels in bridges are treated in detail in reference books by Ziemian [14] and by Xanthakos [230]. As is well known, Japanese experience on bridges is a valuable reference to be cited. The paper presented by Kitada et al. [231] introduced the historical development of Japanese methods and design equations for compression loaded stiffened panels in box-girder bridges.

2.3.3 Stiffened Panels in Marine and Engineering

Stiffened panels also form the compression surfaces of ship hulls, Figure 2.17. The reason that ship hulls encounter longitudinal stresses is bending of hulls under wave action. As a result of increasing demands of marine transport and lack of enough guidance, marine engineers were driven to perform specific researches on stiffened panels that exactly fit their concepts. Generally closely spaced stringers which lead low b/t ratios comprise the ship panels. This configuration is one of the characteristics of ship panels which separate them from those stiffened panels in aeronautical and civil engineering. Also up to 1960s conventional analysis method for ship plating was relied on elastic behaviour which was not an efficient way in design. Moreover, replacement of riveting with welding in those years led to different concerns for marine panels.

A research project named "Built-up Members in Plastic Design" undertaken at Lehigh University Department of Civil Engineering and funded by the Department of the Navy under Naval Ship Engineering Center Contract delivered significant research reports in 1960s on strength of stiffened ship plating. A series of ten tests presented by Lee and Ostapenko [232] and Rapetsreiter et al. [233] on simply

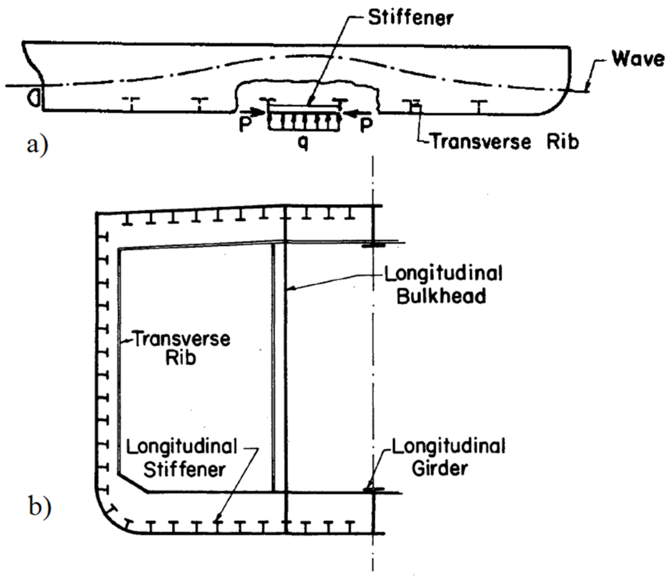

Figure 2.17 Typical ship hull a) Compression loading of panel due to hydrostatic loading b) Cross section of a typical ship hull (from [232])

supported longitudinally stiffened panels investigated effects of lateral loading, residual stresses and geometrical parameters on one to four scale test specimens. Lateral loading was introduced into the specimens to simulate hydrostatic pressure. Beam-column behaviour of panels under lateral and compression loading was observed during the tests. Also the test results revealed that critical strength of panels is not affected by lateral loading whereas axial strength of panels depends on the intensity of lateral loading. The residual stresses were found to have significant impact on critical strength and axial strength of panels with high plate slenderness (b/t). Testing four longitudinally stiffened panels, Kondo and Ostapenko [234] investigated the effects of above parameters under fixed loaded ends boundary condition.

In an attempt to computerize evaluation of stiffened panel strength, Kondo [235] formulated the mathematical equations using moment curvature relationships of beam-columns. Unfortunately his computational tool ruled out local buckling of plating prior to ultimate strength of panel. Therefore, the program served to compute ultimate strength of panels with low plate slenderness. In further studies referring Kondo's [235] work, Tsuiji [236] and Vojta and Ostapenko [237] particularly concerned with the panels with high plate slenderness. Developed computational programs were tested against experimental results and a general agreement was found for design purposes. Considering elastic perfectly plastic material model for stringers and Koiter's type post-buckling behaviour of plate, the relationship between plate critical buckling and post-buckling strengths was also investigated [236]. Both computational efforts neglected strain hardening of panel material and initial geometrical imperfections. Also curves plotted by Tsuiji [236] clearly showed effects of b/t (stringer spacing to skin thickness) ratio on stiffened panel compression strength, Figure 2.18.

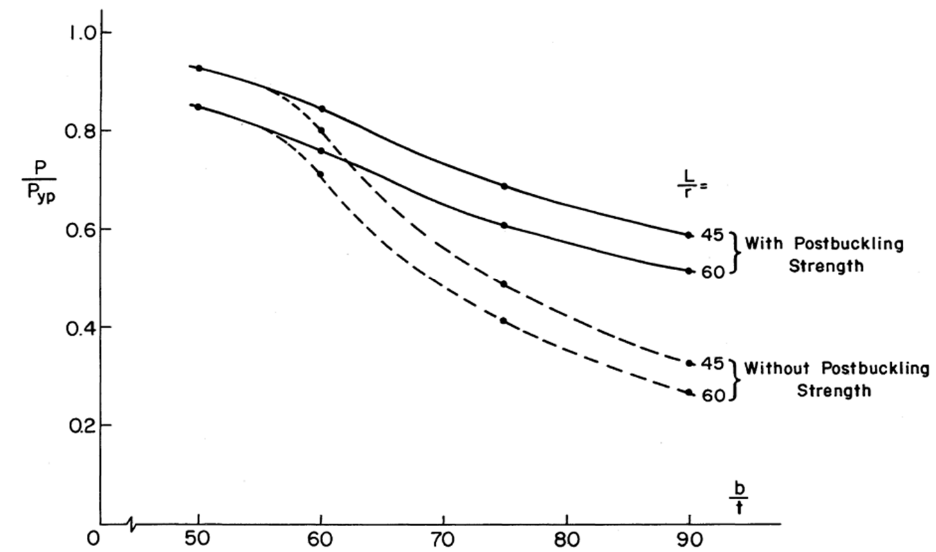

Figure 2.18 Effects of b/t ratio on a simply supported panel strength (from [236])

Ultimate strength design curves for the panels under lateral and compression loads were developed in a following study by Vojta and Ostapenko [238] using developed computer program. Rutledge [239, 240] combined previous computational tools developed in research project and removed elastic-perfectly plastic material model restrictions using a non-linear type definition. The report presented by Ostapenko [241] summarized the findings of the comprehensive research program and underlined key details.

Also many experimental and theoretical investigations were undertaken under the support of Ship Structures Committee (USA) on ship stiffened panels. The experimental program performed by Becker et al. [242] covered seven tests on electron-beam welded stiffened panels under combined compression and lateral loading. A theoretical study presented by Mansour [243] is a very significant reference to be cited. He proceeded to examine existing theoretical approaches for determination of stiffened panel stability. The orthotropic plate theory, energy method, intersecting beams method and strut approach with effective plate width theory were assessed against experimental results in literature. Capabilities and pitfalls of methods in evaluating local buckling and ultimate strength were detailed. A following theoretical study by Mansour and Thayamballi [244] focused on probable failure modes of ship panels in elastic and plastic ranges. An experimental program conducted by Chen et al. [245] undertaken twelve tests of single stringer panels stiffened by T shape stringers. Test specimens were specifically designed to represent ship plating configuration and exhibit various failure modes such as plate buckling and stringer crippling. Intentional geometrical deformations and damages were introduced into specimens to capture impacts on panel strength. The test results revealed that a proper design of single stringer specimen has the potential to represent a full scale one to a certain degree. Another experimental study of simply supported single stringer long specimens performed by Chen et al. [246] explained testing procedure step by step, providing an important reference for those who are interested in compression testing. Also measurement of residual stresses and geometrical imperfections of panel skin and stringer were presented. In following years research programs were extended to cover aluminium alloy stiffened panels used in high speed vessels. Processing initial imperfections and residual stresses and testing 78 MIG (metal inert gas) welded full scale aluminium alloy panels in compression Paik et al. [247] provided an important database for marine engineers. In a subsequent study Paik [248] tested FS (friction stir) welded aluminium stiffened panels and compared the performances with panel tests produced by MIG welding in reference [247]. Figure 2.19 provides collapse mode of a ship panel test specimen.

Figure 2.19 Collapse shape of an axially loaded ship test panel (from [248])

Besides, various investigations were performed by many other researchers to improve the understanding of buckling behaviour of ship panels. Basing on Johnson-Ostenfeld formulation Faulkner et al. [249] derived an effective width equation to be used in ultimate strength assessments of ship panels. Later Faulkner [114] reviewed present effective width proposals for ship panels. This work is important in terms of providing the comparisons of various effective width equations. On the other hand Carlsten [250] derived another effective plate width equation using Perry-Robertson method. Considering initial geometrical imperfections Paik et al. [251] analytically derived an effective width equation for simply supported stiffened panels. Also he combined Perry-Robertson and Johnson-Ostenfeld approaches to propose an ultimate strength equation. A comparison of above Perry-Robertson and Johnson-Ostenfeld methods for the prediction of post-buckling strength of stiffened panels was provided by Soares and Gordo [252].

Somerville et al. [253] presented the measurements of weld induced distortions and residual stresses of stiffened panels. Imperfection sensitivity of buckling behaviour of ship plating and analysing measured imperfections width the aid of Fourier series expansion was presented by Czuijko and Kmiecik [254]. Assuming trigonometric function type initial geometrical imperfections and employing energy principles in an analytical form Byklum and Amdahl [255] derived a method to predict elastic post-buckling response of stiffened panels. Employing plate theory for stringer webs and beam theory for bulb shape flanges elastic stability analysis of stiffened ship panels were carried out analytically by Danielson and Wilmer [256].

In order to provide insight into some of difficulties met in connection with experimental behaviour and theoretical knowledge Gordo and Soares [257-259] tested three bays short, intermediate and long panels. Single bay tests undertaken by many researchers suffered from not satisfactory boundary conditions at loaded ends to capture rational behaviours. In field structures panels are supported by transverse frames. Therefore, neither simply supported nor fixed end boundary conditions provided in most of experimental set-ups fully represents actual behaviour of stiffened panels under compression. Manufacturing three bays specimens which comprise two transverse frames and monitoring behaviour of middle bay during test allows capturing more representative behaviours. In this sense works by Gordo and Soares [257-259] are significant references. A recent experimental study by Xu and Soares [260] investigated collapse behaviour of wide steel stiffened ship panels. The results were compared with the tests of various configurations provided by Gordo and Soares [257-259]. In the concept of marine engineering tests undertaken by Alberg et al. [261] should definitely be mentioned. They tested 21 aluminium panels stiffened by open section L shaped stringers and closed box type stringers under compressive loading. Panels were manufactured utilizing MIG welding and FSW. The test results created a valuable data base for further numerical studies undertaken by many researchers.

The reference edited by Lamb [262] assists ship designers to develop better structural configurations and includes all aspects of structural design of ships. Stiffened panel stability, with local and ultimate strength concerns is also detailed to guide marine engineers.

2.4 Finite Element Method

Foregoing researches constitute a broad overview of theoretical and experimental works on axially loaded columns, plates and stiffened panels, tracing the path of developments from Euler to 21th century. Advent of digital computers in 1960s led to evolution in engineering sciences as well as in structural mechanics. These computers allowed numerical methods to be further advanced. Computational methods in structural mechanics rose as a result of combined actions of theory, numerical techniques and computers. At the present time computational methods accompany the researches with the abilities to simulate linear, non-linear geometric and material properties, complicated boundary conditions and geometrical configurations, imperfections and residual stresses. Computational methods provide reductions in research costs and alleviate the difficulties encountered in preparation of laboratory specimens. Also examination of a wide search space for full scale complicated structures within short period of time offers versatility for investigations.

Of the computational mechanic techniques, Finite Element (FE) method is the most promising one to be deployed into comprehensive research programs. The method discretize the structure into a finite number of elements connected each other by nodes to approximate behaviour of entire system with finite number of degrees of freedom at those nodes. Differential equations of problems are treated using energy principles, most common with total potential energy, and integrated over each element to simulate system characteristics. Assumed functions of nodal parameters are used to evaluate stresses and strains within each element. It approximates solutions with reasonable accuracy, provided that a considerable care is exercised in modelling of structural details. Although the FE method is not the oldest numerical technique in field of mechanics, it has been received the greatest attention as a computational tool due to its implementing features. It follows finite difference and weighted residual methods in the field. Herein no attempt is made to detail the theory of FE method and its numerous features in engineering science. Instead, a brief development history of the method and usage in stability analysis of axially loaded structures are presented. The theory of FE method and different principles behind various implementations of method are well documented in books by Hinton and Owen [263], Zienkiewicz and Taylor [264, 265], Bathe [266] and Crisfield [267, 268]. Following section briefly introduces the development history of the method.

2.4.1 A Brief Historical Overview

The history of FE method begins with the Courant's [269] investigation published in 1943. Looking from a mathematical point of view and using variational principle in conjunction with interpolation over triangular sub-regions he focused on approximate solution of torsion problem. The study was too early to receive required attention, since the computers were not present in those years. In following years Levy [270] generalized a matrix form of force method for sweptback wing analysis. The method evaluates the internal forces directly by equating flexibility matrix. In a further study [271] in 1953 he presented "direct stiffness method" which is based on a direct evaluation of displacements instead of forces to idealize the behaviour of aircraft wings. Evaluation of displacements instead of forces led to development of stiffness matrix. Subsequent studies by Argyris [272, 273] refined previous studies using energy principles, forming the base of matrix structural analysis. The importance of these works lie in the fact that he showed efficiency of using energy principles in matrix structural analysis.

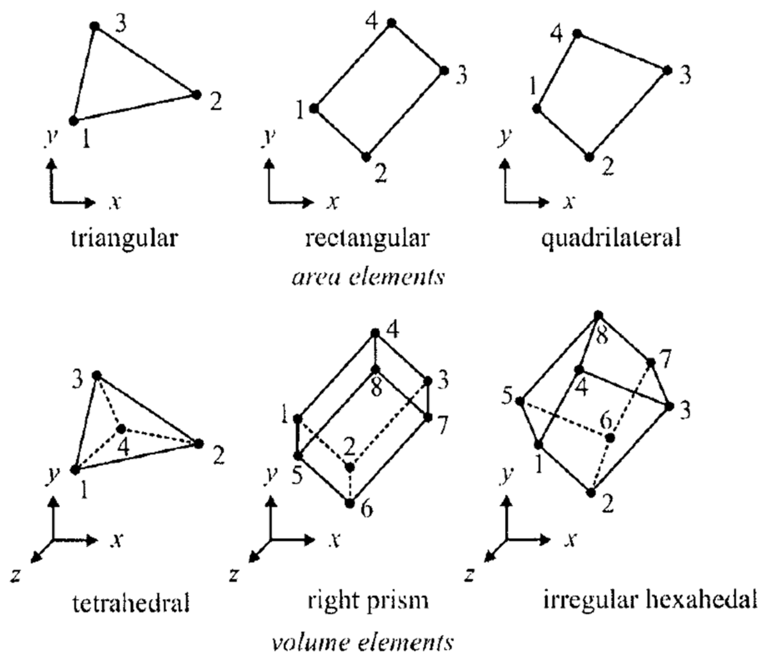

Figure 2.20 A set of structural area and volume elements (from [274])

Aforementioned investigations comprised frame analyses using one dimensional element. Turner et al. [275] were the first to use two dimensional elements to implement a plane stress analysis. And under the name of direct stiffness method they presented stiffness matrices of triangular and rectangular elements for plane stress analysis. In 1960 Clough [276] introduced the name of “finite element” in his paper on plane stress analysis by triangular and rectangular elements. In 1961 Melosh [277] derived stiffness matrix for a rectangular plate bending element. For three dimensional applications Martin [278] developed stiffness matrix of a tetrahedral element. Following, various elements were derived by researchers to proceed into solving of more complicated configurations under various loading and boundary conditions. Figure 2.20 presents a set of finite elements used in today’s structural analysis.

Non-linear structural analysis using FE method began with the investigation of Turner et al. [279]. They incorporated geometric non-linearity in structural analysis developing “geometric stiffness matrix”. Iterative solution technique was adopted by them in conjunction with initial constant stiffness matrix. The developed geometric stiffness matrix later became a significant tool for eigenvalue buckling analysis in literature. The work considered geometric non-linearities in a context of large displacements with small strains. In 1967 Oden [280] presented an investigation which formulated both large displacement and large strain in geometric non-linear FE concept. Attempt to include material non-linear properties in FE procedure did not take much time thanks to the investigation undertaken by Gallagher et al. [281]. Following studies by Pope [282], Marcal and King [283] and Yamada et al. [284] refined and extended the implementation of plastic material behaviour via FE solutions.

Herein, it is not intended to present a complete history of FE element method which is already presented in pertinent books and references. Moreover, the papers by Oden [285] and Felippa [286] gave comprehensive account for the development history of FE method in conjunction with matrix structural analysis. Also it requires a further work to detail the different theories behind the proposed numerous plate and shell elements. For a broader treatment of various elements such as conforming, non-conforming, hybrid and mixed elements, the reader is referred to reference by Long et al. [287].

2.4.2 Eigenvalue Buckling Analysis

FE method has been played a major role in field of stability analysis of structures since 1960s. The use of FE method in buckling analysis of structures can be mainly classified into two categories; eigenvalue buckling analysis and non-linear buckling analysis. The eigenvalue or linearized buckling analysis only considers linear material properties to compute system's initial buckling behaviour and represents Eulerian stability of discretized structures. Disregarding geometric and material non-linear properties it only considers stress stiffening effects by including geometric stiffness matrix. In a mathematical point of view it presumes that the equilibrium is unstable when the stiffness matrix of the system becomes singular;

$$det(K + \lambda K_{\sigma}) = 0 \tag{2.27}$$

λ stands for the load factor in the equation, that is to say the eigenvalue of the equation. The number of λ that satisfies above equation depends on the number of degrees of freedom defined in the system. The smallest load factor multiplied by the load in the system gives critical buckling load. In most cases critical buckling load is the most important one to be used in assessment of system stability. However the greater ones should be also processed to understand the relationship between the loads and system sensitivity. In order to capture corresponding eigenvector of each load factor which represent buckling mode of the system, following eigenvalue equation must be solved;

$$(K + \lambda_i K_{\sigma})\varphi_i = 0 \tag{2.28}$$

where λ_i represents *i'th* eigenvalue and φ_i is the corresponding eigenvector. Buckling load and associated mode should be coupled to gain knowledge on the behaviour of the structure.

The geometric stiffness matrix adopted by Turner et al. [279] contributed very much to eigenvalue buckling analysis. Although they intended to investigate geometric non-linear behaviour of aircraft components, the developed geometric stiffness matrix further became a major tool in stability analysis. Aiming at performing stability analysis Gallagher and Padlog [288] detailed theoretical derivation of geometric stiffness matrix using strain energy principle in 1963. A valuable contribution was made by Martin [289] who based the geometric stiffness matrix on a non-linear strain displacement relation of Green's strain. Derivation of geometric stiffness matrices for plate and shell elements were presented by Kapur and Hartz [290] and Gallagher et al. [291]. Carson [292] presented a detailed formulation of FE plate buckling in conjunction with the energy methods. Carson and Newton [293] adapted rectangular elements for buckling analysis of plates. Comparisons of various elements including triangular ones for plate buckling problems were presented by Clough and Felippa [294]. Studies conducted by Przemieniecki [295, 296] indicated applicability and efficiency of eigenvalue buckling analysis on plates, thin-walled columns and stiffened panels. Fujikubo and Yao [297] employed eigenvalue buckling analysis to assess their formula on local buckling strength of stiffened panels which accounts for effects of residual stresses. Since it was adopted as a computational method eigenvalue buckling analysis has been a major tool for preliminary stability assessments. Solution methods of the eigenvalue problems such as Subspace and Lanczos iterations are well documented by Bathe [266].

Eigenvalue buckling analysis only evaluates bifurcation type buckling behaviour of structures. It predicts the initiation of buckling of a linear elastic structure, and has not the capability to follow the behaviour beyond the bifurcation point. Therefore, presence of initial imperfections, plastic behaviour of materials, residual stresses and stable post-buckling behaviour of plates and plated structures call for methods that account for non-linear actions. In order to seed fully non-linear models with the shape of eigenvectors to be initial geometrical imperfections, eigenvalue buckling analysis today is used by many researchers as a preliminary stage. Since it depicts initial buckling behaviour of structures, eigenvectors are the probable shapes on a non-linear path to collapse. Figure 2.21 presents first five eigen-modes of a representative fuselage panel. In most applications incorporation of 1st mode shape was found to be quite reliable. But, for complicated behaviour it requires to incorporate a combination of different mode shapes. Mode jumping phenomenon can be cited as one of those complicated behaviour which requires consideration of multiple mode shapes.

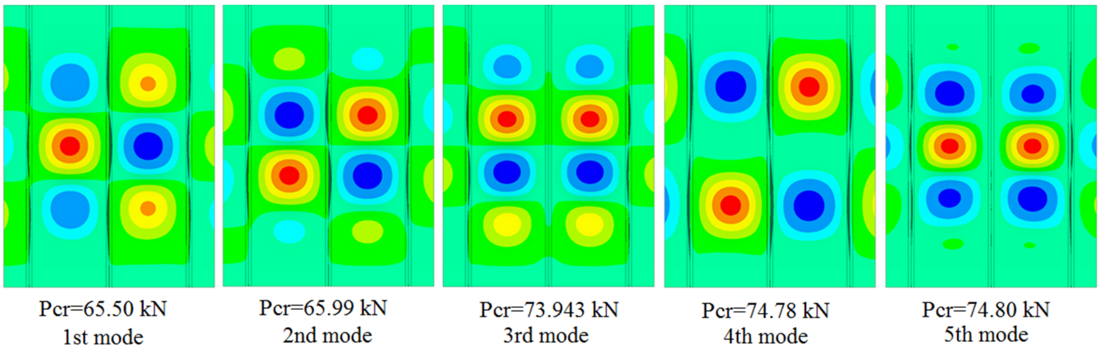

Figure 2.21 Eigen-modes of a fuselage panel

2.4.3 Non-linear Buckling Analysis via FE Method

Non-linear FE analysis requires integration of wide variety of parameters to couple all complexities into a rational solution. Although high fidelity FE models can capture real structural behaviour with very good accuracy, implementation of a non-linear problem would require substantial effort. This effort is undertaken today to solve complex structural mechanics problems including buckling problems which are not amenable to analytical solutions. Geometric and material non-linearities can be cited as two main non-linear behaviours in buckling of axially loaded structural components. The former is related to large deformations during loading and the later one is required to simulate the behaviour beyond the proportional limit of the material. Moreover, presence of initial geometric imperfections and residual stresses are other parameters that compel non-linear properties to be activated. With the intent of tracing the application of non-linear FE method in stability analysis of plates and stiffened panels this section introduces building block studies in the field.

Prior to detailing the works on non-linear buckling studies for plates and stiffened panels via FE method, it would be more convenient to underline the developed methods to solve non-liner equations of discrete systems. Although the buckling problems are handled within same context of FE non-linear analysis of structures, those problems require further precautions to be undertaken to capture instant response shift of buckling nature. Thus, non-linear buckling behaviour imposes significant challenges to FE structural analysis. In the sense of structural behaviour, buckling represents critical points in the load-displacement history. The critical points are divided into bifurcation and limit points. Bifurcation refers the point where two different equilibrium paths coincide and there is no a unique tangent at that point. Stiffness of the structure significantly decreases after bifurcation which leads deflections in the structure to increase significantly. A limit point in stability refers the point at which the tangent to the equilibrium path is zero. The common attribute of those instability behaviours lies in the fact that in both bifurcation and limit points determinant of the stiffness matrix of the system vanishes to be zero. The term collapse or failure refer the level of load corresponding to a critical point beyond the structure cannot withstand further magnitudes of load. According to the type of the structure the bifurcation point may also become limit point of the system. Axially loaded cylindrical shells tend to exhibit this kind of behaviour. However axially loaded plates and stiffened panels usually experience bifurcation points far below the limit points.

Bifurcation buckling is generally considered in the frame of eigenvalue buckling analysis which accounts for linear elasticity with small displacements. Nevertheless, existing initial imperfections, as already noted, lead the deflections to start from the beginning of the loading, hiding the sudden bifurcation behaviour. Such a response calls for non-linear properties to be activated. Also evaluation of limit points for plates and stiffened panels requires non-linear methods, since the limit points take place far above the bifurcation point in those structures. Thus, the non-linear analysis becomes inevitable to compute stability behaviour of plated structures.

Solution of non-linear equations of stability problems via FE method mainly can be classified into two approaches, perturbation and continuation methods [298, 299]. The perturbation methods rely on the approach developed by Koiter [87] who proposed a general method for bifurcation problems of non-linear elasticity. The method considers power series expansion techniques and so approximates equilibrium surfaces only locally around the bifurcation points. Displacements and loads are expanded around the critical point using power series with a single parameter. The slope of the post-critical response is determined by differentiation of parametric representation of load-displacement behaviour. The asymptotic nature of the method raised several questions when considering highly non-linear problems [300]. Incorporation of the perturbation method into non-linear FE solutions was performed by several authors, eg. Thompson and Hunt [301], Ecer [302] and Hangai and Kawamata [303]. Further attempts by Haftka et al. [304], Mallet and Haftka

[305] and Carnoy [306] were also made to extend the perturbation method to predict limit point instabilities.

As opposed to perturbation methods, continuation methods are not confined into a specific region of solution domain [298]. Continuation methods adapt iteration techniques. In a step-by-step manner they compute a set of points in load displacement path to capture stability behaviour. A Newton-Raphson type iteration scheme which linearizes the incremental steps generally dominates the step-by-step procedure of continuation methods. The importance of the linearization in non-linear computational solid mechanics was treated by Hughes and Pister [307]. The pioneering works which adapted Newton-Raphson type iterative technique into stability problems can be cited as the studies by Buechner et al. [308], Riks [309] and Mau and Gallagher [310]. The method can be mathematically delineated as follows;

If we presume a convergence at time t and look for a solution at time $t + \Delta t$ which corresponds to a load increment of Δf^{ext}, the residual load vector is given by;

$$ {}^{t+\Delta t}_{0}r = {}^{t+\Delta t}\lambda f^{ext} - {}^{t}f^{int} \tag{2.29} $$

Left subscripts in the equations refer iteration number. Proceeding to solve first iteration following equation arises;

$$ {}^{t+\Delta t}_{0}K_T \ {}_{1}\delta u = {}^{t+\Delta t}\lambda f^{ext} - {}^{t+\Delta t}_{0}f^{int} \tag{2.30} $$

where K_T represents tangent stiffness matrix and ${}_{1}\delta u$ represents the change in the displacements in first iteration. Equating ${}^{t+\Delta t}_{0}K_T = {}^{t}K_T$ and ${}^{t+\Delta t}_{0}f^{int} = {}^{t}f^{int}$, following equation is employed to evaluate ${}_{1}\delta u$;

$$ {}_{1}\delta u = {}^{t}K_T^{-1}({}^{t+\Delta t}\lambda f^{ext} - {}^{t}f^{int}) \tag{2.31} $$

With above equation first prediction of displacement increment corresponding to applied external loading ${}^{t+\Delta t}\lambda f_{ext}$ is provided. Following, an updated version of the displacement can be obtained;

$$ {}^{t+\Delta t}_{1}u = {}^{t}u + {}_{1}\delta u \tag{2.32} $$

Considering the updated displacements a new internal force vector ${}^{t+\Delta t}_{1}f_{int}$ is developed and new residual force vector becomes;

$$ {}^{t+\Delta t}_{1}r = {}^{t+\Delta t}\lambda f^{ext} - {}^{t}_{1}f^{int} \tag{2.33} $$

An updated tangent stiffness matrix is then incorporated into equation to evaluate next displacement increment;

$$ {}_{2}\delta u = {}^{t+\Delta t}_{1}K_T^{-1}({}^{t+\Delta t}\lambda f^{ext} - {}^{t}_{1}f^{int}) \tag{2.34} $$

Updated displacement vector becomes;

$$ {}^{t+\Delta t}_{2}u = {}^{t+\Delta t}_{1}u + {}_{2}\delta u \tag{2.35} $$

Above process must be repeated until the defined convergence limits for residual forces are satisfied.

$$ \|{}^{t+\Delta t}_{n}r\| / \|{}^{t+\Delta t}_{0}r\| \leq \mathcal{E}_{tol} \tag{2.36} $$

where $\mathcal{E}_{tol}$ is a sufficiently small convergence tolerance.

Figure 2.22 visualizes the Newton-Raphson iterative process for an idealized one degree of freedom case.

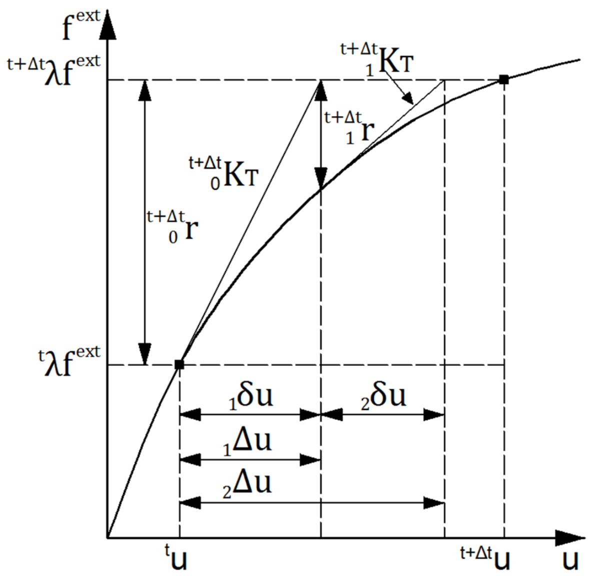

Figure 2.22 Full Newton-Raphson scheme

A simpler approach to reduce the computational cost is also present in the concept of iterative techniques which are called as modified Newton-Raphson methods. These methods consist of replacing the tangential stiffness K_T , which in the standard method is updated in every iteration, by a constant counterpart [311]. The use of initial tangent stiffness throughout all increments and the use of a constant stiffness which is updated at the beginning of each increment are the present options of modified version. The modified versions of the method were used by Oden [312], Zienkiewicz [313] and Owen and Hinton [314]. Although modified versions simplifies the evaluation process of tangent stiffness matrix, they lead to slower convergence rates because of required more iteration within each increment. In this manner a full Newton-Raphson algorithm performs better.

An efficient tracing of non-linear load displacement path to simulate instabilities involved in the structure demands to accurately evaluate limit points. Unfortunately, conventional Newton-Raphson method which evaluates displacement increments for a given fixed load step falls short when the tangent stiffness matrix approaches zero. In a force controlled scheme, as shown in Figure 2.23, when the limit point is reached tangent stiffness matrix becomes perpendicular to external force axis. At this point the tangent stiffness matrix takes a singularity form and convergence cannot be satisfied anymore [299]. This point may represent a local limit point beyond the structure may resist larger magnitudes of loading after a snap-through behaviour. The works presented by Reddien [315] and Rothwell and Drachman [316] detail this ill conditioned singularity problem of Newton-Raphson method in a mathematical point of view.

Some modifications in Newton-Raphson method were made to deal with such behaviours. Regarding this behaviour, force increment technique was replaced with displacement increment to offer more efficient solutions. The displacement controlled Newton-Raphson method dates back to the investigation presented by Argyris [317]. Further improvements were proposed by Roberts and Ashwell [318] and Pian and Tong [319]. The works by Batoz and Dhatt [320], and Powell and Simon [321] contributed very much to development process of displacement controlled non-linear FE analysis. Even though displacement controlled scheme offers more powerful non-linear stability analysis compared to a force controlled one it has a further constraint. In this case the tangent stiffness matrix becomes singular in displacement limit points where the load displacement response is vertical, precluding tracing snap-back behaviour. Figure 2.23 provides a clear vision on the limits of force controlled and displacement controlled Newton-Raphson methods.

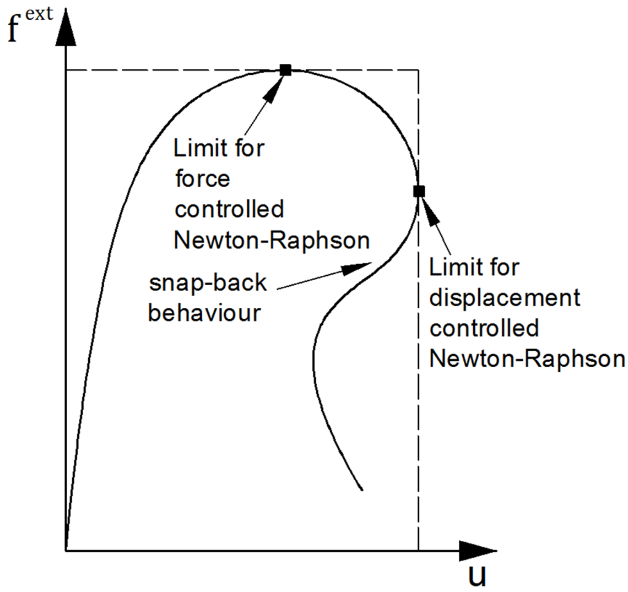

Figure 2.23 Limit points for Newton-Raphson techniques

Although Newton-Raphson methods served as the basis for non-linear FE buckling analysis, further sophistications were required to pass limit points to capture highly non-linear transitions. To this end, we need to refer another continuation technique called arc-length method which is the most popular in tracing very complicated paths such as snap-through and snap-back behaviours. Arc-length method was originally developed by Riks [309, 322] and Wempner [323]. In this method, the constraint involves the incremental nodal displacements and, possibly, also the load parameter increment [324]. In this sense, Crisfield [267] refers the method as a modified form of displacement control technique. Employing the method successfully for highly non-linear behaviours, Crisfield [325] proposed a quadratic control on the constraint which always intersects equilibrium paths. Closed constrain surface as a result of quadratic control provides the successful intersections. The difference between Riks's and Crisfield's approaches lies in the fact that Riks technique iterates along a hyper plane orthogonal to the tangent of the arc-length, Δl, from last converged point whereas Crisfield technique iterates along a hyper sphere. This feature of Crisfield's approach provides more powerful solutions in highly non-linear behaviours [324].

Since the arc-length method introduces both displacement increments, Δu, and load increment, $\Delta\lambda$, as unknown variables, it is required to solve $n+1$ variables in a model which has n degrees of freedom. The load increment is governed by the following;

$$ {}_{i}\Delta u^{T}\ {}_{i}\Delta u + \ {}_{i}\Delta\lambda^{2}\psi^{2} {f^{ext}}^{T} f^{ext} = \Delta l^{2} \qquad (2.37)$$

where ψ stands for scaling parameter to determine load contribution which depends the scaling between the load and displacement terms [267]. The iterations in the method are performed using full or modified Newton-Raphson methods. Adapting an approach proposed by Batoz and Dhatt [320] for displacement control the load increment parameter can be found tracing the quadratic equation given by;

$$a_{1}\ {}_{i}\delta\lambda^{2} + a_{2}\ {}_{i}\delta\lambda + a_{3} = 0 \qquad (2.38)$$

where the coefficients:

$$a_{1} = \delta u_{t}^{T}\delta u_{t} + \psi^{2} {f^{ext}}^{T} f^{ext} \qquad (2.39-a)$$

$$a_{2} = 2\delta u_{t}(\ \Delta u + \delta\bar{u}) + 2\ \ \Delta\lambda\psi^{2} {f^{ext}}^{T} f^{ext} \qquad (2.39-b)$$

$$a_{3} = \left(\ \Delta u + \delta\bar{u}\right)^{T}\left(\ \Delta u + \delta\bar{u}\right) - \Delta l^{2} + \ \Delta\lambda^{2}\psi^{2} {f^{ext}}^{T} f^{ext} \qquad (2.39-c)$$

and δu_{t} is the displacement vector which is associated to load vector;

$$\delta u_{t} = K_{T}^{-1} f^{ext} \qquad (2.40)$$

In modified Newton-Raphson iterative scheme it is enough to compute δu_{t} at the first iteration of each increment. $\delta\bar{u}$ represents iterative displacement resulting from a force controlled Newton-Raphson algorithm;

$$\delta\bar{u} = -K_{T}^{-1} r \qquad (2.41)$$

Incremental displacement for the next iteration can be given by;

$$ {}_{i+1}\delta u = \ {}_{i}\delta\bar{u} + \ {}_{i}\delta\lambda\ {}_{0}\delta u_{t} \qquad (2.41)$$

Figure 2.24 indicates the iterative process of the arc-length method combined with modified type of Newton-Raphson technique on a one degree of freedom idealization with the different approaches of Riks and Crisfield.

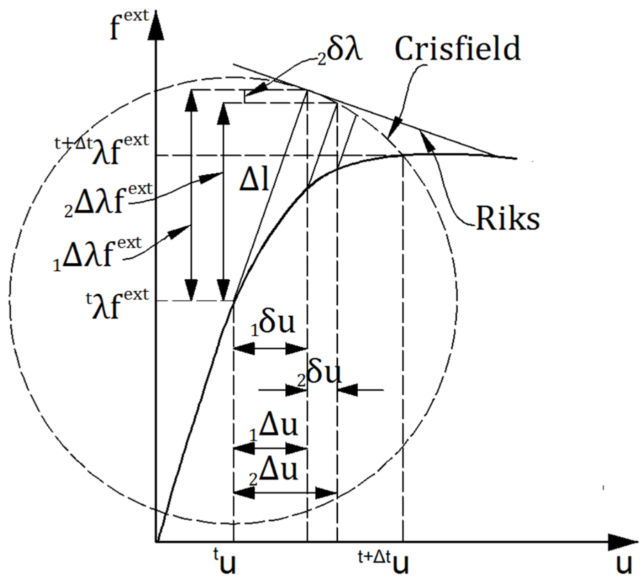

Figure 2.24 Arc-length scheme

In general manner arc-length methods were shown to correlate well with the expected results of highly non-linear problems given wide range of parameters tested. Also, Crisfield [325] indicated that for the practical problems the scaling parameter, ψ, had little effect, so it could be set to zero to simplify the procedure. Setting the ψ to zero leads to constraint surface to be cylindrical rather than spherical. A comprehensive discussion and formulation of the subject are present in the reference by Crisfield [267].

Incorporation of different algorithms into non-linear FE solutions also required to compare the performances of those methods on some benchmark problems. These comparisons generally belong to the years of development process. Presenting detailed formulations, Riks [298] also compared the performances of perturbation and continuation methods. Considering representative benchmark problems Padovan [326] compared the performances Newton-Raphson and arc-length methods. Focusing on singular points in load displacement paths Shi [299] reviewed and compared non-linear FE techniques. Many other investigations were also devoted to assessment of non-linear FE solution techniques for buckling and some proposals on methods such as the works by Lam and Morley [327], Krishnamoorthy et al. [328], Csébfalvi [329], Teng and Luo [330], Lopez [331], Kim and Kim [332], Ronnau [333], Ragon et al. [334], Yuanqi and Zuyan [335], Kwon et al. [336] and Corrêa and Camotim [324].

The methods presented here constitute the main skeleton of the FE solution of non-linear stability problems. Besides, there exist some techniques which are used to improve the quality of Newton-Raphson and arc-length iterations. For instance, line search method is the one that needs to be cited among those methods. It is used in non-linear FE algorithms to optimize the step size during iterations. The mathematics behind line search and other improving techniques can be found in the references by Owen [311] and Crisfield [267].

2.4.4 Non-linear FE Buckling Analysis of Plates and Stiffened Panels

The literature contains significant amount of investigations on plates and stiffened panels using non-linear FE methods. To the knowledge of author FE non-linear buckling analysis of plates was first studied by Murray and Wilson [337] in 1969. Using principle of virtual work and employing incremental equilibrium equations they investigated the post-buckling behaviour of plates by FE method. Adapting a tensor based FE approach in conjunction with triangular elements Vos [338] investigated geometrically non-linear buckling behaviour of plates. Use of Newton-Raphson technique for the iterative procedure was proposed by Roberts and Ashwell [318] for the post-buckling solution of square perfect plates. Kawai and Yoshimura [339] presented a solution procedure which combines FE method and Raleight-Ritz procedure to study buckling of rectangular plates. Pica and Wood [340] used Mindlin shallow shell formulation to analyse post-buckling behaviour of plates.

If the structure exhibits a non-linear material behaviour prior to buckling or in post-buckling range, as indeed the majority of practical thin-walled structures do, the inelastic behaviour of material must be accounted for in analysis stage. Moreover a buckling collapse may arise as a result of strain softening of material, plastic strain localization and energy release through elastic unloading [324]. Initial post-buckling FE analysis for plates with plastic material behaviour considered elastic-perfectly plastic material models. An elastic-perfectly plastic material model for FE plate buckling analysis was adapted by Terazawa et al [341]. Crisfield [342] used rectangular elements with five degrees of freedom for the FE post-buckling analysis of plates. Ilyushin yield criterion with an elastic-perfectly plastic material model was used by him. Modified Newton-Raphson scheme was adapted during the solutions. Lee [343] used virtual work and minimum potential energy theories in conjunction with a full Newton-Raphson iterative FE method to analyse post-buckling behaviour of plates. Elastic-perfectly plastic and linear strain hardening material models were adapted by him under von Mises yield criterion with isotropic hardening material behaviour. The investigation by Roca et al. [344] incorporated both geometrically and material non-linear properties into FE equations of nine node shell element to trace post-buckling behaviour of steel plates. In geometrical non-linear properties they activated only large displacement characteristics and a bilinear kinematic hardening stress-strain diagram with von Mises yield criterion represented the plastic material behaviour.

Although thin-walled structures are composed of plate segments as detailed previously, it was necessary to improve the prediction quality by moving forward from an isolated plate analysis. Serious difficulties encountered in connection of analysis results of constituent elements with design of complicated configurations stimulated focusing on representative models. In this respect, early attempts in the past by aircraft engineers to design wings and fuselages and marine engineers to design ship hulls with bigger FE models created the basis of today's modern design methodologies. A problem of particular interest was the solution time of computational non-linear FE evaluations to represent the behaviour of bigger components with too many degrees of freedom. This challenge was handled with the significant development in computer technology. Today bigger models do not affect the designs much, on account of modern computers' power. Developments in non-linear FE buckling analysis of stiffened panels can be considered within this frame in literature.

In 1976 Crisfield [345] proposed the full section yield criterion to be adapted in FE elasto-plastic buckling analysis of stiffened panels. The theory assumes that behaviour of material is elastic until yield takes place and a sudden fully plastic response of shell element follows this behaviour. It was not a complete representation of the behaviour but was effective in terms of computational cost considering the computers at that time. O'Leary and Harari [346] proposed a simplified approach to analyse ultimate capacity of panels which combines beam elements for stringers and plate elements for panel skin. Towards this aim they modified the stiffness matrix of plate elements to account for a joined beam element. A similar approach was presented by Fujikubo and Kaeding [347] who used plate and beam column elements to simulate non-linear buckling of stiffened panels. Element formulations allowed local plate buckling and overall stringer buckling. Performance of an isoparametric type element with 16 nodes and five degrees of freedom in evaluation of geometric non-linear post-buckling strength of stiffened panels was assessed by Ise [348]. Considering geometrical and material non-linear properties Nordsve and Moan [349] presented a finite element model for compression driven stiffened panels. Cho et al. [350] presented a shell finite element with six degrees of freedom per node to analyse geometrically non-linear post-buckling behaviour of stiffened panels. They also compared performance of element with the proposed elements in literature with five degrees of freedom per node.

2.4.4.1 Building Verified Models

In terms of picturing well adapted FE techniques for the ultimate strength assessment of steel stiffened ship panels, references presented by Paik et al. [351, 352] and Paik and Seo [353, 354] are important. They detailed the techniques of introducing imperfections, non-linearities and boundary condition modelling into FE models to obtain reliable buckling response. Idealization errors for non-linear behaviour of compression loaded aluminium fuselage panels was treated by Campell et al. [355]. Focusing on panels with riveted Z shaped stringers the possible approaches in modelling of material, loading geometrical configuration, rivets, imperfections and fillets are presented with the impacts on collapse load. As discussed in previous sections aluminium materials require non-linear stress-strain curves to be considered in FE models. In this sense, importance of Ramberg-Osgood type non-linear material modelling for aluminium fuselage panels under compression was presented Duarte et al [356]. For aluminium and other materials which exhibit fully non-linear stress-strain behaviour such as stainless steel and some high strength steels, material modelling was detailed by Gardner and Ashraf [39]. Herein it is worth noting that FE modelling of buckling and collapse of compression surfaces with broader treatments of modelling geometric and material non-linearities and non-linear solution algorithms are detailed in a guidance presented by Falzon and Hitchings [357]. This reference is strongly recommended for those readers who are interested in FE modelling of buckling. Considering geometrical non-linear behaviour Belesis and Labeas [358] proposed the use of super element approach in non-linear FE concept to simulate large scale fuselage post-buckling behaviour. The approach has the potential to include material non-linearity to provide complete FE representation of large scale structures.

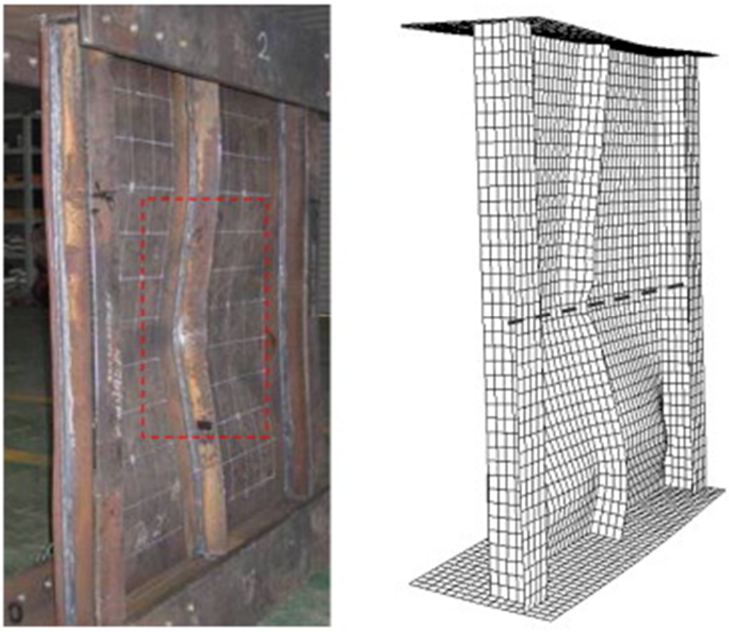

Figure 2.25 Non-linear FE model vs. test for a bridge panel (from [226])

Although today's FE technology has the potential to simulate very complex buckling problems including the stiffened panel behaviour, a great caution must be exercised before running the model and in post-processing of the results. The best way to verify the accuracy of the model is the experimental studies which exactly indicate the behaviour. The motivation for experiments was underlined in previous sections and by Singer et al. [17]. After proving the accuracy of the model the research can be extended via FE models to reduce research costs and save time. In this context, FE analyses are considered as complementary to experimental investigations to achieve a fast final product. The literature contains such verification studies. For bridge panels non-linear FE models were assessed against test results by Choi et al. [226], Figure 2.25.

Chen et al. [245] and Grondin et al. [359] conducted the non-linear FE buckling analyses in conjunction with experimental works for single stringer steel ship panels. Another study on single stringer ship panels which combines experimental and non-linear FE works was presented by Hu and Jiang [360]. In an attempt to simulate effect of corrosion on stiffened panel ultimate capacity, Dunbar et al. [361] calibrated their non-linear FE model against a test result of single stringer ship panel. The measured values were incorporated into FE models to obtain rational results.

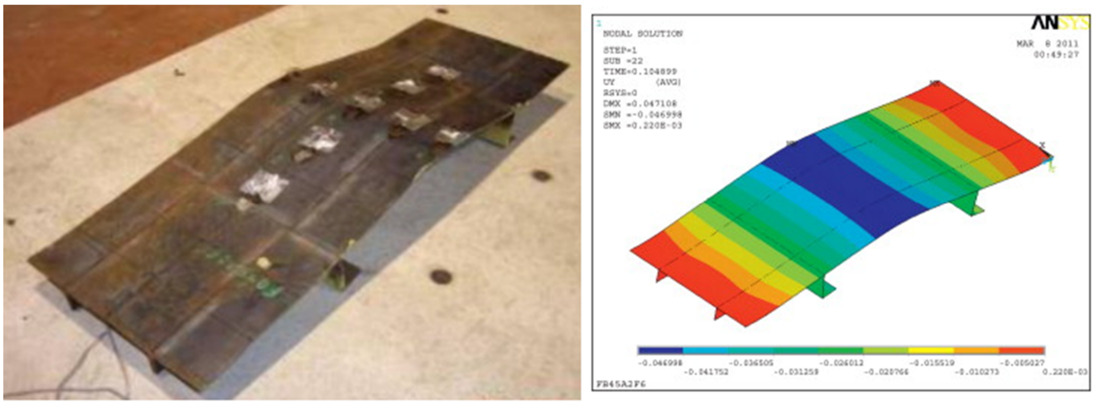

Figure 2.26 Non-linear FE model vs. test for a ship panel (from [362])

Shanmugam and Arockiasamy [363] tested 10 multi-stringer ship panels under different combinations of lateral and axial loadings. Panels were stiffened by longitudinal and transverse stringers. Test behaviours were also simulated with successful non-linear FE models. Comprehensive investigations undertaken by Xu and Soares [362, 364, 365] fit very well to the concept of non-linear FE model verification. Their experimental programs include tests of multi-bay multi-stringer narrow and wide ship panels with flat, L shaped and U shaped stringers. They developed high fidelity non-linear FE models to simulate the tests, Figure 2.26.

Contributions of Queen's University Belfast to the understanding and implementation of aircraft stiffened panels in pre-buckling, post-buckling and collapse regimes are very important for literature. High fidelity FE simulation works give comprehensive account for modelling of compression loaded aircraft panels. Advanced testing facilities at Queen's are used to validate the developed FE models. Within the frame of sub-section modelling of fuselage panels Murphy et al. [155] and Lynch et al. [366] simulated the non-linear buckling and collapse behaviours of single stringer single bay and multi-stringer multi-bay laboratory specimens, Figure

2.27. Both specimens consist of riveted bulb stringers on flat skins. Various FE models were developed with presented details to create representative riveting models. FE simulation results were shown to correlate very well with the tests for complete history of load-displacement path. Further efforts were performed by Özakça et al. [367] and Murphy et al. [368] to simulate the non-linear buckling behaviour of integrally machined and locally sub-stiffened fuselage panels in conjunction with verification tests. Aiming at investigation of performance of various sub-stiffening concepts including prismatic and non-prismatic ones Quinn et al. [369, 370] simulated different types of integrally machined panel tests. Having verified the developed FE models with the experimental results of single bay panels, the studies were extended to investigate the sub-stiffening performance for multi-bay versions of tested panels.

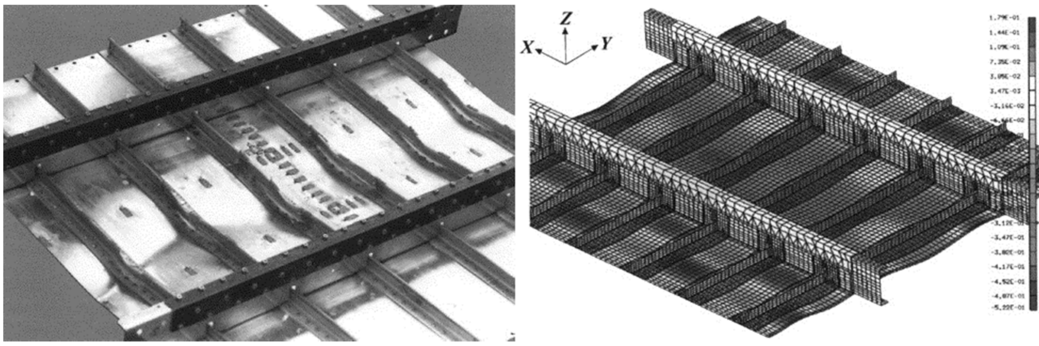

Figure 2.27 Non-linear FE model vs. test for a fuselage panel (from [366])

It should be introduced here that the models developed by Chen et al. [245], Grondin et al. [359] and Hu and Jiang [360] employed measured geometrical imperfections of test specimens in non-linear simulations whereas the works by Xu and Soares [362, 364, 365], Murphy et al. [155, 368], Lynch et al. [366] and Özakça et al. [367] used eigen-mode shapes to represent initial geometrical imperfections. On the other hand Quin et al. [369, 370] incorporated both measured imperfections and eigen-mode shapes into FE models to investigate the impacts. A different approach which implies the use of a single half-wave shape bow imperfection in FE models was employed by Dunbar et al. [361] and Shanmugam and Arockiasamy [363]. Also Chen et al. [245], Grondin et al. [359] and Hu and Jiang [360] introduced measured residual stresses which were induced by welding of stringers into FE models to obtain the effects on panel strength.

2.4.4.2 Non-linear FE models vs. Closed Form Solutions

Practical analysis and design formulations or charts have been very attractive to engineers who are responsible in the field of application. Simple equations are preferred in this field for preliminary designs rather than looking for testing opportunities and building complicated FE models. In this respect, literature contains valuable works for different disciplines which were headed to assess the present equations against the results obtained from testing or non-linear FE simulation. Also many studies were conducted to propose new empirical equations for compression loaded stiffened panels using statistical methods. Zha and Moan [371] simulated the compression loaded aluminium alloy stiffened panel tests to investigate torsional failure modes of flat stringers. Compressive strength prediction methods such as DNV and Eurocode-9 were assessed against test and non-linear FE simulation results. Hughes et al. [372] compared non-linear FE analysis results with orthotropic plate theory and beam method. Paik and Kim's [373] effort for steel ship stiffened panels have been referred widely in literature. Six collapse modes were referred for compression loaded stiffened panels. Various approaches were considered such as orthotropic plate theory, Perry-Robertson approach, effective width method and Johnson-Ostenfield formulation to compare with tests and FE results. In a comprehensive study which combines experimental testing of aluminium alloy marine, aerospace and land based stiffened panels and non-linear FE simulations Paik et al. [374] assessed the prediction methods used in three disciplines. Euler-Johnson, DNV, Eurocode-9 and Aluminium Association approaches were the considered prediction methods in the study. A database of 78 tests of aluminium alloy ship panels was extended employing non-linear FE simulations by Paik et al. [247] and Paik [375] to propose compressive strength empirical equations. MIG welding was used in manufacturing processes of specimens. Equations were generated using statistical regression methods and covered panels stiffened by flat bar, L shaped and T shaped stringers. In a following study Paik [248] employed non-linear FE analysis to simulate the behaviour of aluminium alloy panel tests which were assembled using FSW. He concluded that panels manufactured using FSW have exhibited better performance than that of panels assembled using MIG welding. Closed form empirical equations for compressive strength prediction of a representative plate-stringer combination proposed by Paik and his colleagues can be summarized as follows;

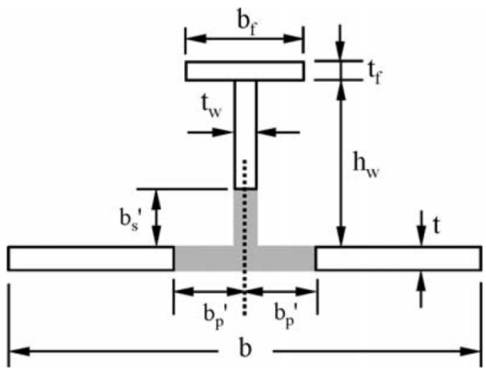

Figure 2.28 Plate stringer combination (from [374])

$$\sigma_u = \frac{\sigma_{Yseq}}{\sqrt{C_1 + C_2(\lambda)^2 + C_3(\beta)^2 + C_4(\lambda\beta)^2 + C_5(\lambda)^4}} \leq \frac{\sigma_{Yseq}}{(\lambda)^2} \tag{2.42}$$

where β denotes plate slenderness ratio

$$\beta = \frac{b}{t}\sqrt{\frac{\sigma_{Yp}}{E}} \tag{2.43}$$

and λ denotes column slenderness ratio

$$\lambda = \frac{a}{\pi r}\sqrt{\frac{\sigma_{Yseq}}{E}} \tag{2.44}$$

r is the radius of gyration, σ_{Yp} is equivalent plate yield stress and σ_{Yseq} is equivalent yield stress of plate stiffener combination. For welded steel panels Paik and Thayamballi [376] proposed the coefficients $C_1 - C_5$ to be ;

$$C_1 = 0.995,\ C_2 = 0.963,\ C_3 = 0.170,\ C_4 = 0.188,\ C_5 = -0.067 \tag{2.45}$$

For MIG welded aluminium alloy stiffened panels Paik [375] and Paik et al. [247] further derived the coefficients;

For the panels with T shaped and L shaped stringers;

$$C_1 = 1.318,\ C_2 = 2.759,\ C_3 = 0.185,\ C_4 = -0.177,\ C_5 = 1.003 \tag{2.46}$$

For the panels with flat bar stringers panel strength would be the minimum of the Eq. 2.47-a evaluated with following coefficients and the Eq. 2.47-b.

$$C_1 = 2.5,\ C_2 = -0.588,\ C_3 = 0.084,\ C_4 = 0.069,\ C_5 = 1.217 \quad (2.47 - a))$$

$$\frac{\sigma_{Yseq}}{\sqrt{-16.297 + 18.776(\lambda) + 17.716(\beta) - 22.507(\lambda\beta)}} \quad (2.47 - b)$$

This concept was shown to correlate well with the test results by Paik. Reviewing the Paik and colleagues' proposals for ship panels Khedmati et al. [377] followed the same path to derive more efficient coefficients which are directly linked to water head, h (pressure). In order to generate a database they performed a comprehensive non-linear FE simulation series of aluminium alloy panels. Introducing the head into formulations allowed evaluating the compressive strength of panels with desired level of lateral loadings. Thus, the coefficients were formulated by Khedmati et al. [377] for the panels with T shaped stringers as follows;

$$C_1 = -0.001h^2 - 0.071h + 0.731 \quad (2.48 - a)$$

$$C_2 = -0.023h + 0.162 \quad (2.48 - b)$$

$$C_3 = -0.057h^2 + 0.235h + 0.483 \quad (2.48 - c)$$

$$C_4 = 0.004h^2 + 0.016h + 0.014 \quad (2.48 - d)$$

$$C_5 = 0.033h^2 - 0.151h + 0.096 \quad (2.48 - e)$$

For the panels for flat bar stringers;

$$C_1 = -0.002h^2 - 0.002h + 1.355 \quad (2.49 - a)$$

$$C_2 = -0.001h^2 + 0.018h + 0.11 \quad (2.49 - b)$$

$$C_3 = 0.008h^2 - 0.102h + 0.081 \quad (2.49 - c)$$

$$C_4 = 0.016h^2 - 0.072h + 0.342 \quad (2.50 - d)$$

$$C_5 = -0.006h^2 + 0.089h - 0.203 \quad (2.49 - e)$$

Zhang and Khan [378] used the test data of steel ship panels present in literature to verify the non-linear FE analyses. They proposed s simple empirical equation for a specific range of geometrical configurations. Choung et al. [379] conducted extensive non-linear FE analyses of wide ship panels and consulted International Association of Classification Societies (IACS) ultimate strength curves for comparisons. Focusing on steel bridge panels Choi et al. [226] undertook non-linear FE simulations. AASHTO prediction technique was then utilized to experience performance of specification. Multiple design specifications such as AASHTO specification, SSRC methods and Eurocode-3 were assessed by Kwon and Park [380] against test and non-linear FE analysis results. Shin et al. [381] developed non-linear FE models for steel bridge panels stiffened by closed shape stringers and presented the results with AASHTO and Eurocode-3 prediction comparisons.

Since no an exact specification is present for aerospace panels, number of researches on assessment of closed form solutions is less than the researches in marine and civil engineering fields. However, this field in aerospace sciences is not completely abandoned. Initial sizing methods such as Euler-Johnson combined with effective width method and crippling strength formulations find some counterparts in recent literature. Bruhn [200] explains all details of initial sizing procedures for aerospace structures. van der Veen [382] examined Euler-Johnson method using the non-linear FE analyses results of fuselage panels stiffened by T shaped stringers. An efficient initial sizing algorithm called equivalent section method and based on effective width approach which accounts for local material property degradation in Heat Affected Zone (HAZ) and residual stresses was followed by Murphy et al. [383] and Wilson et al. [384]. Effect of HAZ on panels strength was represented by reducing the thickness of material within the HAZ with a factor associated with ratio of degraded material strength and parent material strength. Effect of compression residual stresses was also considered using basic approach in literature. Both studies included advanced non-linear FE analyses and laboratory tests. Method was applied to panels which were assembled using laser beam welding and FSW. Method was shown to be satisfactory for initial sizing purposes.

It must be noted here that the non-linear FE simulations performed by Zha and Moan [378], Paik and Kim [373], Paik [248], and Wilson et al. [384] used measured geometrical imperfections of test specimens. On the other hand in the studies by Paik and his colleagues [247, 374, 375] initial imperfections were introduced into FE models using sinusoidal type formulations with the magnitudes assigned after statistical refinement of measured values. Choung et al. [379] also used sinusoidal type formulations for initial geometrical imperfections. Another approach by Khedmati [377], Kwonand and Park [380] and Shin et al. [381] employed single half-wave bow type initial imperfections. And eigen-mode shape imperfections were used by Hughes et al. [372], Choi et al. [226], Zhang and Khan [378] and Murphy et al. [383]. Measured weld induced residual stresses were incorporated into FE models by Paik and colleagues [247, 248, 373, 375] and Wilson et al. [384] whereas Zha and Moan [371], Choung et al. [379], Kwon and Park [380] and Shin et al. [381] used some magnitudes proposed in literature for FE models. HAZ material degradations were represented in FE models using the measured values by Zha and Moan [371], Paik [248], Murphy et al. [383] and Wilson et al. [384]. In the studies by Paik and colleagues [247, 374, 375] HAZ material properties in the FE models were defined using some recommended HAZ stress-strain curves.

2.4.4.3 Non-linear FE Models for Parametric and Sensitivity Studies

In the design of metal stiffened panel structures engineers are confronted with a great number of questions, including effects of parameters such as material properties, geometrical details and manufacturing imperfections. Since most of the today's thin-walled structures work in non-linear range, it is impossible to deploy analytical methods into investigation of these large numbers of parameters. Moreover, experimental methods are not completely appropriate to investigate such parameters in a systematically manner. Most of the parameters such as manufacturing imperfections cannot be controlled in laboratory specimen design. This makes non-linear FE analysis a perfect tool to be employed in investigation of parameters involved in design of stiffened panels. In this manner, various sensitivity studies on parameters were conducted on buckling behaviour of stiffened panels using non-linear FE methods. Grondin et al. [385] proceeded to investigate effects of shape and magnitude of initial imperfections, magnitude of residual stresses, plate slenderness ratio, plate aspect ratio and plate to stringer cross sectional area ratio on compressive strength capacity of steel ship stiffened panel. In another study presented by Sheikh et al. [386] non-linear FE models were developed to characterize plate transverse slenderness, slenderness of web and flanges of stringer, torsional slenderness of the stringer to transverse slenderness of plate ratio effects. Rigo et al.[387] performed a comprehensive numerical sensitivity study with many participants to assess impacts of weld location, HAZ material properties, HAZ width and imperfections on MIG welded aluminium stiffened multi-bay panels. For steel ship stiffened panels Khedmati et al. [388] focused on the effects of plate width to thickness ratio, aspect ratio and stringer type. Another works by Khedmati et al. [389] presented results of a parametric study on aluminium panels which characterized initial geometrical imperfections, HAZ properties and residual stresses. A more recent study by Paulo et al. [390] was devoted to perform a detailed sensitivity study on initial geometrical imperfections for aluminium stiffened panels with open and closed section stringers. Xu and Soares [391] developed non-linear FE models to investigate locally dented multi-bay steel ship panels.

For aircraft panels also there exist some devoted parametric and sensitivity studies to characterize effects of some manufacturing residuals on compressive strength of fuselage and wing panels. Characterisation FSW residual effects and identification of dominant parameters on aluminium fuselage panel initial skin buckling and collapse performances were presented by Murphy et al. [392-394] using non-linear FE models. The investigations were focused on single stringer [392], multi-stringer [393] and multi-stringer and multi-bay panels [394]. HAZ properties and width, magnitude of residual stresses, weld joint width and location were the primary concerns for the assessments. Using non-linear FE models Yoon et al. [395] particularly focused on weld induced HAZ effects on collapse performance of aluminium wing panels. Tweedy et al. [396] conducted non-linear FE analyses to compare the compression performances of stiffened panels assembled using FSW and conventional riveting. Aiming at investigation of buckling and collapse behaviours of aluminium fuselage panels with dents Lang and Kwon [397] conducted non-linear FE analyses.

As with the previous investigations, various investigations in this heading used various techniques to represent manufacturing imperfections in FE models. Sinusoidal type formulations to simulate local mode of geometrical imperfections were used by Grondin et al. [385] and Xu and Soares. Bow type geometrical imperfection was used by Sheikh et al., [386], Rigo et al. [387], Khedmati et al. [389] and Yoon et al. [395]. Eigen-mode shape initial geometrical imperfections was preferred by Khedmati et al. [388]. On the other hand since Paulo et al. [390] focused on geometrical imperfection effects, they used various types of idealizations stated above. A different approach was employed by Murphy et al. [392-394] to seed the models with geometrical imperfections. They used a preliminary stress analysis stage before a fully non-linear collapse analysis, using measured residual stresses to represent weld induced imperfections. Lang and Kwon [397] performed a dynamic impact analysis to represent the dent geometrical imperfections. Residual stresses in FE models were represented by referring yield stress of materials. A fraction of yield stress of parent material was used by Grondin et al. [385] Sheikh et al.[386]. Yield stress of HAZ material was used as magnitude of residual stresses by Rigo et al. [387] and Khedmati et al. [389]. Murphy et al [392-394] based the residual stress magnitude on measured values and varied the magnitudes for parametric study. Lang and Kwon [397] and Xu and Soares [391] used the magnitudes resulted from preliminary analysis stages to represent residual stresses. Rigo et al. [387], Khedmati et al. [389],Yoon et al. [395] and Paulo et al. [390] used the data available in literature to include HAZ material degradation. Measured properties of HAZ were the base for non-linear FE analyses performed by Murphy et al. [392-394].

CHAPTER 3

FINITE ELEMENT SIMULATIONS AGAINST EXPERIMENTS

3.1 Introduction

Lap joints are widely employed in aerospace stiffened panels to assemble the skin and stiffener sub-components together. The assembled panels are required to resist in-service loading conditions without loss of joint integrity for a successful structural design. For large zones of aircraft structure, for example the lower fuselage or upper wing, the extreme loading is compressive and the buckling collapse performance of the panel governs structural design. What is more to increase structural efficiency for panels in insensitive aerodynamic zones, for example elements of the rear fuselage, panels may be designed so that local skin buckling between the stiffeners occurs below the ultimate collapse load. Thus for 'post-buckling' panels, initial skin buckling and panel collapse are key static strength characteristics which must be calculated. These panel stability characteristics are strongly influenced by initial geometric imperfections, typically exhibited in a structure due to sub-component manufacturing and panel assembly processes.

To determine the initial buckling, post-buckling and collapse response of a stiffened panel empirical and semi-empirical design formula [200, 382] or the Finite Element (FE) method, employing non-linear material and geometric analysis procedures may be used. The design formulas rely on applying simplifying assumptions, modelling the panel structure as a series of plates and columns. Using the FE method it is possible to model panel joints in great detail and predict panel behaviour under loading with a high level of accuracy. However, when modelling large wing and fuselage panel structures such detailed analysis becomes computationally expensive. Moreover, when modelling large structures the impact of local joint behaviour on global static strength performance may be weakened, creating a link between appropriate panel and joint idealisation and the size of the modelled panel structure. Thus this study presents coupled computational and experimental analysis, aimed at developing modelling guidelines for lap joined stiffened panel structure which accounts for the size of the structure being modelled. Three varying size panel structures, representing lap-joined fuselage panels, are investigated. Two levels of modelling fidelity are employed to model each panel specimen with the analysis results used to develop idealisation guidelines.

The chapter is organised as follows: Section 2 briefly summarizes key background literature. Section 3 details the validating experimental work, Section 4 presents the computational analysis of the experimental specimens. Section 5 documents the results from the coupled computational and experimental analysis. Section 6 concludes the work with a summary of the developed idealisation guidelines.

3.2 Panel Experimental Analysis

To develop relationships between panel idealisation and the size of the modelled panel structure three coupled experimental and simulation case studies are presented. Each case study considers a similar panel design but a different size specimen, with each having validating experimental results to benchmark the simulation predicted static strength behaviour. Three panel specimen designs already available in the literature are examined [392-394]. Each design is representative of compression critical aircraft fuselage structure. The panel specimen designs are presented in Figure 3.1 and Table 3.1. The smallest specimen consists of a single longitudinal stiffener plus attached skin (S1), the middle size specimen consists of three longitudinal stiffeners (S3) and the largest specimen consists of five longitudinal and two lateral stiffeners (S7).

Each specimen was manufactured using standard aerospace materials (stiffeners AA7075 extrusions, skin AA2024 sheet). The longitudinal stiffeners of specimens S1 and S3 were assembled to the skin using FSW. The central three longitudinal stiffeners for specimens S7 were assembled to the skin using FSW, with the edge longitudinal stiffeners and the lateral stiffeners assembled to the welded skin-stiffener structure using standard aerospace countersunk rivets and a standard manual riveting process. Each specimen was tested under uniform compression loading. Before testing the specimen ends were cast in cerrobend or epoxy tooling resin, allowing simultaneously the uniform compression loading of the specimens and clamped loading edge boundary conditions. During the tests specimen loading, end-shortening and strain data from key specimen locations were recorded at short load intervals.

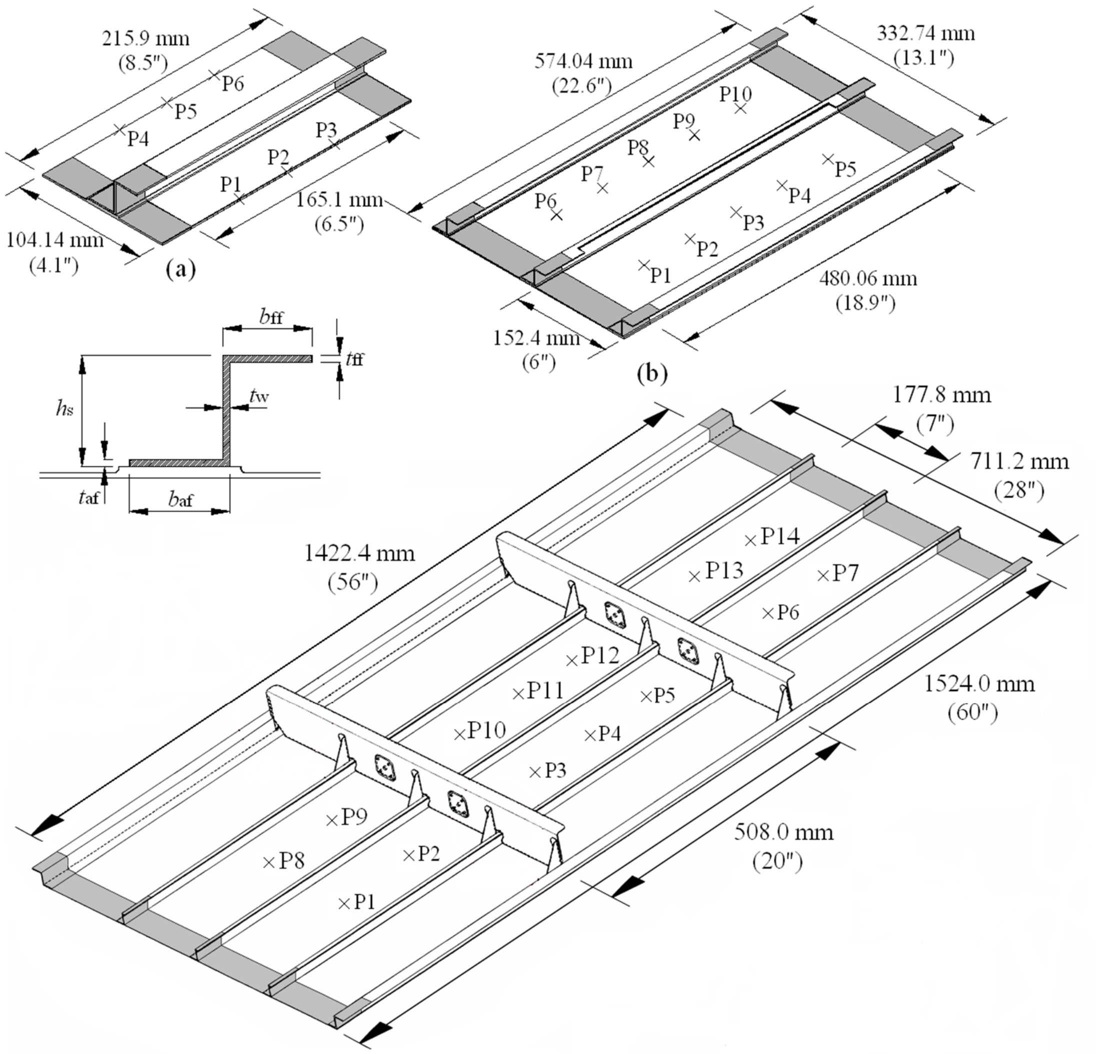

Figure 3.1. Test specimens.

For all specimens additional supplementary measurements and tests were undertaken to determine the basic specimen material properties. As the specimens were welded further experimental measurements were undertaken to capture the size of the degraded material zone around the weld joint (typically called the Heat Affected Zone – HAZ), and its associated material properties. Further information on the case study specimens, individual test setups and experimental results can be found in the individual references [392-394].

Table 3.1. Cross sectional dimensions

	Multi-stiffener panel		Multi-bay panel	
	Edge stiffeners (mm) welded	Central stiffeners (mm) welded	Edge stiffeners (mm) riveted	Central stiffeners (mm) welded
h_s	25.4	25.4	25.4	25.4
b_{ff}	20.32	7.3	22.86	10.16
b_{af}	22.86	22.86	20.32	20.32
t_w	1.6	1.6	3.175	2.032
t_{ff}	1.6	1.6	3.175	2.032
t_{af}	1.6	1.6	3.175	2.032
t_{skin}	1.2		2.032	

3.3 Panel Computational Analysis

For any analysis the structure must be idealised with appreciation of the possible structural behaviour as the computational model must accurately represent such behaviour. Optimised stiffened panels are susceptible to local skin and stiffener buckling behaviour as well as global stiffener buckling behaviour. An appropriate idealisation is therefore to represent the stiffener individual web and flange components along with the panel skin as an assemblage of shell or solid elements. This approach is essential to enable both the local and global buckling modes of the structure to be predicted. In the literature the vast majority of preceding work has used shell elements [392-394], generating acceptable panel strength predictions. Herein each case study specimen will be modelled twice, in the first instance using the well-practised shell element idealisation, and then using the more novel solid-shell element idealisation. For each case study and each idealisation the accuracy of the predicted panel static strength performance along with the computational expense of the analysis will be presented and analysed, thus enabling the advantages and disadvantages of both element type idealisations to be understood.

Modelling with the two structural element types the local idealisation of the skin-stiffener lap joints may be modelled with two unique high fidelity idealisations. In the shell model rigid link MPCs are used to represent the connected zones of the skin-stiffener interfaces. The remaining interface zones are modelled using contact gap elements. To represent the connected zones of the skin-stiffener interfaces in the solid-shell element models, the upper nodes of the panel skin and the lower nodes of the stiffener flange are merged. In the remaining interface zones surface to surface contact elements are used. Figure 3.2 depicts a schematic of the two local lap joint idealisations. The shell elements are located at the mid-plane thickness of each segment of specimen skin, web or flange. Using solid-shell elements there is no need for such mid-plane idealisation. The total model cross-sectional area of both idealisations is equal and corresponds exactly to the individual test specimen cross-sectional areas.

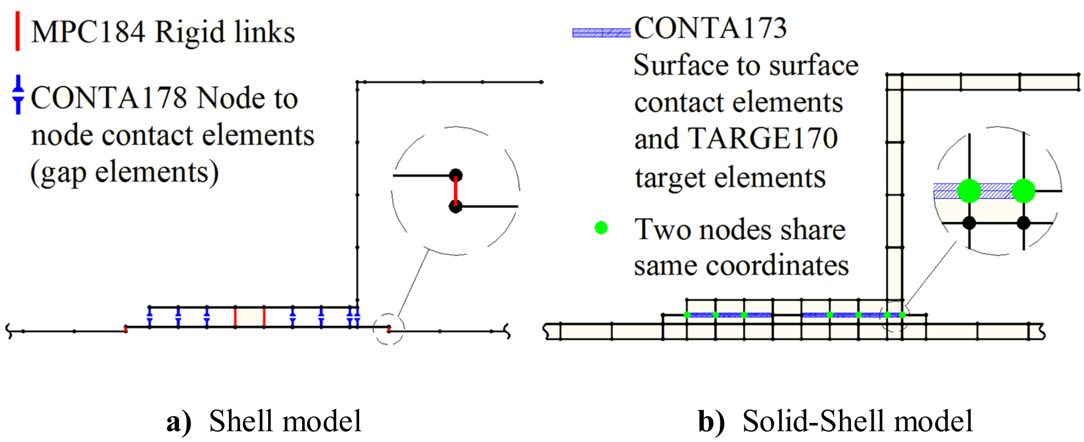

Figure 3.2 Lap joint idealisations

For any FE analysis an element and mesh convergence study must be preformed to determine an appropriate model mesh for a particular element formulation. When examining the buckling collapse behaviour of stiffened panels the aim is the definition of the minimum mesh density required to accurately represent the structures possible buckling waveforms. Based on a series of element and mesh convergence studies, which examined the buckling behaviour of rectangular plates with geometries and boundary conditions designed to represent those of specimen individual skin, flange and web units, appropriate element formulations and mesh densities were initially defined. For the shell models a four noded element, Shell181 [21], with six degrees of freedom at each node along with a mesh density of the order of 5.0 mm (Figures 3.3-3.5) was determined most appropriate for this study. To represent contact and sliding at the shell model skin-stiffener interfaces a two noded contact element, Conta178 [398], with three degrees of freedom at each node was coupled with the developed shell mesh. For the solid-shell models an element with continuum solid element topology and featuring eight node connectivity with three degrees of freedom at each node, Solsh190 [398], was found most appropriate. For the solid-shell models an identical mesh to the shell models was determined most appropriate for this study (Figures 3.3-3.5) along with Conta173 and Target170 elements [398] selected to represent panel interface contact.

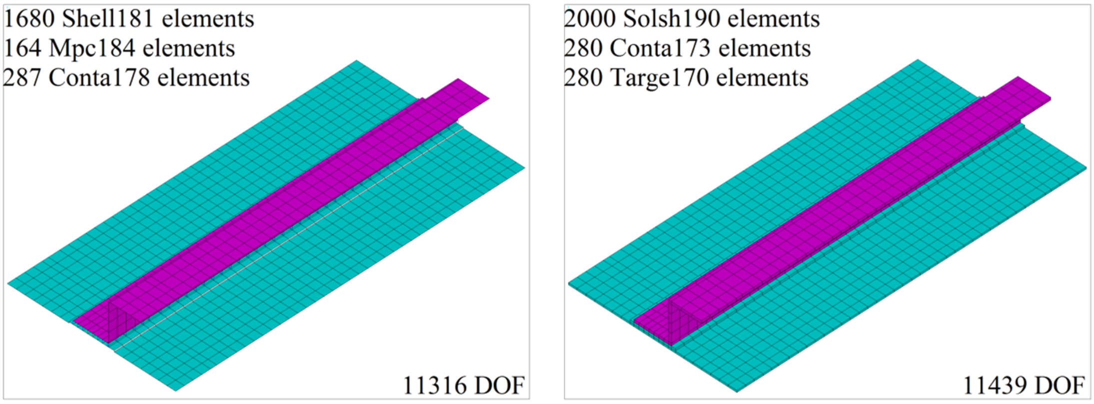

a) Shell model **b)** Solid-Shell model

Figure 3.3 FE mesh for specimen S1

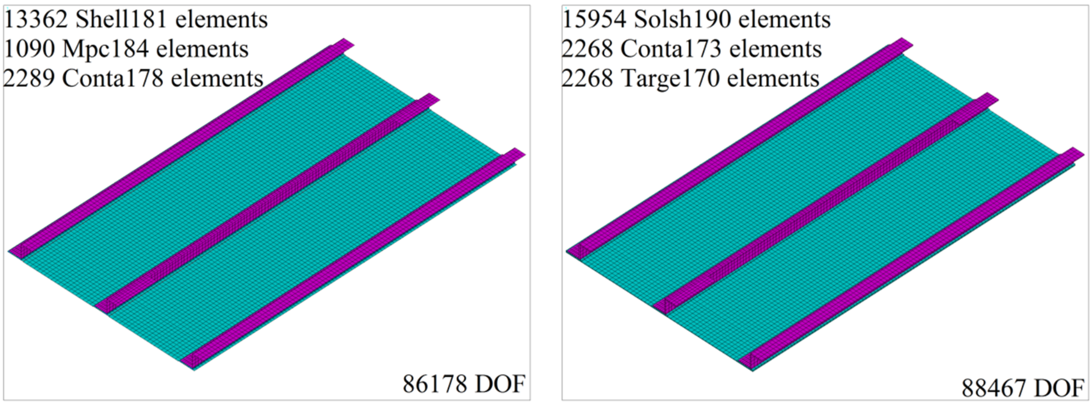

a) Shell model **b)** Solid-Shell model

Figure 3.4 FE mesh for specimen S3

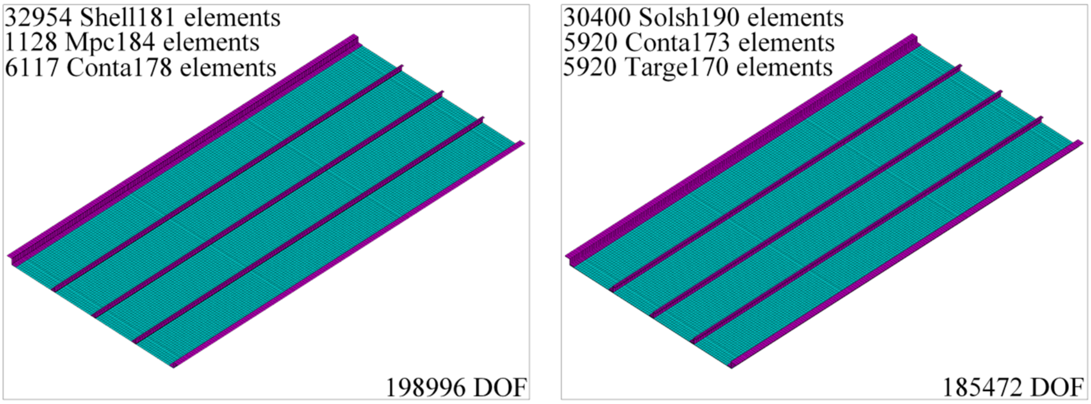

a) Shell model **b)** Solid-Shell model

Figure 3.5 FE mesh for specimen S7

Material curves were incorporated into the simulations using a multi-linear isotropic strain hardening material model [21]. Skin and stiffener material properties were generated experimentally using coupons taken from the same material batches used for specimen manufacture. Specimen weld degraded material properties were also experimentally determined and again incorporated into the simulations using a multi-linear isotropic strain hardening material model.

As initial geometric imperfections can lead to widely varying initial buckling and collapse behaviour great care was taken when generating initial imperfections. In considering the case study specimen design and manufacture, the main source of specimen geometric imperfections results from the thermal and mechanical stresses developed during the welding assembly processes. Using the FE method it is possible to represent weld induced geometric imperfections [394]. To do so, a simplified residual stress state is introduced into an initial FE model of the as-designed perfect specimen structure. When the residual stresses are introduced to the model, the structure is no longer in equilibrium, and a non-linear geometric analysis is carried out to establish static equilibrium. The equilibrium calculation generates a distorted structure, and a slightly modified stress state. This step represents the unclamping of the assembled structure from any fixturing required during the welding process [394]. A second stage simulation is then required to represent additional manufacturing processes, for example attaching the riveted stiffeners of specimen S7 and test preparation processes such as clamping and casting specimen ends. To model these processes the stressed and deformed mesh output of the first analysis has appropriate nodes (for example the skin nodes along rivet lines or the skin nodes within clamped and cast areas) displaced back to a zero out-of-plane location before a second non-linear geometric analysis is carried out to establish static equilibrium.

Applying this approach here to generate specimen imperfections will help further assess the impact of panel size and element type on the prediction of imperfections and there impact on predicted buckling behaviour. An initial state command, INISTATE [21], is used to define the initial stress state in both model types. For each specimen the same magnitude of stress is applied over the same volume of specimen material for each idealisation.

Having created an imperfect specimen model a final analysis is performed representing the compression test. The analysis applies the test loads and boundary conditions to the imperfect model. To represent specimen loading, a uniform axial displacement is applied to the nodes at the lower end of the model, while the axial displacement of the nodes at the opposite end of the model are restrained in the same direction. To represent the specimen cast ends and the stiffener flanges which are constrained within edge guides during test (specimen S7), the out-of-plane displacements of the nodes within these zones are restrained. For the shell models the single mid-plane nodes will be constrained against out-of-plane displacements, and for the solid-shell models at least two nodes through the thickness of the skin, web or flange will be constrained from out-of-plane displacements. As multiple adjacent longitudinal and lateral nodes are restrained within all the cast and edge guide zones the impact on the specimen behaviour due to this difference in the two idealisation boundary conditions is hard to quantify. However, it is important to note this subtle boundary condition difference with change of element type. Were this will have a greater impact is in representing the lateral stiffeners of specimen S7. Experimentally the lateral stiffeners were constrained from out-of-plane displacements using a series of tie rods connected from the lateral stiffeners to remote anchor points [394]. In the simulations the lateral stiffeners are not modelled but represented using displacement boundary conditions. Within the shell models the skin nodes along the lateral stiffener rivet lines are constrained from out-of-plane displacements. To represent the lateral stiffeners within the solid-shell models all nodes through the skin thickness along the rivet lines are constrained from out-of-plane displacements. In this case the different boundary conditions will impact on panel behaviour as only a single line of multiple adjacent lateral nodes are restrained from out-of-plane displacements, resulting in different levels of rotational constraint about the lateral rivet lines. Thus when examining the simulation results for S7 it will be important to recognise that the shell and solid-shell models have different lateral stiffener boundary conditions and that both are approximate idealisations of the real experimental setup.

For all simulation stages a displacement controlled incremental-iterative Newton-Raphson solution procedure was used. During the analysis the end-shortening load is applied monotonically in small increments representing the test conditions. During loading the instability of the skin develops depending on the initial imperfection pattern across the skin segments, and with marginally different initial conditions at different locations marginally different buckling loads will be calculated. Where possible to allow direct comparison between the experimental and computational results initial skin buckling is determine using the average strain method. The method plots the load against the mid-plane strain at a selected location, with initial buckling defined to have occurred when a sharp break is seen in the data. Based on early simulation observations in which a range of initial buckling locations where observed a number of locations were selected to calculate initial buckling for each specimen. A total of six locations are examined for specimen S1, ten locations for S3 and fourteen locations for S7, Figure 3.1. For specimen S7 initial buckling is expected within the specimen central zone as the test boundary conditions stabilise the outer skin bays. Finally, the ultimate specimen collapse load is defined as the maximum experimental or computational load carried by the specimen or model.

3.4 Experimental and Simulation Results

3.4.1 Specimen S1

The performance of three test specimens is presented in reference [399], with one instrumented to capture initial skin buckling behaviour. This specimen experienced initial skin buckling at 16.6 kN and failed in a crippling mode at 71.7 kN. The skin buckling load was calculated using strain gauge data from location P5, see Figure 3.1. The specimen skin segments initially buckled into single longitudinal half-waves

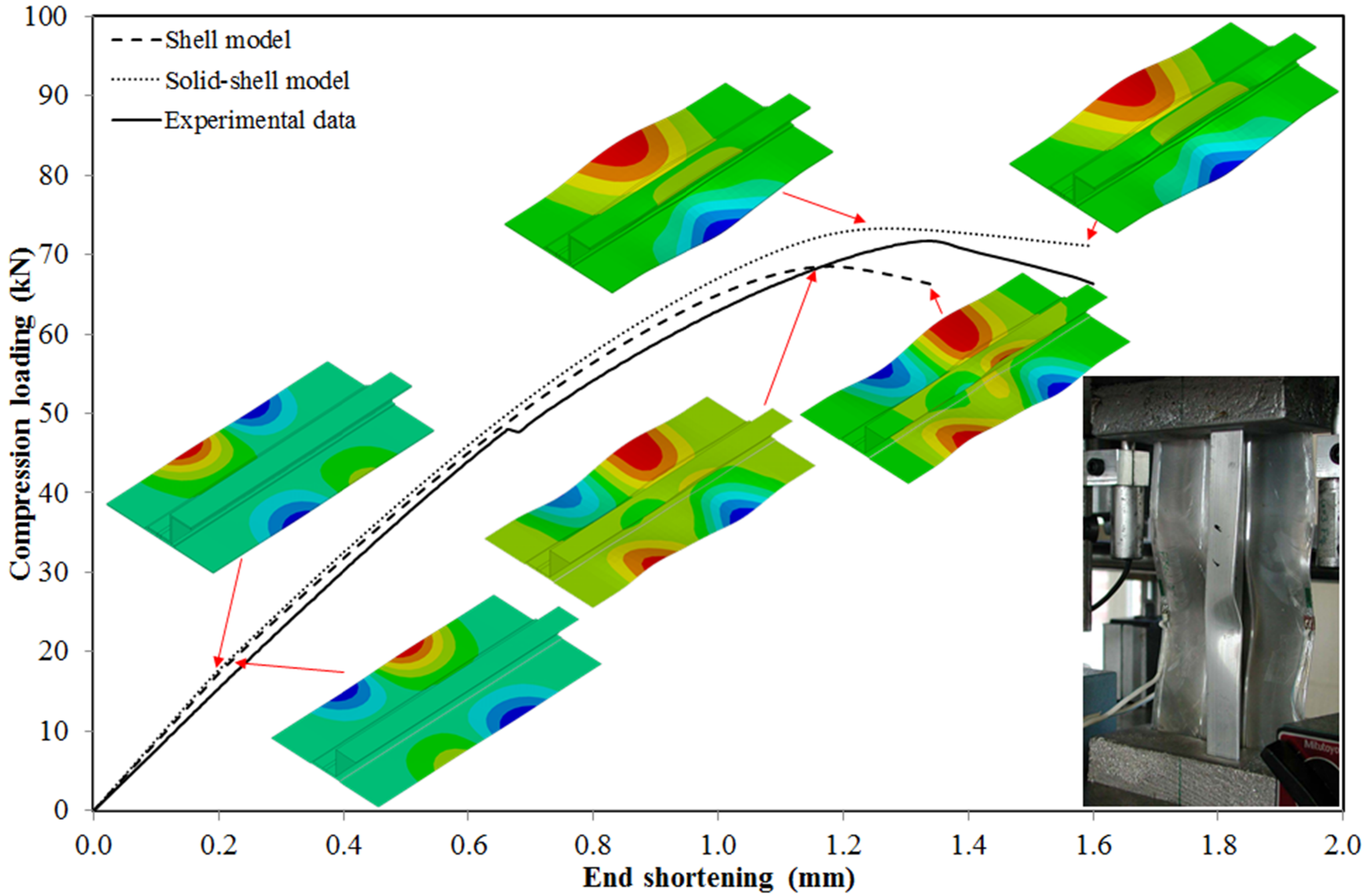

Figure 3.6 Load versus end shortening curves for S1

before changing mode into two longitudinal half-waves at 48.0 kN. At specimen collapse the skin segments rotated in the opposite direction to the stiffener web and free flange just below the mid-plane of the specimen. The specimen skin-stiffener weld remained intact up to and during specimen collapse. Figure 3.6 presents the measured load versus end-shortening curve. The results of the Finite Element analyse will be discussed next. The figure also presents a final test image of the specimen at which stage the weld joint has failed due to post collapse end-shortening of the specimen.

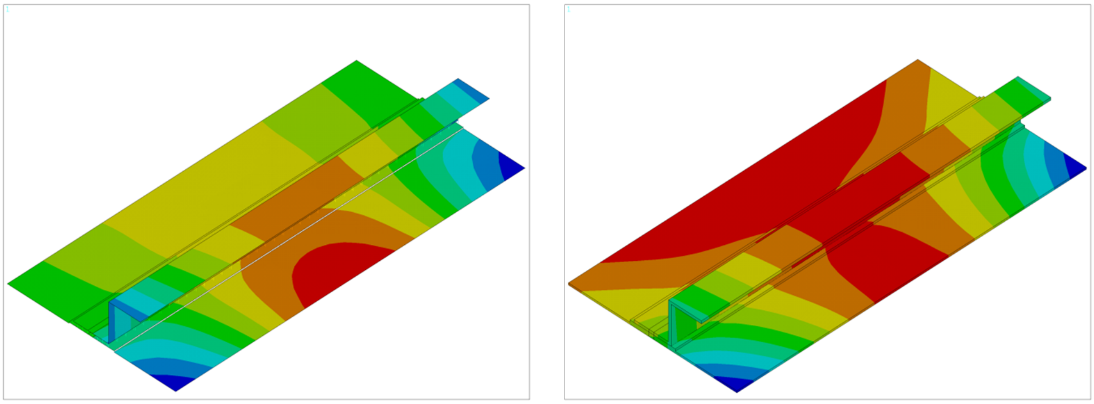

a) Shell model **b)** Solid-Shell model

Figure 3.7 Specimen S1 predicted initial geometric imperfection patterns

Considering the simulation predicted behaviour, Figure 3.7 presents the initial specimen geometric imperfection patterns induced by modelling the idealised welding residual stress state. Figure 3.8 presents the key magnitudes of the geometric imperfections once the test boundary conditions have been applied to the models. The simulations predict the same imperfection pattern with the shell model predicting marginally larger magnitudes. This highlights the potential impact of the two element type boundary condition idealisations, with the shell model only having the single mid-plane nodes constrained against out-of-plane displacements but the solid-shell models having at least two nodes through the thickness of the skin, web or flange constrained from out-of-plane displacements. Unfortunately for this specimen there is no experimental geometric imperfection data available. However if we examine the initial axial stiffness data in Figure 6 the solid-shell model predicts a 16.7% greater stiffness and the shell model a 12.8% greater stiffness than that measured during experimental specimen test. This suggests that the real specimen imperfection is larger in magnitude than that generated by the idealised residual stress state.

The simulation predicted initial skin buckling loads are presented in Table 3.2. Both simulations predict initial asymmetric skin segment buckling with two longitudinal half-waves, however the initial buckle waves of the shell and solid-shell models are in opposite directions, Figure 3.6. The shell model initially buckles at 17.5 kN at location P5, and the solid-shell model initially buckles at 16.2 kN at location P4. Unexpectedly, the shell model buckling loads are greater in magnitude despite greater geometric imperfection magnitudes and the more heavily constrained cast end boundary conditions.

Table 3.2 Local skin buckling load results for single stiffener specimen

	Skin local buckling load (kN)				
	Shell181	**Solsh190**	**% difference**	**a**	**b**
P1	17.9	17.7	1.12	7.83	6.63
P2	17.9	17.1	4.47	7.83	3.01
P3	19.8	17.6	11.11	19.28	6.02
P4	18.2	16.2	10.99	9.64	-2.41
P5	17.5	16.3	6.86	5.42	-1.81
P6	17.6	16.7	5.11	6.02	0.60

[a,b]Percentage differents based on experimental data (16.6 kN) for Shell181 and Solsh190 models

The range of calculated buckling loads for the shell model is marginally larger (13.1%) than that predicted by the solid-shell model (9.3%). This highlights the importance of location when calculating and comparing buckling behaviour. Variation in the predicted buckling load at a single location ranges from 1.1% at location P1 to 11.1% at location P3.

Figure 3.9 presents average strain data at the six locations defined in Figure 3.1. It is evident from the strain data that the solid-shell model predicts a skin mode change at 32.7 kN, this results in a single longitudinal half-wave within each specimen skin segment, Figure 3.6. It is worth noting that it is not possible to detect this mode change in the predicted load versus end-shortening curve.

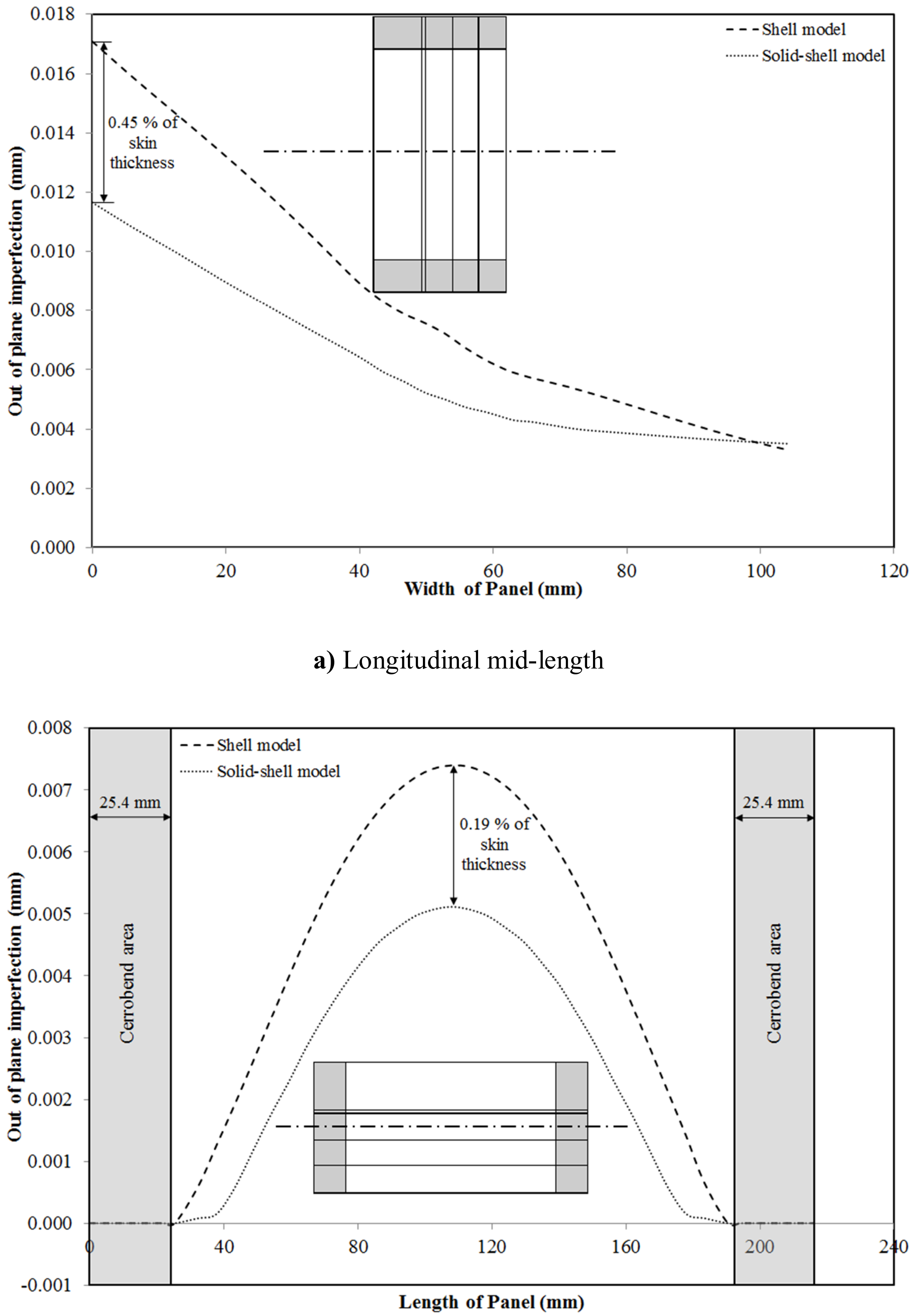

a) Longitudinal mid-length

b) Lateral mid-length

Figure 3.8 Predicted geometric imperfections of specimen S1

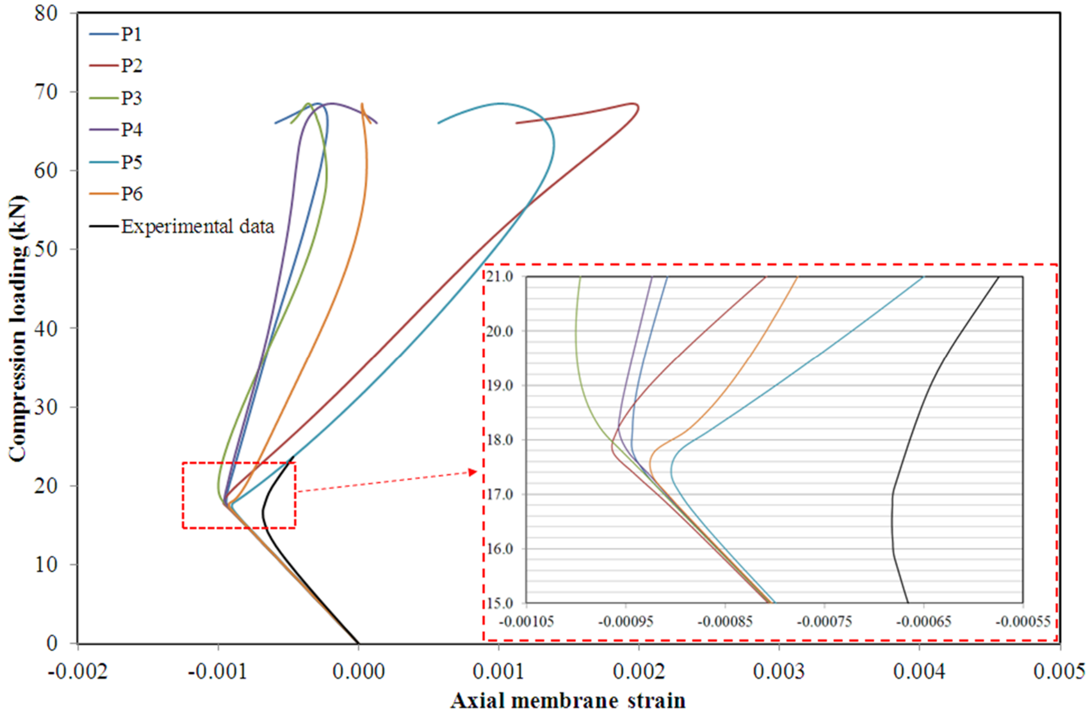

a) Shell model average strain data

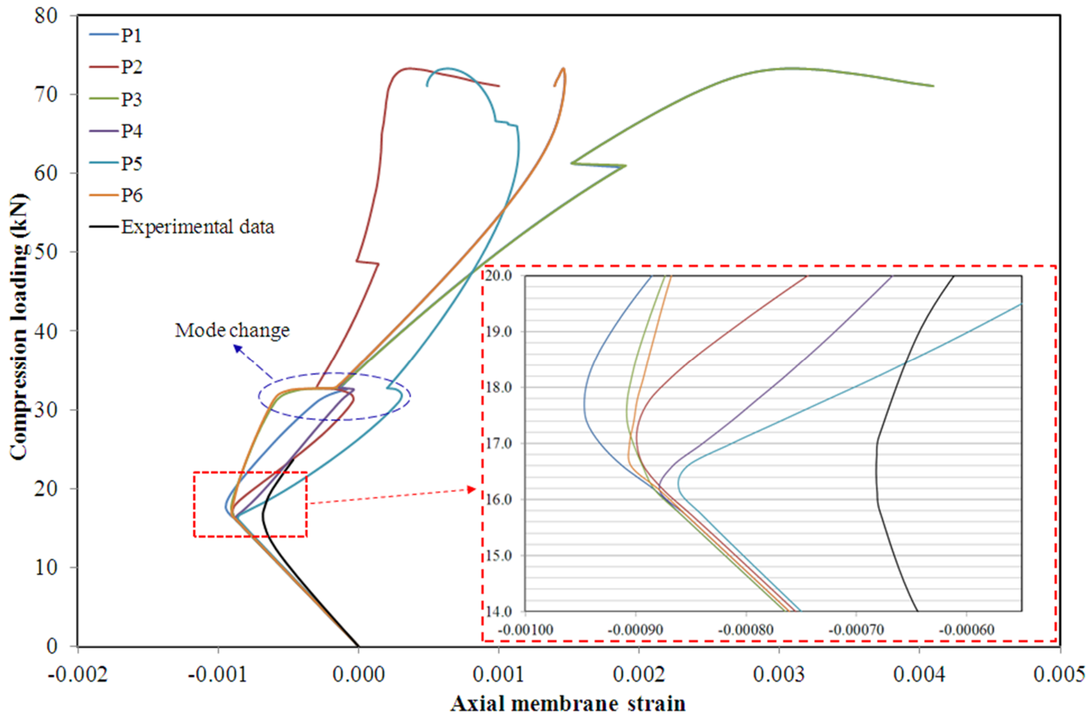

b) Solid-shell model average strain data

Figure 3.9 Average strain versus load curves for specimen S1

The collapse load predictions are 68.5 kN and 73.3 kN for the shell model and the solid-shell model respectively. The shell model predicts a very similar collapse mode to the experimental behaviour, under predicting the experimental collapse load by 4.5%. The solid-shell model predicts a different collapse mode and a higher collapse load (2.2%) than that measured experimentally. The mode change identified within the average strain data of the solid-shell model results in increased skin and stiffener flange buckle wave-lengths and ultimately this leads to larger skin and flange buckle-waves at specimen collapse, which was not seen in the physical testing.

Examining the computational cost, the solid-shell model took approximately 3.56 times longer to reach maximum load than the shell model. Also it is worth noting that the shell model experienced convergence difficulties after reaching the maximum load and could not achieve the ultimate target end-shortening of 1.6 mm. The solid-shell model experienced no such difficulty.

3.4.2 Specimen S3

This specimen was tested by Murphy et al. [393]. The skin buckling load of specimen S3 was calculated to be 21.5 kN using strain gauge data from location P8, see Figure 3.1. The skin bays buckled with five approximately equal length half-waves with almost the equivalent asymmetric pattern in each bay. However, in one of the skin bays two of the buckle half-waves, in the region of P1 and P2, combined into a single half-wave. Specimen failure was measured at a load of 166.4 kN with the central stiffener buckling with combined global flexure and local stiffener flange and web buckling. Figure 3.10 presents the measured load versus end-shortening curve for specimen S3.

Figure 3.11 presents the predicted initial specimen geometric imperfection patterns induced by modelling the idealised welding residual stress state and Figure 3.12 presents the imperfection magnitudes once the test boundary conditions have been applied to the models. The simulations predict the same imperfection pattern with again the shell model predicting marginally larger magnitudes. In this case it is not clear that the different shell and solid-shell cast end boundary conditions are responsible for the magnitude difference. Comparing with the available experimental

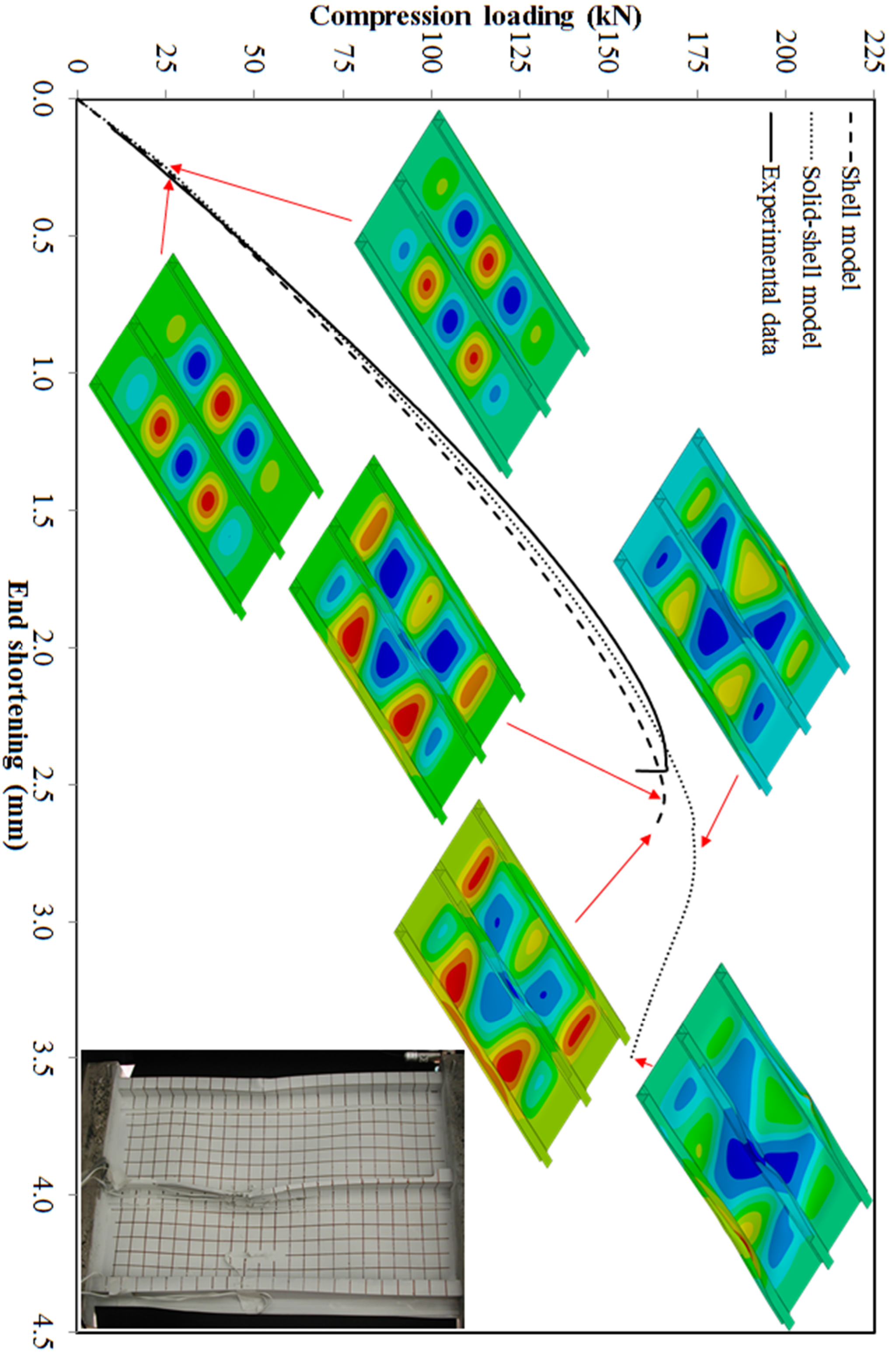

Figure 3.10 Load versus end shortening curves for S3

was 120% the skin thickness, with the shell model which predicts the larger imperfection having an equivalent imperfection magnitude of only 9.15%. In this case the shell model predicts a 6.3% greater initial specimen stiffness and the solid-imperfection data the maximum out-of-plane magnitude of the curvature parallel to the specimen stiffeners (measured from the specimen edge to the specimen centre) shell model a 10.3% greater stiffness than the magnitude measured experimentally. Again this indicates that the real specimen imperfection is larger in magnitude than that generated by the idealised residual stress state.

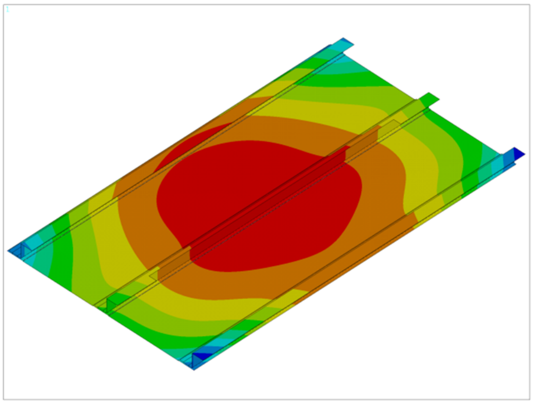

Shell181 model

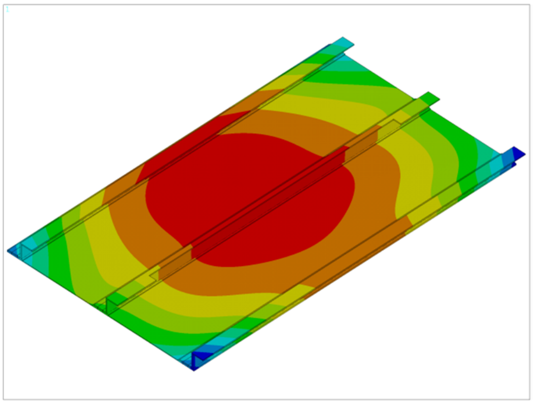

Solsh190 model

Figure 3.11 Specimen S3 predicted initial geometric imperfection patterns

Table 3.3 presents the calculated skin buckling loads and Figure 3.13 presents the interpreted strain data. The models predict very similar skin buckling modes consisting of five half-waves within each skin bay, as shown in Figure 3.10. The predicted skin buckling modes are similar to the experimental buckling wave pattern except for the combined half-waves located at P1 and P2 as noted earlier. The shell model initially buckles at 23.2 kN calculated at locations P2, P4 and P8, and the solid-shell model initially buckles at 23.2 kN at P8. The maximum variation at a single location is 4.7% (at P7) and for the majority of the skin bay locations the shell model predicts greater or equal skin buckling loads when compared to the solid-shell model predictions. The variation in the predicted buckling loads over the ten sample points for the shell model is 27.2%. As seen in the specimen S1 results the scatter for the solid-shell model is marginally smaller in comparison to the shell model predictions with a 21.6% variation. In general the predicted buckling loads are not as close to the measured experimental behaviour as those predicted for specimen S1.

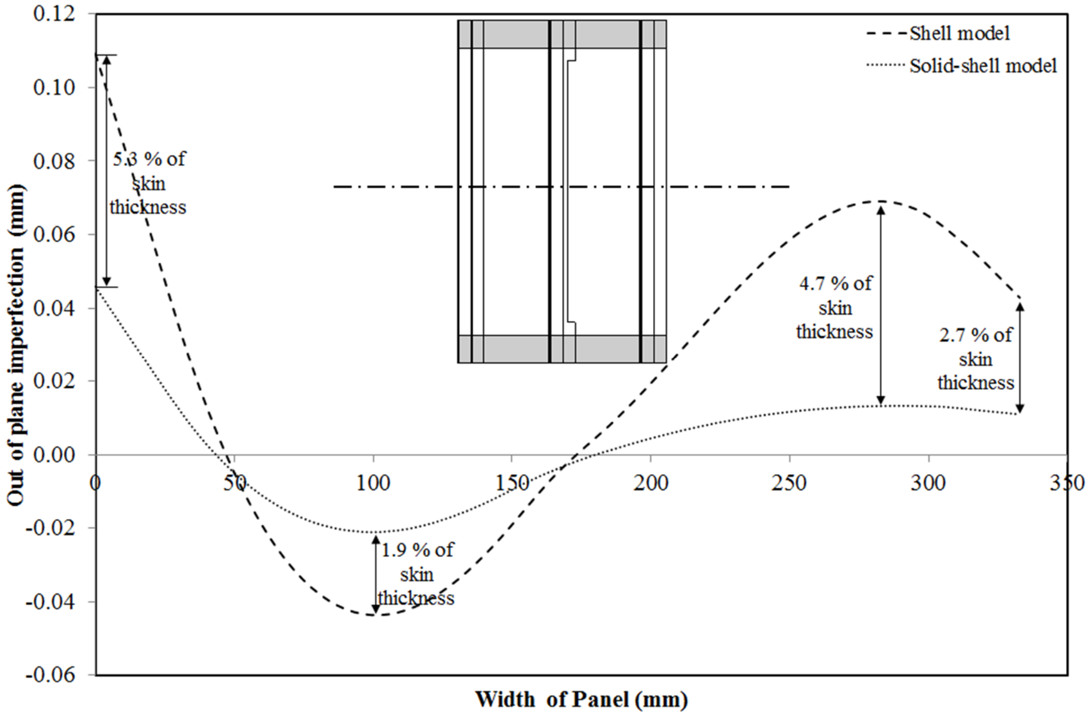

a) Longitudinal mid-length

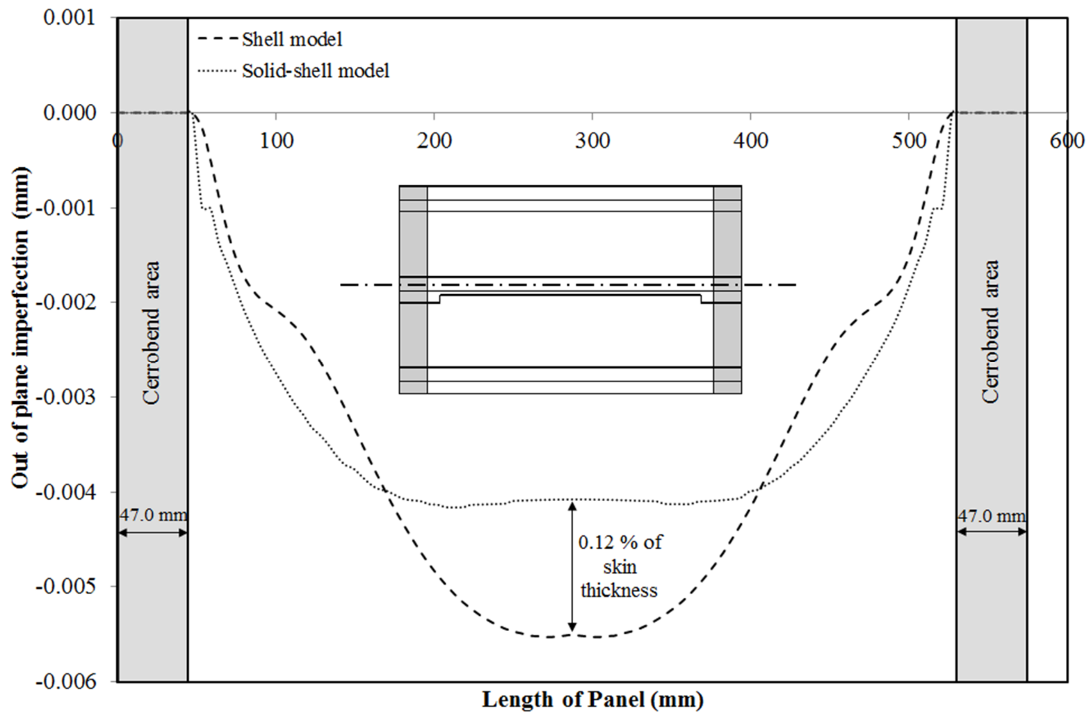

b) Lateral mid-length

Figure 3.12 Predicted geometric imperfections of specimen S3

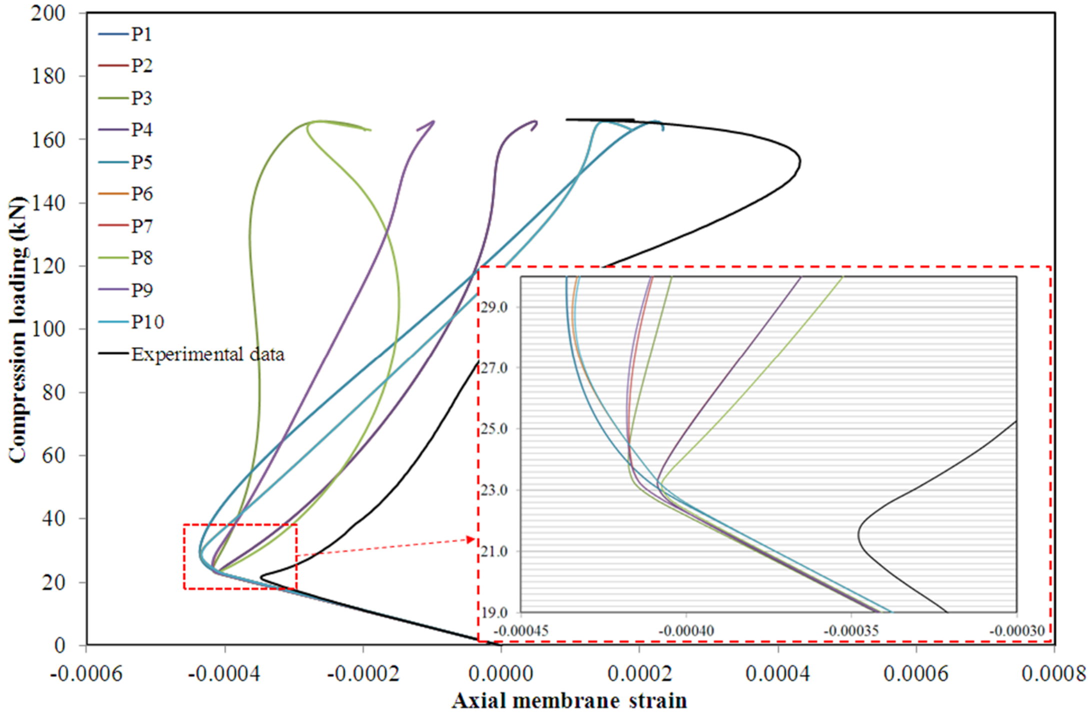

a) Shell model average strain data

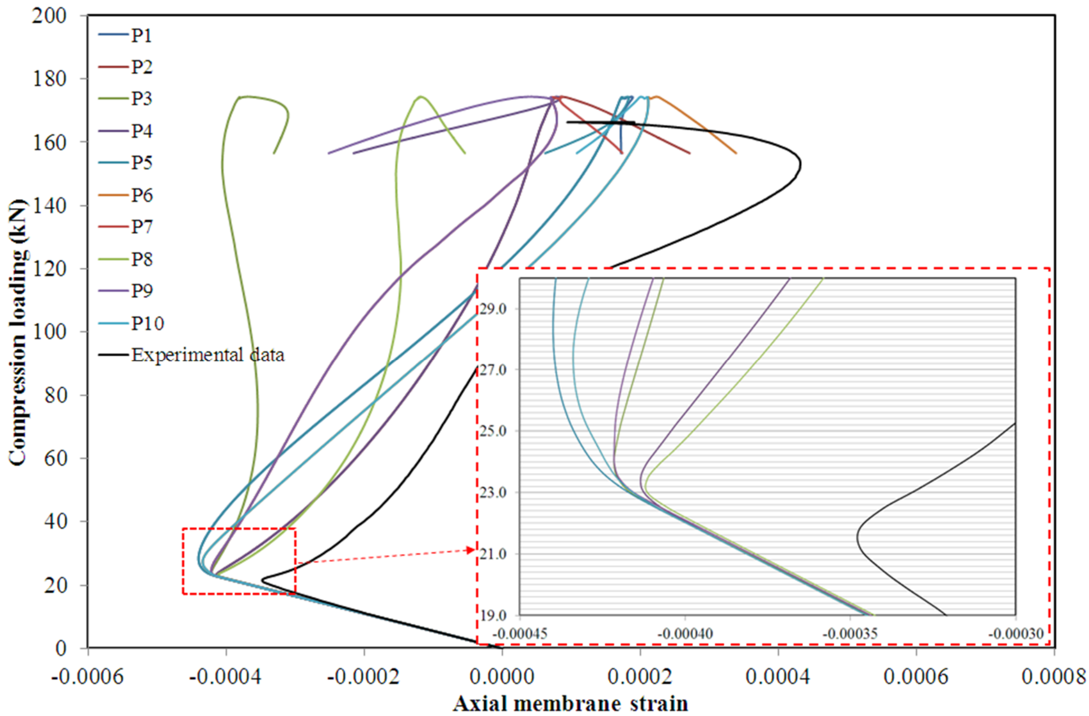

b) Solid-shell model average strain data

Figure 3.13 Average strain versus load curves for specimen S3

Examining collapse behaviour both models predict similar central stiffener global flexure and local stiffener flange and web buckling as observed experimentally, Figure 3.10. The shell model is conservative; predicting collapse 0.4% below the experimental value, the solid-shell model over predicts the experimental collapse load by 4.8%. The predicted collapse loads are closer than those predicted for specimen S1.

Table 3.3 Local skin buckling load results for multi-stiffener specimen

	Skin local buckling load (kN)				
	Shell181	**Solsh190**	**% difference**	**a**	**b**
P1	29.5	28.2	4.41	37.21	31.16
P2	23.2	23.4	-0.86	7.91	8.84
P3	23.9	23.9	0.00	11.16	11.16
P4	23.2	23.4	-0.86	7.91	8.84
P5	29.5	28.2	4.41	37.21	31.16
P6	28.7	27.4	4.53	33.49	27.44
P7	25.5	24.3	4.71	18.60	13.02
P8	23.2	23.2	0.00	7.91	7.91
P9	25.5	24.3	4.71	18.60	13.02
P10	28.7	27.4	4.53	33.49	27.44

[a,b]Percentage differents based on experimental data (21.5 kN) for Shell181 and Solsh190 models

In this case the solid-shell model required 3.22 times more CPU time to reach a maximum specimen load when compared with the shell model. Again the Newton-Raphson solution method performs well for the solid-shell model but again convergence issues emerged for the shell model beyond the maximum specimen load.

3.4.3 Specimen S7

Specimen S7 initially buckles with four approximately equal length half-waves within the specimen central skin bays. The central skin bays buckle with an asymmetric pattern. In this case only strain gauge data is available from a single side of the specimen skin at location P11 (Figure 3.1) to calculate a buckling load. The extracted load versus strain curve does not have a distinct behaviour to establish an

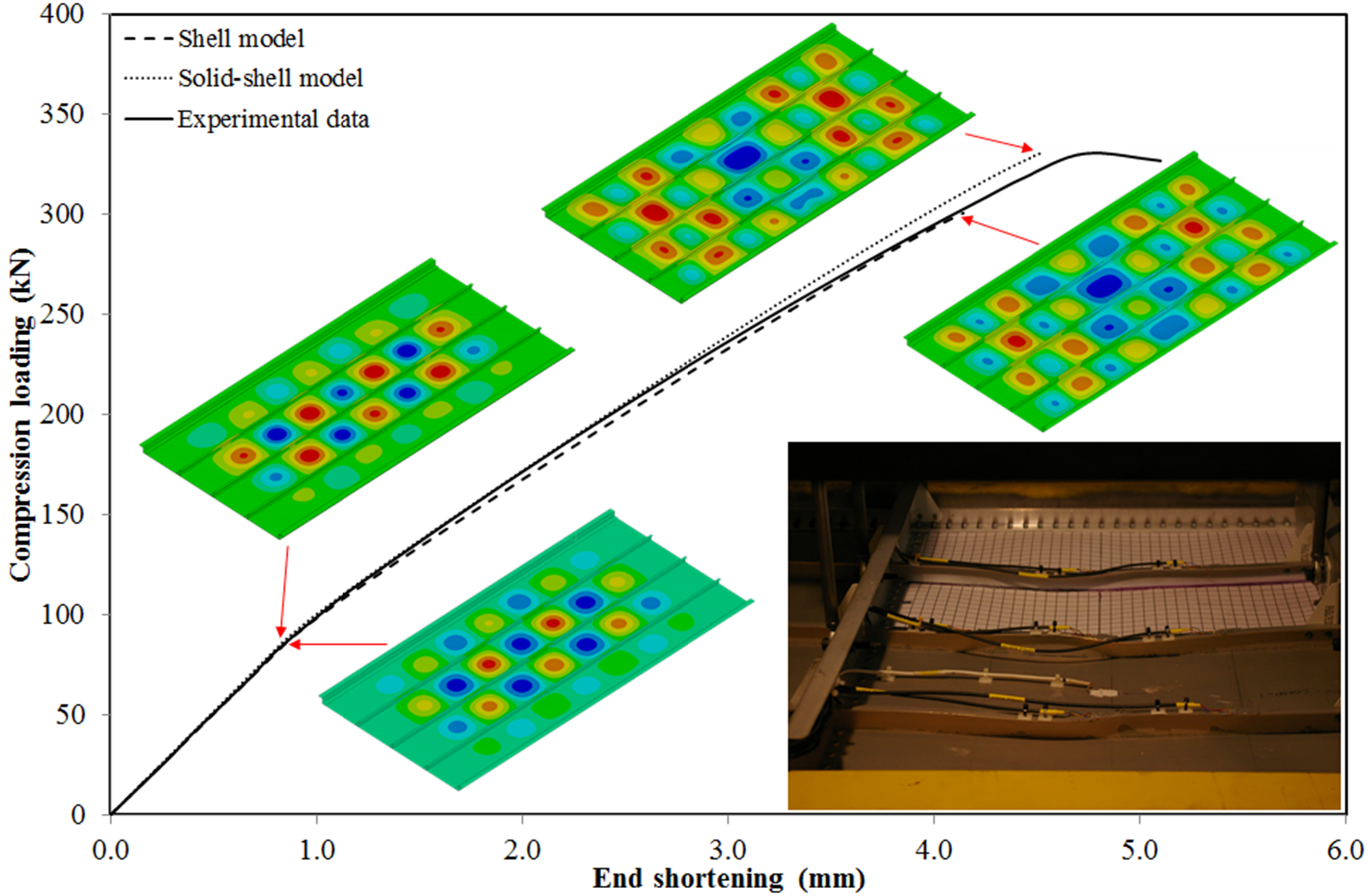

Figure 3.14 Load versus end shortening curves for **S7**

initial buckling load, thus a mathematical curve fitting method was used to determine a buckling load level of 89.7 kN.

For specimen S7 weld joint integrity was maintained through initial skin buckling, post-buckling and overall specimen collapse. The specimen failed at 336.8 kN by combined stiffener global flexure and local free flange instability at the mid-plane of the specimen. Figure 3.14 presents the measured load versus end-shortening curve plus a post collapse image of the specimen.

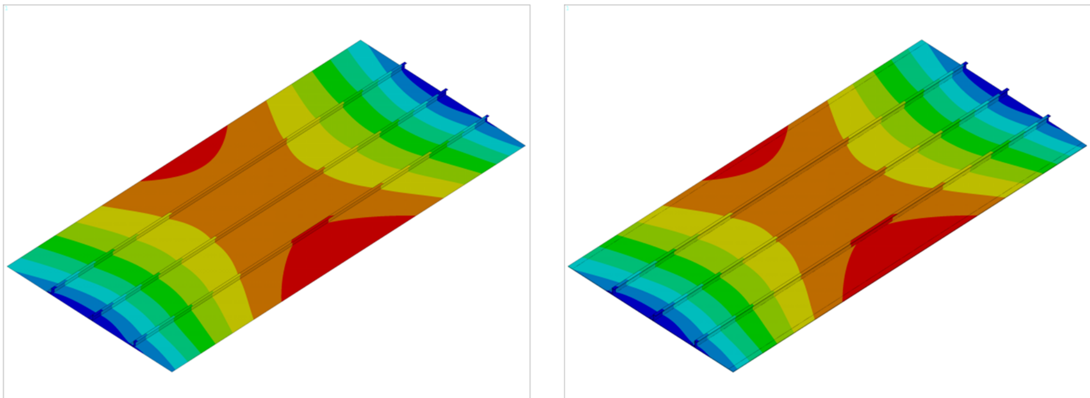

Figure 3.15 Specimen S7 predicted initial geometric imperfection patterns

Figure 3.15 presents the predicted initial specimen geometric imperfection patterns induced by modelling the idealised welding residual stress state. Again both modelling approaches predict the same initial geometric imperfection patterns when the idealised welding residual stress state is introduced into the perfect geometry models. However once the lateral stiffeners and test boundary conditions have been applied larger differences in magnitude and the final direction of imperfections is evident, Figure 3.16. This is primarily due to the imperfection simulation used to represent the attachment of the riveted lateral stiffeners; in which the skin nodes along the lateral stiffener rivet lines are displaced back to their zero out-of-plane location. For the shell model the single mid-plane nodes are displaced back to their zero out-of-plane location, and for the solid-shell model the nodes at the top and the bottom of the skin, through its thickness, are both displaced back to their zero out-of-plane locations. This enforces reduced longitudinal rotations around the lateral stiffener rivet lines and this significantly impacts the final form of the panel

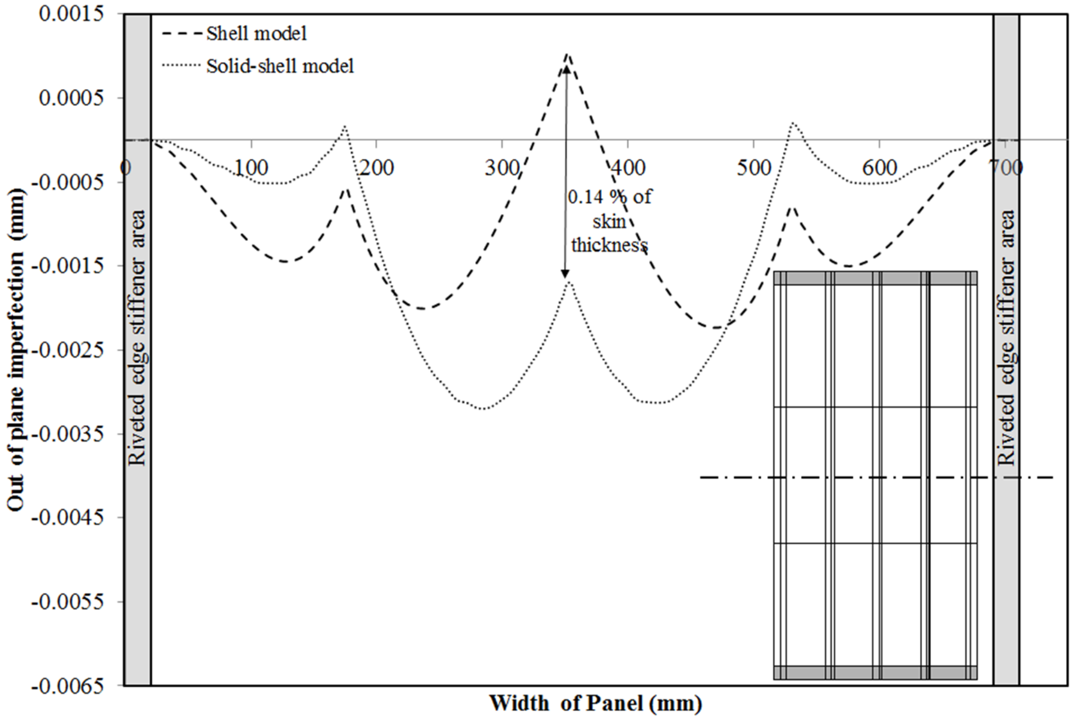

a) Longitudinal mid-length

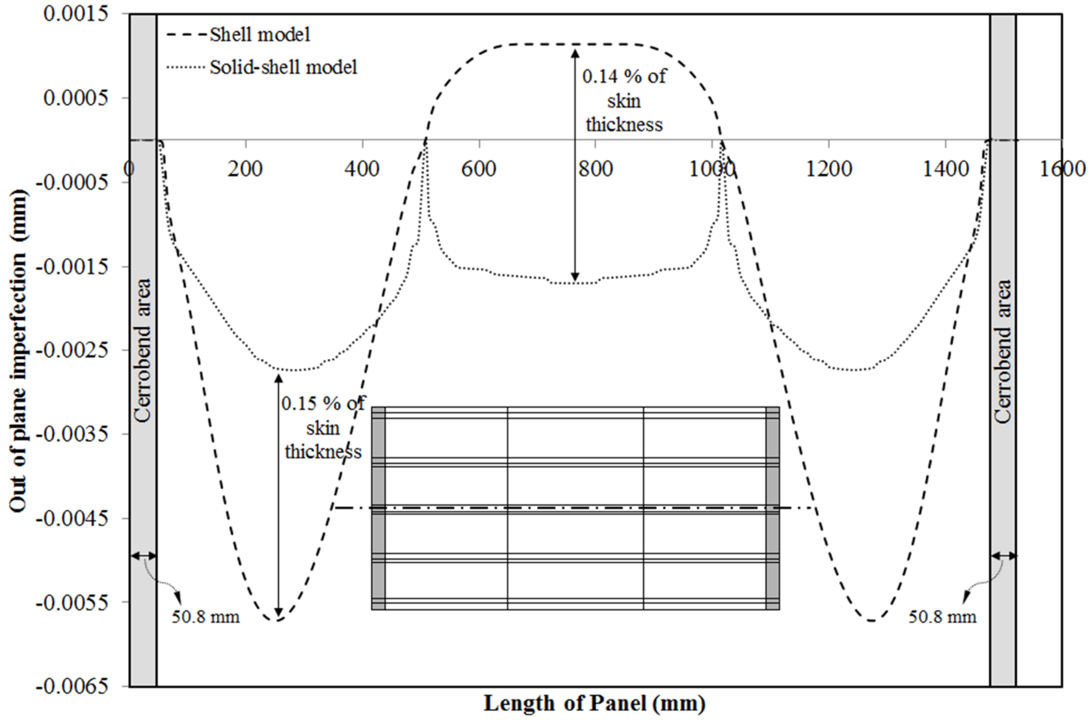

b) Lateral mid-length

Figure 3.16 Predicted geometric imperfections of specimen S7

imperfection. There is no experimental geometric imperfection data available for this specimen. However, comparing the initial stiffness predictions of the two FE models and measured test specimen stiffness, Figure 3.14, the solid-shell model predicts an initial stiffness 1.2% greater than the measured initial stiffness and the shell model predicts an initial stiffness 1.1% less than the measured initial stiffness.

Figures 3.17 and Table 3.4 presents the skin buckling behaviour of the two FE models and the experimental specimen. The two FE models predict three longitudinal half-waves within the central specimen bays and two half-waves in the outer bays. The two models predict similar buckling loads, with the shell model predicting initial buckling 3.0% below the experimental value at 87.0 kN (P2-6 and P9-13) and the shell model predicting initial buckling 3.6% below the experimental value at 86.5 kN (P2-6 and P9-13). The variation in skin buckling load predictions between the fourteen analysis locations is 14.9 % and 14.5% for the shell model and the solid-shell model respectively. Variation at a single location between the two models is very small, with a maximum difference of just 1%. In general the predicted buckling loads are closer to the measured experimental behaviour than those predicted for specimen S3. In addition variation in skin buckling load predictions between the analysis locations and at a single location are consistently smaller than that seen for specimen S3.

The employed displacement controlled Newton-Raphson method fails to converge before capturing the collapse of both FE models. Although both FE models fail to converge the solid-shell model precedes approximately 10% further than the shell model. The arc-length and non-linear stabilisation theories are available to deal with convergence problems throughout a post-buckling analysis. Since the arc-length method is a load controlled method and it is intended to represent the real displacement controlled specimen tests, it is not preferred in the present study. When using the non-linear stabilisation method artificial dampers are added to the structural system. When buckling occurs large displacements occur over small load steps and the artificial dampers then generate resistive forces to stabilise the problem. Stabilisation can help with convergence problems, but it can also affect accuracy if the stabilisation energy or f orces are too large. Herein there are two reasons not to utilise the nonlinear stabilization method in the present study. First the current

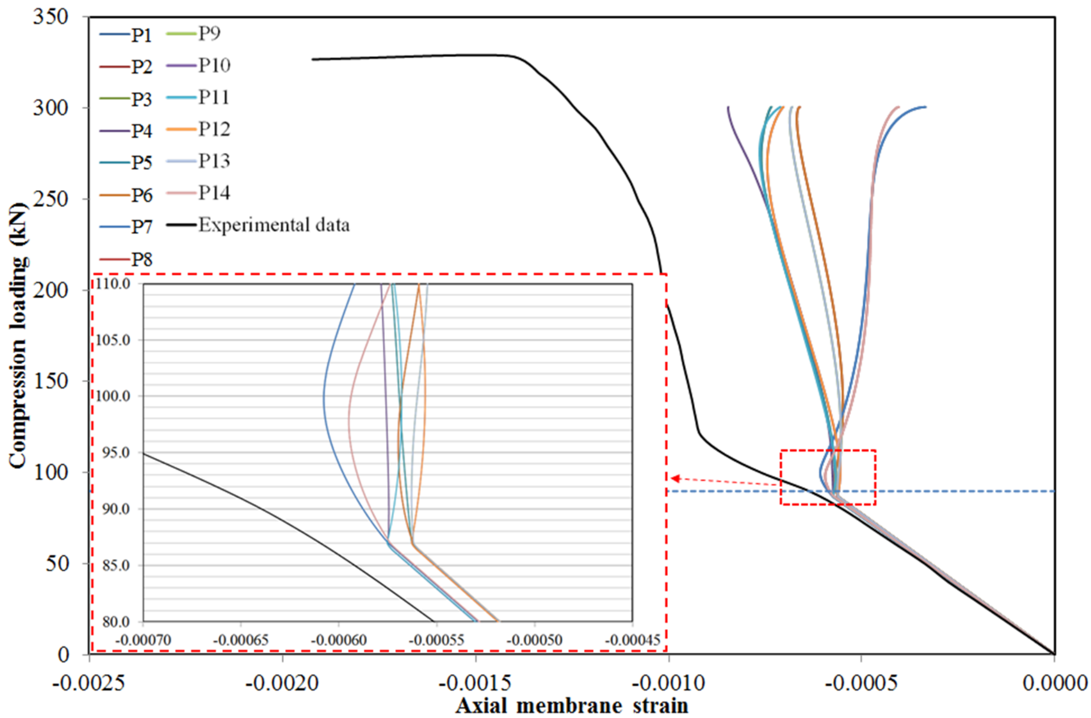

a) Shell model average strain data

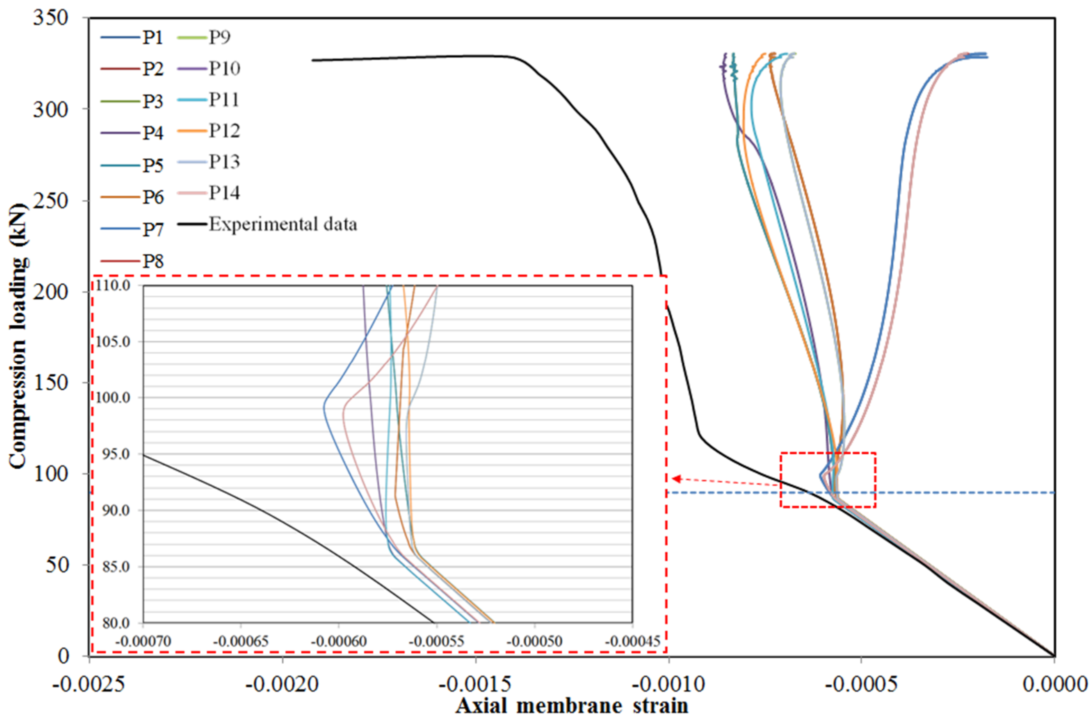

b) Solid-shell model average strain data

Figure 3.17 Average strain versus load curves for specimen S7

specimen models are very large in terms of degrees of freedom. Therefore, it is very difficult to control the non-linear stabilisation method over these models with an optimum energy dissipation ratio or damping factor. Secondly the models are developed to compare buckling predictions and artificial dampers would change the response of the individual models making comparisons of the two models more difficult.

Table 3.4 Local skin buckling load results for multi-bay specimen

	Skin local buckling load (kN)				
	Shell181	**Solsh190**	**% difference**	**a**	**b**
P1	100.0	99.0	1.00	11.48	10.37
P2	87.0	86.5	0.57	-3.01	-3.57
P3	87.0	86.5	0.57	-3.01	-3.57
P4	87.0	86.5	0.57	-3.01	-3.57
P5	87.0	86.5	0.57	-3.01	-3.57
P6	87.0	86.5	0.57	-3.01	-3.57
P7	100.0	99.0	1.00	11.48	10.37
P8	98.0	98.5	-0.51	9.25	9.81
P9	87.0	86.5	0.57	-3.01	-3.57
P10	87.0	86.5	0.57	-3.01	-3.57
P11	87.0	86.5	0.57	-3.01	-3.57
P12	87.0	86.5	0.57	-3.01	-3.57
P13	87.0	86.5	0.57	-3.01	-3.57
P14	98.0	98.5	-0.51	9.25	9.81

[a,b] Percentage differents based on experimental data (89.7 kN) for Shell181 and Solsh190 models

Examining the solution time, the solid-shell model required 2.84 times more CPU time to reach the maximum converged iteration compared to the shell model.

3.5. Conclusions

The presented research herein is focused on modelling and addressing the static strength behaviour of lap jointed stiffened panels representing subcomponents of fuselage structure. To this end accompanying the experimental studies and employing the ANSYS FE package two FE models are developed to assess and compare local skin buckling and collapse characteristics. First model is build up with Shell181 element which is a four node element with six degrees of freedom at each node. The second model is developed utilizing Solsh190 solid shell element which is an eight node element with three degrees of freedom at each node. To understand the variation in the experimental and computational results and remove or reduce the potential uncertainties, from FE analyses and address the effects of scale and number of stiffeners on the prediction response three panels with different configurations are considered. In order to obtain two models with closer degrees of freedom as possible, the mesh densities of models are intended to be closer as possible. To generate representative models the geometry of weld joints were taken directly from the specimens measured joint geometry and HAZ material properties obtained from coupon tests are incorporated into the FE models. The initial imperfection state of panel configurations are considered to be residual stress state based on the magnitude of the specimen measured residual stress and FE element models are developed to represent these imperfection states. It is pertinent here to mention that the residual stresses resulted from mechanical millings are not included into FE models. Only the weld induced residual stresses are taken into consideration. Obtaining FE models as representative as possible, displacement controlled Newton-Raphson method is applied to models through collapse. The local skin buckling, and collapse characteristics of experimental tests and FE models are compared each other to address the reliability of FE models. Also the other outputs from non-linear analyses, such as initial stiffnesses and solution times (CPU time), of developed FE models are considered to be important in the evaluation of modelling. Finally, in the light of above and obtained results the following conclusions can be drawn.

- It is demonstrated that weld induced initial distortions can be computationally simulated. The magnitude and shapes of obtained initial geometrical imperfections after two stages of analyses are reasonable and within the limits of real life aerospace applications which is 10 % of skin thickness.

- For the examined specimens with different configurations, the predictions of strength are of reasonable accuracy compared to the experimental results, with scatters of -4.45 to +2.22 percent and -0.37 to +4.78 percent for the single stiffener specimen and multi-stiffener specimen respectively. Both multi-bay specimen models failed to converge before observing the collapse load. For single stiffener specimen Solsh190 model has better prediction of collapse load. However for the big specimen Shell181 model predicts collapse load closer to experimental one.

- Shell181 model is conservative in terms of collapse load and axial stiffness compared to Solsh190 model for both single stiffener and multi-stiffener specimen configurations examined.

- Importantly, the simulation results imply that as the specimen model gets larger two simulation methods predicts closer initial axial stiffness to each other and to experimental measurements as can be observed from quantified results and load vs. end shortening curves.

- Considering the collapse mode shapes, in the single stiffener specimen models Shell181 model predicts the collapse mode similar to experimental mode. But Solsh190 model ends up with a different collapse mode resulting from different local skin buckling modes and mode change in Solsh190 model. However both models predict similar collapse modes which are very close to experimental one for the multi-stiffener specimen. Although both modelling approaches failed to converge in multi-bay specimen modelling, they have same mode shapes from very beginning to final converged solution. This behaviour is associated with the scale effect.

- Convergence is a general problem for Shell181 models. In simulation of single stiffener and multi-stiffener specimens Shell181 model experiences convergence difficulties some after reaching the ultimate load and displacement controlled Newton-Raphson method cannot proceed further. In simulation of multi-bay specimen Shell181 model fails before reaching collapse load. On the other hand, Solsh190 model performs well and does not encounter such a problem in simulations of single stiffener and multi-stiffener specimens. But in simulation of multi-bay specimen due to boundary conditions of unloaded edges and lateral frames Solsh190 model fails too.

- The extracted local skin buckling loads from different points for all specimen models suggest the location of point on the panel from where the local skin buckling load is predicted is important. During the non-linear analysis the displacement load is applied slowly representing the real test conditions and the weakest points lost stability first. The predicted local skin buckling loads from six points for the single stiffener specimen exhibit 13.14 and 9.26 percent variations for the Shell181 model and Solsh190 model respectively. And for the multi-bay specimen modelling the variation is within 27.15 percent for Shell181 model and within 21.55 percent for Solsh190 model. For the multi-bay specimen these variations become 14.94 % and 14.45 % for Shell181 model and Solsh190 model respectively. As it can be observed from the percent variations Solsh190 models have narrower scatters compared to Shell181 models.

- Examining the local skin buckling mode shapes, in the single stiffener specimen modelling two FE models predict different local skin buckling modes. Both models predict two half-waves along panel length but asymmetric to each other resulting from magnitudes of imperfection levels and differences of structural and contact element characteristics. As the panel gets larger, impact of the differences in features of finite elements reduces on panel response that very similar local skin buckling modes are predicted in multi-stiffener and multi-bay specimen models.

- For the single stiffener specimen modelling two models predict local skin buckling load for the same location of points with a maximum difference of 11.11 %. However for the multi-stiffener and multi-bay specimen models the maximum difference of local skin buckling load for the same points are 4.71 % and 1.0 %. This again demonstrates for the stiffened panel configurations investigated that as the panel becomes larger the impact of the different FE modelling methodologies on the response reduces.

- For the single stiffener specimen models the closer predictions of local skin buckling loads to test results differ by 5.42 % and 0.60 % for Shell181 model and Solsh190 model respectively. Although same procedures are applied in both configuration models, the closer predictions of multi-stiffener specimen models differ by 7.91%. And the closer predictions for multi-bay specimen differ by 3.01 % and 3.57 % for Shell181 and Solsh190 models respectively.

- Finally considering the solution times of two FE models, Solsh190 model needs approximately three times more CPU time to reach the ultimate load compared to Shell181 model.

Three lap jointed stiffened panels with different configurations, one with single stiffener, other with multi-stiffener and the third with multi-stiffener and multi-bay have been modelled with two different FE approaches. The simulation work has demonstrated the appropriateness of FE idealisations and simulation procedures. The obtained static strength results have been compared to each other and with experimental works and the important response characteristics for the both modelling approaches have been pointed out. Revealed outputs should be taken in to consideration in collapse simulations of lap jointed stiffened panels.

CHAPTER 4

AN INVESTIGATION ON FAILURE OF FSW LAP JOINTS THROUGH STIFFENED PANEL POST-BUCKING

4.1 Introduction

Advanced welding methods have already started to replace conventional riveting in the assembling process of aircraft components. Friction Stir Welding (FSW) which is a solid state process is one of those advanced welding methods and has many advantages compared to some other welding techniques. For example it has the capability to weld successfully some metallic alloys which cannot be welded by traditional fusion welding processes like arc-welding (TIG, MIG) or laser welding [400], generates low levels of distortions, provides better retention of baseline mechanical properties, creates lower residual stresses [401]. And also FSW has the advantage of joining speed when compared to riveting in assemblage process as a common property of all welding methods [402]. The fundamental aspects, metallurgical and microstructural consequences of FSW have been addressed in detail in literature [403, 404]. Another prominent advantage of FSW is the ability of dealing with lap joints. In aircraft fuselage production the lap joints play an important role which yields as a result of riveting or welding the extruded stringers on a flat skin.

The performance of the welded panels depends on integrity of weld joint through panel buckling, post-buckling and collapse. Level of stresses and material properties in the vicinity of the weld joint characterize the performance of joint. Little imperfections in the joint or high level of stresses may lead to separation of welded parts thus may cause a premature failure of panel before reaching ultimate capacity of perfect configuration. Considering the stability behaviour, the delamination and separation of skin and stringer for composite stiffened panels have been received a great attention. Using the theory of fracture mechanics and employing different damage laws (generally stress based) the studies were conducted to simulate the skin-stringer delamination through post-buckling [405-408]. But the mechanics of the interface between skin and stringer which has the potential to change the panel collapse performance has not documented in detail so far for metal panels which are assembled by FSW technology. So in present study main attention is focused on understanding failure of FSW lap joints during the compressive loading. Towards this aim, an extended study which couples experimental testing and non-linear computational simulation capabilities was undertaken. The experimental program comprises compression loaded five crippling specimens with different geometrical configurations along with several coupon tests to characterize material properties. Utilizing measured material properties the generated experimental data is then employed to validate non-linear FE simulation models. With the intent of capturing the mechanics of weld joints, results of FE models through compression loading histories are investigated. Outcomes of present study will lead to an improved understanding of mechanics involved at weld joints and promisingly build a basis for more accurate and reliable fuselage panel designs.

The study is organized as follows: Section two treats the geometric and material characteristics of test specimens and gives the details of developed nonlinear FE model. Section three presents the results of experimental studies along with the results obtained from developed FE models. Using the confirmed FE model results, section four extends the study to focus on weld joint behaviour. And section five concludes the study with summary of findings and suggestions.

4.2 Test Specimens and Developed FE Models

4.2.1 Test Specimens

Tested crippling specimens are representative of fuselage structure of a commercial aircraft and consist of single stringer. All test specimens shares same geometry of extruded Z shaped stringer (7075-T76511) while skin (2024-T3) thicknesses and widths of specimens are different. Figure 4.1 presents general configuration of test specimens. With the intent of generating knowledge on FSW weld joint behaviour and take a detailed look at mechanics of joints, two different weld geometries were generated. The first is continuous weld which begins at one end of specimen and ends at other end without a break. The second weld geometry is named as start-stop weld and as opposed to continuous weld there is a certain distance of weld interruption at centre lines of specimens along their lengths. The start-stop weld design creates a potential failure location during compression loading and ease investigation of failure mechanics. The weld itself and two types of weld geometries are depicted in Figure 4.2. In addition to two different weld designs, to increase the potential of failure and expand the knowledge for simulation environment a third design which is named as joggled specimen was manufactured. In this specimen a discontinuous weld (start-stop) combined with local skin thickness change at the centre of weld gap and associated stringer joggle. This kind of design will provide an eccentric loading for weld joint and ease separation failure of skin-stringer interface. Figure 4.2 presents the geometry of joggled specimen. Table 4.1 provides all dimensional details and naming convention of specimens.

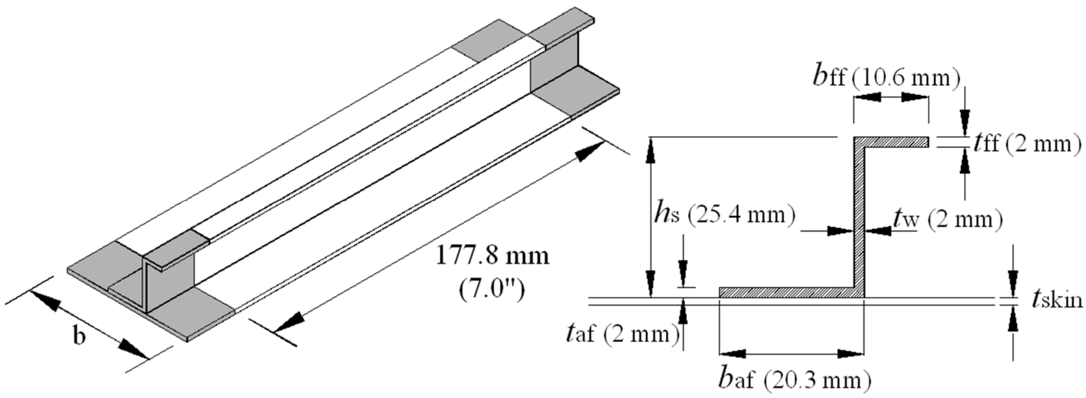

Figure 4.1 Specimens configuration

Welding leads to degradation and loss of mechanical properties in the vicinity of weld joint and generates residual stresses. In order to determine the specimens' material properties compression coupon tests were undertaken for both parent material (unwelded) and degraded material within Heat Affected Zone (HAZ). As present study focuses on the weld joint mechanics, the material properties of weld nugget have to be accounted for. To achieve this aim an additional coupon test was undertaken to measure stress-strain relationship of very locally located weld joint material. Then the stress-strain data from coupon tests were employed to generate

Ramberg-Osgood relationships for parent and HAZ materials. Knock down factor which represents the ratio of degraded material yield strength within the HAZ over parent material yield strength was measured to be 0.8 for skin and stringer. On the other hand weld joint material was idealized to possess a bilinear stress-strain relationship. The reason of this kind of idealization will be detailed in following section. Figure 4.2 presents the obtained stress-strain curves of parent materials and weld joint material. The widths of HAZ for the subcomponent panels were determined utilizing a series of Vickers micro-hardness cross-sections and the magnitude of residual stress was measured using the hole drilling method. Cerrobend bases were casts at top and bottom ends of specimens (shaded areas in Figure 4.1) to provide uniform compression loading and fully clamped boundary conditions while the unloaded edges of specimens were kept free.

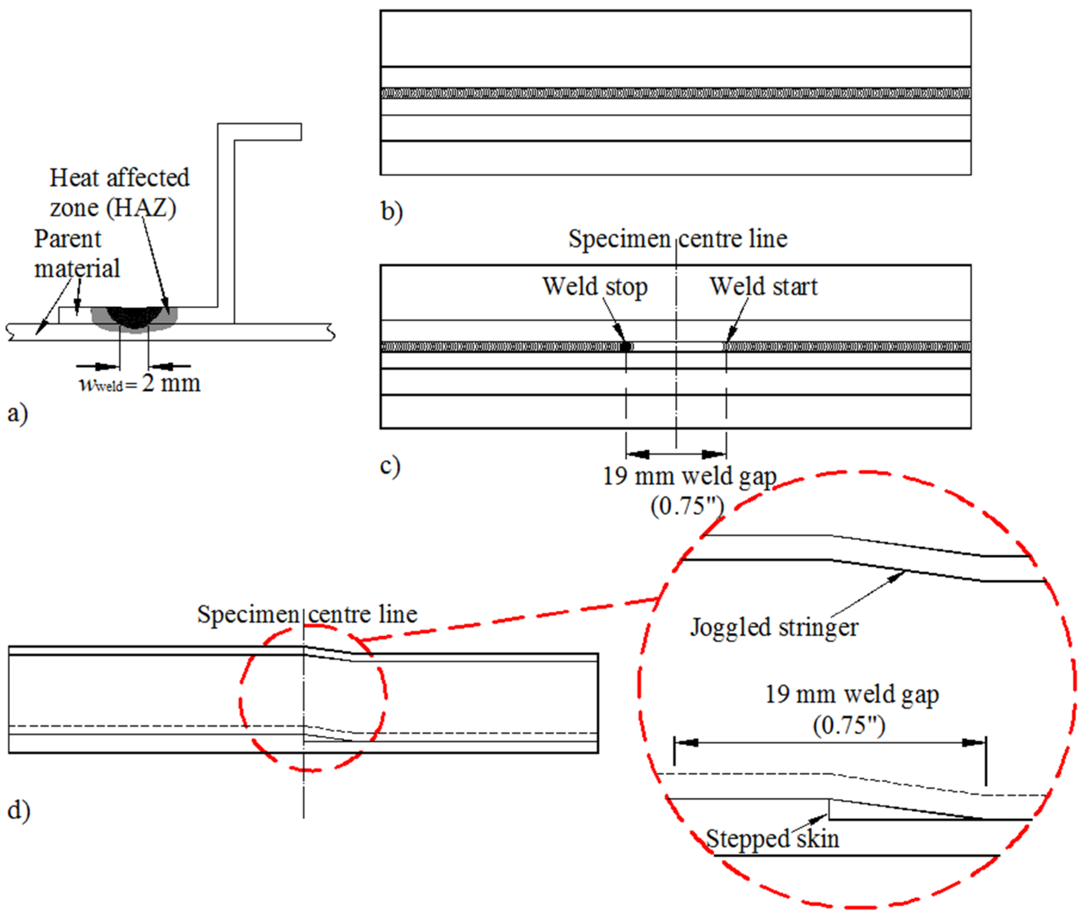

Figure 4.2 Weld details a) FSW b) continuous weld c) start-stop weld d) joggled specimen

Table 4.1. Specimens' details

Specimen	t_{skin} mm (inch)	b mm (inch)	Naming conven.
SD 080-080	2.032 (0.08)	50.8 (2)	skin thickness
SD 080-080 SS	2.032 (0.08)	50.8 (2)	start-stop weld
SD 100-080	2.54 (0.1)	63.5 (2.5)	100-080 SS
SD 100-080 SS	2.54 (0.1)	63.5 (2.5)	stringer
SD 080/100-080 JS	2.032/2.54 (0.08/0.1)	63.5 (2.5)	thickness

4.2.2 FE Idealizations

Shell elements are employed in most of research programs to investigate the stability behaviour of stiffened panels. Experiences showed that the shell elements are successful in prediction of the static strength behaviour [366, 372, 374, 375, 387, 393, 409-411]. Also compared to solid shell elements, they are effective in terms of computational time. Rigid links which are used to model rigid constraints between two deformable bodies or as rigid components to transmit forces and moments were used by Murphy et al. [393] to model the weld joint between skin and stringer shell elements. The model exhibited successful predictions of local skin buckling and collapse behaviours.

The present study is aiming at investigating the failure mechanics of FSW joints. A model developed using shell elements [393] and modelling the weld joint with rigid links would not be convenient to investigate the mechanics of skin-stringer interface. Consequently in present study a different modelling approach is presented. Solid shell elements (Solsh190) defined within ANSYS commercial FE program are used in the modelling. Solsh190 is used for simulating thin to moderately thick shell structures. The element possesses the continuum solid element topology and features eight nodes connectivity with three degrees of freedom at each node: translations in the nodal x, y and z directions. The element has plasticity, large deflection and large strain capabilities. Solsh190 is a 3-D solid element free of locking in bending dominant situations. The element formulation is based on logarithmic strain and true stress measures [398]. Figure 3 presents the details of FE idealisation and views of joggled specimen at specimen centre line. In order to obtain reliable results a fine mesh is created for the regions of skin and stringer in contact, Figure 3. The weld joint is represented by merging the nodes of stringer bottom and skin top within the measured weld joint width. In developed FE model the joint maintains its integrity through non-linear collapse analysis and the main attention is focused on behaviour of joint.

Another complication with developing a FE model for lap jointed panels is the need to simulate the physics of contact at the unwelded skin-stringer interface. For the sake of comprehension and appropriate correspondence with behaviour of test specimens the contact condition between unwelded skin and stringer interface is modelled using Conta173 surface to surface contact elements and Targe170 target elements, Figure 4.3.

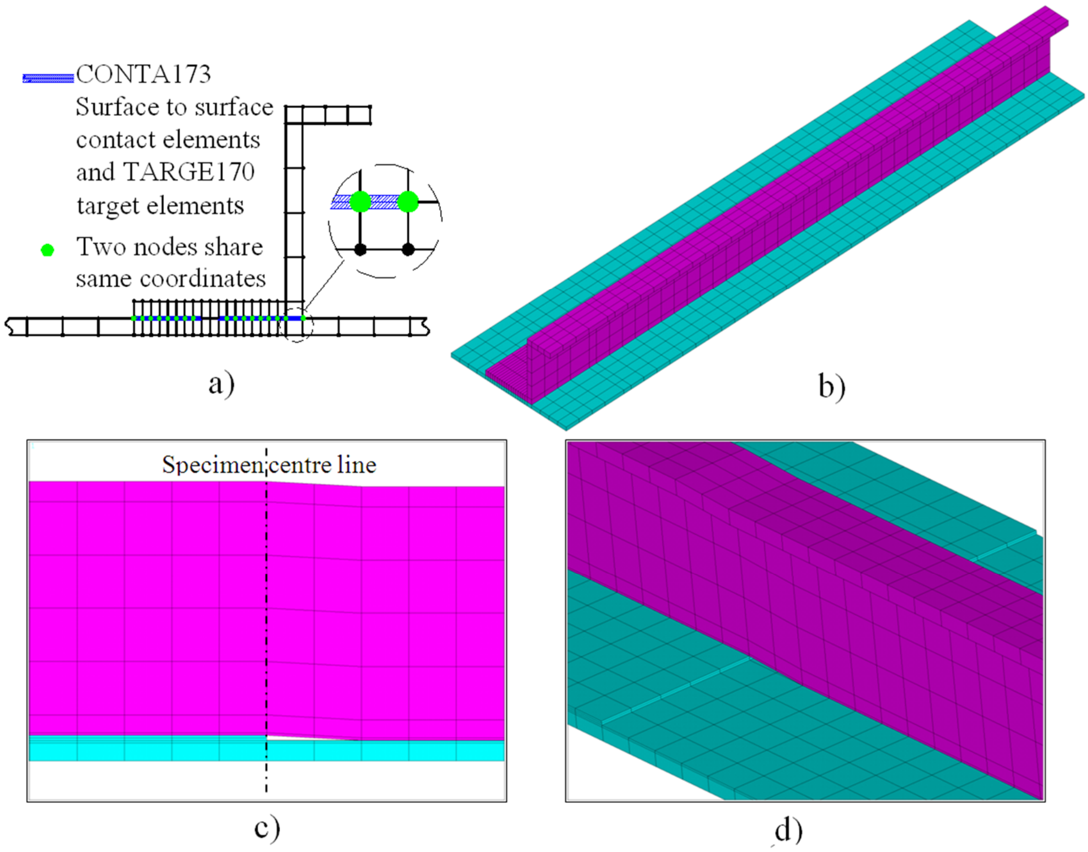

Figure 4.3 FE idealization a) cross section b) FE model c) joggled specimen side view d) joggled specimen 3D view

The stress-strain curves obtained from coupon tests for skin, stringer and weld joint materials converted to logarithmic strain and true stress measures since the developed FE model use Solsh190 element which formulation is based on this kind of measure, Figure 4.4. Then the curves are idealised as piece-wise linear portions and incorporated into the FE model using isotropic hardening rule available within the ANSYS simulation software. These curves also are used to generate similar curves by incorporating knock down factor (reduction factor of materials yield stresses, $\sigma_{0.1\%}$ and $\sigma_{0.2\%}$) for HAZ materials which have elastic modulus equal to parent materials'. Figure 4.5 illustrates the spread of materials on the cross section of specimen model. The reason of employing a bilinear stress-strain relationship for the weld joint material is the desire to obtain a clear observation of the material yield during compression loading.

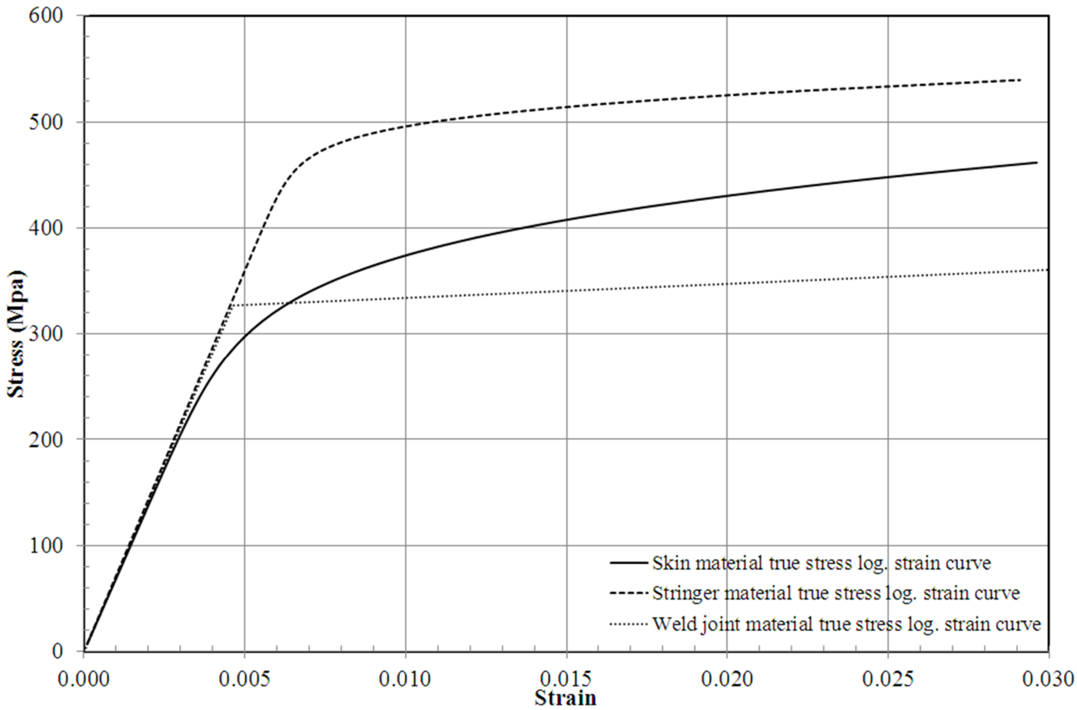

Figure 4.4 Stress-strain curves

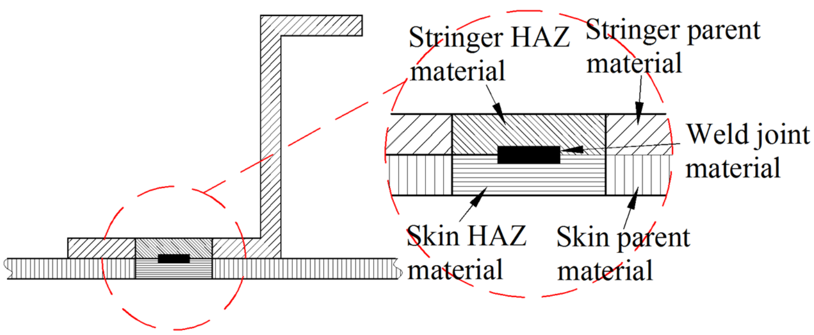

Figure 4.5 Spread of materials on cross sectional area

Geometrical imperfections are important in stability behaviour of thin walled structures and the magnitudes and shapes must be carefully handled. Because even small changes in structure may sometimes produce significant changes in its response [120]. Also bifurcation points can be avoided with the aid of geometrical imperfections. In a bifurcation analysis the stiffness matrix of the linearized FE equation becomes singular at a bifurcation point and the Newton-Raphson solver cannot proceed further [395]. In numerical studies a standard procedure to set the geometrical imperfections is to incorporate shape of a buckling mode. In case of absence of geometrical imperfection data this approach is satisfactory to capture stability behaviour [355, 366, 372, 402].

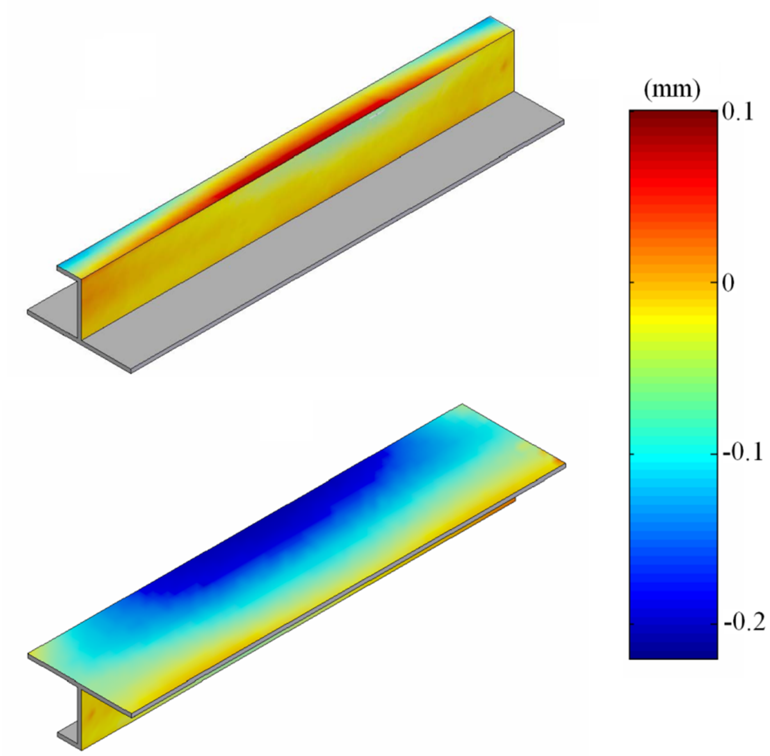

Figure 4.6 CMM plot for specimen SD 080-080

Since the main goal of the present work is to investigate the weld joint behaviour, deformation of test specimens through compression loading is very significant in terms of skin-stringer interaction. Predicting close collapse loads to test specimens but different collapse mode shapes would not be satisfactory to assess weld joint integrity. As is well known deformation of compression specimens through loading are promoted by initial geometrical imperfections. In order to simulate initial geometrical imperfections of test specimens and capture similar collapse mode shapes via FE models, specimens were scanned using Coordinate Measuring Machine (CMM) prior to testing. Figure 4.6 presents CMM plot of specimen SD

080-080. This type of geometrical imperfection is very close to specimen buckling mode. Therefore convenient buckling modes for specimens were scaled and introduced into simulation models to successfully capture collapse modes of test specimens.

Obtaining geometric distortions very close to test specimens' the testing boundary conditions are imposed to the specimen models in order to develop numerical models to be as representative of the experimental set up as possible. A uniform axial displacement (0.005 mm/step) is applied to nodes of one end with the axial displacement at the opposite end restrained.

4.3 Simulation Against Testing

This section introduces the results of experiments and corresponding simulation models. Verifying the employed simulations FE models are used to propose a measure to assess failure of FSW lap joints. Subsections of this section are created according to geometrical configurations of panels. For example SD 080-080 and SD 080-080-SS specimens only differ in the weld configurations. So it is convenient to gather those configurations under same heading.

4.3.1 SD 080-080 and SD 080-080-SS

Collapse of specimen SD 080-080 was by crippling with a collapse load of 69.48 kN. Weld joint integrity was maintained with this specimen through testing. Employing FE model the collapse load of specimen was computed as being 65.11 kN which is 6.29 % less than the experimentally measured. The same collapse mode as resulted in testing was captured via FE model, Figure 4.7. Despite a 6.29 % under-prediction of collapse load, evaluated stiffness of this specimen model is almost identical with the test specimen as can be seen in end shortening vs. compression loading figure, Figure

Specimen SD 080-080-SS performed a collapse at a load level of 66.91 kN by a crippling mode. Considering the collapse load, introducing a weld joint gap caused 3.70 % reduction of strength for this geometrical design. As with the previous test, this specimen demonstrated a weld joint integrity through loading history. 64.86 kN collapse load was computed with FE model for the SD 080-080-SS which differs by 3.06 % with experimentally measured.

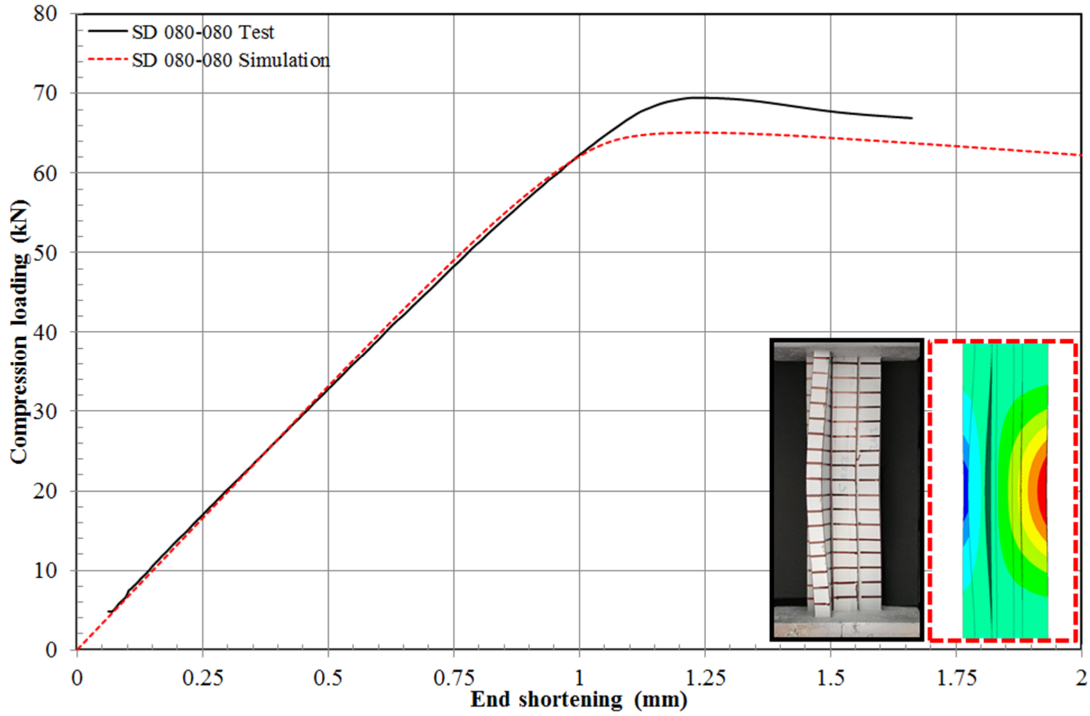

Figure 4.7 Compression loading vs. end shortening for SD 080-080

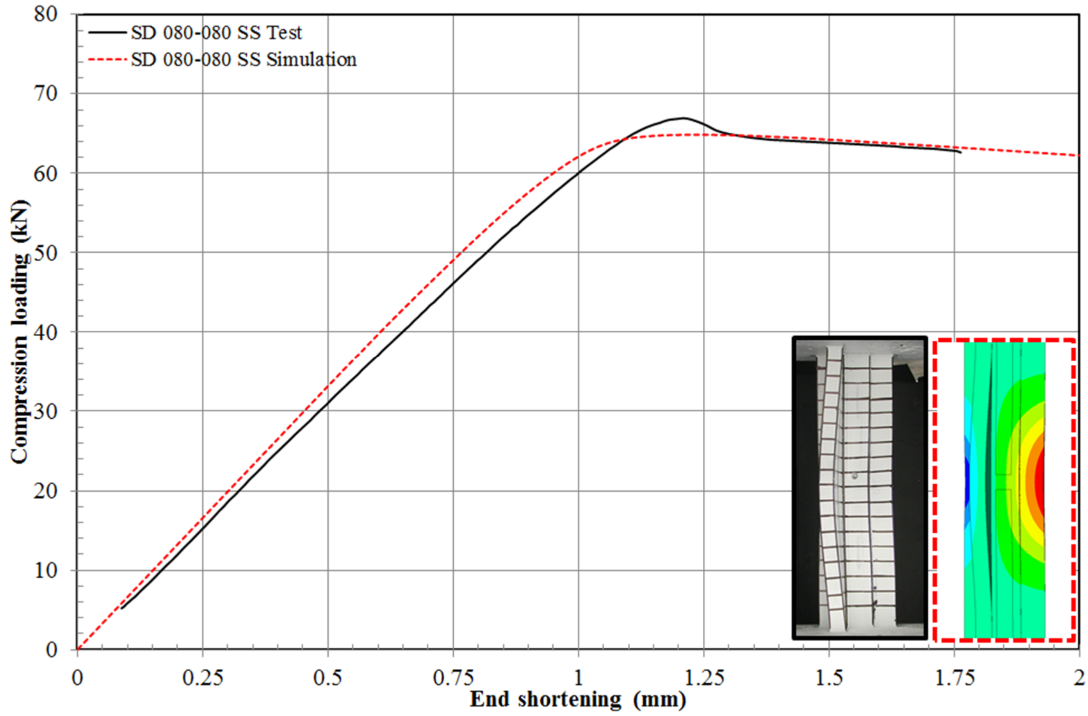

Figure 4.8 Compression loading vs. end shortening for SD 080-080 SS

Figure 4.8 presents end shortening curves for this design and collapse mode shapes. Again FE model successfully predicted the collapse mode shape as depicted in

Figure 4.8. Examining the reduction in collapse load due to weld gap with this geometrical configuration, again a minor difference was captured via FE models.

4.3.2 SD 100-080 and SD 100-080-SS

A collapse load of 81.77 kN was measured for the specimen SD 100-080. Collapse mode shape of this specimen is different compared to previous tests but could be classified as crippling mode. Weld joint integrity of this specimen was also maintained through testing. For this configuration 79.03 kN collapse load was predicted by FE model which is 3.35 % less than that of experimentally measured. Figure 4.9 provides attained end shortening vs. compression loading curves for SD 100-080 and collapse mode shapes as well. Examining Figure 4.9, it can be seen that identical collapse mode shape with the test specimen was captured with the aid of FE model.

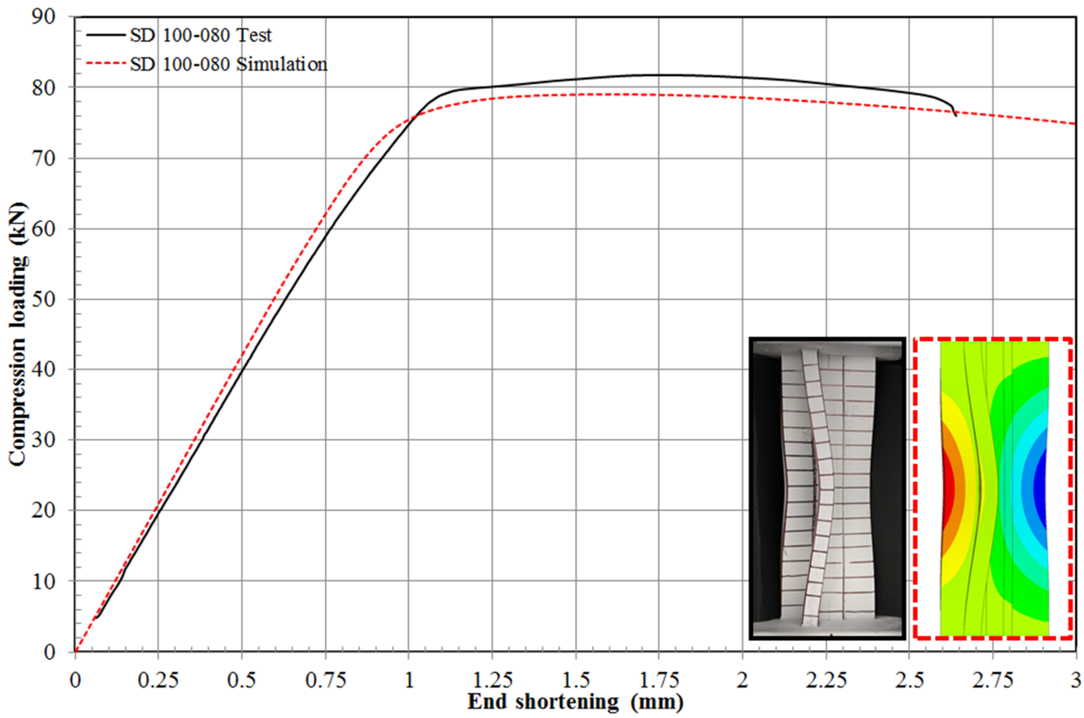

Figure 4.9 Compression loading vs. end shortening for SD 100-080

Specimen SD 100-080-SS achieved a collapse load of 78.31 kN corresponding to 4.23 % associated strength reduction by weld gap. Same crippling mode of continuously welded specimen was attained for this design which means weld gap had no effect on the collapse mode shape as with previous configurations, Figure 4.10. Weld joint integrity of this specimen again was maintained. 78.86 kN collapse load was computed for this specimen. The computed load is very close to experimentally measured as can be seen in end shortening vs. compression loading curves in Figure 4.10. Although a moderate reduction of collapse load due to start-stop weld was recorded in testing, simulation model evaluated a minor reduction. FE model successfully captured identical collapse mode shape of experimentally obtained, Figure 4.10.

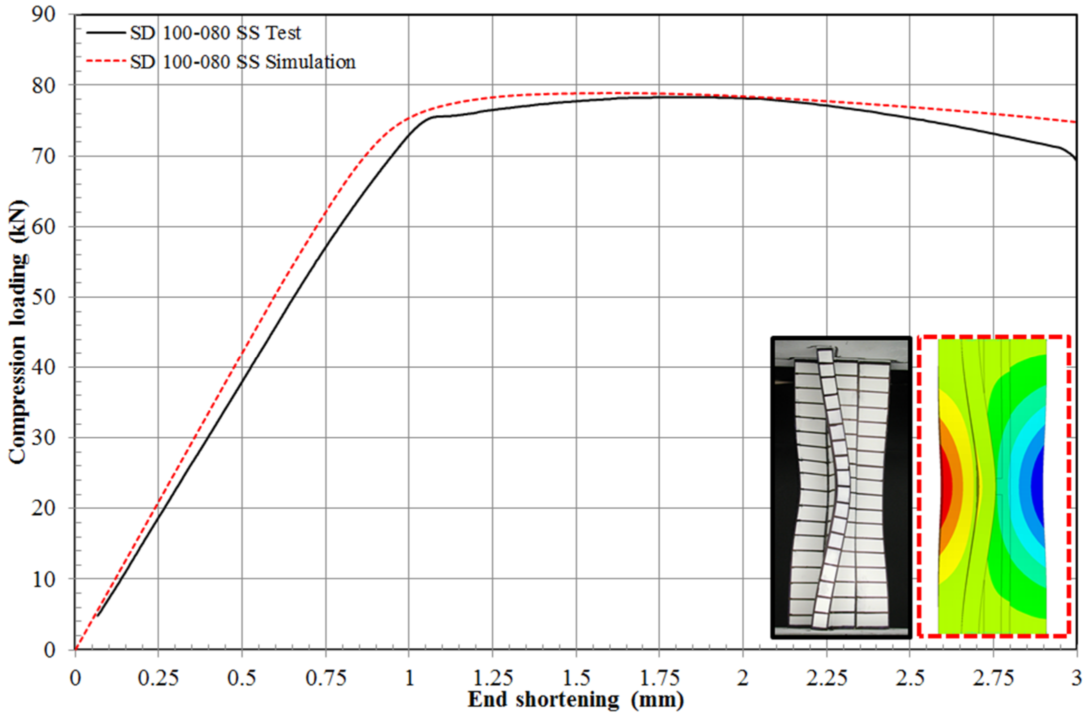

Figure 4.10 Compression loading vs. end shortening for SD 100-080 SS

4.3.3 SD 080/100-080 JS (Joggled specimen)

Specimen SD 080/100-080 JS failed with weld joint failure just before achieving collapse of perfect specimen as can be seen in Figure 4.11. Weld joint failure occurred at a load level of 71.54 kN with failure initiating at the edge of the weld start-stop. It is worth noting that weld gap and skin step have significant influences on the weld joint failure. Particularly introduction of skin step at weld gap promotes weld joint failure. This behaviour is caused by the post-buckling deformations of the global structure and is potentially magnified by local secondary bending effects (due to local change in the load path neutral axis). The mechanics at the weld start and weld stop is thus complex and unfortunately cannot be investigated experimentally. FE model which assumes an inseparable weld joint, predicted a collapse load of

71.64 kN. Considering collapse load of simulation model it can be concluded that failure of weld joint occurred at a load level close to collapse load of perfect specimen. Figure 4.11 presents end shortening vs. compression loading responses of specimen and FE model. Failure mode shape of specimen and collapse mode shape of FE model are also presented in Figure 4.11. It is evident that resulted mode shape of specimen and predicted by FE model are same, Figure 4.11.

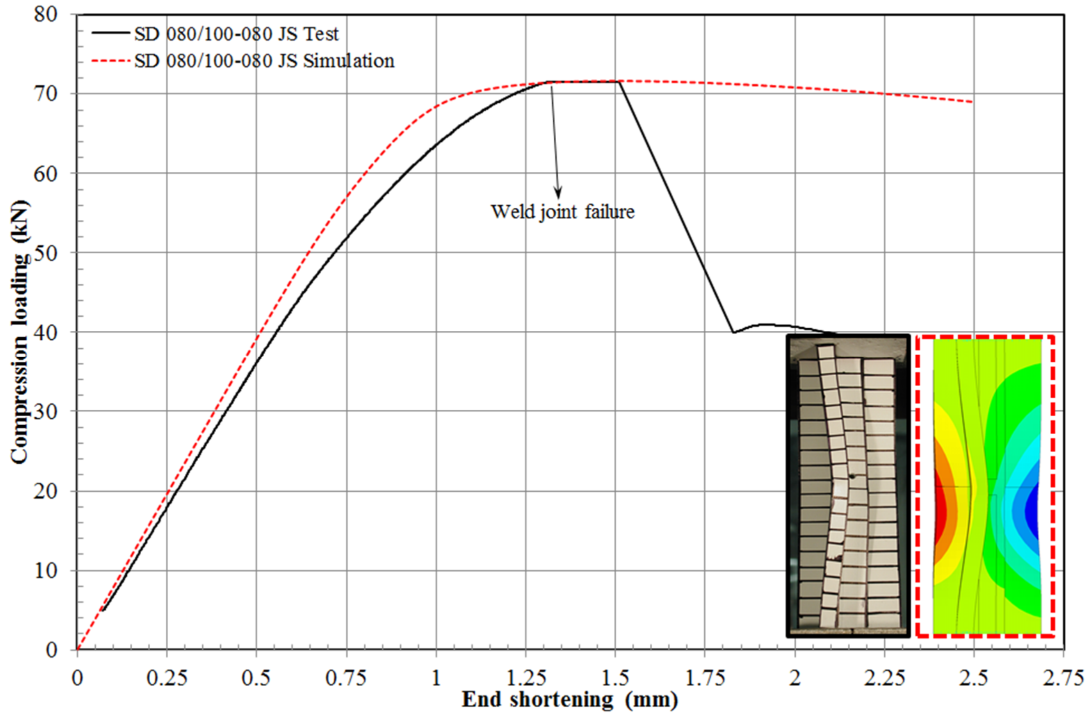

Figure 4.11 Compression loading vs. end shortening for SD 080/100-080 JS

4.3.4 Summary

Except specimen SD 080/100-080 JS, failure for all specimens was by crippling. This type of crippling failure indicates that capacities of high strength stringers are fully exploited. Weld joint gaps (start-stop welds) caused on average 4 % strength reduction compared to the equivalent cross-section continuous weld specimens. This reduction in performance is believed to relate to discontinuous skin-stringer connection and resultant reduction of skin-stringer shared support within the post-buckling domain. But only minor strength reductions were captured by means of FE models. Despite the measured strength reductions, discontinuous welds did not cause any change in collapse mode shapes and all start-stop specimens ultimately failed in a crippling mode as designed.

Failure of specimen SD 080/100-080 JS (joggled specimen) was a weld joint failure which inspired this study to investigate FSW joint behaviour. Failure of joint initiated at the edge of weld start-stop. Unfortunately to understand the complex mechanics at failure location there is no experimental opportunity to employ. Results presented in this section demonstrate that in general FE predictions are in good agreement with test results. Therefore, utilizing FE software with activating geometrical and material non-linearity capabilities and simulating the contact physics at unwelded skin-stringer interface a detailed investigation can be undertaken. Thus following section treats the investigation of weld joint mechanics via developed FE models.

4.4 Weld Joint Behaviour

The application of a stress based criteria may be considered as a measure for joint failure. However, this approach raises difficulties in combination of components of stress tensor. In the study conducted by Reimers [412], a stress based criteria was proposed to assess weld joint integrity. That study focused on weld joints which is formed by welding L shaped stringers on curved skins. So the configuration is different than that of panel configurations considered here. In the preliminary stages of the present study the proposed stress formulation by Reimers [412] was applied to characterize behaviour of joints but the criteria failed to explain the weld joint failure of joggled specimen. Probably this is because of created eccentricity for the joggled specimen and the stress components proposed by Reimers [412] could not represent the case. Accordingly with the intent of proposing a general measure, equivalent plastic strain (EPS) development at weld joints was investigated. The results through end shortening history of simulation models suggested that EPS has the potential to be a measure to assess weld joint failure. In assessment of weld joint integrity it is essential to capture the developed maximum EPS at weld joint. Simulation results suggest that maximum EPS does not take place at centre lines for constant skin thickness specimen models. So the EPS developments which have maximum magnitudes were taken as reference in assessment process. Investigation of contact condition at the unwelded skin-stringer interface through buckling, post-buckling and collapse of specimen has the potential to explain mechanics of skin-stringer interaction and separation. Since the contact physics is modelled using surface to surface contact elements (Conta173 elements), it is possible to capture the interaction through the compression loading. So in the following subsections accompanying EPS measurement, contact opening distance plots are also employed to characterize behaviours. Contact opening distance plots are extracted for collapse load and introduced final end shortening levels of each simulation model to capture the development of openings through loading history.

4.4.1 SD 080-080 and SD 080-080-SS

Skin-stringer contact interaction at collapse and final end shortening levels are depicted in Figure 4.12. At collapse load level contact opening distance at stringer edge is 0.32 mm. This distance increases to be 0.68 mm at final end shortening of 2 mm. Location of maximum opening distance remains same through compression loading. Also it is worth noting that local skin buckling promotes the development of contact opening. Onset of opening occurs just before local skin buckling and gains very small magnitudes. After local skin buckling, contact opening changes the behaviour and increases very sharply. Weld joint EPS details for specimen model SD 080-080 are presented in Figure 4.13. Examining developed maximum EPS, specimen weld joint receives 0.59 % EPS at collapse load and 2.05 % EPS at final end shortening of 2 mm. At panel centre line received EPS at collapse load level is 0.27 %. And at final end shortening level EPS for this location is 0.79 %.

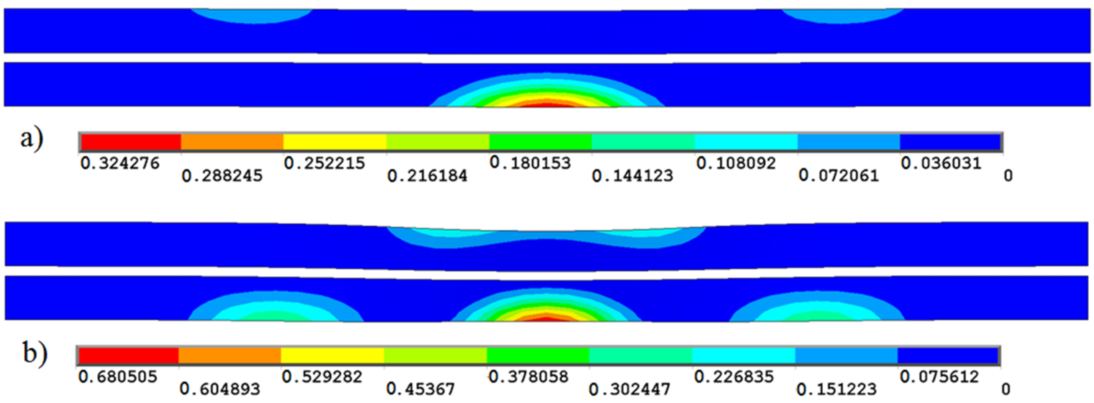

Figure 4.12 SD 080-080 contact opening a) at collapse b) at final end shortening

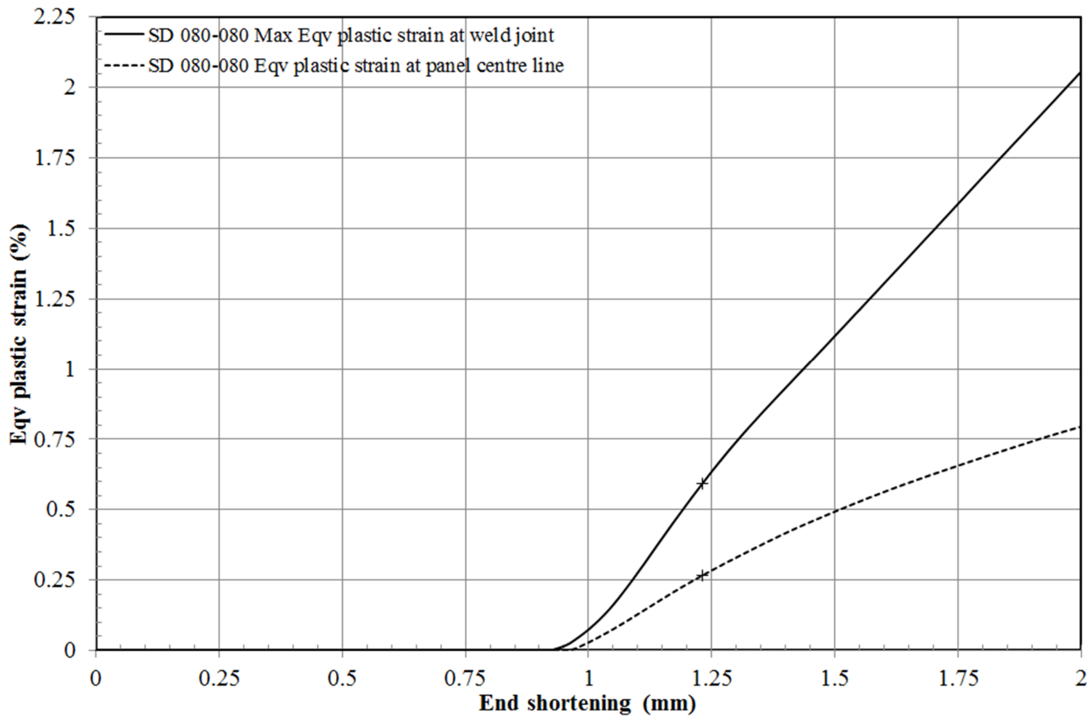

Figure 4.13 Contact behaviour and EPS at weld joint for SD 080-080 SS

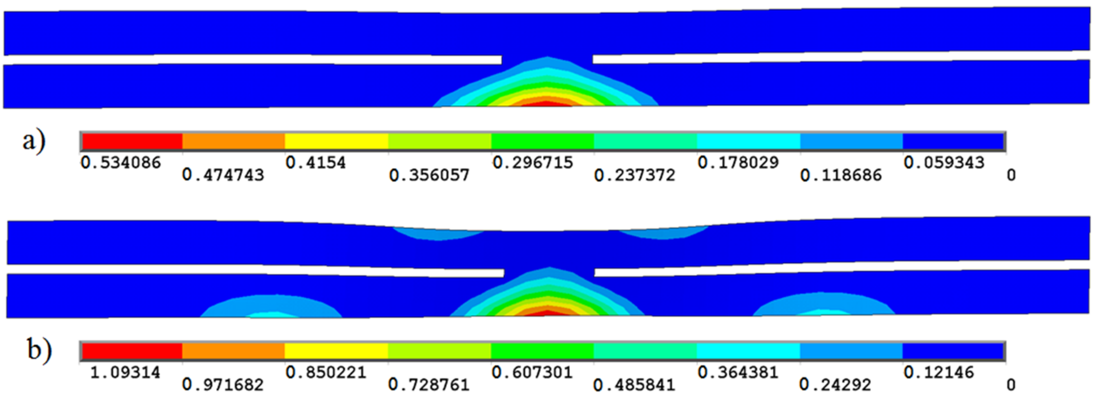

Figure 4.14 SD 080-080 SS contact opening a) at collapse b) at final end shortening

Figure 4.14 details contact opening plots for specimen model SD 080-080-SS. 0.53 mm contact opening was captured at stringer edge at collapse load level. In Figure 4.14 it is evident that also opening occurs at created weld gap. This means that weld gap leads to 66 % more opening distance at stringer edge for this configuration. Predicted opening distance at final end shortening of 2 mm is 1.09 mm at stringer edge. Again location of maximum opening remained same through compression loading. 0.60 % maximum EPS was predicted at collapse load level and increased to 1.98 % at final end shortening of 2 mm. 0.60 % maximum EPS is just slightly higher than the predicted 0.59 % EPS for SD 080-080. And the location of maximum EPS also remains same. Level of EPS at the edge of weld start-stop is 0.50 % at collapse load level and close to maximum predicted EPS at weld joint, Figure 4.15. This level of EPS at the edge of weld start-stop proofs the potential of start-stop weld to lead a joint failure compared to predicted EPS for equivalent continuous weld specimen. EPS for this location increases to be 1.34 % at level of final end shortening.

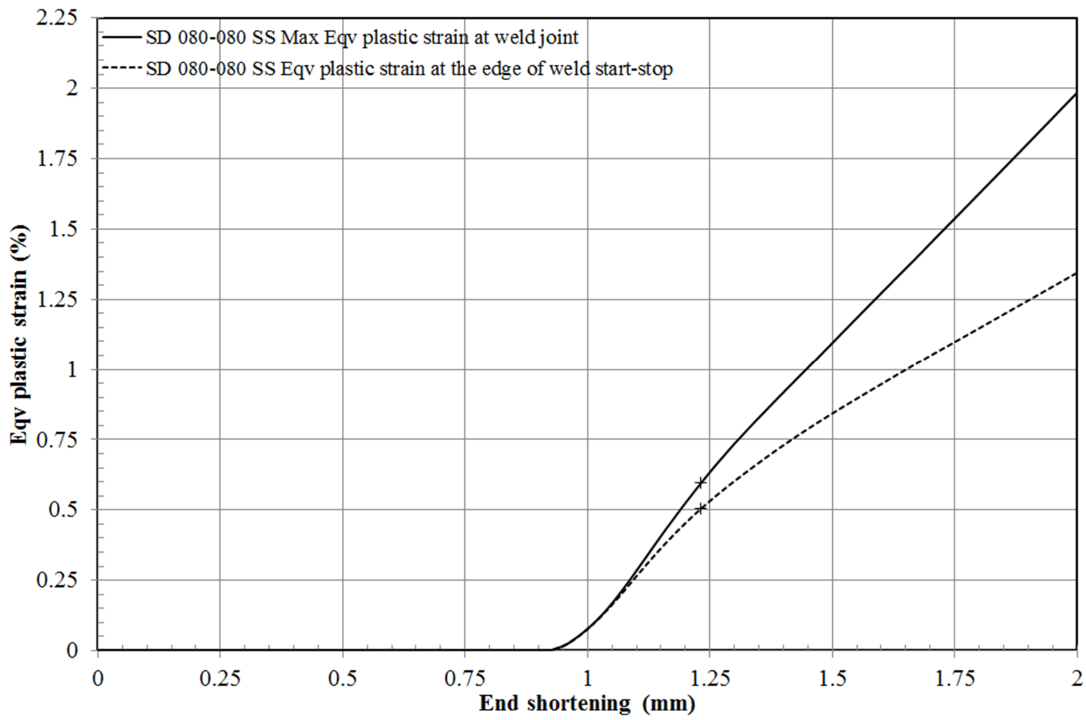

Figure 4.15 SD 080-080 SS EPS at weld joint

4.4.2 SD 100-080 and SD 100-080-SS

Figure 4.16 provides contact opening distance plots for specimen model SD 100-080. Since specimen model SD 100-080 exhibited a different crippling mode, skin-stringer contact interaction changed significantly as expected, Figure 4.16. For this type of crippling mode maximum opening occurred at a different location than specimen centre line, Figure 4.16. At collapse load level 0.09 mm maximum opening distance was computed. As opposed to behaviour of previous set maximum opening jumps to other side of stringer through the loading and ends up with 0.66 mm magnitude at final end shortening level of 3 mm. This behaviour is attributed to collapse mode shape of this specimen model. Weld joint receives 1.24 % maximum EPS at collapse load level and at final end shortening level of 3mm EPS increases to be 3.34 % for this location, Figure 4.17. The EPS at panel centre line at collapse load level is 0.36 %. The level of EPS increases to be 1.46 % for this location at final end shortening level.

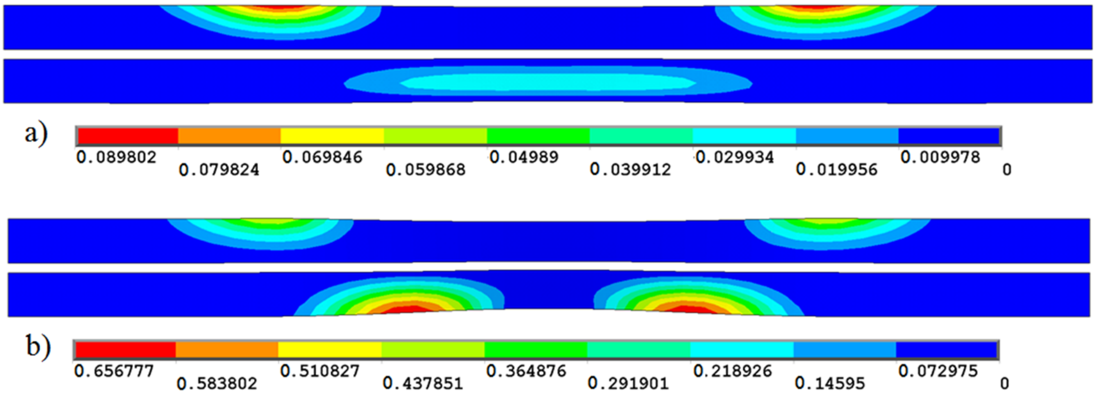

Figure 4.16 SD 100-080 contact opening a) at collapse b) at final end shortening

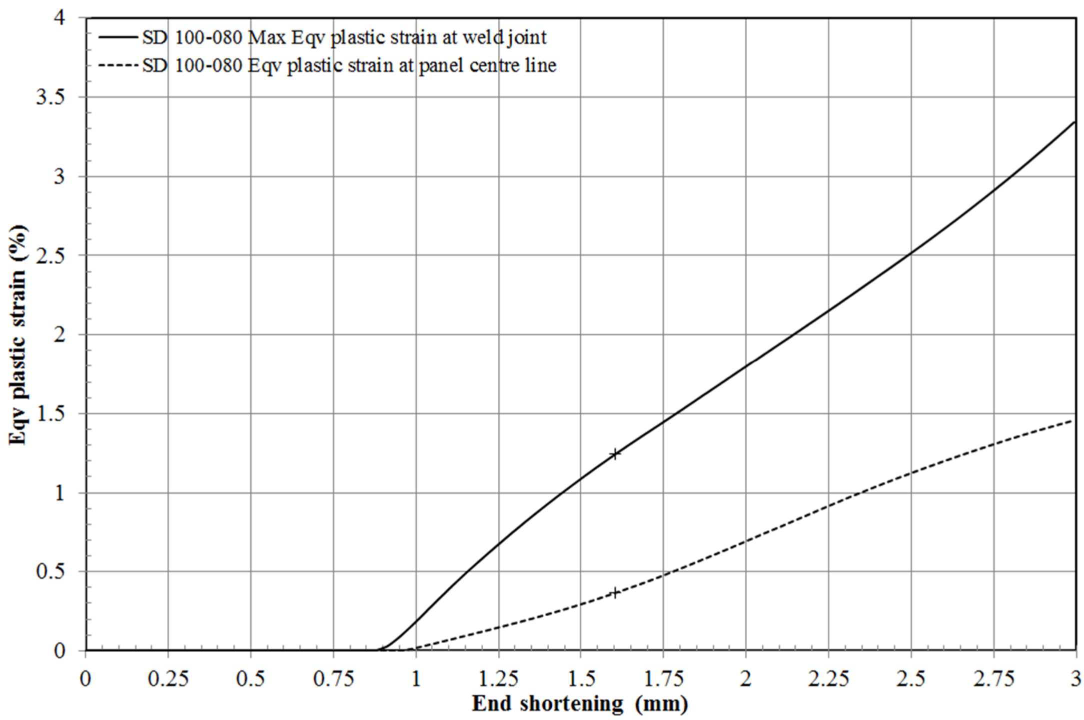

Figure 4.17 SD 100-080 EPS at weld joint

Figure 4.18 presents the contact opening plots for start-stop specimen model SD 100-080-SS. Figure 4.18 shows the significant contact loss at weld gap for this configuration. For this crippling type of collapse weld gap did not caused much more opening distances, Figure 4.18. Because maximum opening occurred at different location than panel centre line. Maximum EPS at weld joint at collapse load level was predicted to be 1.25 % and increased to be 3.40 % at final end shortening level.

At the edge of weld start-stop 0.57 % EPS was computed at collapse load level, Figure 4.19. For this location the EPS increased to be 1.94 % at final end shortening. It should be noted that although weld start-stops could not promote maximum EPS to occur at start-stop edge locations, they significantly increased magnitude of EPS.

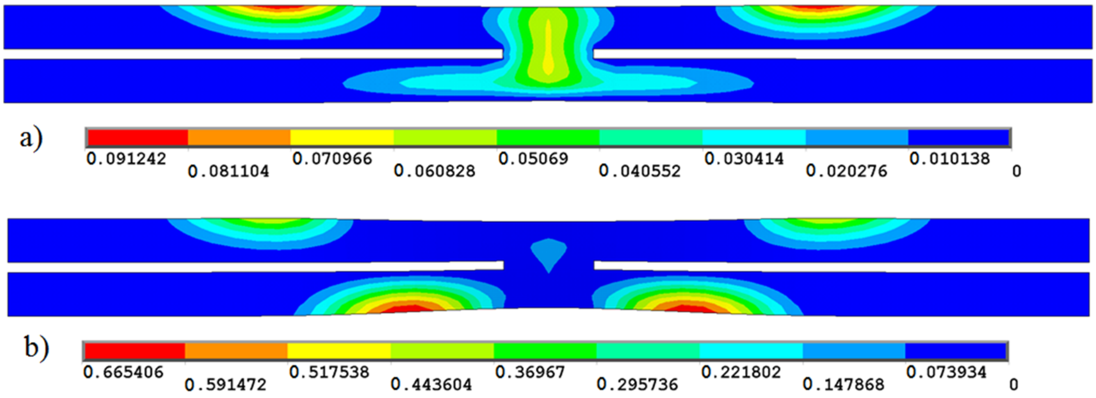

Figure 4.18 SD 100-080 SS contact opening a) at collapse b) at final end shortening

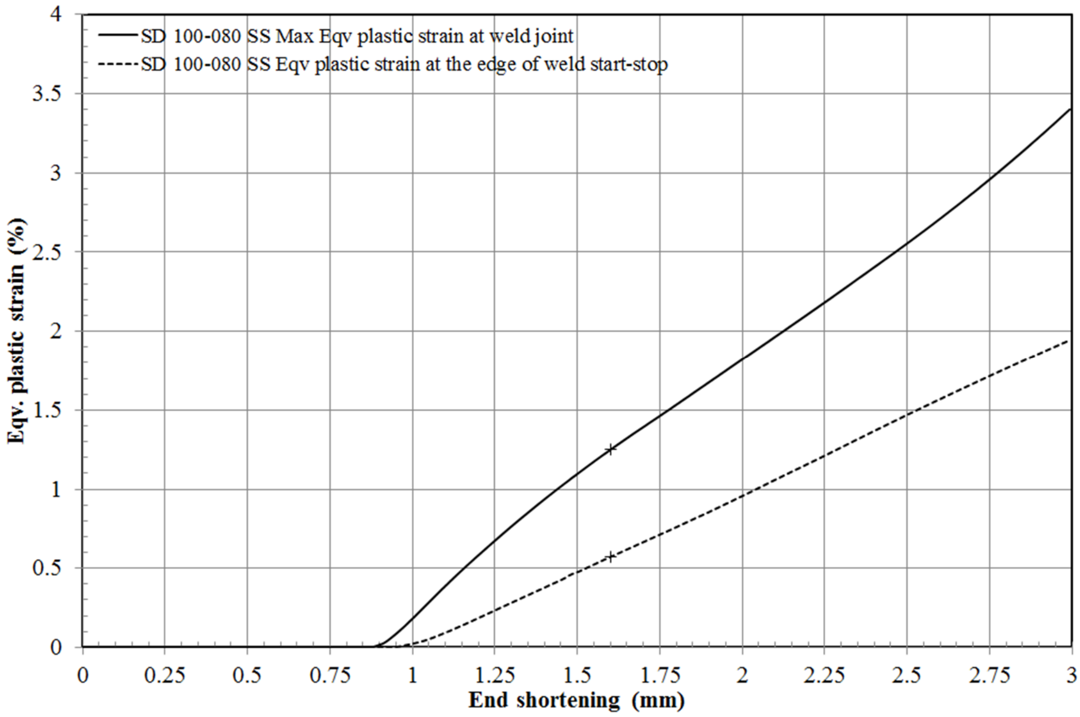

Figure 4.19 SD 100-080 SS EPS at weld joint

4.4.3 SD 080/100-080-JS (Joggled specimen)

Skin-stringer contact interaction for specimen model 080/100-080-JS are presented in Figure 4.20. Failure of this specimen was a weld joint failure as detailed in previous section. Investigation of FE model of this specimen with an assumption of inseparable weld revealed significant drawbacks to assess weld joint failure. As expected specimen model 080/100-080-JS exhibits very distinct behaviours compared to previous specimen models. Examining the contact behaviour at weld gap, stringer entirely loss contact across the width of the flange at level of collapse load, Figure 4.20. Also it should be noted that as opposed to previous specimen models onset of contact openings begin with initiation of compression loading. These behaviours are related to incorporated stepped skin and associated eccentric loading. 0.44 mm maximum opening occurs at panel centre line at collapse load level. Beyond the collapse maximum opening changes location and 0.58 mm opening occurs at final end shortening level of 2.5 mm. Magnitudes of openings are not very large. But entire contact loss at specimen centre is enough to understand the skin-stringer interaction.

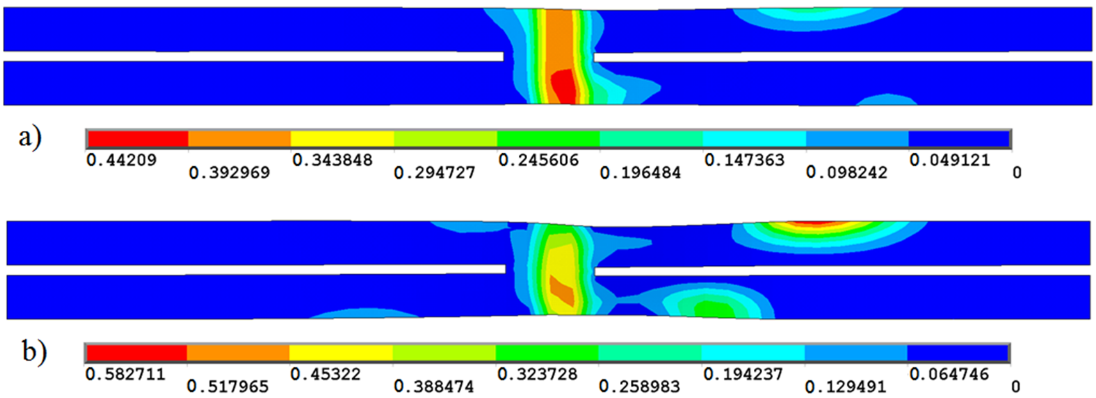

Figure 4.20 SD 080/100-080 JS contact opening a) at collapse b) at final end shortening

Considering the received EPS at the edge of weld start-stop it is obvious that joint is exposed to significant amount of EPS, Figure 4.21. And stepped skin design leads EPS to initiate at early end shortening level compared to previous designs as can be seen in Figure 4.21. Start-stop weld with stepped skin design successfully promotes maximum EPS to be at the edge of weld stat-stop. At collapse load level EPS at joint is 1.64 %. Among the predicted EPSs for all previous specimen models, this magnitude is 31 % higher than the largest EPS prediction (EPS prediction of SD 100-080-SS was 1.25 %). This behaviour explains weld joint failure of test specimen. EPS increases to be 3.70 % at final end shortening of 2.5 mm. This magnitude of EPS is very large compared to obtained ones for previous models. Therefore captured EPS behaviour at joint through compression loading suggests that EPS has the potential to be a measure in designs of FSW fuselage panels.

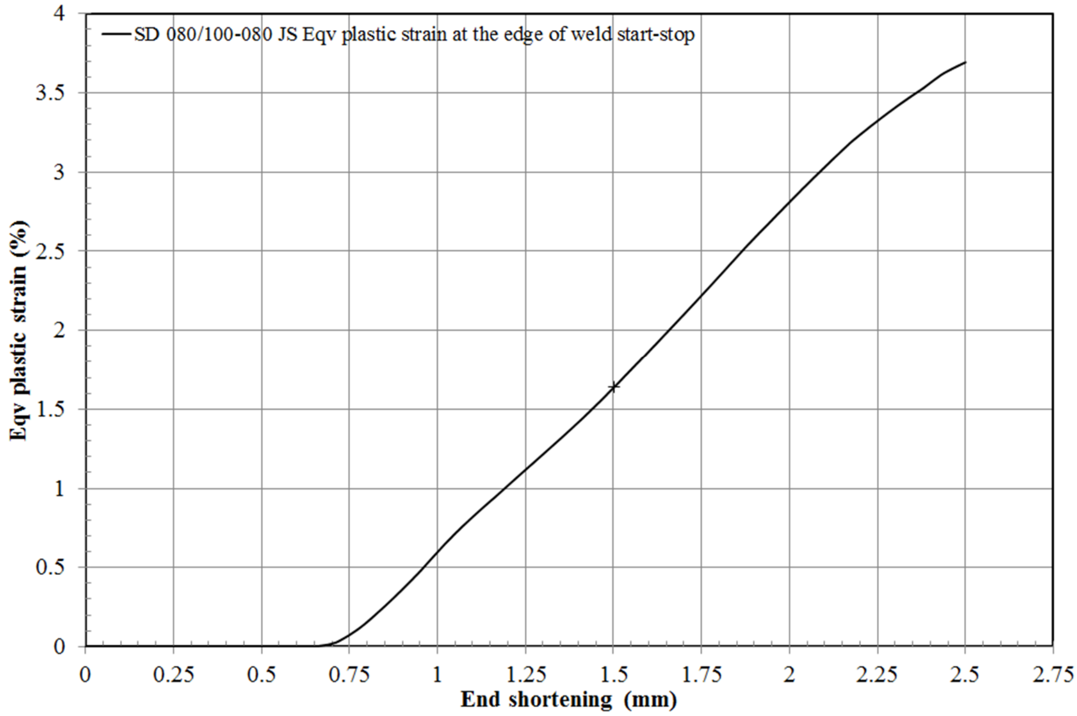

Figure 4.21 SD 080/100-080 JS EPS at weld joint

4.5 Summary and Conclusions

Today's novel and fully engineered aircrafts require adoption of new structural assembly methods such as FSW which has many advantages compared to traditional riveting. However FSW raises significant concerns such as the need to consider weld joint integrity under service loads. Because as is well known performance of welded panels depends on weld joint integrity and a failure at weld joint before achieving collapse of panel may cause detrimental strength reductions. Herein, experimental and FE simulation capabilities were coupled with the intent of generating knowledge to present an efficient procedure to assess weld joint failure. Out of five experiments, one specimen exhibited weld joint failure under compression loading before reaching collapse load of perfect configuration. It is worth noting that there is no chance to capture the complicated mechanics of joint failure during the experimental study. To investigate joint behaviour and detail the study with the aid of simulation capabilities, FE models of five test specimens were built. Weld induced residual stresses, material degradation in HAZ and contact conditions at unwelded skin-stringer interface were accounted for in FE models. To set the initial imperfections weld induced distortions were simulated. The loading and boundary conditions were incorporated into FE models as well in such a way that would represent test conditions. Combining the experimental and simulation results following conclusions can be made.

Test results draw particular attention to 4 % on average strength reductions due start-stop weld created at the centre of specimens. But no weld joint failure was occurred due to weld gap and start–stop specimens failed in a crippling mode as designed. Also no change in collapse mode shapes occurred due to start-stop weld compared to equivalent continuous weld specimens. Specimen 080/100-080-JS which has a stepped skin design failed with weld joint failure before achieving collapse load. Predicted collapse modes and loads by FE models were generally in good agreement with the modes and loads observed in the tests. Extracted contact plots showed the skin-stringer interaction at unwelded interface. Contact plots demonstrated that openings are concentrate at the centre lines of specimens as expected. Importantly with the contact plots openings were captured at the weld gaps for start-stop specimens. These plots confirm that compression loaded stiffened panels are sensitive to weld gaps and skin-stringer contact losses occur at gap locations. Employed EPS measure to assess weld joint integrity seems to be successful to explain the mechanics at weld joints. Predicted EPS magnitudes at collapse load levels for the start-stop specimens are significantly larger than that of predicted for equivalent continuous weld specimens. These computed magnitudes confirm the detrimental effect of weld gaps in terms of joint integrity. Predicted EPS for the specimen SD 080/100-080 JS which exhibited a weld joint failure is significantly higher than that of predicted for all previous specimens. Weld joint failure of this test specimen can be explained employing this approach. The magnitudes detailed for specimen SD 080/100-080 JS can be used in computational evaluations of stiffened panels manufactured by welding 7075-T76511 stringers on 2024-T3 skin. The proposed method which is based on present study on subcomponent panels can be deployed in future fuselage designs to remove premature failure of weld joint and associated strength reduction. To compensate for uncertainties inherent in the simulations, EPS magnitudes predicted here should be factored before adopting the evaluations.

CHAPTER 5

BUCKLING/POST-BUCKLING STRENGTH OF FSW AIRCRAFT STIFFENED PANELS

5.1 Introduction

To reduce the manufacturing cost and mass of aircraft aluminium stiffened panels significant research has been conducted on welding fabrication [1-17]. The key manufacturing challenges include the development of processing methods which robustly produce high quality joints but which do not significantly degrade the local material properties. Typically the aluminium alloys used in aircraft applications are heat treated to maximise static strength and thus the introduction of an intense localised heat source can degrade local joint material properties. This has focused research on the use of welding processes which can concentrate heat input (e.g. Laser Beam Welding, LBW), or processes which work at lower temperatures than traditional fusion processes (e.g. Friction Stir Welding, FSW), and has resulted in the development of new aerospace weldable alloys [18]. The introduction of localised heat, the thermal conductivity of aluminium alloy and the thin-walled nature of aerospace stiffened panels make the task of minimising or controlling welding process residual panel distortion another major manufacturing challenge. Panel distortion arises due to the development of high transient thermal strains in the joint region during welding. When heat is applied compressive stresses are induced in the surrounding material due to thermal expansion. When the joint is formed and the cooling begins, the contraction of the local joint is resisted by the surrounding material creating tensile residual stresses. Some of the developed stress state may be relieved by the structure distorting, with the remaining stress state typically complex in nature. The optimisation of welding process parameters and the introduction of pre- and post-weld heat or mechanical treatments to minimise the final component residual stress and distortion state is key to the use of welding within the manufacture of aircraft thin-walled stiffened panels.

Major developments have been seen in all of the noted manufacturing challenges and the largest questions now occupy the themes of designing, analysing and verifying the generic use of welded aircraft stiffened panels. The herein work focuses on the static strength requirements of stiffened panels with this article aiming to demonstrate the static strength potential of a large scale welded aircraft panel with multiple lateral and longitudinal stiffener bays, verifying that the behaviour demonstrated during collapse is dominated by typical panel behaviour, and not by weld joint strength limitations. Such behaviour is required to maximise the strength to weight ratio of the panel structure. Having proved the large scale welded aircraft panel performance, detailed Finite Element simulation is then undertaken to determine the sensitivity of panel static strength performance to varying levels of welding process residual effects. Finally, with the developed experimental data it is possible to validate a previously published analysis procedure for static strength design which acknowledges the key welding altered panel properties, but to date has only been validated against small scale coupon experimental results [12].

The study is organised as follows: Section 2 briefly introduces the FSW process and reviews the state-of-the-art in the static strength verification of FSW in aerospace stiffened panel assembly. Section 3 and 4 present respectively the experimental and simulation components of the study, and Section 5 presents the combined results. Section 6 outlines the verification of the previously published design method and Section 7 concludes the chapter with a summary of the key findings.

5.2 Background

5.2.1 Stiffened panels

Stiffened panels dominate the wing, fuselage and empennage structure of aircraft. These are thin-walled structures, which exhibit structural instability when loaded in compression, potentially failing with stress levels lower than the material limits of their sub-components. The strength analysis of potentially unstable structures is dependent on component geometric dimensions, boundary conditions, load type, initial geometric and stress imperfections, as well as material properties. Thus stiffened panels are typically idealised as plate and column sub-components for static strength analysis [19]. For stiffened panels designed to operate in the post-buckled region, the panel skin may experience initial instability through localised skin segments buckling between lateral and longitudinal stiffeners. This initial buckling does not constitute panel failure as the panel can be designed to have the stiffeners carry additional loading until they become unstable and collapse. Moreover the support of the stiffeners enables a portion of the skin to carry load beyond the point of initial skin buckling, increasing the efficiency of the panel design. The ability to accurately predict the initial buckling, post-buckling and failure collapse behaviour of aircraft stiffened panels is therefore essential to aircraft design [20].

5.2.2 Friction Stir Welding

As indicated in the introduction significant research has been undertaken to develop welding technology capable of replacing riveting as the primary fabrication method for the production of aerospace stiffened panels. The key advantage of welding is the potential speed of the joining process when compared to riveting [1, 4-7]. In addition the removal of the vast majority of mechanical fasteners and the potential to select more structurally efficient stiffener pitching may enable reduced final panel weight. Although welding has many potential advantages the heat necessary for joining typically results in residual welding effects. The performance of thin-walled structures is potentially sensitive to these residual welding effects and therefore to minimise any impact FSW is of particular interest given its processing temperatures are typically lower than classical welding methods, resulting in the potential for reduced residual stress and distortion in fabricated panels, and reduced mechanical property degradation (in terms of ductility and strength [21]).

The FSW process is a solid state joining technique which uses local frictional heating to produce continuous solid-state seams. The process joins material by plasticizing and then consolidating the material around the weld line. A cylindrical, shouldered tool with a protruding pin is rotated and plunged into the components to be joined at the start of the weld line. The tool continues rotating and traverses forward in the direction of welding. Frictional heat is generated between the wear resistant tool and the component material. As the tool proceeds, the friction heats the surrounding material and rapidly produces a plasticized zone around the pin. This heat causes the local material to soften to a temperature below that of the material melting temperature and typically within the material's forging temperature range. As the tool moves forward metal flows to the back of the pin where it is extruded behind the tool. It then consolidates and cools to form the bond. To produce a lap joint, considered herein, the pin must extend a small amount through the bottom of the top component and into the bottom component, creating a metallic bond between the two components. A schematic drawing of the lap joint welding process used herein is shown in Figure 5.1.

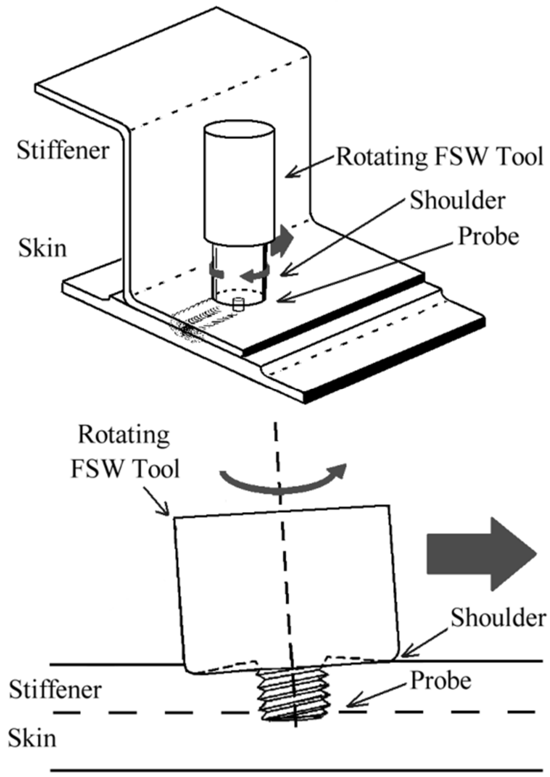

Figure 5.1 A Schematic of the lap joint welding process

5.2.3 Static strength of aerospace FSW panels

FSW has been investigated as a rivet replacement technology for panel construction within spacecraft launch vehicles [3, 8]. First simple coupon testing was undertaken to check the basic shear strength of welded lap joints. These tests demonstrated the potential for FSW joints to exceed the lap shear strength of traditional riveted joints [3]. To assess skin-stiffener weld joint strength under representative panel loading (longitudinal compression), single-stiffener compression specimens (112 x 533 mm) where then tested [3]. These specimen tests where designed with a reduced effective length compared to the real application enabling the welded skin-stiffener assemblies to be loaded to extremely high compression stress levels, much higher than would be possible within a panel with a representative effective length. The experimental results demonstrated the panel weld joint strength in the post-buckling region, with the welded specimens exhibiting a higher average initial buckling load than the equivalent riveted specimens (+16 per cent), but showing a marginally lower average crippling failure load (-7.7 per cent).

A single-stiffener specimen does not necessarily represent the behaviour of a vehicle panel, containing a focused cross-section it typically contains a higher percentage cross-sectional area of weld affected material. Moreover a single-stiffener specimen contains only a single set of welding process effects, whereas a vehicle panel will be subjected to multiple welding processes and the potential compounding of weld induced effects. Thus in the final stage of the launch vehicle research study equivalent welded and riveted large-scale multi-stiffener panel specimens (838 x 1524 mm) were designed, manufactured and experimentally tested under static compression loading [8]. Both specimens exhibited large initial geometric imperfections and initial skin buckling well below the predicted values. Pre-buckling global stiffness of both panels was approximately equal; however the welded panel exhibited a lower post-buckling stiffness and a 20 per cent lower failure load than the riveted panel. These results emphasise the potential impact of welding process effects and the importance of including these within strength analysis methods. Moreover the variation in welded and riveted specimen performance between the single and multiple-stiffener specimens reinforces the importance of ultimately testing at the full scale level.

FSW has also been investigated as a rivet replacement technology for fuselage manufacture [13, 14]. Again, the work first examined reduced effective length single-stiffener compression specimens (104 x 215 mm) [13]. For each specimen tested, weld joint integrity was maintained throughout local skin buckling, post-buckling and ultimate specimen failure, verifying weld joint performance. In this work no equivalent riveted specimens were tested but an attempt was made to quantify the impact of welding process effects on specimen static strength performance via computational studies modelling the experimentally tested single-stiffener specimen design. The computational results determined that initial specimen skin buckling was principally influenced by the magnitude of the welding induced residual stresses and the resultant geometric distortions. The computational results also determined that the level of material property degradation within the Heat Affected Zone (HAZ) and the welding induced residual stresses had the greatest influence on specimen collapse. Overall the simulations determined significant sensitivity to the examined range of welding process residual effects, with a maximum variation in initial specimen skin buckling load of 15% and for specimen collapse load a maximum variation of 9%.

A second stage of research examined multi stiffener panels (334 x 575 mm) again with a reduced effective length [14]. Test specimen weld joint integrity was maintained throughout initial skin buckling, post-buckling and ultimate specimen failure, verifying weld joint performance. Again using experimentally validated Finite Element models the impact of welding process effects where studied. This work determined that for the examined multi stiffener panels, initial skin buckling was predominantly influenced by the magnitude of welding induced residual stresses and associated geometric distortions. In contrast, the panel collapse behaviour was determined to be most sensitive to the lateral width of the weld joint, and the magnitude of the welding induced residual stresses. Overall the simulations again determined a significant sensitivity to the examined range of welding process residual effects, with a maximum variation in initial specimen skin buckling load of 59.4% and for specimen collapse load a maximum variation of 7.0%.

These second stage tests allowed a more realistic percentage volume of welding process affected material within the specimens but the specimen's reduced effective length compared to actual fuselage structure will have artificially constrained geometric imperfections induced by the welding process and impacted on panel residual stresses. Thus a final research stage is required with a specimen with multiple lateral and longitudinal stiffener bays, representing full scale fuselage structure. Moreover such experimental work would enable the extension of the simulation based analysis on the impact of individual welding process effects on panel static strength.

FSW has also been investigated as an assembly method for the integrally stiffened panels found on the upper wing cover of commercial aircraft [16]. No experimental test data is presented but detailed Finite Element simulations demonstrate the potential impact of weld joint material property degradation on the maximum buckling load of the assembled wing structure.

Finally, modifications to conventional aircraft panel static strength design methods have been proposed [12]. Single-stiffener specimen results have established that standard panel buckling analysis procedures must be altered to account for the weld joint geometry and process altered material properties. However the proposed modifications have not been experimentally validated with full scale specimens, which compose multiple lateral and longitudinal stiffener bays, a task which is appropriate to be undertaken herein.

5.2.4 Summary

The FSW process induces complicated coupled thermal, mechanical and metallurgical behaviour resulting in residual effects within the fabricated panels. Results from both single stiffener and multi-stiffener aerospace specimen tests and coupled simulation studies have demonstrated that panel static strength performance is influenced by the residual welding effects. To date neither experimental data nor accompanying sensitivity studies on the impact of welding process effects on full scale aerospace panel structures with multiple lateral and longitudinal stiffener bays is available. Moreover as such experimental work is not available the proposed modified static strength analysis methods [12] for welded aircraft structures are as yet unvalidated for panel structure with multiple lateral and longitudinal stiffener bays.

5.3 Validation

5.3.1 Specimen Design

In order to fill the identified gap in experimental knowledge, a test programme was developed to demonstrate the static strength potential of a sample welded aircraft fuselage panel with multiple lateral and longitudinal stiffener bays under uniform compression loading. To represent realistic aircraft structure a conventional panel design was created based on generic design requirements for a single aisle civil transport aircraft fuselage. An intermediate magnitude fuselage panel ultimate loading intensity was first specified (of the order of 450 N/mm) along with typical fuselage design constraints on plastic material behaviour and initial skin buckling. A series of standard aerospace minimum manufacturing, fatigue and damage tolerance requirements were also specified to ensure a realistic design. A test specimen configuration of five lateral stringer bays and three longitudinal frame bays was then developed from the representative panel design, Figure 5.2.

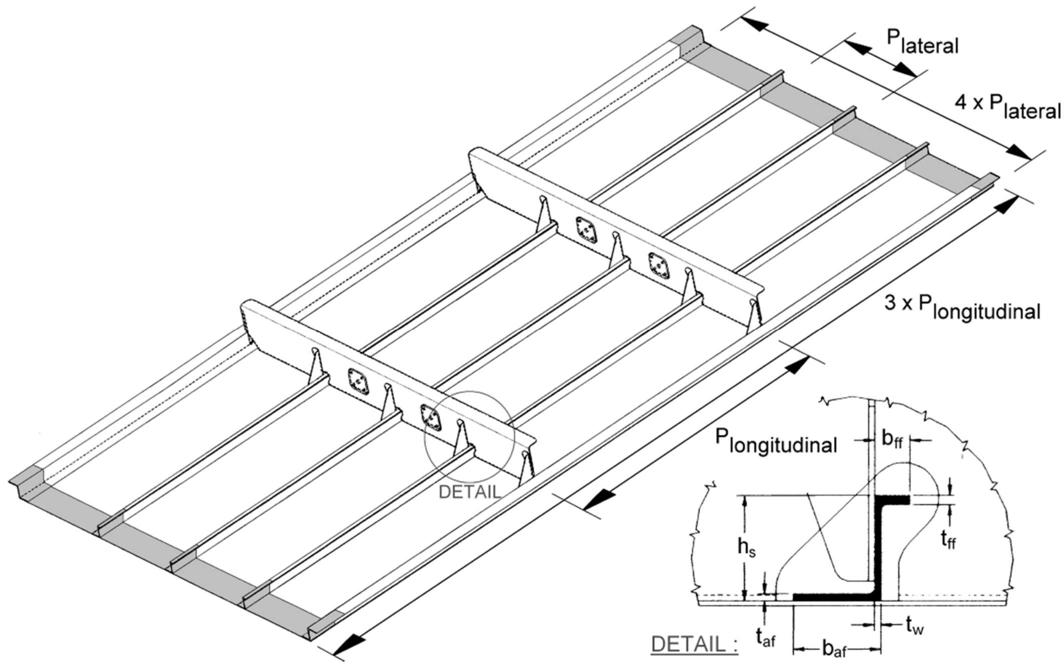

Figure 5.2 Compression specimen design

The resulting specimen design consisted of a constant thickness skin of standard fuselage skin material (AA2024), extruded Z-section longitudinal stringers, and press formed C-section lateral frames, both in a standard fuselage stiffener material (AA7075). The central three stringers were designed with a continuous weld joint to the skin via the lower wider Z-section flange, hereafter referred to as the attached flange. The two edge stringers, which were marginally oversized to promote specimen failure within the specimen central zone away from the specimen boundaries, where attached to the skin via standard aerospace counter-sunk fasteners, again with the aim of promoting specimen failure inside the specimen central zone. The specimen lateral frames where also attached to the skin via standard aerospace counter-sunk fasteners and at each stringer-frame intersection a stringer opening was designed to allow the uninterrupted passage of the stringers. Cleats (AA2024) where also attached at each stringer-frame intersection, designed to offer the stringers additional support against instability [22].

5.3.2 Specimen Manufacture

The specimen skin was initially cut to size in the width but cut marginally over sized in the length (i.e. in the loading direction). The central stringers were also cut marginally over sized and welded to the skin with continuous flange lap welds. Once welded the skin-stringer structure was inspected before the lateral frames and edge stringers were attached. Once fabricated the specimen ends were cast in epoxy tooling resin and machined parallel, allowing simultaneously the uniform compression loading of the specimen and clamped loading edge boundary conditions. Applying clamped boundary conditions at the specimen loading ends, stabilises the upper and lower specimen frame bays, thereby again promoting failure of the specimen within its central zone.

5.3.3 Specimen Test

The specimen was tested in a 1,500 kN capacity hydraulic testing machine at Queen's University Belfast. Two edge guides, fixed to the lower loading platen were slotted onto the free flanges of the edge stringers. These support members were designed to stop out-of-plane deformation of the edge stringer free flanges during testing, stabilising the edge stringers and promoting failure to occur in the specimen central zone. An end-shortening gap was designed between the top of the edge guides and the upper loading platen. In order to support the specimen lateral frames from out-of-plane deflection during test, a series of horizontal tie rods connected each frame to remote lateral anchor points. The specimen was strain gauged with gauge locations selected to enable the definition of initial specimen buckling and post-buckling collapse behaviour. Specimen end-shortening was measured during test using calibrated displacement transducers. The specimen was loaded monotonically, in displacement control, at a rate of 0.25 mm per minute until failure occurred. Load, deflection and strain data were recorded at set load intervals during test.

5.3.4 Supplementary Tests

A series of supplementary measurements and tests were also undertaken to determine the impact of welding on the final fabricated test specimen. Micro hardness mapping was undertaken on a series of weld cross-section coupons, sectioned from equivalent specimen joints. Using the generated hardness data and semi-empirical models, similar to those developed by Myhr & Grong [23], the weld joint material properties were calculated. In order to understand the residual stress magnitudes present within the specimen a series of measurements via the hole-drilling method [24] were performed on similar scale specimens which were fabricated from the same batch materials and using the same welding process parameters.

In addition material tests were undertaken to determine the batch material properties for each of the specimen skin, stringer and frame sub-components. These material tests were performed in accordance with the ASTM compressive material testing standards [25]. Post-test the captured material property data was processed for use within Finite Element simulations, in addition the data was fitted with the Ramberg-Osgood parameters [26] thus enabling its use with standard aerospace static strength analysis methods [19, 28-29].

5.4 Sensitivity Study

Based on the experimental test programme outlined in Section 3 an accompanying Finite Element (FE) simulation programme was developed to computationally determine the sensitivity of the specimen's static strength performance to varying levels of welding process residual effects. First, a FE simulation was created to model the behaviour of the experimental panel specimen under compression loading conditions and including the experimentally measured welding process residual effects. The ability of this simulation to predict the specimen's initial buckling and collapse behaviour was then assessed against the generated experimental data. Having validated the prediction capability of the simulation the welding process residual effects were then systematically varied with a Design Of Experiment (DOE) simulation series to identify the key process effects which impact static strength. Having identified the key process effects a series of simulation parametric studies were then completed to understand the detailed nature of the relationship between the magnitude of the key welding effects and the specimen's initial buckling and collapse performance.

5.4.1 Simulation Procedure

Using the FE method and employing non-linear material and geometric analysis procedures previous research has shown that the static strength performance of stiffened panels with welding process residual effects can be simulated [12, 14]. Previous work has concluded that to represent the typical buckling failure modes of a stiffened panel the structure must be idealised as an assemblage of inter-connected shells, with the stiffener web and flanges, along with the panel skin components represented with 3D shell elements. In addition, the stiffener-skin joints must be accurately represented with the weld connection along with any contact conditions between the stiffener and skin modelled [9]. Based on this preceding knowledge Figure 5.3 schematically outlines the mid-plane shell element representation of the experimental compression test specimen. Figure 5.4 schematically outlines the local stiffener-skin joint idealisation, where the skin and stiffener attached flange nodes in the weld joint zone are connected via rigid link elements, and the skin and stiffener attached flange nodes outside the weld joint zone are connected via uni-axial contact elements.

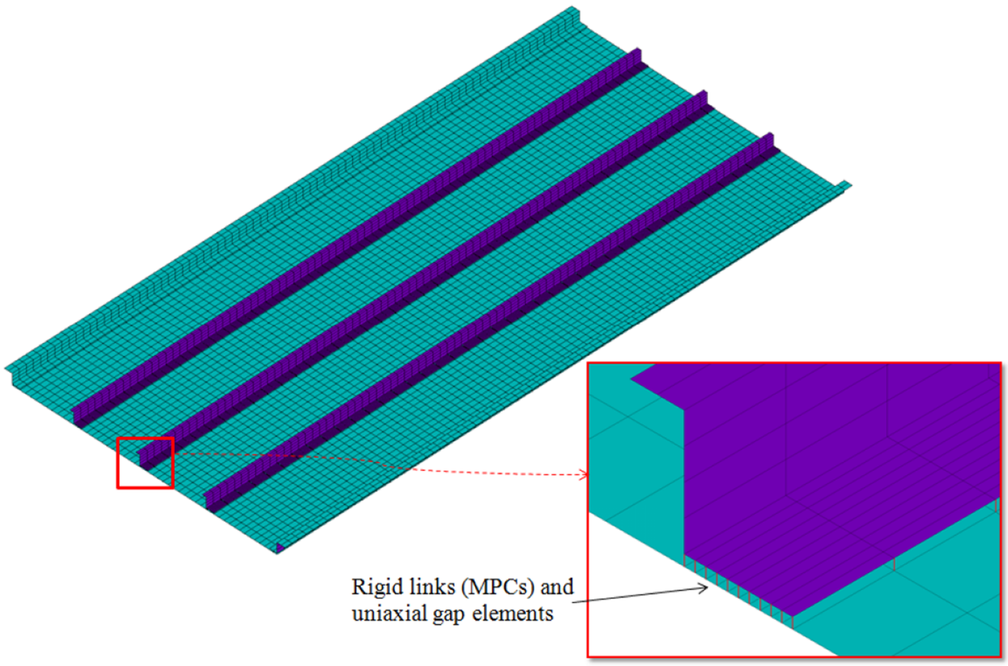

Figure 5.3 Compression specimen mesh

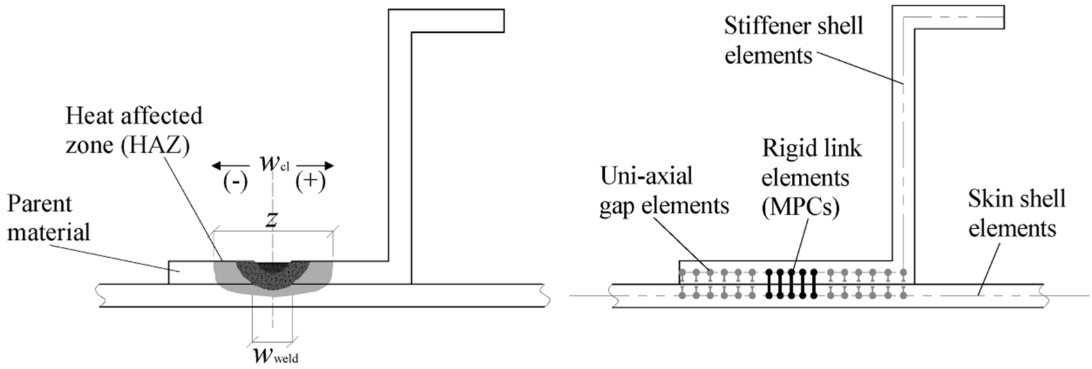

Figure 5.4 Skin-stringer joint idealisation

Applying the element selection and mesh convergence procedures outlined in Murphy et al. [30] a 4-node 3D finite strain shell element with 6 degrees of freedom at each node was selected to represent all panel skin and stiffener components. With the selected element, the convergence study defined a minimum mesh density of twelve nodes per buckle half wave for the panel skin segments. The final mesh for each analysis was defined considering the minimum mesh density and the desire to have a consistent mesh pattern across the complete simulation programme, Figure 5.3.

The loading and boundary conditions applied to the model were designed to represent the experimental test setup outlined in Section 3.3. To model the test specimen ends, the out-of-plane displacements of the nodes within the panel zones that were cast in epoxy resin in the experimental tests were restrained. To represent specimen loading, a uniform axial displacement was applied to the lower end of the model, while the axial displacement at the opposite end was restrained, again in the axial direction. The edge stringer free flanges constrained within the edge guides where constrained from out-of-plane displacements, again corresponding with the experimental setup. Finally, to represent the lateral specimen frames along with their out-of-plane displacement constrains via their tie rod connection to the experimental anchor points, simple-support conditions where applied to the model skin nodes across the specimen width at the frame fastener centre line planes.

Stress-strain curves obtained from the material tests outlined in Section 3.4 were incorporated into a multi-linear isotropic strain hardening material model available within the FE simulation software. For the computational analysis a displacement controlled incremental-iterative Newton-Raphson solution procedure was used [27]. To determine initial skin buckling the average strain method was used [31], both in the experimental and computational analysis, therefore allowing direct comparison of the results. The method plots the load against the mid-plane strain at the centre of the skin bay, with buckling defined to have occurred when a sharp break is seen in the data. The strain data used for each experimental and computational calculation was taken from the same central specimen skin bay. For ultimate collapse load definition, the maximum experimental or computational load carried by the specimen was used.

5.4.2 Welding Process Residual Effects

Based on the previous research on Friction Stir lap welding [12, 14, 32-36] a total of five welding process residual effects were identified for inclusion within the FE simulation programme:

a) The width of the effective weld joint (w_{weld}), Figure 5.4.

b) The location of the effective weld joint centre (w_{cl}), Figure 5.4.

c) The effective strength of the HAZ material (k_z) – this factor relates the degraded strength of the HAZ material to the original parent material strength, k_z being equal to the ratio of HAZ material proof stress to parent material proof stress.

d) The width of the HAZ (z), Figure 5.4.

e) The peak tensile magnitude of welding induced residual stress (F_{rs}) – the residual stress is defined as a percentage of the original parent material proof stress.

Table 5.1 summarises the range of welding process effect magnitudes under consideration. The selected magnitudes represent generic bounding values based on typical fuselage materials and joint geometries, with minimum degrading magnitudes intended to represent optimised welding parameters and pre- or post-weld heat or mechanical treatments, with maximum degrading magnitudes designed to represent non-optimised welding parameters with no pre- or post-weld heat or mechanical treatments.

Table 5.1 Test specimen welding process residual effect magnitudes

Welding process effect	Test specimen	Lower boundary	Upper boundary
Width of the effective weld joint (w_{weld})	t_{af}	t_{af}	$3t_{af}$
Location of the effective weld joint centre (w_{cl})	$-t_{af}$	$-t_{af}$	$+t_{af}$
Effective strength of the HAZ material (k_z)	0.8	0.7	0.9
Width of the HAZ (z)	$6t_{af}$	$4t_{af}$	$8t_{af}$
Peak tensile magnitude of welding induced residual stress (F_{rs})	60%	20%	60%

5.4.3 Modelling Welding Residual Effects

The inclusion of the degraded material properties in the HAZ was achieved by modelling the shell elements properties within the specimen zones within the HAZ width with HAZ material properties obtained from the supplementary experimental tests outlined in Section 3.4. The remaining specimen zones where modelled with the parent material properties obtained from the coupon tests, again outlined in Section 3.4. Representing the location of the effective weld joint centre and joint width was achieved by modelling the correct combination of rigid link and uni-axial contact elements between the relevant skin and stiffener attached flange nodes along each welded skin-stringer joint line, Figure 5.4.

The inclusion of the weld induced residual stress within the computational simulations required a three-step analysis:

- *1st analysis step* – The post weld residual stress state is initially idealised as a uniform tensile zone centred on each of the specimen's skin-stringer weld lines and an initially uniform equalising compression zone elsewhere within the model. The perfect mesh of the test specimen, without edge stringers or frames, is modelled with the idealised post weld residual stress state and with minimum boundary conditions to prevent rigid body translations or rotations. This step represents the unclamping of the welded skin and stringers from their fixturing required for the welding process [37-38]. When the residual stresses are introduced to the model, the structure is no longer in equilibrium, and a non-linear geometric analysis is carried out to establish static equilibrium. The equilibrium calculation generates a distorted structure, and a slightly modified stress state.

- *2nd analysis step* – Having created an imperfect initial geometry and stress model for the skin and three central welded stringers a second simulation stage is completed to represent the mechanical fastener attachment of the specimen frames and edge stringers. The stressed and deformed mesh of the *1st analysis step* has the skin nodes along the edge stringer and frame fastener centre lines displaced to a zero out-of-plane location and the absent stiffeners then added to the model, and a non-linear geometric analysis carried out to establish static equilibrium. Note the absent stiffener geometry is modelled through-out the analysis but in the preceding step their material stiffness is modelled at a fraction of the true value, and in the *2nd* and *3rd analysis step* the true material stiffness is represented.

- *3rd analysis step* – Having created an imperfect specimen geometry and stress state which represents the specimen manufacturing process the third analysis describes the specimen compression testing. The analysis starts with the stressed and deformed mesh produced by the *2nd analysis step* and the test loads and boundary conditions described previously, Section 4.1, are applied to the imperfect specimen model to predict the specimen behaviour under test.

Figure 5.5 presents the stress imperfection and Figure 5.6 the geometric imperfection generated by each step undertaken to create an imperfect specimen model.

5.4.4 Identification of Key Welding Process Residual Effects

Examining the five identified residual effects potentially requires significant computational effort if for example the five residual effects where examined at four independent levels across their magnitude ranges then a total of 4^5 or 1024 simulations would be required for a full factorial simulation series. Given this potential computational expense a fractional factorial approach, the Taguchi method [39], is used herein to govern the simulations. In this method a special orthogonal array is used to define a simulation series such that the understanding of the individual and combined influence of input factors (in this case the welding process residual effects) on the output results (the specimen static strength performance) is achieved from a minimum number of simulations. Table 5.2 presents the two-level orthogonal array used to study the five selected welding process residual effects. Based on the simulation series an ANalysis Of VAriance (ANOVA) is preformed on the predicted initial skin buckling and ultimate collapse loads allowing the influence of each residual effect to be numerically characterised.

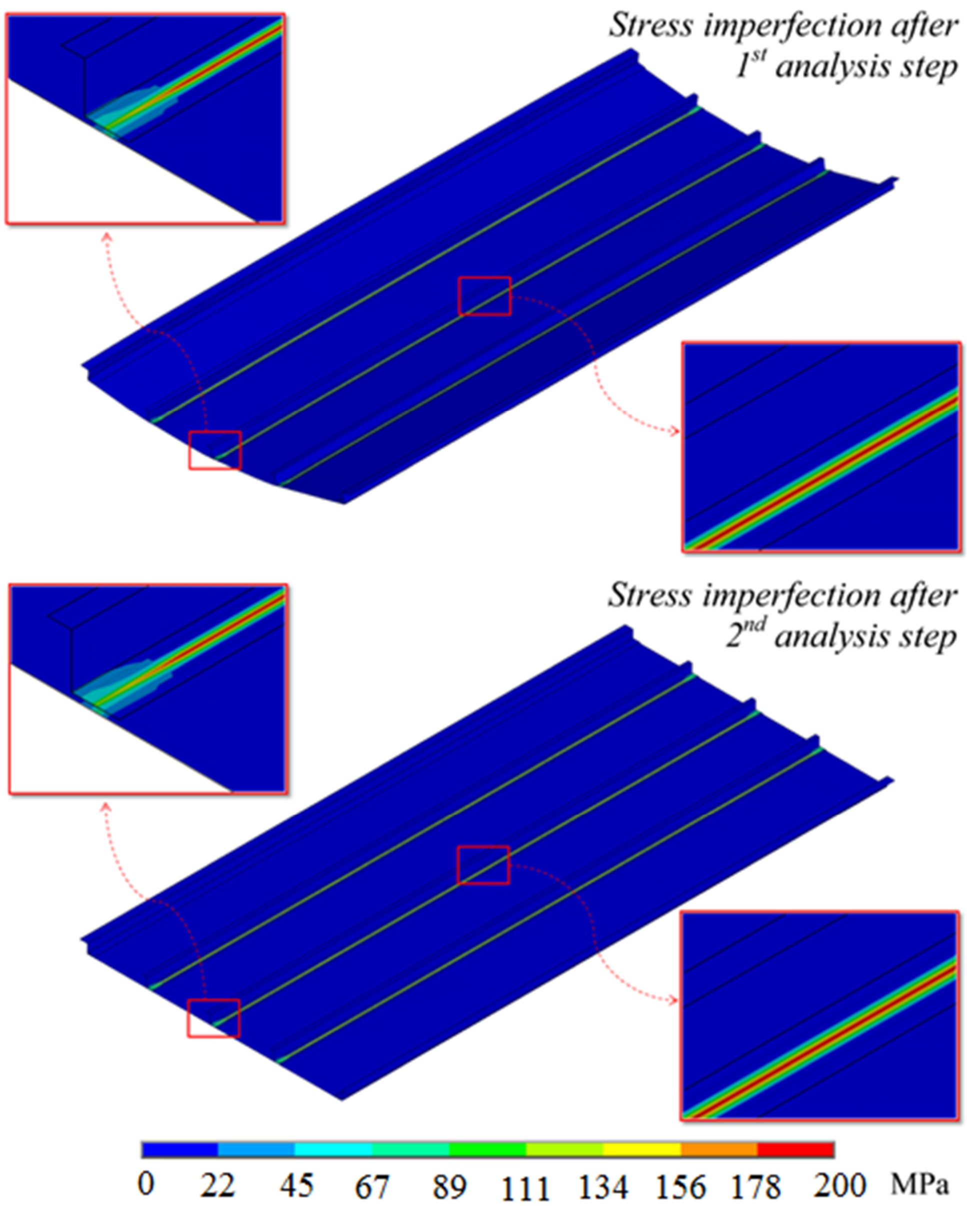

Figure 5.5 Initial stress imperfection development (von Mises stress)

Table 5.2 Fractional factorial simulation series.

Sim. No	w_{weld}	w_{cl}	Interaction $(w_{weld})\times(w_{cl})$	k_z	z	F_{rs}	Interaction $(w_{weld})\times(F_{rs})$	Interaction $(w_{cl})\times(F_{rs})$
1	t_{af}	$-t_{af}$	1	0.7	$4t_{af}$	20%	1	1
2	t_{af}	$-t_{af}$	1	0.7	$8t_{af}$	60%	2	2
3	$3t_{af}$	$+t_{af}$	1	0.9	$4t_{af}$	20%	2	2
4	$3t_{af}$	$+t_{af}$	1	0.9	$8t_{af}$	60%	1	1
5	t_{af}	$-t_{af}$	1	0.9	$4t_{af}$	20%	1	1
6	t_{af}	$-t_{af}$	1	0.9	$8t_{af}$	60%	2	2
7	$3t_{af}$	$+t_{af}$	1	0.7	$4t_{af}$	20%	2	2
8	$3t_{af}$	$+t_{af}$	1	0.7	$8t_{af}$	60%	1	1
9	t_{af}	$+t_{af}$	2	0.9	$4t_{af}$	60%	2	1
10	t_{af}	$+t_{af}$	2	0.9	$8t_{af}$	20%	1	2
11	$3t_{af}$	$-t_{af}$	2	0.7	$4t_{af}$	60%	1	2
12	$3t_{af}$	$-t_{af}$	2	0.7	$8t_{af}$	20%	2	1
13	t_{af}	$+t_{af}$	2	0.7	$4t_{af}$	60%	2	1
14	t_{af}	$+t_{af}$	2	0.7	$8t_{af}$	20%	1	2
15	$3t_{af}$	$-t_{af}$	2	0.9	$4t_{af}$	60%	1	2
16	$3t_{af}$	$-t_{af}$	2	0.9	$8t_{af}$	20%	2	1

5.4.5 Parametric Study of Key Welding Process Residual Effects

As the results from a fractional factorial simulation series are influenced by the range of effect magnitudes analysed, a series of additional simulations were performed to confirm and define the form of the key relationships. The studied effect magnitude ranges were based on the identified boundaries outlined in Table 5.1. During the parametric studies the non-varying process effects were set to represent the experimental specimen measured effect magnitudes, also outlined in Table 5.1.

5.5 Results

5.5.1 Compression Specimen Experimental Results

Table 5.3 presents the measured specimen initial buckling and collapse performance. The test specimen performed as designed, with initial buckling and ultimate failure occurring within the central zone of the specimen. The specimen failed at 336.8 kN by combined stiffener global flexure and local free flange instability, Figure 5.7. Prior to ultimate failure initial skin bay buckling occurred at 27 per cent of the ultimate test load. Weld joint integrity was maintained throughout initial skin buckling, post-buckling and overall specimen collapse, demonstrating the static strength potential of welded aircraft panels with multiple lateral and longitudinal stiffener bays. The demonstrated behaviour during test was dominated by typical panel stability with the strength of the local weld joints not limiting performance.

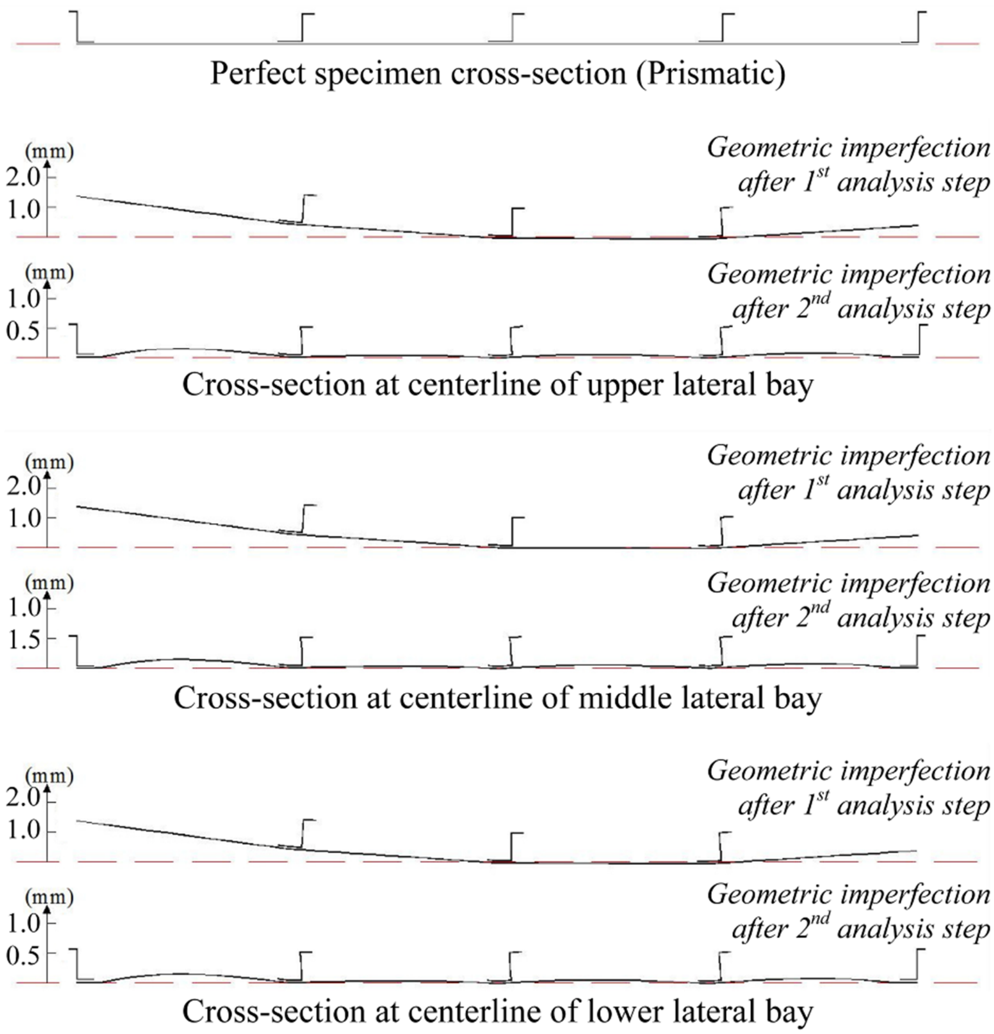

Figure 5.6 Initial geometric imperfection development

5.5.2 Baseline Simulation Results

Table 5.3 presents the predicted specimen initial buckling and collapse performance when the test specimen residual effect magnitudes are represented within the model,

Table 5.2. Specimen failure is predicted to occur at 342.2 kN by combined stiffener global flexure and local free flange instability, and initial skin buckling is predicted to occur at 91.0 kN. The simulation thus marginally over-predicts the load to cause initial skin buckling by 1.4 per cent and the collapse load by 1.6 per cent, correctly predicting the mode of collapse. Clearly the accuracy of the simulation prediction is very high and thus appropriate for further analysis on the influence of the welding residual process effects.

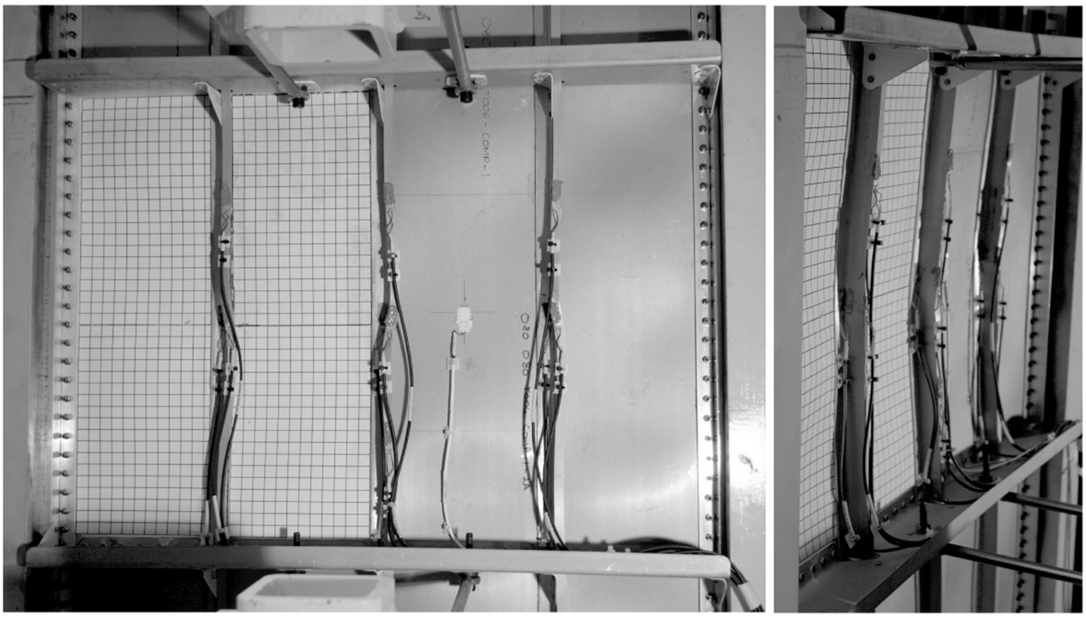

Figure 5.7 Specimen ultimate collapse mode

For completeness a 'perfect' baseline simulation was also analysed, representing the test specimen weld joint width and location but with zero material property degradation and welding induced residual stress (w_{weld}=t_{af}, w_{cl}=-t_{af}, k_z=1.0, z=0, F_{rs}=0%). This enables an estimation of the total performance impact of the specimen material property degradation and welding induced residual stress on performance. Specimen initial skin buckling was predicted to occur at 96.5 kN (6.0 per cent higher than the test specimen simulation). The 'perfect' baseline simulation predicted specimen collapse to occur at 352.7 kN by combined stiffener global flexure and local free flange instability, the same failure mode as the test specimen simulation, but at a 3.1 per cent higher load.

Table 5.3 Specimen skin buckling and collapse loads

Specimen	Experimental results	Simulation prediction	Modified static strength design method prediction
Initial skin buckling (kN)	89.7	91.0	86.3
Specimen collapse (kN)	336.8	342.2	293.8
Initial buckling to collapse ratio (%)	27	27	29
Collapse mode	Combined stiffener global flexure and local free flange instability	Combined stiffener global flexure and local free flange instability	Combined stiffener global flexure and local free flange instability

5.5.3 Fractional Factorial Simulation Series

5.5.3.1 Initial skin buckling

The results of the fractional factorial simulation series defined in Table 5.2 are presented in Table 5.4. Examining the results from the sixteen simulations the maximum variation in predicted initial skin buckling load is 19.0 per cent (17.1 kN) indicating the extreme range of performance for the full range of welding process residual effect under consideration. The outcome of the ANOVA analysis, Table 5.5, establishes that the dominant factor influencing initial skin buckling is the location of the effective weld joint centre with an individual contribution of 54.7 per cent. The width of the effective weld joint is determined to have the second greatest influence on initial skin buckling, with an individual contribution of 21.6 per cent. The ANOVA analysis also identifies a small level of interaction between the location of the effective weld joint centre and the width of the effective weld joint (1.8 per cent). Thus in total the examined physical joint characteristics (location, width plus interaction) account for a total contribution of 78.1 per cent. This is potentially not surprising as the weld joints define the lateral width of the central specimen skin bays and significantly influence the skin bay boundary conditions, effectively defining the rotational constraint provided by the stringers.

Table 5.4 Fractional factorial simulation series results

Simulation number	Local skin buckling load (kN)	Collapse load [1] (kN)
1	94.8	355.2
2	91.0	335.1
3	108.1	351.1
4	105.9	340.7
5	94.8	355.2
6	91.0	354.1
7	108.1	351.0
8	105.9	340.5
9	101.2	331.9
10	105.0	328.5
11	95.2	329.9
12	104.5	355.0
13	101.2	331.8
14	105.0	336.2
15	95.2	329.9
16	104.5	355.2
Experimental specimen [2]	91.0	342.2
Perfect specimen [3]	96.5	352.7

[1] *All simulations predicted the specimen collapse mode as 'Combined stiffener global flexure and local free flange instability'*

[2] *Simulation predictions with test specimen weld effects modelled ($w_{weld}=t_{af}$, $w_{cl}=-t_{af}$, $k_z=0.8$, $z=6$, $F_{rs}=60\%$)*

[3] *Simulation predictions with perfect specimen weld effects modelled ($w_{weld}=t_{af}$, $w_{cl}=-t_{af}$, $k_z=1.0$, $z=0$, $F_{rs}=0\%$)*

The ANOVA analysis also identifies the peak tensile magnitude of welding induced residual stress as the third most significant effect on initial buckling (16.6 per cent). Two interactions which include the residual stress effect indicate further impact totalling 3 per cent, Table 5.5. Understandably the peak tensile residual stress will impact on the magnitude of the initial specimen geometric imperfection and this along with the compressive residual stresses in the skin will impact on stability behaviour. The ANOVA analysis identifies that the strength of the HAZ material and the width of the HAZ have no significant influence on initial skin buckling. This is confirmed by examining the specimen stress levels at initial buckling, which are all within the elastic material range.

Table 5.5 Initial skin buckling and collapse load ANOVA analysis results

	Initial skin buckling load (% contribution)	Collapse load (% contribution)
w_{weld}	21.6	0.6
w_{cl}	54.7	10.2
k_z	0.0	0.0
z	2.3	0.0
F_{rs}	16.6	29.4
Interaction $(w_{weld})\times(w_{cl})$	1.8	23.8
Interaction $(w_{weld})\times(F_{rs})$	2.3	6.8
Interaction $(w_{cl})\times(F_{rs})$	0.7	7.2
Unidentified contribution	0.0	22.0

5.5.3.2 Collapse

Considering the results of the sixteen simulations, Table 5.4, the maximum variation in simulated specimen collapse load is 8 per cent (26.7 kN). This magnitude of prediction range suggests that the collapse performance of the specimen is less sensitive to the weld effects and the range of magnitudes examined than initial skin buckling performance. All sixteen simulations experience specimen failure within the central zone, with a combined stiffener global flexure and local free flange instability mode. Figure 5.8 depicts the predicted load versus end-shortening curves and collapse modes for the maximum (simulation number 1, Table 5.4) and minimum (simulation number 10) collapse predictions.

The bounding simulations (number 1 and 10) predicted collapse loads both compare well with the test result. Both simulations predict the same axial stiffness up to initial skin buckling. Beyond this region the curves diverge and the higher post-buckling axial stiffness of simulation 10 leads ultimately to a higher collapse load. The collapse modes of the two bounding simulations are also presented in Figure 5.8, where marginal differences in mode peak location and form can be observed.

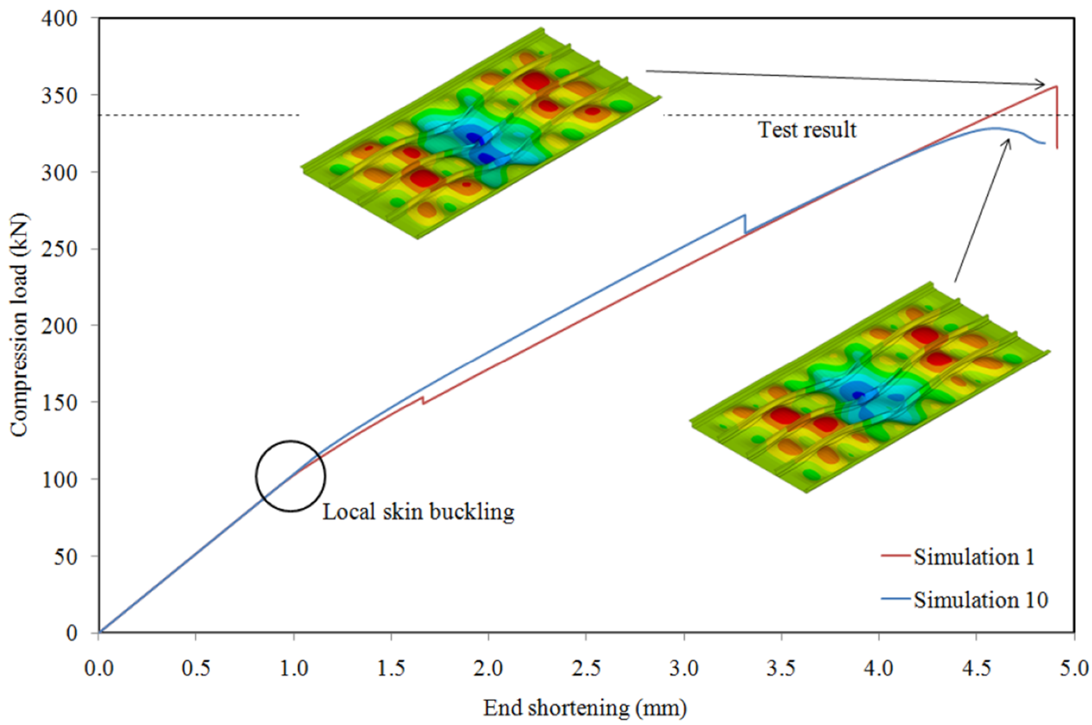

Figure 5.8 Load versus end shortening curves

The collapse ANOVA analysis reveals that the two dominant effects on specimen performance are the peak tensile magnitude of welding induced residual stress and the location of the effective weld joint centre, with individual contributions of 29.4 per cent and 10.2 per cent respectively, Table 5.5. The ANOVA analysis also identifies a significant level of interaction between the location of the effective weld joint centre and the width of the effective weld joint (23.8 per cent). Thus in total the examined physical joint characteristics (location, width plus interaction) account for a total contribution of 34.6 per cent. Smaller but significant interactions are also seen between the width of the effective weld joint, the location of the effective weld joint centre and the tensile residual stress.

The ANOVA analysis again identifies that the strength of the HAZ material and the width of the HAZ have no significant influence on specimen collapse. This is confirmed by examining the specimen local stress levels at collapse, which are within the initial plastic material range. Finally it is worth noting the significant magnitude of unidentified percentage contributions within the ANOVA collapse analysis (22 per cent in total). This reflects the complication of the post-buckling collapse analysis and confirms the need for a second phase parametric examination of the key effects, which is presented next.

5.4 Parametric Study

The ANOVA analysis identifies three significant effects, namely the width of the effective weld joint, the location of the effective weld joint centre, and the peak tensile residual stress, which impact specimen initial buckling and collapse performance, Table 5.5. Of these identified effects the tensile residual stress is potentially the most difficult to control, whereas the location of the effective weld joint centre may be manipulated through the selection of welding process parameters [32-33] and welding direction (as FSW joints are not symmetric with respect to the seam due to the rotation of the tool). The width of the effective weld joint can also be effectively manipulated via the design of the welding tool and process parameters [32-33, 40]. Therefore in the parameter study a single discrete weld joint configuration has been studied, representing the mean of the physical joint characteristics under consideration (w_{weld}=2t_{af} and w_{cl}=0). However, given the challenge of controlling residual stress the magnitude of the welding induced residual stress was examined in detail at seven individual magnitudes (5%, 10%, 20%, 30%, 40%, 50% and 60% of the original parent material proof stress).

5.4.1 Initial Skin Buckling

The specimen initial skin buckling modes and loads for the parametric results are presented in Figure 5.9. Examining the results it can be seen that the buckling load decreases continuously with higher magnitudes of initial residual stress. There is an approximately linear relationship between the magnitude of welding induced residual stress and the buckling performance (a reduction of 89 N for each per cent increase in stress magnitude). Across the simulation series there is only small deviations in the predicted skin buckling wave forms, however as the residual stress is increased specimen lateral edge bay buckles become more visible, Figure 5.9.

5.4.2 Collapse

Figure 5.10 presents the collapse results of the parametric study. Examining the results it can be seen clearly that there is only a very slight variation in the specimen

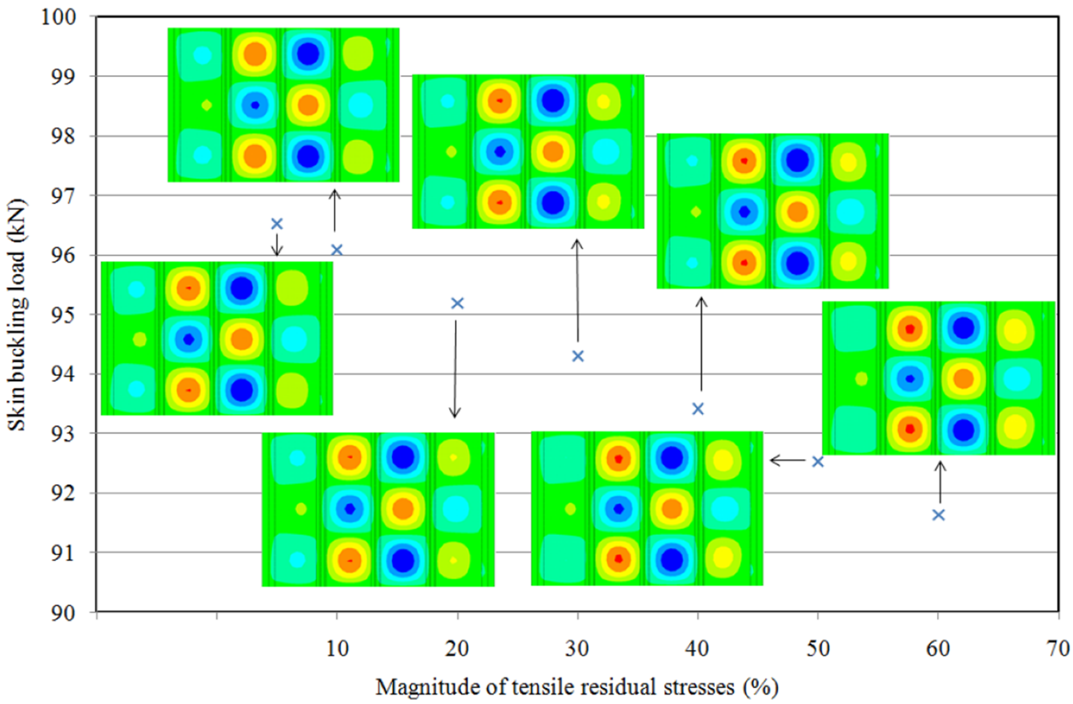

Figure 5.9 Specimen initial skin buckling parametric analysis results

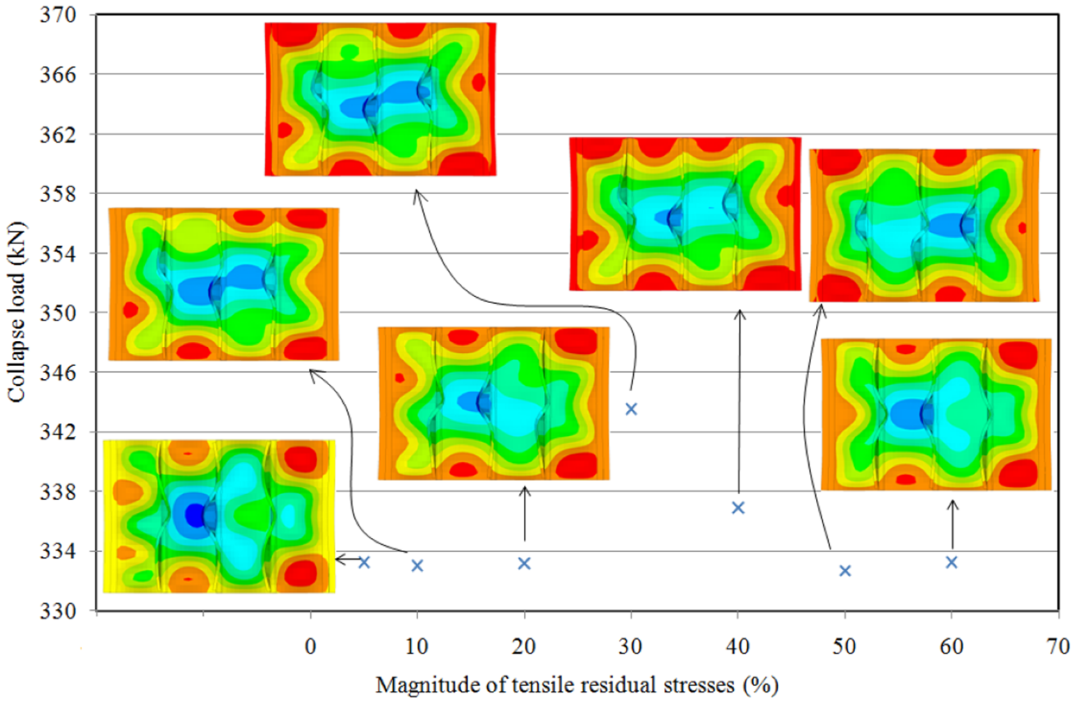

Figure 5.10 Specimen collapse parametric analysis results

collapse load with varying magnitudes of initial residual stress. No simple relationship is visible between the magnitude of initial residual stress and the collapse performance. Across the simulation series the maximum variation in simulated specimen collapse load is 3.3 per cent (10.9 kN). The variation present is visible in the predicted collapse modes, Figure 5.10, with small deviations in the ultimate buckling wave modes (with all simulations predicting central specimen failure, occurring by combined stiffener global flexure and local free flange instability).

5.5 Summary

The experimental work has demonstrated the potential static strength of panel stiffener to skin joints under large panel buckling collapse behaviour, with weld joint integrity maintained through initial skin buckling, post-buckling, and ultimate panel collapse. The numerical simulations achieved excellent agreement with the specimen test behaviour and the results of the fractional factorial simulation series and ANOVA analysis determined the dominant effects influencing specimen static strength as the width of the effective weld joint, the location of the effective weld joint centre, and the peak tensile residual stress. Overall the ANOVA computational analysis determined a relatively modest impact on static strength for the full scale panel specimen examined and the effect magnitude ranges analysed (19 per cent for initial skin buckling and 8 per cent for collapse load). The parametric computational analysis confirmed the initial ANOVA findings and defined an approximately linear relationship between the magnitude of welding induced residual stress and the initial skin buckling performance.

5.6 Modified Static Strength Design Method

As noted in the background section previous work [12] has proposed modifications to conventional aircraft panel static strength design methods [19, 28-29] to acknowledge welding altered panel properties. Single-stiffener specimen results have established that the standard aerospace stiffened panel static strength analysis procedures must be altered to account for the weld joint geometry and process altered material properties. To examine the accuracy of the previously published static strength design method on larger welded panel structures the ‘fully factored’ analysis method outlined in reference 12 was performed on the current specimen. Table 5.3 presents the analysis results.

The predicted specimen performance was reasonably close to the experimental results, with the initial buckling behaviour marginally under predicted (–3.8 per cent). In the case of collapse performance the under prediction was larger, –12.8 per cent, with the correct specimen failure mode predicted. The accuracy of these predictions is considered good given that the basic conventional analysis methods, into which the modifications are incorporated, contain empirical data and conservative simplifying assumptions which generally weaken accuracy [20]. In addition, the modified methods do not account for welding induced residual stresses or welding specific distortions.

5.7 Conclusions

Despite considerable developments on the manufacturing challenges associated with aircraft stiffened panel FSW assembly; significant questions remain with respect to static strength performance and design and analysis methods. To date studies have focused at smaller scale test specimens but herein a large scale welded aircraft panel with multiple lateral and longitudinal stiffener bays has been tested, verifying that the panel behaviour is not limited by weld joint failure. Moreover detailed FE simulations have determined the dominant effects influencing large scale panel static strength as the width and location of the effective weld joint, and the peak tensile residual stress. However in general the computational analysis demonstrates the relatively modest impact that welding effects have on the static strength of full scale panel structure, significantly lower than that demonstrated in preceding work on smaller panel specimens. In addition, a previously published static strength design method has been validated on the large scale test specimen results, indicating accurate predictions are possible with simple hand calculations if the analysis methods acknowledge the altered panel properties.

CHAPTER 6

CONCLUSIONS

6.1 Stiffened Panels as Building Blocks of Thin-Walled Structures

In many engineering disciplines the promising capabilities of plate stable buckling behaviour is facilitated to build efficient structures. Nevertheless, further actions have to be undertaken for plates in order to compensate extreme loading conditions. Increasing thickness of plate is an alternative to improve the buckling performance of structural components. However such a way would lead to expensive designs in terms of engineering practices with waste of material. To arrive at a reliable solution and overcome this challenge with efficiency based approach, stiffening of plate elements have been a robust engineering based technique in field. In this context, stringers are attached on flat plates to constitute stiffened panels which will serve as more powerful building blocks for structures. The bending and compression capacities of stringers combined with post-buckling reserve of thin flat plate (skin) constitute the key force behind the high performance of stiffened panels. Although stringers on flat plates create efficient structural segments, they reduce the predictability of structural behaviour by provoking complicated geometrical configurations. There exist several instability modes for this kind of thin-walled structures such as global and local buckling related to stringer or skin behaviour. A more complicated case is the interaction buckling of skin and stringers which plays a major role in practice and calls for careful prediction techniques.

Since stiffened panels constitute the skin of many thin-walled structures in several engineering disciplines, performance evaluations of those panels by different techniques have been a major interest for engineering design. Aircraft fuselages and wings, ship hulls and bridge components are the examples of the application fields of stiffened panels. Literature contains analytical investigations, experimental works and numerical methods to provide an improved understanding of buckling behaviour of stiffened panels. Complicated configurations of panels and non-linear performances of plated structures do not allow employing fully adapted analytical methods to predict the response those structures. For a while experimental techniques in conjunction with high resolution monitoring devices were governed the researches in this field. Results obtained from the experimental works provided significant information on buckling behaviour and sensitivity of stiffened panels. However, experimental programs have the limitations in terms of representing behaviour of actual structures. Also the costs of the programs do not allow the researchers to try many configurations with different design parameters and representative scales. Invent of computers and accompanying developments in high performance numerical techniques opened up new ways of engineering prediction techniques. Today FE method has the potential to simulate the buckling behaviour of stiffened panels accounting for complicated boundary conditions, non-linear material and geometric properties, initial geometrical imperfections and residual stresses. Although this method has the potential to simulate buckling and post-buckling behaviour of stiffened panels, building of the models and interpretation of the model response call for great care and experience.

6.2 Undertaken Research

In this thesis experimental and computational techniques are combined to investigate buckling, post-buckling and collapse behaviour of stiffened panels. Aircraft panels are the main components of the investigations in this study. Test specimens are representative of fuselage structures of commercial aircrafts. Results of many experiments on single stringer and multi-stringer panels were presented. In aircraft panels it is desirable to design the components that would exhibit initial skin buckling at a small fraction of panel collapse load. This attribute requires monitoring of two distinct stability behaviours of panels carefully from the beginning of compression loading to collapse. Experimental results include load-displacement curves of tests, monitored strain gage curves to determine initial skin buckling, and some figures of the specimens pictured during the tests. Representative fuselage specimens were made of high performance aluminium alloy materials. As a result of design requirement of fuselages panel, skin and stringers have different material characteristics. Since the stringers are the main load carrying members for panels, they have superior stress-strain curves compared to that of skin properties. Investigated panels were manufactured using FSW technology which has many advantages compared to traditional riveting techniques as detailed in previous sections. Although many researches are present in literature on metallic stiffened panels, there is no complete knowledge on performances of panels manufactured by FSW. Since the aerospace industry seeks for the effects of this novel assembling technique on aircraft panels, it is compulsory to investigate the field in detail.

Non-linear FE simulations of compression loaded stiffened panels accompanied the research as a complementary tool to extend the works to develop high fidelity virtual test models, trace the behaviours locally and perform some parametric studies. Measured material properties of parent materials, HAZ materials and residual stresses were incorporated into FE models to represent effects of manufacturing residuals. Weld induced initial geometric imperfections were imposed to models by a preliminary analysis stage. Shell elements and solid shell elements available within the ANSYS simulation software were used to represent the skin and stringers. Boundary conditions of the FE models were created in such a way that would represent the test specimens' boundaries. Due to advantageous features displacement controlled Newton-Raphson method was employed to simulate compression loading. The validation simulations exhibited performances very close to behaviours of test specimens. Having obtained good prediction results, FE models were used to investigate some characteristics which are important for the panels in service conditions. Chapter 3 presents coupled computational and experimental analysis, aimed at developing modelling guidelines for lap joined stiffened panel structure which accounts for the size of the structure being modelled. Three varying size panel structures, representing lap-joined fuselage panels, are investigated. Two levels of modelling fidelity are employed to model each panel specimen with the analysis results used to develop idealisation guidelines. In order to develop basic criteria for a possible weld joint failure for stiffened panels under compressive loading, in Chapter 4 different weld configurations of five specimens were modelled with solid shell elements. The stress and straining conditions at start-stop welds and continuous welds were investigated. It was found that EPS has the potential to be a measure for the assessment of weld joint integrity of panels manufactured by FSW. The characterisation of effects of FSW residuals on a large scale panel with multi-bays and multi-stringers was performed in Chapter 5. Weld joint width, location of weld joint centre, HAZ material strength, width of HAZ and magnitude of residual stresses were the investigated parameters. Experimental results, FE simulations and statistical techniques were used to characterize the dominant parameters on panel compression behaviour including initial skin buckling and collapse.

6.3 Further Works

Experimental and simulation works employed in this thesis are capable of investigation of aircraft stiffened panels. The non-linear FE models developed in this thesis proved the suitability of simulating the local skin buckling and collapse of panels with highly non-linear behaviours. However there are still much work to do to fully characterise the behaviour of stiffened panels with different configurations and material properties. Also there exists a significant void in the experimental and simulation works of today's researches in terms of representing very large scales components. Today' investigated characteristics of sub-component panels are extended to design very large scales of fuselages and wing structures. However, there are some questions in this process such as the reliability of such approach. Unfortunately, the scale of the structures does not allow big experiments to be undertaken. Also required time to solve the non-linear compression behaviour of those full scale structures asks for ultrahigh performance computers which are not present today for commercial use. But some engineering techniques should be provided to link small scale specimen behaviour to design of full scale structures.

REFERENCES

[1] L. Euler (1744). Methodus Inveniendi Lineas Curves Maximi Minvive Porprietate Gaudentes. Lausanne. Marcum Michaelem Bosquet.

[2] T. Young (1807). A course of Lectures on Natural Philosophy and the Mechanical Arts. London.

[3] G. R. Kirchhoff (1859). Über das Gleichgewicht und die Bewegung eines unendlich dünnen elastischen Stabes. *Journal Mathematik (Crelle).* **56**, 285-313.

[4] T. von Kármán (1908). Die Knickfestigkeit gerader Stäbe. *Physikalische Zeitschrift.* **9**, 136.

[5] H. M. Westergaard and W. R. Osgood (1928). Strength of Steel Columns. *Transactions ASME.* **50**, 65-80.

[6] H. Scheffler (1858). Theorie der Festigkeit gegen das Zernicken. Braunschweig.

[7] A. Considère (1889). Résistance des pièces comprimées. *Congrès Internationale des Procédés de Construction*. 371.

[8] F. Engesser (1889). Die Knickfestigkeit gerader Stäbe. *Zeitschrift für Architektur und Ingenieurwesen.* **35**, 455.

[9] F. Engesser (1899). Uberdie Knickfestigkeit grader Stäbe. *Zeitschrift für Architektur und Ingenieurwesen.* **35**,

[10] T. von Kármán (1910). Untersuchungen über Knickfestigkeit, Mitteilungen über Forschungsarbeiten auf dem Gebiet des Ingenieurwesens, Verin deutscher Ingenieure. Berlin.

[11] F. R. Shanley (1947). Inelastic column theory. *Journal of Aeronautical Sciences.* **14**, 261-268.

[12] N. J. Hoff (1954). Buckling and Stability. *Journal of the Royal Aeronautical Society.* **58**, 3-52.

[13] F. Bleich (1952). Buckling Strength of Metal Structures. New York. McGraw-Hill.

[14] R. D. Ziemian (2010). Guide to Stability Design Criteria for Metal Structures (6th Edition). Wiley.

[15] W.-W. Yu and R. A. LaBoube (2010). Cold-Formed Steel Design (4th Edition). Wiley.

[16] G. J. Hancock, T. M. Murray and D. S. Ellifritt (2001). Cold-Formed Steel Structures to the AISI Specification. New York. Marcel Dekker Inc.

[17] J. Singer, J. Arbocz and T. Weller (1998). Buckling experiments: Experimental Methods in Buckling of Thin-Walled Structures. Volume1: Basic Concepts, Columns, Beams and Plates. 1. Chichester. Wiley.

[18] A. G. Pugsley (1932). Torsional Instability in Struts. *Aircraft Engineering.* **4**, 229-230.

[19] S. P. Timoshenko (1945). Theory of Bending,Torsion and Buckling of Thin-Walled Members of Open Cross Section. *Journal of the Franklin Instutute.* **239**, 343-361.

[20] J. N. Goodier (1941). The Buckling of Compressed Bars by Torsion And Flexure. Ithaca, New York. Cornell University Experiment Station.

[21] P. J. Fang (1965). Torsional-Flexural Buckling of Thin-Walled Open Sections. Ithaca, New York. Cornell University.

[22] A. Chajes and W. G. (1965). Torsional-Flexural Buckling of Thin-Walled Members. *Journal of Structural Division, ASCE Proceedings.* **91**, 103-124.

[23] A. Chajes, P. J. Fang and G. Winter (1966). Torsional-Flexural Buckling, Elastic and Inelastic, of Cold-Formed Thin-Walled Columns. Ithaca, New York. Engineering Research Bulletin, Cornell University, 66-1.

[24] T. B. Peköz and G. Winter (1969). Torsional-Flexural Buckling of Thin-Walled Sections under Eccentric Load. *Journal of Structural Division, ASCE Proceedings.* **95**, 941-963.

[25] L. S. Beedle and L. Tall (1960). Basic Column Strength. *ASCE Journal of the Structural Division.* **86**, 139-173.

[26] M. A. Batterman and B. G. Johnston (1967). Behavior and Maximum Strength of Metal Columns. *ASCE Journal of the Structural Division.* **93**, 205-230.

[27] G. A. Alpsten and L. Tall (1969). Residual Stresses in Heavy Welded Shapes. Bethlehem, Pennsylvania. Fritz Laboratory Reports. Paper 334.

[28] J. Brozzetti, G. A. Alpsten and L. Tall (1970). Welding Parameters, Thick Plates and Column Strength. Bethlehem, Pennsylvania. Fritz Laboratory Reports. Paper 337.

[29] R. Bjorhovde (1972). Deterministic and Probabilistic Approaches to the Strength of Steel Columns. Ph.D. dissertation. Lehigh University.

[30] L. S. Beedle (1990). Why Are Specifications Different. *Journal of Constructional Steel Research.* **17**, 3-31.

[31] AISC (2005). Specification for Structural Steel Buildings. 360-05. Chicago, IL. American Institute of Steel Construction.

[32] R. Bjorhovde and L. Tall (1971). Maximum Column Strength and Multiple Column Curve Concept. Bethlehem, Pennsylvania. Fritz Laboratory Reports. Paper 345.

[33] H. Beer and G. Schultz (1970). Theoretical Basis for European Column Curves. *Construction Métalique.* **3**,

[34] EN 1993-1-1 Eurocode 3 (2005). Design of Steel Structures-Part 1.1. Brussels, Belgium. European Committe for Standardisation.

[35] J. Jacquet (1970). Column Test and Statistical Analysis of Their Results. *Construction Métalique.* **3**,

[36] N. Tebedge, W. F. Chen and L. Tall (1972). Experimental Studies on Column Strength of European Heavy Shapes. Bethelem, Pennsylvania. Fritz Laboratory Reports. Paper 351.7.

[37] (1976). European Convention for Constructional Steelwork (ECCS). Manual on Stability of Steel Structures. publ. 22.

[38] R. M. Jones (2006). Buckling of Bars, Plates and Shells. Blacksburg, Virginia. Bull Ridge Publishing.

[39] L. Gardner and M. Ashraf (2006). Structural design for non-linear metallic materials. *Engineering Structures.* **28**, 926-934.

[40] K. J. R. Rasmussen and J. Rondal (2000). Strength curves for aluminium alloy columns. *Engineering Structures.* **22**, 1505-1517.

[41] Y. Kim and T. Pekoz (2010). Ultimate flexural strength of aluminum sections. *Thin-Walled Structures.* **48**, 857-865.

[42] W. Ramberg and W. R. Osgood (1943). Determination of Stress -Strain Curves by Three Parameters. Technical note No. 902. Washington (DC). National Advisory Committe for Aeronautics (NACA).

[43] A. Cevik, N. Atmaca, T. Ekmekyapar and I. H. Guzelbey (2009). Flexural buckling load prediction of aluminium alloy columns using soft computing techniques. *Expert Systems with Applications.* **36**, 6332-6342.

[44] B. G. Johnston (1961). Buckling Behavior Above Tangent Modulus Load. *Journal of the Engineering Mechanics Division. ASCE proceedings.* **87**, 79-100.

[45] B. G. Johnston (1964). The Inelastic Buckling Gradient. Michigan. The University of Michigan Industry Program of the College of Engineering.

[46] B. G. Johnston (1961). Behavior of an Inelastic Buckling Model Between the Tangent Modulus and Shanley Loads. Michigan. The University of Michigan Industry Program of the College of Engineering.

[47] R. Hariri (1967). Post-buckling behavior of Tee-Shaped Aluminum Columns. Ph.D dissertation. University of Michigan.

[48] J. R. Kissel and R. L. Ferry (2002). Aluminum Structures-a guide to their specifications and design. New York. Wiley.

[49] R. J. Brungraber and J. W. Clark (1962). Strength of Welded Aluminum Columns. *Transactions ASCE.* **127**, 202-226.

[50] Y. F. W. Lai and D. A. Nethercot (1992). Strength of aluminum members containing local transverse welds. *Engineering Structures.* **14**, 241-254.

[51] (2005). AA 2005, Specification for Aluminum Structures, Aluminum Association. Arlington, VA.

[52] P. Arnault (1967). Recherche sur le flambement des profiles en alliages legers. Paris. Centre Technique Industriel de la Construction Metallique (CTICM).

[53] A. Bernard, F. Frey, J. Janss and C. Massonnet (1973). Recherches sur le comportement au flambement de barres en aluminium. *IABSE Mem.* **33**, 1-32.

[54] H. Djalaly and D. Sfintesco (1972). Recherches sur flambement de barres en aluminium. Reports of the working commissions, IABSE. Paris. International Colloqium on Column Strength.

[55] K. Kloppel and W. Barsch (1973). versuche zum Kapitel 'Stabilitatsfalle' der Nefassung von DIN 4113. *Aluminium.* **10**, 690-699.

[56] F. M. Mazzolani (1995). Aluminum alloy structures. London. E & FN Spon.

[57] EN 1999-1-1 Eurocode 9 (2007). Design of Aluminium Structures-Part 1.1. Brussels, Belgium. European Committe for Standardisation.

[58] R. G. Driver, G. Y. Grondin and L. Teh (2003). Centrally Loaded Column Research Inventory. Structural Stability Research Council, Task Group 1, University of Missouri-Rolla.

[59] (1983). ESDU Data Sheet 01.01.01, Strength of Struts.

[60] (1989). ESDU Data Sheet 89007, Flexural and Torsional-Flexural Buckling of Thin-Walled Open Section Struts.

[61] (1947). ESDU Data Sheet 01.01.10, Torsional Instability of Stringers and Struts of Angle Section.

[62] (1977). ESDU Data Sheet 77030, Buckling of Struts. Lipped and Unlipped Z Sections.

[63] (1976). ESDU Data Sheet 76023, Buckling of Struts. Lipped and Unlipped Channel Sections.

[64] (1962). ESDU Data Sheet 01.01.08, Local Instability of Struts with Flat Sides.

[65] (1978). ESDU Data Sheet 78020, Local Buckling and Crippling of I, Z and Channel Section Struts.

[66] G. H. Bryan (1891). On the Stability of a Plane Plate Under Thrusts in its Own Plane with Applications to the Buckling of the Sides of a Ship. *Proceedings London Mathematical Society.* **22**, 54-67.

[67] E. Ventsel and T. Krauthammer (2001). Thin Plates and Shells: Theory, Analysis and Applications. New York. Marcel Dekker.

[68] S. P. Timoshenko (1936). Theory of Elastic Stability. 1st edition. New York. McGraw-Hill.

[69] F. N. Hill (1940). Chart for Critical Compressive Stress of Flat Rectangular Plates. Technical note No. 773. Washington. National Advisory Committe for Aeronautics (NACA).

[70] G. Gerard and H. Becker (1957). Hanbook of Structural Stability, Part I, Buckling of Flat Plates. Technical note No. 3781. Washington. National Advisory Committe for Aeronautics (NACA).

[71] E. E. Lundquist (1939). Local Instability of Symmetrical Rectangular Tubes under Axial Compression. Technical note No. 686. Washington. National Advisory Committe for Aeronautics (NACA).

[72] E. E. Lundquist (1939). Local Instability of Centrally Loaded Columns of Channel Section and Z-Section. Technical note No. 722. Washington. National Advisory Committe for Aeronautics (NACA).

[73] E. Z. Stowell and E. E. Lundquist (1939). Instability of Columns with I, Z, Channel and Rectangular Tube Sections. Technical note No. 743. Washington. National Advisory Committe for Aeronautics (NACA).

[74] E. E. Lundquist and E. Z. Stowell (1942). Critical Compressive Stress for Flat Rectangular Plates Supported along All Edges and Elastically Restrained against Rotation along the Unloaded Edges. Technical note No. 733. Washington. National Advisory Committe for Aeronautics (NACA).

[75] E. E. Lundquist and E. Z. Stowell (1942). Critical Compressive Stress for Outstanding Flanges. Technical note No. 734. Washington. National Advisory Committe for Aeronautics (NACA).

[76] P. P. Bijlaard (1938). A theory of Plastic Stability and its Application to Thin Plates of Structural Steel. *Proceedings Royal Netherlands Academy of Sciences.* **7**, 731-743.

[77] P. P. Bijlaard (1940-41). Theory of Plastic Stability of Thin Plates. *International Association for Bridge and Structural Engineering*. Zurich. 45-69.

[78] P. P. Bijlaard (1947). Some Contributions to Theory of Elastic and Plastic Stability. *International Association for Bridge and Structural Engineering*. 17-80.

[79] P. P. Bijlaard (1949). Theory and Tests on the Plastic Stability of Plates and Shells. *Journal of Aeronautical Sciences.* **16**, 529-541.

[80] P. P. Bijlaard (1956). Theory and Theory of Plastic Buckling of Plates and Application to Simply Supported Plates Subjected to Bending or Eccentric Compression in Their Plane. *Journal of Applied Mechanics.* **23**, 27-34.

[81] P. P. Bijlaard (1957). Buckling of Plates Under Non-Homogeneous Stress. *Journal of the Engineering Mechanics Division. ASCE proceedings.* **83**, 1293.

[82] A. A. Ilyushin (1947). Stability of Plates and Shells Beyond the Proportional Limit. Technical memo. No. 1116. Washington. National Advisory Committe for Aeronautics (NACA).

[83] A. A. Ilyushin (1947). The Elasto-Plastic Stability of Plates. Technical memo. No. 1188. Washington. National Advisory Committe for Aeronautics (NACA).

[84] E. Z. Stowell (1948). A Unified Theory of Plastic Buckling of Columns and Plates. Technical note No. 1556. Washington. National Advisory Committe for Aeronautics (NACA).

[85] (1983). ESDU Data Sheet 83044, Plasticity Correction Factors for Plate Buckling.

[86] (1972). ESDU Data Sheet 72019, Buckling of Flat Isotropic Plates Under Uniaxial and Biaxial Loading.

[87] W. T. Koiter (1945 (English Translation: NASA Technical report no. AFFDL-TR70-25, 1970)). On the Stability of Elastic Equlibrium (Dissertation in Dutch). PhD. Technical University of Delft.

[88] H. L. Davidson (1965). Post-buckling Behavior of Long Rectangular Plates. Bethlehem, Pennsylvania. Fritz Laboratory Reports. Paper 248.15.

[89] M. J. Sewell (1965). The static perturbation technique in buckling problems. *Journal of the Mechanics and Physics of Solids.* **13**, 247-265.

[90] J. M. T. Thompson (1965). Discrete branching points in the general theory of elastic stability. *Journal of the Mechanics and Physics of Solids.* **13**, 295-310.

[91] W. J. Supple (1969). Initial post-buckling behaviour of a class of elastic structural systems. *International Journal of Non-Linear Mechanics.* **4**, 23-36.

[92] P. D. Simão, A. M. Girão Coelho and F. S. K. Bijlaard (2012). Influence of splices on the buckling of columns. *International Journal of Non-Linear Mechanics.* **47**, 806-822.

[93] R. Hill (1958). A General Theory of Uniqueness and Stability in Elastic-Plastic Solids. *Journal of the Mechanics and Physics of Solids.* **6**, 236-249.

[94] R. Hill (1961). Bifurcation and Uniqueness in Non-linear Mechanics of Continua. *Society for Industrial and Applied Mathematics.* 155-164.

[95] J. W. Hutchinson (1973). Postbifurcation Behavior in the Plastic Range. *Journal of the Mechanics and Physics of Solids.* **21**, 163-190.

[96] J. W. Hutchinson (1974). Plastic Buckling. *Advances in Applied Mechanics.* **14**, 67-144.

[97] L. Schuman and G. Back (1930). Strength of Rectangular Flat Plates Under Edge Compression. Technical report No. 356. National Advisory Committe for Aeronautics (NACA).

[98] R. W. Sweeney (1933). The Strength of Hull Plating Under Compression. Progress Reports 1 & 2. U.S. Experimental Model Basin

[99] J. Montgomerie (1934). Experiments on the Compression of Samples of Deck Plating and the Application of the Results to Determine a Safe Limiting Thickness for Weather Decks in Certain Conditions of Loading. *Journal of the Society of Naval Architects of Japan.* **54**,

[100] R. Lahde and H. Wagner (1936). Experimental Studies of the Effective Width of Buckled Sheets. Technical memo. No. 814. Washington. National Advisory Committe for Aeronautics (NACA).

[101] J. M. Frankland (1940). The Strength of Ship Plating Under Edge Compression. Progress Report 469. U.S. Experimental Model Basin

[102] W. Muckle (1948). Resistance to Buckling of Light Alloy Plates. *Transactions North East Coast Institution of Engineers and Shipbuilders.* **64**, 223-269.

[103] T. von Kármán, E. E. Sechler and L. H. Donnell (1932). The Strength of Thin Plates in Compression. *Transactions ASME.* **54**, 53-57.

[104] H. L. Cox (1933). Buckling of Thin Plates in Compression.

[105] E. E. Sechler (1933). The Ultimate Strength of Thin Flat Sheets in Compression. Publication 27. Pasedana. Guggenhein Aeronautics Laboratory, California Institute of Technology.

[106] K. Marguerre (1937). The Apparent Width of the Plate in Compression. Technical memo. No. 833. Washington. National Advisory Committe for Aeronautics (NACA).

[107] W. Ramberg, A. E. McPherson and S. Levy (1939). Experimental Study of Deformation and of Effective Width in Axially Loaded Sheet-Stringer Panels. Technical Note. No. 684. Washington. National Advisory Committe for Aeronautics (NACA).

[108] AISI (2007). Specification for the Design of Cold-Formed Steel Structural Members. Washington, DC. Americal Iron and Steel Institute.

[109] G. Winter (1947). Strength of Thin Steel Compression Flanges. *Transactions ASCE.* **112**, 527-576.

[110] G. Winter, W. Lansing and R. B. McCalley (1950). Four Papers on the Performance of Thin Walled Steel Structures. Reprint 33. Ithaca, New York. Cornell University Engineering Experimental Station.

[111] V. Kalyanaraman, T. Peköz and G. Winter (1977). Unstiffened Compression Elements. *Journal of the Structural Division, ASCE Proceedings.* **103**, 1833-1848.

[112] G. Winter (1970). Commentary on the 1968 Edition of the Specification for the Design of Cold-Formed Steel Structural Members. New York. American Iron and Steel Institute.

[113] A. L. Jombock and J. W. Clark (1962). Post-Buckling Behavior of Flat Plates. *Transactions ASCE.* **127**, 227-240.

[114] D. Faulkner (1975). A Review of Effective Plating for Use in the Analysis of Stiffened Plating in Bending and Compression. *Journal of Ship Research.* **19**, 1-17.

[115] N. C. Lind, M. K. Ravindra and G. Schorn (1976). Empirical Effective Width Formula. *ASCE Journal of the Structural Division.* **102**, 1741-1757.

[116] J. Roorda and K. Venkataramaiah (1979). Effective Width of Cold-Formed Steel Plates. *Canadian Journal of Civil Engineering.* **6**, 381-389.

[117] J. Rhodes (2002). Buckling of Thin Plates and members-and Early Work on Rectangular Tubes. *Thin-Walled Structures.* **40**, 87-108.

[118] W. Cui and A. E. Mansour (1998). Effects of welding distortions and residual stresses on the ultimate strength of long rectangular plates under uniaxial compression. *Marine Structures.* **11**, 251-269.

[119] J. K. Paik (2008). Some Recent Advances in the Concepts of Plate-Effectiveness Evaluation. *Thin-Walled Structures.* **46**, 1035-1046.

[120] L. A. Godoy (1996). Thin-Walled Structures with Structural Imperfections: Analysis and Behavior. Oxford. Pergamon.

[121] P. C. Hu, E. E. Lundquist and S. B. Batdorf (1946). Effects of Small Deviations from Flatness on Effective Width and Buckling of Plates. Technical note No. 1124. Washington. National Advisory Committe for Aeronautics (NACA).

[122] N. Yamaki (1959). Postbuckling Behavior of Rectangular Plates with Small Initial Curvature Loaded in Edge Compression. *Journal of Applied Mechanics. Transactions ASME.* **26**, 407-414.

[123] N. Yamaki (1961). Experiments on the Postbuckling Behavior of Square Plates Loaded in Edge Compression. *Journal of Applied Mechanics. Transactions ASME.* **28**, 238-244.

[124] G. G. Pope (1968). On the Bifurcational Buckling of Elastic Beams, Plates and Shallow Shells. Aeronautical Quarterly, vol XIX.

[125] M. Kmiecik (1971). Behaviour of axially loaded simply supported long rectangular plates having initial deformations. Report No. R84. Trondheim. Ship Research Institute.

[126] M. Kmiecik, T. Jastrzebski and J. Kuniar (1995). Statistics of Ship Plating Distortions. *Marine Structures.* **8**, 119-132.

[127] J. Rhodes, J. M. Harvey and W. C. Fok (1975). The Load-Carrying Capcity of Initially Imperfect Eccentrically Loaded Plates. *International Journal of Mechanical Sciences.* **17**, 161-175.

[128] J. Rhodes and J. M. Harvey (1977). Examination of Plate Post-Buckling Behavior. *ASCE Journal of Engineerin Mechanics Division.* **103**, 461-478.

[129] J. B. Dwight and A. T. Ractliffe (1969). The Strength of Thin Plates in Compression. *Thin-Walled Steel Structures*. K. C. Rockey and H. W. Hill. London. 3-34.

[130] J. W. Hutchinson and B. Budiansky (1974). Analytical and Numerical Study of the Effects of Initial Imperfections on the Inelastic Buckling of a Cruciform Column. *Proceedings IUTAM Symp. on Buckling of Structures*. Harvard University.

[131] C. D. Bradfield (1980). Tests on Plates Loaded in In-Plane Compression. *Journal of Constructional Steel Research.* **1**, 27-37.

[132] K. Masubuchi (1980). Analysis of welded structures-residual stresses, distortion and their consequence. New York. Pergamon.

[133] M. Ahmadzadeh, B. Farshi, H. R. Salimi and A. Hoseini Fard (2011). Residual stresses due to gas arc welding of aluminum alloy joints by numerical simulations. *International Journal of Material Forming.* 1-15.

[134] N. R. N. Rao and L. Tall (1961). Residual Stresses in Welded Plates. Bethlehem, Pennsylvania. Fritz Laboratory Reports. Paper 249.7.

[135] H. Becker, R. Goldman and J. Pozerycki (1970). Compressive Strength of Ship Hull Girders: Part I Unstiffened Plates. Washington. Ship Structures Committee (USA). Report SSC-217.

[136] P. A. Frieze, P. J. Dowling and R. E. Hobbs (1977). Ultimate Load Behavior of Plates in Compression. *Steel Plated Structures*. P. J. Dowling, J. E. Harding and P. A. Frieze. London. 24-50.

[137] J. D. White (1977). Longitudinal Shrinkage of a Single Pass Weld. Report CUED/C-Struct/TR.57. University of Cambridge, UK.

[138] J. D. White (1977). Longitudinal Stresses in a Member Containing Non-Interacting Welds. Report CUED/C-Struct/TR.58. University of Cambridge, UK.

[139] C. D. Bradfield (1979). Tests on Single Plates Under In-Plane Compression with Controlled Residual Stressesand Initial Out of Flatness. Report CUED/C-Struct/TR.78. University of Cambridge, UK.

[140] M. R. Bambach and K. J. R. Rasmussen (2002). Tests on Unstiffened Elements under Combined Compression and Bending. Research Report R818. Sydney. Department of Civil Engineering University of Sydney.

[141] M. R. Bambach and K. J. R. Rasmussen (2002). Elastic and Plastic Effective Width Equations for Unstiffened Elements. Research Report R819. Sydney. Department of Civil Engineering University of Sydney.

[142] S. P. Timoshenko (1921). Über die Stabilität Versteifter Platten. *Der Eisenbau.* **12**, 147-163.

[143] F. Schleicher (1934). Problems in the Stability of Full Walled Steel Girders (in German). *Der Bauingenieur.* **15**, 505.

[144] A. S. Lokshin (1935). On the Calculation of Plates with Ribs (in Russian). *Journal of Applied Mathematics and Mechanics.* **2**, 225.

[145] R. Barbré (1936). Buckling Stress of Rectangular Plates with Longitudinal Stiffeners Under Uniform Compression (in German). *Der Bauingenieur.* **17**, 268-273.

[146] D. F. Windenburg (1938). The Elastic Stability of Tee Stiffeners. Report 457. U.S. Experimental Model Basin

[147] E. Chwalla (1934). The General Stability Problem of a Plate Reinforced Angles Along Its Edges (in German). *Ingenieur Archiv.* **5**, 54-65.

[148] T. K. Steele and C. T. Wang (1953). The Effect of the Torsional Rigidity of a Single Stiffener on the Buckling Characteristics of a Panel Subjected to Axial Compression with Large Deflections. *Journal of the Aeronautical Sciences (Institute of the Aeronautical Sciences).* **20**, 12-18.

[149] F. Schleicher and R. Barbré (1937). On the Stability of Stiffened Rectangular Plates Having Initial Deflections (in German). *Bauing.* **18**, 665.

[150] H. Fröhlich (1937). Stability of a Uniformly Compressed Rectangular Plate with Crossing Stiffeners (in German). *Bauing.* **18**, 673.

[151] www.airbus.com (2011).

[152] J. S. Newel (1930). The Strength of Aluminum Alloy Sheets. *Airway Age.* **11**, 1420-1424.

[153] J. S. Newel (1932). Data on the Strength of Aircraft Materials. *Aviation Engineering.* **6**, 11-14.

[154] E. E. Lundquist (1933). Comparison of Three Methods for Calculating the Compressive Strength of Flat and Slightly Curved Sheet and Stiffener Combinations. Technical note No. 455. Washington. National Advisory Committe for Aeronautics (NACA).

[155] A. Murphy, M. Price, A. Gibson and C. G. Amstrong (2004). Efficient non-linear idealisations of aircraft fuselage panels in compression. *Finite Elements in Analysis and Design.* **40**, 1977-1993.

[156] E. E. Sechler (1937). Stress Distribution in Stiffened Panels Under Compression. *Journal of Aeronautical Sciences.* **4**, 320-333.

[157] H. B. Dickinson and J. R. Fischel (1938). Measurement of Stiffener Stresses and Effective Widths in Stiffened Panels. *Journal of Aeronautical Sciences.* **6**, 249-254.

[158] E. R. Reff (1939). Empirical Formulas for Allowable Compression Loads in Stiffened Sheet Panels. *Journal of the Aeronautical Sciences (Institute of the Aeronautical Sciences).* **6**, 505-510.

[159] R. Barbré (1939). Stability of Rectangular Plates with Longitudinal or Transverse Stiffeners Under Uniform Compression. Technical memo. No. 904. Washington. National Advisory Committe for Aeronautics (NACA).

[160] L. G. Dunn (1940). An Investigation of Sheet-Stiffener Panels Subjected to Compression Loads with Particular Reference to Torsionally Weak Stiffeners. Technical note No. 752. Washington. National Advisory Committe for Aeronautics (NACA).

[161] C. B. Hutchins (1934). The Relative Strength of Stiffener and Sheet Attachment Methods. Ph.D. California Institute of Technology.

[162] W. L. Howland (1936). Effect of Rivet Spacing on Stiffened Thin Sheet Under Compression. *Journal of the Aeronautical Sciences (Institute of the Aeronautical Sciences).* **3**, 434-439.

[163] M. Holt (1943). Tests of Aluminum-Alloy Stiffened-Sheet Specimens Cut from an Airplane Wing. Technical note No. 883. Washington. National Advisory Committe for Aeronautics (NACA).

[164] H. L. Cox, F. R. Thurston and E. P. Coleman (1945). Compression Tests on Seven Panels of Monocoque Construction. R & M No. 2042. Aeronautical Research Council (U.K.).

[165] J. W. Semonian and J. P. Peterson (1955). An Analysis of the Stability and Ultimate Compressive Strength of Short Sheet-Stringer Panels with Special Reference to the Influence of Riveted Connection Between Sheet and Stringer. Technical note No. 3431. Washington. National Advisory Committe for Aeronautics (NACA).

[166] S. Levy and W. D. Kroll (1948). Primary Instability of Open-Section Stringers Attached to Sheet. *Journal of the Aeronautical Sciences (Institute of the Aeronautical Sciences).* **15**, 581-591.

[167] C. A. Rossman, L. M. Bartone and C. V. Dobrowski (1944). Compressive Strength of Flat Panels with Z-Section Stiffeners. ARR No. 4B03. Washington. National Advisory Committe for Aeronautics (NACA).

[168] E. H. Schuette, S. Barab and L. McCracken (1946). Compressive Strength of Aluminum-Alloy Flat panels with Longitudinal Formed Hat-Section Stiffeners.

Technical note No. 1157. Washington. National Advisory Committe for Aeronautics (NACA).

[169] N. F. Dow, W. A. Hickman and B. W. Rosen (1954). Data on the Compressive Strength of Skin-Stringer Panels of Various Materials. Technical note No. 3064. Washington. National Advisory Committe for Aeronautics (NACA).

[170] H. B. Crocket (1942). Predicting Stiffener and Stiffened Panel Crippling Stresses. *Journal of the Aeronautical Sciences (Institute of the Aeronautical Sciences).* **9**, 501-509.

[171] B. E. Gatewood and E. L. Williams (1951). Allowable Compressive Stresses in Aircraft Structures. *Journal of the Aeronautical Sciences (Institute of the Aeronautical Sciences).* **18**, 657-664.

[172] P. P. Bijlaard (1955). On the Buckling of Stringer Panels Including Forced Crippling. *Journal of the Aeronautical Sciences (Institute of the Aeronautical Sciences).* **22**, 491-501.

[173] G. Gerard (1957). Hanbook of Structural Stability, Part V, Compressive Strength of Flat Stiffened Panels. Technical note No. 3785. Washington. National Advisory Committe for Aeronautics (NACA).

[174] G. Gerard (1957). Hanbook of Structural Stability, Part IV, Failure of Plates and Composite Elements. Technical note No. 3784. Washington. National Advisory Committe for Aeronautics (NACA).

[175] G. Gerard (1958). The Crippling Strength of Compression Elements. *Journal of the Aerospace Sciences.* **25**, 37-52.

[176] M. C. Y. Niu (1988). Airframe Structural Design: Practical Design Information and Data on Aircraft Structures. Hong Kong. Hong Kong Conmilit Press Ltd.

[177] S. Yusuff (1958). Buckling Phenomena of Stiffened Panels. *Journal of the Aerospace Sciences.* **25**, 507-514.

[178] S. Yusuff (1974). An Investigation of Short Wave Buckling of Stiffened Panels by Energy Method. *Journal of Applied Mechanics.* **41**, 1131-1133.

[179] S. Yusuff (1976). Buckling and Failure of Flat Stiffened Panels. *Journal of Aircraft.* **13**, 198-204.

[180] H. L. Sujata (1961). Plastic Buckling of Longitudinally Stiffened Plates. *Journal of the Aerospace Sciences.* **28**, 864-871.

[181] H. L. Sujata (1962). The Effective Plate Width of Longitudinally Stiffened Plates at Plastic Buckling. *Journal of the Aerospace Sciences.* **29**, 269-274.

[182] S. W. McClaren, J. C. McQueen and A. P. Martin (1967). Comparison of Integrally Formed Compression Panel Efficiencies with Other Aerospace Panel Concepts. 8th Structural Dynamics and Materials Conference. American Institute of Aeronautics and Astronautics.

[183] J. C. McQueen, S. W. McClaren and A. P. Martin (1969). Integrally formed structures - A new stiffened panel concept. Astrodynamics Conference. American Institute of Aeronautics and Astronautics.

[184] A. van der Neut (1974). Mode Interaction with Stiffened Panels. Report VTH-180. Delft. Delft University of Technology Department of Aeronautical Engineering.

[185] A. Rothwell (1981). An Experimental Investigation of the Post-buckling Efficiency of Z-Section Stringer-Skin Panels. *Aeronautical Journal.* **85**, 29-33.

[186] J. C. Ekvall and D. J. Chellman (1988). Evaluation of aluminum-lithium alloys in compression-stiffened aircraft structures. *Journal of Aircraft.* **25**, 1001-1008.

[187] D. J. Chellman, J. C. Ekvall, L. Bakow and R. R. Flores (1991). Compression crippling behavior of elevated temperature aluminum alloys. 32nd Structures, Structural Dynamics, and Materials Conference. American Institute of Aeronautics and Astronautics.

[188] E. K. Hoffman, R. A. Hafley, J. A. Wagner, D. C. Jegley, R. W. Pecquet, C. M. Blum and W. J. Arbegast Compression Buckling Behavior of Large-Scale Friction Stir Welded and Riveted 2090-T83 Al-Li Alloy Skin-Stiffener Panels. TM-2002-211770. Washington. National Aeronautics and Space Administration (NASA).

[189] (1976). ESDU Data Sheet 70003, Local Buckling of Compression Panels with Unflanged Integral Stiffeners.

[190] (1976). ESDU Data Sheet 71014, Local Buckling of Compression Panels with Flanged Stringers.

[191] (1974). ESDU Data Sheet 02.01.34, Estimation of the Initial Buckling Stress Under Uniaxial Compression of a skin with Integral Unflanged Stiffeners.

[192] (1974). ESDU Data Sheet 02.01.35, Estimation of the Initial Buckling Stress Under Uniaxial Compression of a skin with Z-Section Stringers.

[193] (1974). ESDU Data Sheet 02.01.36, Estimation of the Initial Buckling Stress Under Uniaxial Compression of a skin with Top Hat Section Stringers.

[194] (1990). ESDU Data Sheet 02.01.08, Buckling in Compression of Sheet Between Rivets.

[195] (1976). ESDU Data Sheet 02.01.09, Inter-rivet Buckling Curves for Specific Materials.

[196] (1977). ESDU Data Sheet 02.01.16, Strength of Stringers in Panel in Compression.

[197] (1982). ESDU Data Sheet 02.01.17, Nomogram for Strength of Stringers in Compression.

[198] (2008). ESDU Data Sheet 98016, Elastic Buckling of Flat Isotropic Stiffened Panels and Struts in Compression.

[199] (2008). ESDU Data Sheet 01001, Elasto-plastic Buckling of Flat Isotropic Stiffened Panels and Struts in Compression.

[200] E. F. Bruhn (1973). Analysis and Design of Flight Vehicle Structures (1st ed.). Tri-State Offset Company.

[201] M. C. Y. Niu (1999). Airframe Stress Analysis and Sizing (2nd ed.). Hong Kong. Hong Kong Conmilit Press Ltd.

[202] B. Åkesson (2007). Plate Buckling in Bridges and other Structures. London. Taylor & Francis Group.

[203] N. W. Murray (1973). Buckling of Stiffened Panels Loaded Axially and in Bending. *The Structural Engineer.* **51**, 285-301.

[204] N. W. Murray (1975). Analysis and Design of Stiffened Plates for Collapse Load. *The Structural Engineer.* **53**, 153-158.

[205] N. W. Murray (1981). Some Basic Plastic Mechanisms in Thin walled Structures. *International Journal of Mechanical Sciences.* **23**, 703-713.

[206] N. W. Murray (1984). Introduction to the Theory of Thin-Walled Structures. Oxford: Clarendon Press.

[207] M. R. Horne and R. Narayanan (1975). An Approximate Methodfor the Design of Stiffened Steel Compression Panels. *Proceedings of the Institution of Civil Engineers, Part II.* **59**, 501-514.

[208] M. R. Horne and R. Narayanan (1976). The Strength of Straitened Welded Steel Stiffened Plates. *The Structural Engineer.* **54**, 437-443.

[209] M. R. Horne and R. Narayanan (1976). Strength of Axially Loaded Stiffened Panels,. *IABSE.* **36**, 125-157.

[210] M. R. Horne and R. Narayanan (1977). Design of Axially Loaded Stiffened Stiffened Panels. *Journal of Structural Division, ASCE.* **103**, 2243-2257.

[211] J. B. Dwight and G. H. Little (1976). Stiffened Steel Compression Flanges: A Simpler Approach. *The Structural Engineer.* **54**, 501-505.

[212] P. J. Dowling and S. Chatterjee (1977). Design of Box Girder Compression Flanges. *2nd International Colloquium on Stability*. Brussels. 153.

[213] S. Chatterjee (1978). Ultimate Load Analysis and Design of Stiffened Plates in Compression. Ph.D. Ph.D. thesis, Imperial College, University of London.

[214] M. S. Troitsky (1976). Stiffened Plates: Bending Stability and Vibrations. New York. Elsevier.

[215] A. N. Sherbourne, C. Y. Liaw and C. Marsh (1971). Stiffened Plates in Uniaxial Compression. *IABSE.* **31**, 145-177.

[216] C. Massonnet and R. Maquoi (1973). New Theory and Tests on the Ultimate Strength of Stiffened Box Girders. *Steel Box Girder Bridges, Proceedings of the Institution of Civil Engineers*. 131-144.

[217] N. W. Murray and W. Katzer (1983). The Collpase Behaviour of Stiffened Steel Plates Which Have High Aspect Ratios Under Axial Compression. *Instability and Plastic Collapse of Steel Structures*. L. J. Morris. 432-445.

[218] D. G. Williams (1971). Some Examples of the Elastic Behaviour of Initially Deformed Bridge Panels. *Civil Engineering and Public Works Review*.

[219] N. C. Lind (1973). Buckling of Longitudinally Stiffened Sheets. *Journal of Structural Division, ASCE.* **99**, 1686-1691.

[220] O. K. Bedair (1998). A contribution to the stability of stiffened plates under uniform compression. *Computers & Structures.* **66**, 535-570.

[221] R. Barbré, H. Schmidt and S. Riemann (1982). Traglastversuche an Längsgestauchten, Durch Wulstflachstähle Versteiften Blechen mit Freien Längsrändern. *Der Stahlbau.* **51**, 321-332.

[222] J. Scheer and J. Vayas (1983). Traglastversuche an Längsgestauchten, Rechteckplatten mit Allseitiger Lagerung. *Der Stahlbau.* **52**, 78-84.

[223] K. Roik (1976). Effective Breadth and Shear Lag in Plate Girder Bridges with Elastic and Elasto-plastic Material Behaviour. *Steel Plated Structures*. London. 169-195.

[224] P. Dubas (1976). Plated Structures with Closed-Section Stiffeners. *Steel Plated Structures*. London. 266-283.

[225] E. Steen (1989). Elastic buckling and postbuckling of eccentrically stiffened plates. *International Journal of Solids and Structures.* **25**, 751-768.

[226] B. H. Choi, M. O. Hwang, T. Y. Yoon and C. H. Yoo (2009). Experimental study of inelastic buckling strength and stiffness requirements for longitudinally stiffened panels. *Engineering Structures.* **31**, 1141-1153.

[227] S. Sridharan and P. Mao-Hua (1989). Performance of axially compressed stiffened panels. *International Journal of Solids and Structures.* **25**, 879-899.

[228] O. K. Bedair (1997). The elastic behaviour of multi-stiffened plates under uniform compression. *Thin-Walled Structures.* **27**, 311-335.

[229] Y. Galéa and P. O. Martin (2010). Longitudinally stiffened plates in Eurocode 3: Calculation of the global critical buckling stress. *Journal of Constructional Steel Research.* **66**, 1345-1353.

[230] P. P. Xanthakos (1994). Theory and Design of Bridges. Washington. John Wiley & Sons.

[231] T. Kitada, T. Yamaguchi, M. Matsumura, J. Okada, K. Ono and N. Ochi (2002). New technologies of steel bridges in Japan. *Journal of Constructional Steel Research.* **58**, 21-70.

[232] T. Lee and A. Ostapenko (1960). Tests on Longitudinally Stiffened Plate Panels Subjected to Lateral and Axial Loading. Bethlehem, Pennsylvania. Fritz Laboratory Reports. Paper 248.4.

[233] R. H. Rampetsreiter, T. Lee and A. Ostapenko (1962). Tests on Longitudinally Stiffened Plate Panels: Effects of Residual Stresses and Rotational Restraint by Stiffeners. Bethlehem, Pennsylvania. Fritz Laboratory Reports. Paper 248.5.

[234] J. Kondo and A. Ostapenko (1964). Tests on Longitudinally Stiffened Plate Panels with Fixed Ends. Bethlehem, Pennsylvania. Fritz Laboratory Reports. Paper 248.12.

[235] J. Kondo (1965). Ultimate Strength of Longitudinally Stiffened Plate Panels Subjected to Combined Axial and Lateral Loading. Bethlehem, Pennsylvania. Fritz Laboratory Reports. Paper 248.13.

[236] T. Tsuiji (1965). Strength of Longitudinally Stiffened Plate Panels. Bethlehem, Pennsylvania. Fritz Laboratory Reports. Paper 248.14.

[237] J. Vojta and A. Ostapenko (1967). Ultimate Strength of Longitudinally Stiffened Plate Panels with Large b/t. Bethlehem, Pennsylvania. Fritz Laboratory Reports. Paper 248.18.

[238] J. Vojta and A. Ostapenko (1967). Ultimate Strength Design Curves for Longitudinally Stiffened Plate Panels with Large b/t. Bethlehem, Pennsylvania. Fritz Laboratory Reports. Paper 248.19.

[239] D. R. Rutledge (1968). Computer Program for Ultimate Strength of Longitudinally Stiffened Panels: Large and Small b/t, General Material Properties. Bethlehem, Pennsylvania. Fritz Laboratory Reports. Paper 248.23.

[240] D. R. Rutledge (1968). Ultimate Strength of Longitudinally Stiffened Panels: Large and Small b/t, General Material Properties. Bethlehem, Pennsylvania. Fritz Laboratory Reports. Paper 248.24.

[241] A. Ostapenko (1969). Final report on Research Project: Longitudinally Stiffened Plate Panels Under Lateral and Axial Loads (Ship Bottom Plating). Bethlehem, Pennsylvania. Fritz Laboratory Reports. Paper 248.28.

[242] H. Becker, A. Colao, R. Goldman and J. Pozerycki (1971). Compressive Strength of Ship Hull Girders: Part II Stiffened Plates. Washington. Ship Structures Committee (USA). Report SSC-223.

[243] A. E. Mansour (1977). Gross Panel Strength Under Combined Loading. Washington. Ship Structures Committee (USA). Report SSC-270.

[244] A. E. Mansour and A. Thayamballi (1980). Ultimate Strength of a Ship's Hull Girder in Plastic and Buckling Modes. Washington. Ship Structures Committee (USA). Report SSC-299.

[245] Q. Chen, T. J. E. Zimmerman, D. D. DeGeer and B. W. Kennedy (1997). Strength and Stability Testing of Stiffened Plate Components. Washington. Ship Structures Committee (USA). Report SSC-399.

[246] Q. Chen, R. S. Hanson and G. Y. Grondin (2004). Interactive Buckling testing of Stiffened Steel Plate Panels. Washington. Ship Structures Committee (USA). Report SSC-433.

[247] J. K. Paik, A. Thayamballi, J. Y. Ryu, J. H. Hang, J. K. Seo, S. W. Park, S. K. Soe, C. Renaud and N. I. Kim (2008). Mechanical Collpase Testing on Aluminum Stiffened Panels For Marine Applications. Washington. Ship Structures Committee (USA). Report SSC-451.

[248] J. K. Paik (2009). Buckling Collapse Testing on Friction Stir Welded Aluminum Stiffened Plate Structures. Washington. Ship Structures Committee (USA). Report SSC-456.

[249] D. Faulkner, J. C. Adachak, J. G. Snyder and M. F. Vetter (1973). Synthesis of Welded Grillages to Withstand Compression and Normal Loads. *Computers & Structures.* **3**, 221-246.

[250] C. A. Carlsen (1977). Simplified Collapse Analysis of Stiffened Plates. *Norwegian Maritime Research.* **4**, 20-36.

[251] J. K. Paik, A. K. Thayamballi and D. H. Kim (1999). An analytical method for the ultimate compressive strength and effective plating of stiffened panels. *Journal of Constructional Steel Research.* **49**, 43-68.

[252] C. G. Soares and J. M. Gordo (1997). Design Methods for Stiffened Plates Under Predominantly Uniaxial Compression. *Marine Structures.* **10**, 465-497.

[253] W. L. Somerville, J. W. Swan and J. D. Clarke (1977). Measurement of Residual Stresses and distortions in Stiffened Panels. *Journal of Strain Analysis.* **12**, 107-116.

[254] M. Kmiecik (1975). Behaviour of axially loaded simply supported long rectangular plates having initial deformations. Report No. 4-S. Technical University of Szceczin. Ship Research Institute.

[255] E. Byklum and J. Amdahl (2002). A simplified method for elastic large deflection analysis of plates and stiffened panels due to local buckling. *Thin-Walled Structures.* **40**, 925-953.

[256] D. A. Danielson and A. Wilmer (2004). Buckling of stiffened plates with bulb flat flanges. *International Journal of Solids and Structures.* **41**, 6407-6427.

[257] J. M. Gordo and C. G. Soares (2008). Compressive tests on short continuous panels. *Marine Structures.* **21**, 113-137.

[258] J. M. Gordo and C. G. Soares (2011). Compressive tests on stiffened panels of intermediate slenderness. *Thin-Walled Structures.* **49**, 782-794.

[259] J. M. Gordo and C. G. Soares (2008). Compressive Tests on Long Continuous Stiffened Panel. *27th International Conference on Offshore Mechanics and Artic Engineering (OMAE 2008)*.

[260] M. C. Xu and C. G. Soares (2013). Experimental study on the collapse strength of wide stiffened panels. *Marine Structures.* **30**, 33-62.

[261] A. Aalberg, M. Langseth and P. K. Larsen (2001). Stiffened aluminium panels subjected to axial compression. *Thin-Walled Structures.* **39**, 861-885.

[262] T. Lamb (2003). Ship Design and Construction. 1 & 2. Jersey. Society of Naval Architects and Marine Engineers.

[263] E. Hinton and D. R. J. Owen (1979). An Introduction to Finite Element Computations. Swansea. Pineridge Press Limited.

[264] O. C. Zienkiewicz and R. L. Taylor (2000). Finite Element Method, Volume 1: The Basis. Butterworth-Heinemann.

[265] O. C. Zienkiewicz and R. L. Taylor (2000). Finite Element Method, Volume 2: Solid Mechanics. Butterworth-Heinemann.

[266] K. J. Bathe (1996). Finite Element Procedures. Prentice Hall.

[267] M. A. Crisfield (1991). Non-linear Finite Element Analysis of Solids and Structures, Volume 1: Essentials. Chichester. John Wiley & Sons.

[268] M. A. Crisfield (1997). Non-linear Finite Element Analysis of Solids and Structures, Volume 2: Advanced Topics. Chichester. John Wiley & Sons.

[269] R. Courant (1943). Variational Methods for the Solution of Problems of Equilibrium and Vibration. *Bulletin of the American Mathematical Society.* **49**, 1-23.

[270] S. Levy (1947). Computation of Influence Coefficients for Aircraft Structures with Discontinuities and Sweepback. *Journal of Aeronautical Sciences.* **14**, 547-560.

[271] S. Levy (1953). Structural Analysis and Influence Coefficients for Delta Wings. *Journal of Aeronautical Sciences.* **20**, 449-454.

[272] J. H. Argyris (1954). Energy Theorems and Structural Analysis. *Aircraft Engineering.* **26**, 347-356 (Oct.), 383-387 (Nov.).

[273] J. H. Argyris (1955). Energy Theorems and Structural Analysis. *Aircraft Engineering.* **27**, 42-58 (Feb.), 80-94 (March), 125-134 (April), 145-158 (May).

[274] E. Madenci and I. Guven (2006). The Finite Element Method and Applications in Engineering Using Ansys. Springer.

[275] M. J. Turner, R. W. Clough, H. C. Martin and L. J. Topp (1956). Stiffness and Deflection Analysis of Complex Structures. *Journal of Aeronautical Sciences.* **23**, 805-824.

[276] R. W. Clough (1960). The Finite Element Method in Plane Stress Analysis. *Proceedings ASCE, 2nd Conference on Electronic Computation*. Pittsburgh. 345-378.

[277] R. J. Melosh (1961). A stiffness Matrix for the Analysis of Thin Plates in Bending. *Journal of the Aerospace Sciences.* **28**, 34-42.

[278] H. C. Martin (1961). Plane Elasticity Problems and the Direct Stiffness Method. *The Trend in Engineering.* **13**, 5-19.

[279] M. J. Turner, E. Dill, H. C. Martin and R. J. Melosh (1960). Large Deflections of Structures Subjected to Heating and External Loads. *Journal of Aeronautical Sciences.* **27**, 97-107.

[280] J. T. Oden (1967). Numerical Formulation of Non-Linear Elasticity Problems. *Journal of Structural Division, ASCE.* **93**, 235-255.

[281] R. H. Gallagher, J. Padlog and P. P. Bijlaard (1962). Stress Analysis of Heated Compex Shapes. *Journal of American Rocket Society.* **32**, 700-707.

[282] G. G. Pope (1965). A Discrete Element method for Analysis of Plane Elastic-Plastic Stress Problems, TR SM65-10. Royal Aircraft Establishment.

[283] P. V. Marcal and I. P. King (1967). Elastic-Plastic Analysis of Two Dimensional Stress Systems by the Finite Element Method. *International Journal of Mechanical Sciences.* **9**, 143-155.

[284] Y. Yamada (1968). Plastic Stress-Strain Matrix and Its Application for the Solution of Elasto-Plastic Problems by the Finite Element Method. *International Journal of Mechanical Sciences.* **10**, 343-354.

[285] J. T. Oden (1990). Historical Comments on Finite Elements. *Proceedings of ACM Conference on History of Scientific and Numeric Computation*. S. G. Nash. 125-130.

[286] C. A. Felippa (2001). A Historical Outline of Matrix Structural Analysis: A Play in Three Acts. *Computers & Structures.* **79**, 1313-1324.

[287] Y. Q. Long, S. Cen and Z. F. Long (2009). Advanced Finite Element Method in Structural Engineering. Berlin. Springer-Verlag.

[288] R. H. Gallagher and J. Padlog (1963). Discrete Element Approach to Structural Instability Analysis. *Aiaa Journal.* **1**, 1437-1439.

[289] H. C. Martin (1966). On the Derivation of Stiffness Matrices for the Analysis of Large Deflection and Stability Problems. *Matrix Methods in Structural Mechanics*. AFFDL-TR-66-80, Air Force Institute of Technology. 697-716.

[290] K. K. Kapur and B. J. Hartz (1966). Stability of Plates Using the Finite Element Method. *Journal of Engineerin Mechanics Division, ASCE.* **92**, 177-195.

[291] R. H. Gallagher, R. A. Gellatly, J. Padlog and R. H. Mallett (1967). Discrete Element Procedure for Thin Shell Instability Analysis. *Aiaa Journal.* **5**, 138-144.

[292] W. G. Carson (1968). Plate Buckling Analysis by Finite Element Method. Ms.C. Auburn University.

[293] W. G. Carson and R. E. Newton (1969). Plate Buckling Analysis Using A Fully Compatible Finite Element. *Aiaa Journal.* **7**, 527-529.

[294] R. W. Clough and C. A. Felippa (1969). A Refined Quadrilateral Element for Analysis of Plate Bending. *Matrix Methods in Structural Mechanics*. AFFDL-TR-68-150, Wright Patterson AFB, Ohio. 399-440.

[295] J. Przemieniecki (1968). Discrete Element Methods for Stability Analysis of Complex Structures. *The Aeronautical Journal.* **72**, 1077-1086.

[296] J. S. Przemieniecki (1972). Finite Element Structural Analysis of Local Instability. *13th Structures, Structural Dynamics, and Materials Conference.*

[297] M. Fujikubo and T. Yao (1999). Elastic Local Buckling Strength of Stiffened Plate Considering Plate/Stiffener Interaction and Welding Residual Stress. *Marine Structures.* **12**, 543-564.

[298] E. Riks (1984). Some Computational Aspects of the Stability Analysis of Nonlinear Structures. *Computer Methods in Applied Mechanics and Engineering.* **47**, 219-259.

[299] J. Shi (1996). Computing Critical-Points and Secondary Paths in Nonlinear Structural Stability Analysis by the Finite-Element Method. *Computers & Structures.* **58**, 203-220.

[300] R. H. Gallagher (1973). The Finite Element Method in Shell Stability Analysis. *Computers & Structures.* **3**, 543-557.

[301] J. M. T. Thompson and G. W. Hunt (1973). A General Theory of Elastic Stability. New York. Wiley.

[302] A. Ecer (1973). Finite Element Analysis of the Post-buckling Behaviour of Structures. *Aiaa Journal.* **11**, 1532-1538.

[303] Y. Hangai and S. Kawamata (1972). Perturbation Method in the Analysis of Geometrically Non-linear and Stability problem. *Advances in Computational Methods in Structural Mechanics and Design*. J. T. e. a. Oden. The University of Alabama, Huntsville. 473-492.

[304] R. T. Haftka, R. H. Mallet and W. Nachbar (1971). Adaptation of Koiter's Method to Finite Element Analysis of Snap-Through Buckling Behaviour. *International Journal of Solids and Structures.* **7**, 1427-1447.

[305] R. H. Mallet and R. T. Haftka (1972). Progress in Nonlinear Finite Element Analysis Using Asymptotic Solution Techniques. *Advances in Computational Methods in Structural Mechanics and Design*. J. T. e. a. Oden. The University of Alabama, Huntsville. 357-374.

[306] E. Carnoy (1980). Postbuckling Analysis of Elastic Structures by the Finite-Element Method. *Computer Methods in Applied Mechanics and Engineering.* **23**, 143-174.

[307] T. J. R. Hughes and K. Pister (1978). Consistent Linearization in Mechanics of Solids and Structures. *Computers & Structures.* **8**, 391-397.

[308] H. F. Buechner, M. W. Johnson and R. H. Moore (1965). The Calculation of Equilibrium States of Elastic Bodies by Newton's Method. *9th Mid Western Mechanics Conference*. Madison.

[309] E. Riks (1972). The Application of Newton's Method to the Problem of Elastic Stability. *Journal of Applied Mechanics.* **39**, 1060-1066.

[310] S. T. Mau and R. H. Gallagher (1972). A Finite Element Procedure for Nonlinear Prebuckling and Initial Post Buckling Analysis, CR 1936. Washington. National Aeronautics and Space Administration (NASA).

[311] E. d. S. Neto, D. Peric and D. J. Owen (2008). Computational Methods for Plasticity: Theory and Applications. John Wiley & Sons.

[312] J. T. Oden (1969). Finite Element Applications in Non-linear Structural Analysis. *Finite Element Methods*. Venderbilt University Tennessee.

[313] O. C. Zienkiewicz (1971). The Finite Element in Engineering Science. London. McGraw-Hill.

[314] D. R. J. Owen and E. Hinton (1980). Finite Elements in Plasticity: Theory and Practice. Swansea. Pineridge Press.

[315] G. W. Reddien (1978). On Newton's Method for Singular Problems. *SIAM Journal on Numerical Analysis.* 993-996.

[316] E. Rothwell and B. Drachman (1989). A Unified Approach to Solving Ill-Conditioned Matrix Problems. *International Journal for Numerical Methods in Engineering.* **28**, 609-620.

[317] J. H. Argyris (1965). Continua and Discontinua. *Matrix Methods in Structural Mechanics*. AFFDL-TR-66-80, Wright Patterson AFB, Ohio. 11-189.

[318] T. M. Roberts and D. G. Ashwell (1971). The Use of Finite Element Mid-increment Stiffness Matrices in the Post-buckling Analysis of Imperfect Structures. *International Journal of Solids and Structures.* **7**, 805-823.

[319] T. H. H. Pian and P. Tong (1970). Variational Formulation of Finite Displacement Analysis. *IUTAM Symposium on High Speed Computing of Elastic Structures*. Liege.

[320] J. L. Batoz and G. Dhatt (1979). Incremental Displacement Algorithms for Nonlinear Problems. *International Journal for Numerical Methods in Engineering.* **14**, 1262-1267.

[321] G. Powell and J. Simons (1981). Improved Iteration Strategy for Nonlinear Structures. *International Journal for Numerical Methods in Engineering.* **17**, 1455-1467.

[322] E. Riks (1979). An Incremental Approach to the Solution of Snapping and Buckling Problems. *International Journal of Solids and Structures.* **15**, 529-551.

[323] G. A. Wempner (1971). Discrete Approximations Related to Nonlinear Theories of Solids. *International Journal of Solids and Structures.* **7**, 1581-1599.

[324] M. Ritto-Correa and D. Camotim (2008). On the arc-length and other quadratic control methods: Established, less known and new implementation procedures. *Computers & Structures.* **86**, 1353-1368.

[325] M. A. Crisfield (1981). A Fast Incremental-Iterative Solution Procedure That Handles Snap-Through. *Computers & Structures.* **13**, 55-62.

[326] J. Padovan (1985). Solving Postbuckling Collapse of Structures. *Finite Elements in Analysis and Design.* **1**, 363-385.

[327] W. F. Lam and C. T. Morley (1992). Arc-Length Method for Passing Limit Points in Structural Calculation. *Journal of Structural Engineering, ASCE.* **118**, 169-185.

[328] C. S. Krishnamoorthy, G. Ramesh and K. U. Dinesh (1996). Post-buckling analysis of structures by three-parameter constrained solution techniques. *Finite Elements in Analysis and Design.* **22**, 109-142.

[329] A. Csébfalvi (1998). A Non-linear Path-following Method for Computing the Equilibrium Curve of Structures. *Annals of Operation Research.* **81**, 15-23.

[330] J. G. Teng and Y. F. Luo (1998). A User Controlled Arc-length Method for Convergence to Predefined Deformation Set. *Communications In Numerical Methods in Engineering.* **14**, 51-58.

[331] S. Lopez (2001). Geometrically nonlinear analysis of plates and cylindrical shells by a predictor-corrector method. *Computers & Structures.* **79**, 1405-1415.

[332] J. H. Kim and Y. H. Kim (2001). A predictor-corrector method for structural nonlinear analysis. *Computer Methods in Applied Mechanics and Engineering.* **191**, 959-974.

[333] A. Ronnau (2001). Solving Buckling Problems and Computing Critical Points Using the Multigrid Method. Ph.D. University of Illinois at Urbana-Champaign.

[334] S. A. Ragon, Z. Gurdal and L. T. Watson (2002). A comparison of three algorithms for tracing nonlinear equilibrium paths of structural systems. *International Journal of Solids and Structures.* **39**, 689-698.

[335] L. Yuanqi and Z. Shen (2004). Improvements on the Arc-length Type Method. *Acta Mechanica Sinica.* **20**, 542-550.

[336] Y. D. Kwon, H. W. Kwon and B. S. Lim (2005). Nonlinear Analysis Using Load-displacement Control. *Structural Engineering and Mechanics.* **19**, 153-172.

[337] D. W. Murray and E. L. Wilson (1969). Finite Element Post-buckling Analysis of Thin Elastic Plates. *Aiaa Journal.* **7**, 1915-1920.

[338] R. G. Vos (1970). Finite Element Analysis of Plate Buckling and Postbuckling. Ph.D. Rice University.

[339] T. Kawai and N. Yoshimura (1971). Analysis of Large Deflection of Plates by the Finite Element Method. *International Journal for Numerical Methods in Engineering.* **1**, 123-133.

[340] A. Pica and R. D. Wood (1980). Post Buckling Behaviour of Plates and Shells Using a Mindlin Shallow Shell Formulation. *Computers & Structures.* **12**, 759-768.

[341] K. Terazawa, Y. Ueda and M. Matsuishi (1969). Elasto-plastic Buckling of Plates by Finite Element Method. *ASCE Annual Meeting and national Meeting on Water Resources Engineering*. New Orleans. Paper 845.

[342] M. A. Crisfield (1973). Large Deflection Elasto-plastic Buckling Analysis of Plate Using Finite Elements, Report LR 593. Crowthorne, Berkshire. TRRL.

[343] H. P. Lee (1977). Non-linear Finite Element Analysis of Thin-Walled Members. Ph.D. McGill University.

[344] P. Roca, E. Mirambell and J. Costa (1996). Geometric and material nonlinearities in steel plates. *Journal of Structural Engineering, ASCE.* **122**, 1427-1436.

[345] M. A. Crisfield (1976). Large Deflection Elasto-plastic Buckling Analysis of Eccentrically Stiffened Plates Using Finite Elements, Report LR 725. Crowthorne, Berkshire. TRRL.

[346] J. R. Oleary and I. Harari (1985). Finite-Element Analysis of Stiffened Plates. *Computers & Structures.* **21**, 973-985.

[347] M. Fujikubo and P. Kaeding (2002). New simplified approach to collapse analysis of stiffened plates. *Marine Structures.* **15**, 251-283.

[348] G. Ise (1982). Analysis of Eccentrically Stiffened Wide Panels. Recent Advances in Non-linear Computational Mechanics. Swansea. Pineridge Press.

[349] N. T. Nordsve and T. Moan (1980). Numerical collapse analysis of compression members. *Computers & Structures.* **12**, 521-531.

[350] C. Chahngmin, P. Hoon and L. Sung (1995). Buckling and postbuckling analysis using an assumed strain element with six DOF per node. 36th Structures,

Structural Dynamics and Materials Conference. American Institute of Aeronautics and Astronautics.

[351] J. K. Paik, B. J. Kim and J. K. Seo (2008). Methods for ultimate limit state assessment of ships and ship-shaped offshore structures: Part I - Unstiffened plates. *Ocean Engineering.* **35**, 261-270.

[352] J. K. Paik, B. J. Kim and J. K. Seo (2008). Methods for ultimate limit state assessment of ships and ship-shaped offshore structures: Part II - stiffened panels. *Ocean Engineering.* **35**, 271-280.

[353] J. K. Paik and J. K. Seo (2009). Nonlinear finite element method models for ultimate strength analysis of steel stiffened-plate structures under combined biaxial compression and lateral pressure actions-Part I: Plate elements. *Thin-Walled Structures.* **47**, 1008-1017.

[354] J. K. Paik and J. K. Seo (2009). Nonlinear finite element method models for ultimate strength analysis of steel stiffened-plate structures under combined biaxial compression and lateral pressure actions-Part II: Stiffened panels. *Thin-Walled Structures.* **47**, 998-1007.

[355] J. Campbell, L. Hetey and R. Vignjevic (2012). Non-linear idealisation error analysis of a metallic stiffened panel loaded in compression. *Thin-Walled Structures.* **54**, 44-53.

[356] A. Perez-Duarte, R. Muzzolini, J. C. Ehrstrom and S. van der Veen (2002). On Material Models for Static Sizing of Compression Driven Airframe Structure. 43rd AIAA/ASME/ASCE/AHS/ASC Structures, Structural Dynamics, and Materials Conference. American Institute of Aeronautics and Astronautics.

[357] B. G. Falzon and D. Hitchings (2007). An Introduction to Modelling Buckling and Collapse, 2nd ed. Glasgow. NAFEMS.

[358] S. Belesis and G. N. Labeas (2010). Development of an Efficient Engineering Methodology for Non-linear Damage and Post-buckling Analysis of Large Scale Structures. *International Journal of Structural Integrity.* **1**, 126-139.

[359] G. Y. Grondin, Q. Chen, A. E. Elwi and J. J. Cheng (1998). Stiffened steel plates under compression and bending. *Journal of Constructional Steel Research.* **45**, 125-148.

[360] S. Z. Hu and L. Jiang (1998). A finite element simulation of the test procedure of stiffened panels. *Marine Structures.* **11**, 75-99.

[361] T. E. Dunbar, N. Pegg, F. Taheri and L. Jiang (2004). A computational investigation of the effects of localized corrosion on plates and stiffened panels. *Marine Structures.* **17**, 385-402.

[362] M. Xu and C. Guedes Soares (2012). Assessment of the ultimate strength of narrow stiffened panel test specimens. *Thin-Walled Structures.* **55**, 11-21.

[363] N. E. Shanmugam and M. Arockiasamy (1996). Local buckling of stiffened plates in offshore structures. *Journal of Constructional Steel Research.* **38**, 41-59.

[364] M. C. Xu and C. G. Soares (2012). Numerical assessment of experiments on the ultimate strength of stiffened panels. *Engineering Structures.* **45**, 460-471.

[365] M. C. Xu and C. G. Soares (2013). Comparisons of calculations with experiments on the ultimate strength of wide stiffened panels. *Marine Structures.* **31**, 82-101.

[366] C. Lynch, A. Murphy, M. Price and A. Gibson (2004). The computational post buckling analysis of fuselage stiffened panels loaded in compression. *Thin-Walled Structures.* **42**, 1445-1464.

[367] M. Özakca, A. Murphy and S. van der Veen (2006). Buckling and Post-buckling of Sub-stiffened or Locally Tailored Aluminium Panels. *ICAS 25th Congress of International Council of the Aeronautical Sciences*. Hamburg, Germany.

[368] A. Murphy, D. Quinn, P. Mawhinney and M. Özakca (2006). Tailoring Static Strength Performance of Metallic Stiffened Panels by Selective Local Sub-Stiffening *47th AIAA/ASME/ASCE/AHS/ASC Structures, Structural Dynamics, and Materials Conference*. Newport, Rhode Island.

[369] D. Quinn, A. Murphy, W. McEwan and F. Lemaitre (2009). Stiffened panel stability behaviour and performance gains with plate prismatic sub-stiffening. *Thin-Walled Structures.* **47**, 1457-1468.

[370] D. Quinn, A. Murphy, W. McEwan and F. Lemaitre (2010). Non-prismatic sub-stiffening for stiffened panel plates-Stability behaviour and performance gains. *Thin-Walled Structures.* **48**, 401-413.

[371] Y. F. Zha and T. Moan (2001). Ultimate strength of stiffened aluminium panels with predominantly torsional failure modes. *Thin-Walled Structures.* **39**, 631-648.

[372] O. F. Hughes, B. Ghosh and Y. Chen (2004). Improved prediction of simultaneous local and overall buckling of stiffened panels. *Thin-Walled Structures.* **42**, 827-856.

[373] J. K. Paik and B. J. Kim (2002). Ultimate strength formulations for stiffened panels under combined axial load, in-plane bending and lateral pressure: a benchmark study. *Thin-Walled Structures.* **40**, 45-83.

[374] J. K. Paik, S. van der Veen, A. Duran and M. Collette (2005). Ultimate compressive strength design methods of aluminum welded stiffened panel structures for aerospace, marine and land-based applications: A benchmark study. *Thin-Walled Structures.* **43**, 1550-1566.

[375] J. K. Paik (2007). Empirical formulations for predicting the ultimate compressive strength of welded aluminum stiffened panels. *Thin-Walled Structures.* **45**, 171-184.

[376] J. K. Paik and A. K. Thayamballi (2003). Ultimate Limit State Design of Steel-Plated Structures. Chichester, UK. John Wiley & Sons.

[377] M. R. Khedmati, M. R. Zareei and P. Rigo (2010). Empirical formulations for estimation of ultimate strength of continuous stiffened aluminium plates under combined in-plane compression and lateral pressure. *Thin-Walled Structures.* **48**, 274-289.

[378] S. M. Zhang and I. Khan (2009). Buckling and ultimate capability of plates and stiffened panels in axial compression. *Marine Structures.* **22**, 791-808.

[379] J. Choung, J. M. Nam and T. B. Ha (2012). Slenderness ratio distribution and load-shortening behaviors of stiffened panels. *Marine Structures.* **26**, 42-57.

[380] Y. B. Kwon and H. S. Park (2011). Compression tests of longitudinally stiffened plates undergoing distortional buckling. *Journal of Constructional Steel Research.* **67**, 1212-1224.

[381] D. K. Shin, V. A. Le and K. Kim (2013). In-plane ultimate compressive strengths of HPS deck panel system stiffened with U-shaped ribs. *Thin-Walled Structures.* **63**, 70-81.

[382] S. van der Veen and D. Coatta (2004). Stiffened Panels in Compression: Redirecting Loads Toward High-Strength Stiffeners. 45th AIAA/ASME/ASCE/AHS/ASC Structures, Structural Dynamics & Materials Conference. American Institute of Aeronautics and Astronautics.

[383] A. Murphy, F. Lynch, M. Price and A. Gibson (2006). Modified Stiffened Panel Analysis Methods for Laser Beam and Friction Stir Welded Aircraft Panels. *Proceedings of the Institution of Mechanical Engineers, Part G: Journal of Aerospace Engineering.* **220**, 267-278.

[384] R. Wilson, A. Murphy, M. A. Price and C. Glazebrook (2012). A preliminary structural design procedure for laser beam welded airframe stiffened panels. *Thin-Walled Structures.* **55**, 37-50.

[385] G. Y. Grondin, A. E. Elwi and J. J. R. Cheng (1999). Buckling of stiffened steel plates - a parametric study. *Journal of Constructional Steel Research.* **50**, 151-175.

[386] I. A. Sheikh, G. Y. Grondin and A. E. Elwi (2002). Stiffened steel plates under uniaxial compression. *Journal of Constructional Steel Research.* **58**, 1061-1080.

[387] P. Rigo, R. Sarghiuta, S. Estefen, E. Lehmann, S. C. Otelea, I. Pasqualino, B. C. Simonsen, Z. Wan and T. Yao (2003). Sensitivity analysis on ultimate strength of aluminium stiffened panels. *Marine Structures.* **16**, 437-468.

[388] M. R. Khedmati, M. Rastani and K. Ghavami (2009). Ultimate strength and ductility characteristics of intermittently welded stiffened plates. *Journal of Constructional Steel Research.* **65**, 599-610.

[389] M. R. Khedmati, M. R. Zareei and P. Rigo (2009). Sensitivity analysis on the elastic buckling and ultimate strength of continuous stiffened aluminium plates under combined in-plane compression and lateral pressure. *Thin-Walled Structures.* **47**, 1232-1245.

[390] R. M. F. Paulo, F. Teixeira-Dias and R. A. F. Valente (2013). Numerical simulation of aluminium stiffened panels subjected to axial compression: Sensitivity analyses to initial geometrical imperfections and material properties. *Thin-Walled Structures.* **62**, 65-74.

[391] M. C. Xu and C. Guedes Soares (2013). Assessment of residual ultimate strength for wide dented stiffened panels subjected to compressive loads. *Engineering Structures.* **49**, 316-328.

[392] A. Murphy, W. McCune, M. Price, R. Curran, D. Quinn and R. Wilson (2006). The Characterization of Friction Stir Welding Process Effects on Stiffened Panel Buckling Performance. 47th AIAA/ASME/ASCE/AHS/ASC Structures, Structural Dynamics, and Materials Conference. American Institute of Aeronautics and Astronautics.

[393] A. Murphy, W. McCune, D. Quinn and M. Price (2007). The characterisation of friction stir welding process effects on stiffened panel buckling performance. *Thin-Walled Structures.* **45**, 339-351.

[394] A. Murphy, T. Ekmekyapar, M. Özakça, K. Poston, G. Moore and M. Elliott (2012). Buckling/Post-Buckling Strength of Friction Stir Welded Aircraft Stiffened Panels. *Proceedings of the Institution of Mechanical Engineers, Part G: Journal of Aerospace Engineering.*

[395] J. W. Yoon, G. H. Bray, R. A. F. Valente and T. E. R. Childs (2009). Buckling analysis for an integrally stiffened panel structure with a friction stir weld. *Thin-Walled Structures.* **47**, 1608-1622.

[396] B. Tweedy, S. Sellmeyer, A. Jahn and D. Burford (2006). Static Strength Comparison of Riveted versus Friction Stir Welded Stiffened Panels. 47th AIAA/ASME/ASCE/AHS/ASC Structures, Structural Dynamics, and Materials Conference. American Institute of Aeronautics and Astronautics.

[397] N. C. Lang and Y. W. Kwon (2007). Investigation of the Effect of Metallic Fuselage Dents on Compressive Failure Loads. *Journal of Aircraft.* **44**, 2026-2033.

[398] ANSYS ANSYS User manual. PA, USA. ANSYS Inc.

[399] A. Murphy, M. Price and P. Wang (2005). The integration of strength and process modeling of friction-stir-welded fuselage panels. Austin, TX, United states. 2815-2829.

[400] A. Bastier, M. H. Maitournam, F. Roger and K. D. Van (2008). Modelling of the residual state of friction stir welded plates. *Journal of Materials Processing Technology.* **200**, 25-37.

[401] J. Q. Su, T. W. Nelson, R. Mishra and M. Mahoney (2003). Microstructural investigation friction stir welded 7050-T651 aluminium. *Acta Materialia.* **51**, 713-729.

[402] R. Wilson, A. Murphy, M. A. Price and C. Glazebrook (2012). A preliminary structural design procedure for laser beam welded airframe stiffened panels. *Thin-Walled Structures.* **55**, 37-50.

[403] R. S. Mishra and Z. Y. Ma (2005). Friction stir welding and processing. *Materials Science & Engineering R-Reports.* **50**, 1-78.

[404] R. Nandan, T. DebRoy and H. K. D. H. Bhadeshia (2008). Recent advances in friction-stir welding - Process, weldment structure and properties. *Progress in Materials Science.* **53**, 980-1023.

[405] R. Degenhardt, A. Kling, K. Rohwer, A. C. Orifici and R. S. Thomson (2008). Design and analysis of stiffened composite panels including post-buckling and collapse. *Computers & Structures.* **86**, 919-929.

[406] R. Krueger, J. G. Ratcliffe and P. J. Minguet (2009). Panel stiffener debonding analysis using a shell/3D modeling technique. *Composites Science and Technology.* **69**, 2352-2362.

[407] C. Meeks, E. Greenhalgh and B. G. Falzon (2005). Stiffener debonding mechanisms in post-buckled CFRP aerospace panels. *Composites Part a-Applied Science and Manufacturing.* **36**, 934-946.

[408] A. C. Orifici, R. S. Thomson, R. Degenhardt, A. Kling, K. Rohwer and J. Bayandor (2008). Degradation investigation in a postbuckling composite stiffened fuselage panel. *Composite Structures.* **82**, 217-224.

[409] B. Tweedy, S. Sellmeyer, A. Jahn and D. Burford (2006). Static Strength Comparison of Riveted versus Friction Stir Welded Stiffened Panels. *47th AIAA/ASME/ASCE/AHS/ASC Structures, Structural Dynamics, and Materials Conference* Newport, Rhode Island.

[410] M. R. Khedmati, A. Bayatfar and P. Rigo (2010). Post-buckling behaviour and strength of multi-stiffened aluminium panels under combined axial compression and lateral pressure. *Marine Structures.* **23**, 39-66.

[411] M. R. Khedmati and K. Ghavami (2009). A numerical assessment of the buckling/ultimate strength characteristics of stiffened aluminium plates with fixed/floating transverse frames. *Thin-Walled Structures.* **47**, 1373-1386.

[412] P. Reimers and A. Gorba (2003). Nonlinear Buckling Analysis on Welded Airbus Fuselage Panels. *3rd FENet Annual Industry Meeting, Ensuring Fitness for Purpose of FEA*. Hamburg, Germany.